České vysoké učení technické v Praze
Fakulta jaderná a fyzikálně inženýrská

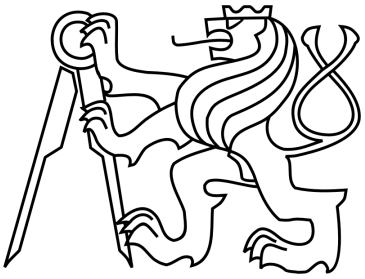

HABILITAČNÍ PRÁCE

Diffractive Electroproduction of Vector Mesons off Nuclei: Selected Topics

Praha, 2018 **RNDr. Ján Nemčík, CSc.**

Preface

This habilitation thesis includes a part of my original and pioneering results published during the period of about fifteen years after obtaining the doctoral degree. The corresponding papers were published in high-ranking journals and have a very good citation. Most of results, obtained already more than twenty years ago, are still actual presently and represent thus the basis of theoretical description of diffractive electroproduction of vector mesons off nuclei.

Within this field the main emphasize is devoted to investigation of effects occuring in interactions with both nucleon and nuclear targets. The theoretical description of the diffractive process of vector meson production is based on the light-cone (LC) quantum-chromodynamics dipole approach using the rigourous path integral technique, which allows to incorporate naturally the color transparency and coherence length effects. Besides the quark shadowing I included also the nuclear suppression of gluons at small values of Bjorken x_{Bj} within the same LC approach treating it as shadowing corrections for the higher Fock states containing gluons.

All these effects were analysed in elastic (coherent) and quasielastic (incoherent) production of different vector mesons off nuclei. I discussed possibilities for separated study of color transparency and the onset of coherence length effects.

A part of presented papers is devoted to investigation of anomalies in production of (2S) radially excited vector mesons. From the specific behavior of the nucleus-to-nucleon ratio of production cross sections as function of the photon energy and virtuality one can study a shape of radial wave functions with the corresponding position of the node.

Investigating different aspects of diffractive electroproduction of vector mesons, the presented papers are divided into four chapters and are collected in the Appendix.

Contents

1. Introduction

The dynamics of vector meson (ρ, Φ, J/Ψ, Υ, ...) production is presently a hot topic evolved intensively during last three decades. Currently the photoproduction of vector mesons represents one of the intensive channels in ultra-peripheral collisions of heavy ions (UPC) studied by experiments [1, 2] at the Large Hadron Collider (LHC) at CERN. If the nucleus remains in the ground state, $\gamma A \to V A$, such reaction is called *coherent*, otherwise we call it *incoherent*.

Discovery of J/Ψ in 1973 confirmed the idea of charm quark and gave a basis for its further investigations, which were affected also by new experiments situated on more developed accelerators using more and more powerful electronics. Later, at the beginning of 90's the experiments with relativistic heavy-ion collisions [3] stimulated the enhanced interest about charmonium suppression as a possible indication of the quark-gluon plasma formation. That fact has given a further motivation to continue in investigation of space-time pattern of charmonium production and opened new possibilities to analyze various corresponding phenomena occuring in interactions off nuclei.

In diffractive electroproduction of vector mesons one should include and study two main phenomena occuring in interactions with nuclear targets: the color transparency (absorption) and coherence (shadowing) length effets.

1.1. Color transparency

One of the fundamental phenomenon coming from the quantum-chromodynamics (QCD) is color transparency (CT) studied intensively almost three last decades. This effect manifests itself as more transparent nuclear medium for colorless hadronic wave packets than predicted by the Glauber model. Besides the nuclear medium becomes more transparent for smaller transverse sizes r of the hadron.

The CT phenomenon can be treated either in the hadronic or in the quark basis. The former approach leads to Gribov's inelastic corrections [4], the latter one manifests itself as a result of color screening [5, 6] (see also the review [7]). Although these two approaches are complementary, the quark-gluon interpretation is more intuitive and straightforward. Colorless objects (hadrons) can interact only because the color is distributed inside them. Consequently, a point-like colorless object is bare of any interaction with external color field. Therefore its cross section vanishes $\sigma(r) \propto r^2$ at $r \to 0$ [5]. This fact naturally explains the correlation between the cross sections of hadrons and their sizes [8, 9, 10].

In the classical probabilistic approach the final state absorption of the produced

meson can be estimated through the survival probability $W(z,b)$ of the vector meson produced at the point with longitudinal coordinate z and impact parameter $\vec{b}$,

$$W(z,b) = exp\left[-\sigma_{in}^{VN}\int\limits_{z}^{\infty} dz'\,\rho_A(b,z')\right] , \tag{1.1}$$

where $\rho_A(b,z)$ is the nuclear density and σ_{in}^{VN} is the inelastic VN cross section.

Going beyond the classical approach, which is represented by the vector dominance model (VDM), the diffractive process initiating the production of the vector meson on a bound nucleon is $\gamma^* N \to \bar{q}q N$ (with possible glue). Such a process of diffractive electroproduction of vector mesons off nuclei is very effective and sensitive for study of CT. A photon of high virtuality Q^2 is expected to produce a pair with a small $\sim 1/Q^2$ transverse separation [1]. Then CT manifests itself as a vanishing absorption of the small sized colorless $\bar{q}q$ wave packet during propagation through the nucleus. However, the transverse size of the colorless pair may evolve during the time of propagation due to transverse motion of the quarks. Besides, the medium filters out large size configurations which have larger absorption cross section, an effect known as *c*olor filtering. Eventually, the resulting distribution amplitude of the $\bar{q}q$ wave packet must be projected onto the wave function of the vector meson V.

Dynamical evolution of the small size $\bar{q}q$ pair to a normal size vector meson is controlled by the time scale called formation time. Due to uncertainty principle, one needs time interval to resolve different levels V (the ground state) or V' (the next excited state) in the final state. In the rest frame of the nucleus this formation time is Lorentz dilated,

$$t_f = \frac{2\,\nu}{{m'_V}^2 - m_V^2} , \tag{1.2}$$

where ν is the photon energy; m_V and m'_V is the mass of a vector meson in the $1S$ ground state and $2S$ radially excited state, respectively.

A rigorous quantum-mechanical description of the pair evolution was suggested in [11] and is based on the light-cone Green function technique. This approach is presented below in Sect. 2.

According to quark-hadron duality we expect an equivalent description of diffractive vector meson production also in the hadronic basis. Such a description is presented in [12] and looks quite different. Here the incident photon may produce different states on a bound nucleon, the V meson ground state or an excited state. Those states propagate through the nucleus experiencing multiple diagonal and off-diagonal diffractive interactions, and eventually the ground state is detected.

[1] For production of light vector mesons (ρ^0, Φ^0) very asymmetric pairs can be possible when the q or $\bar{q}$ carry almost the whole photon momentum. As a results the $\bar{q}q$ pair can have a large separation, see Chapter 2 and Eq. (2.12). Not so for production of charmonia where one can use the nonrelativistic approximation, $\alpha = 0.5$, with rather high accuracy.

Comparing the both descriptions, neither of them can be calculated exactly, and therefore each has advantages and shortcomings as was discussed in [13]. However, they are complementary and rely on different approximations and their comparison may provide a scale for the theoretical uncertainty involved.

1.2. Effects of quantum coherence; shadowing of quarks and gluons

In contrast to final state absorption, the quark shadowing is a pure quantum-mechanical effect resulting from destructive interference of the amplitudes for which the interaction takes place on different bound nucleons. This phenomenon is also known to cause nuclear suppression. It can be interpreted as a competition between the different nucleons participating in the reaction: since the total probability cannot exceed one, each participating nucleon diminishes the chances of others to contribute to the process.

Calculating nuclear absporption at small energies using the Glauber formula one should not expect any shadowing due to smallness of the photoproduction cross section. However, it has been realized back in the 60s (see the review [14]) that the photon can interact via its hadronic fluctuations. During propagation of these fluctuations through a medium they may interact with a large hadronic cross section, which causes shadowing. Consequently, shadowing effets reflect the distance from the absorption point when the pointlike photon becomes the hadronlike $\bar{q}q$ pair. This may be also interpreted as a lifetime of $\bar{q}q$ fluctuation providing the time scale which controls shadowing. Again, it can be estimated relying on the uncertainty principle and Lorentz time dilation as,

$$t_c = \frac{2\,\nu}{Q^2 + m_V^2}\ . \tag{1.3}$$

It is usually called coherence time, but we also will use the term coherence length (CL), since light-cone kinematics is assumed, $l_c = t_c$ (similarly, for formation length $l_f = t_f$). CL is related to the longitudinal momentum transfer $q_c = 1/l_c$ in the process $\gamma^* N \to V N$, which controls the interference of the production amplitudes from different nucleons.

1.3. Mixing of absorption and shadowing

There are many reactions where the initial state shadowing has been indeed observed experimentally since no final state absorption is expected. For example the total photoabsorption cross section on nuclei (see [14]), the inclusive deep-inelastic cross section [15, 16], the total neutrino-nucleus cross section [17], the Drell-Yan reaction of dilepton production [18, 19], etc. However, in the case of electroproduction of vector mesons off nuclei, it is difficult to study separately

shadowing and absorption effects as two different sources of nuclear suppression since they occur with the same cross section. For this reason one should study differences in manifestations of these effects in the two limiting cases [11], what can be illustrated within VDM.

In the low energy limit of small l_c, shorter than the mean internucleon spacing $\sim 2\,fm$, only the final state absorption matters. Then the ratio of the quasielastic (or incoherent) $\gamma^* A \to V X$ and $\gamma^* N \to V X$ cross sections, usually called nuclear transparency, reads,

$$Tr_A^{inc}\Big|_{l_c \ll R_A} \equiv \frac{\sigma_V^{\gamma^* A}}{A\,\sigma_V^{\gamma^* N}} = \frac{1}{A}\int d^2b \int\limits_{-\infty}^{\infty} dz\,\rho_A(b,z)\,\exp\left[-\sigma_{in}^{VN}\int\limits_z^{\infty} dz'\,\rho_A(b,z')\right]$$
$$= \frac{1}{A\,\sigma_{in}^{VN}}\int d^2b\,\Big\{1-\exp\Big[-\sigma_{in}^{VN}\,T(b)\Big]\Big\} = \frac{\sigma_{in}^{VA}}{A\,\sigma_{in}^{VN}}\ . \qquad (1.4)$$

In the high energy limit of long l_c the expression for nuclear transparency takes a different form,

$$Tr_A^{inc}\Big|_{l_c \gg R_A} = \int d^2b\,T_A(b)\,\exp\left[-\sigma_{in}^{VN}\,T_A(b)\right]\ , \qquad (1.5)$$

where we assume $\sigma_{el}^{VN} \ll \sigma_{in}^{VN}$ for the sake of simplicity. $T_A(b)$ is the nuclear thickness function

$$T_A(b) = \int\limits_{-\infty}^{\infty} dz\,\rho_A(b,z)\ . \qquad (1.6)$$

The exact expression beyond VDM which interpolates between the low and high energy regimes (1.4) and (1.5) can be found in [20].

The expression Eq. (1.5) clearly demonstrates that at large energies corresponding to long l_c the vector meson attenuates along the whole nucleus thickness, but only along roughly half of that length in (1.4). This confirms our expectation that nuclear shadowing also contributes to Eq. (1.5) increasing suppression.

The problem of separation of CT and CL effects arises especially in production of light vector mesons (ρ^0, Φ^0) [13]. In this case the coherence length is larger or comparable with the formation one starting from the photoproduction limit up to $Q^2 \sim 1 \div 2\,\mathrm{GeV}^2$. In charmonium production [21], however, there is a strong inequality $l_f > l_c$ independently of Q^2 and ν. It leads to a different scenario of CT-CL mixing compared to production of light vector mesons as is discussed in Chapter 3.

In exclusive production of vector mesons at high energies besides quark shadowing discussed in Chapters 3 and 4 we included also gluon shadowing (GS) corrections as an important phenomenon at small Bjorken-x_{Bj} [13]. The GS effect also suppresses electroproduction of vector mesons as is discussed in Chapter 5. In terms of the light-cone QCD approach the process of gluon shadowing is related to the inclusion of higher Fock components, $|\bar{q}q\,nG\rangle$, containing gluons

[22]. Such fluctuations might be quite heavy compared to the simplest $|\bar{q}q\rangle$ fluctuation, therefore, they have a shorter lifetime [23] and need a higher energy to be relevant.

It was shown in [24, 21] that for electroproduction of charmonia off nuclei the gluon shadowing starts to be important at c.m. collision energy $\sqrt{s} \geq 30-60\,\mathrm{GeV}$ depending on nuclear target A and photon virtuality Q^2. However, we have found that in incoherent electroproduction of charmonia off nuclei [21] the gluon shadowing contribution to overall suppression is quite small within the kinematic range important for investigation of CT.

1.4. Outline of the habilitation thesis

In the next Chapter 2 we present a short review of the light-cone (LC) dipole approach to diffractive electroproduction of vector mesons in the rest frame of the nucleon target. The key ingredient of this approach is the universal interaction cross section for a colorless quark-antiquark dipole and a nucleon presented in Sect. 2.1. The Sect. 2.2 is devoted to description of the LC wave function for a quark-antiquark fluctuation of the virtual photon. Here we treat the both, free and interacting $\bar{q}q$ pairs of the photon. The model for the LC wave function of a vector meson is described in Sect. 2.3. As a rigorous test of the model we present in Sect. 2.4 calculations of the cross section of elastic electroproduction of ρ and ϕ mesons off a nucleon target. We found a good agreement with available data as function of the collision energy and photon virtuality Q^2.

Chapter 3 is devoted to incoherent production of vector mesons off nuclei. In Sect. 3.1 the absorption is incorporated using the path integral formalism by introducing an imaginary part of the potential into the two-dimensional LC Schrödinger equation for the Green function. Different limiting cases of short and long coherence and formation lengths are considered in Sections 3.1.1, 3.1.2 and 3.1.3, respectively. The exact expression Eq. (3.10) presented in Section 3.1.4 for the cross section of incoherent vector meson production represents the general case with no restrictions on the magnitude of the coherence length. Numerical calculations and comparison with available data are presented in Sect. 3.2.

Coherent production of vector mesons off nuclei leaving the nucleus intact is studied in Chapter 4. The formalism described in Sect. 4.1 is simpler than in the case of incoherent production. The calculations and the comparison with data are presented in Sect. 4.2. Here we show that the effect of CT on the Q^2 dependence of nuclear transparency at $l_c = const$ is weaker than in the case of incoherent production and is difficult to be detected at low energies since the cross section is small.

At large energies the exclusive production of vector mesons is controlled by the small-x_{Bj} physics, and gluon shadowing becomes an important phenomenon. In Chapter 5 gluon shadowing is calculated and included in the calculations for nuclear transparency.

The results of the present habilitation thesis are summarized and discussed in Sect. 6.

2. Short review of the light-cone dipole phenomenology for $\gamma^* N \to V\ N$

In the light-cone dipole approach the amplitude of a diffractive process is treated as elastic scattering of a $\bar{q}q$ fluctuation of the incident particle. The elastic amplitude is given by convolution of the universal flavor independent dipole cross section for the $\bar{q}q$ interaction with a nucleon, $\sigma_{\bar{q}q}$, [5] and the initial and final wave functions. Then for the exclusive photo- or electroproduction of vector mesons $\gamma^* N \to V\ N$ the forward production amplitude can be represented in the quantum-mechanical form

$$\mathcal{M}_{\gamma^* N \to V N}(s, Q^2) = \langle V | \sigma^N_{\bar{q}q}(\vec{\rho}, s) | \gamma^* \rangle = \int\limits_0^1 d\alpha \int d^2 r\ \Psi^*_V(\vec{r}, \alpha)\, \sigma_{\bar{q}q}(\vec{r}, s)\, \Psi_{\gamma^*}(\vec{r}, \alpha, Q^2) \tag{2.1}$$

with the normalization

$$\left.\frac{d\sigma}{dt}\right|_{t=0} = \frac{|\mathcal{M}|^2}{16\,\pi}. \tag{2.2}$$

For calculations of the photoproduction amplitude one needs to know the following ingredients of Eq. (2.1): (i) the dipole cross section $\sigma_{\bar{q}q}(\vec{r}, s)$ which depends on the $\bar{q}q$ transverse separation $\vec{r}$ and the c.m. energy squared s. (ii) The light-cone (LC) wave function of the photon $\Psi_{\gamma^*}(\vec{r}, \alpha, Q^2)$ which also depends on the photon virtuality Q^2 and the relative share α of the photon momentum carried by the quark. (iii) The LC wave function $\Psi_V(\vec{r}, \alpha)$ of the vector meson.

Note that in the LC formalism the photon and meson wave functions contain also higher Fock states $|\bar{q}q\rangle$, $|\bar{q}qG\rangle$, $|\bar{q}q2G\rangle$, etc. The effects of higher Fock states are implicitly incorporated into the energy dependence of the dipole cross section $\sigma_{\bar{q}q}(\vec{r}, s)$ as is given in Eq. (2.1). However, as for nuclear targets, one must explicitly include the higher Fock states because their eikonalization leads to gluon shadowing as will be dicussed in Chapter 5.

2.1. Phenomenological dipole cross section

The dipole cross section $\sigma_{\bar{q}q}(\vec{r}, s)$ represents the interaction of a $\bar{q}q$ dipole of transverse separation $\vec{r}$ with a nucleon [5]. It is a flavor independent universal

function of $\vec{r}$ and energy and allows to describe in a uniform way various high energy processes. It is known to vanish quadratically $\sigma_{\bar{q}q}(r,s) \propto r^2$ as $r \to 0$ due to color screening (CT property) and cannot be predicted reliably because of poorly known higher order pQCD corrections and nonperturbative effects. Detailed discussion about the dipole cross section $\sigma_{\bar{q}q}(\vec{r},s)$ can be found in [13].

There are several popular parameterizations of $\sigma_{\bar{q}q}(\vec{r},s)$. The first group of parametrizations suggested in [25, 26, 27, 28, 29] reflects the fact that at small separations the dipole cross section should be a function of r and $x_{Bj} \sim 1/(r^2\,s)$ to reproduce the Bjorken scaling. It well describes data for deep-inelastic scattering (DIS) at small x_{Bj} and medium and high Q^2. However, at small Q^2 it cannot be correct since it predicts energy independent hadronic cross sections. Besides, x_{Bj} is not any more a proper variable at small Q^2 and should be replaced by energy. For this reason we used in calculations also the parameterization suggested in [30], which is similar to one in [25, 26, 27, 28, 29], but contains an explicit dependence on energy. In this case our approach will be valid down to the limit of real photoproduction. This parametrizatnion has the following form:

$$\sigma_{\bar{q}q}(r,s) \;\; = \;\; \sigma_0(s)\left[1 - e^{-r^2/r_0^2(s)}\right] \; . \tag{2.3}$$

It correctly reproduces the hadronic cross sections for the choice

$$\sigma_0(s) = \sigma_{tot}^{\pi p}(s)\left[1 + \frac{3}{8}\frac{r_0^2(s)}{\langle r_{ch}^2\rangle}\right] \text{ mb} \; , \tag{2.4}$$

$$r_0(s) = 0.88\left(\frac{s}{s_0}\right)^{-0.14} \text{ fm} \; . \tag{2.5}$$

Here $\langle r_{ch}^2\rangle = 0.44\,\text{fm}^2$ is the mean pion charge radius squared; $s_0 = 1000\,\text{GeV}^2$. The cross section $\sigma_{tot}^{\pi p}(s)$ was fitted to data in [31, 32],

$$\sigma_{tot}^{\pi p}(s) = 23.6\,\left(\frac{s}{s_0}\right)^{0.079} + 0.432\,\left(\frac{s}{s_0}\right)^{-0.45} \text{ mb}\,, \tag{2.6}$$

containing the Pomeron and Reggeon parts as was presented and discussed in [13].

The dipole cross section Eqs.(2.3) – (2.6) provides the imaginary part of the elastic amplitude. It is known, however, that the energy dependence of the total cross section generates also a real part [33],

$$\sigma_{\bar{q}q}(r,s) \Rightarrow \left(1 - i\,\frac{\pi}{2}\,\frac{\partial}{\partial \ln(s)}\right)\,\sigma_{\bar{q}q}(r,s)\,. \tag{2.7}$$

The energy dependence of the dipole cross section Eq. (2.3) is rather steep at small r leading to a large real part which should not be neglected. For instance, the photoproduction amplitude of $\gamma N \to J/\Psi N$ rises $\propto s^{0.2}$ and the real-to-imaginary part ratio is over 30%.

Although the form of Eq. (2.3) successfully describes data for DIS at small x only up to $Q^2 \approx 10 \div 20\,\mathrm{GeV}^2$ we prefer this parameterization for study of vector meson electroproduction. The reason is that we want to study CT effects predominantly in the range $Q^2 \leq 20\,\mathrm{GeV}^2$ and in addition the parameterization in Eq. (2.3) describes the transition toward photoproduction limit better than parameterizations presented in [25, 26, 27, 28, 29].

2.2. The $\bar{q}q$ wave function of the photon

The perturbative distribution amplitude ("wave function") of the $\bar{q}q$ Fock component of the photon has the following form for transversely (T) and longitudinally (L) polarized photons [34, 35, 36],

$$\Psi^{T,L}_{\bar{q}q}(\vec{r},\alpha) = \frac{\sqrt{N_C\,\alpha_{em}}}{2\,\pi}\; Z_q\,\bar{\chi}\,\hat{O}^{T,L}\,\chi\,K_0(\epsilon\,r) \tag{2.8}$$

where χ and $\bar{\chi}$ are the spinors of the quark and antiquark, respectively; Z_q is the quark charge; $N_C = 3$ is the number of colors. $K_0(\epsilon r)$ is a modified Bessel function with

$$\epsilon^2 = \alpha\,(1-\alpha)\,Q^2 + m_q^2\;, \tag{2.9}$$

where m_q is the quark mass, and α is the fraction of the LC momentum of the photon carried by the quark. The operators $\widehat{O}^{T,L}$ read,

$$\widehat{O}^T = m_q\;\vec{\sigma}\cdot\vec{e} + i\,(1-2\alpha)\,(\vec{\sigma}\cdot\vec{n})\,(\vec{e}\cdot\vec{\nabla}_r) + (\vec{\sigma}\times\vec{e})\cdot\vec{\nabla}_r\;, \tag{2.10}$$

$$\widehat{O}^L = 2\,Q\,\alpha(1-\alpha)\,(\vec{\sigma}\cdot\vec{n})\;. \tag{2.11}$$

Here $\vec{\nabla}_r$ acts on transverse coordinate $\vec{r}$; $\vec{e}$ is the polarization vector of the photon and $\vec{n}$ is a unit vector parallel to the photon momentum.

In general, the transverse $\bar{q}q$ separation is controlled by the distribution amplitude Eq. (2.8) with the mean value,

$$\langle r\rangle \sim \frac{1}{\epsilon} = \frac{1}{\sqrt{Q^2\,\alpha\,(1-\alpha)+m_q^2}}\,. \tag{2.12}$$

For production of light vector mesons very asymmetric $\bar{q}q$ pairs with α or $(1-\alpha) \lesssim m_q^2/Q^2$ become possible. Consequently, the mean transverse separation $\langle r\rangle \sim 1/m_q$ is huge since one must use current quark masses within pQCD. However, that is not the case of heavy vector meson production due to large quark masses and corresponding nonperturbative interaction effects between heavy Q and $\bar{Q}$ are rather weak. Despite of this fact for completeness we include these nonperturbative interaction effects in all calculations using from [30, 13] the corresponding phenomenology based on the light-cone Green function approach.

The Green function $G_{\bar{q}q}(z_1,\vec{r}_1;z_2,\vec{r}_2)$ describes the propagation of an interacting $\bar{q}q$ pair between points with longitudinal coordinates z_1 and z_2 and with initial

and final separations $\vec{r}_1$ and $\vec{r}_2$. This Green function satisfies the two-dimensional Schrödinger equation,

$$i\frac{d}{dz_2}\,G_{\bar{q}q}(z_1,\vec{r}_1;z_2,\vec{r}_2) = \left[\frac{\epsilon^2-\Delta_{r_2}}{2\,\nu\,\alpha\,(1-\alpha)} + V_{\bar{q}q}(z_2,\vec{r}_2,\alpha)\right] G_{\bar{q}q}(z_1,\vec{r}_1;z_2,\vec{r}_2)\ . \tag{2.13}$$

Here ν is the photon energy. The Laplacian Δ_r acts on the coordinate r.

The imaginary part of the LC potential $V_{\bar{q}q}(z_2,\vec{r}_2,\alpha)$ in (2.13) is responsible for attenuation of the $\bar{q}q$ in the medium, while the real part represents the interaction between the q and $\bar{q}$. This potential is supposed to provide the correct LC wave functions of vector mesons. For the sake of simplicity we use the oscillator form of the potential,

$$\mathrm{Re}\,V_{\bar{q}q}(z_2,\vec{r}_2,\alpha) = \frac{a^4(\alpha)\,\vec{r}_2^{\,2}}{2\,\nu\,\alpha(1-\alpha)}\ , \tag{2.14}$$

which leads to a Gaussian r-dependence of the LC wave function of the meson ground state. The shape of the function $a(\alpha)$ will be discussed below in this section.

In this case the equation (2.13) has an analytical solution, the harmonic oscillator Green function [37],

$$\begin{aligned} G_{\bar{q}q}(z_1,\vec{r}_1;z_2,\vec{r}_2) \ &= \\ &\frac{a^2(\alpha)}{2\,\pi\,i\sin(\omega\,\Delta z)}\exp\left\{\frac{i\,a^2(\alpha)}{\sin(\omega\,\Delta z)}\left[(r_1^2+r_2^2)\cos(\omega\,\Delta z) - 2\,\vec{r}_1\cdot\vec{r}_2\right]\right\} \\ &\times\exp\left[-\frac{i\,\epsilon^2\,\Delta z}{2\,\nu\,\alpha\,(1-\alpha)}\right]\ , \end{aligned} \tag{2.15}$$

where $\Delta z = z_2 - z_1$ and

$$\omega = \frac{a^2(\alpha)}{\nu\ \alpha(1-\alpha)}\ . \tag{2.16}$$

The boundary condition is $G_{\bar{q}q}(z_1,\vec{r}_1;z_2,\vec{r}_2)|_{z_2=z_1} = \delta^2(\vec{r}_1-\vec{r}_2)$.

If we write the transverse part as

$$\bar{\chi}\,\widehat{O}^T\chi = A + \vec{B}\cdot\vec{\nabla}_{r_1}\ , \tag{2.17}$$

then the distribution functions read,

$$\Psi^T_{\bar{q}q}(\vec{r},\alpha) = Z_q\sqrt{\alpha_{em}}\ \left[A\,\Phi_0(\epsilon,r,\lambda) + \vec{B}\,\vec{\Phi}_1(\epsilon,r,\lambda)\right]\ , \tag{2.18}$$

$$\Psi^L_{\bar{q}q}(\vec{r},\alpha) = 2\,Z_q\sqrt{\alpha_{em}}\,Q\,\alpha(1-\alpha)\,\bar{\chi}\ \vec{\sigma}\cdot\vec{n}\ \chi\,\Phi_0(\epsilon,r,\lambda)\ , \tag{2.19}$$

where

$$\lambda = \frac{2\,a^2(\alpha)}{\epsilon^2}\ . \tag{2.20}$$

The functions $\Phi_{0,1}$ in Eqs. (2.18) and (2.19) are defined as

$$\Phi_0(\epsilon,r,\lambda) = \frac{1}{4\pi}\int\limits_0^\infty dt\,\frac{\lambda}{\mathrm{sh}(\lambda t)}\exp\left[-\frac{\lambda\epsilon^2 r^2}{4}\,\mathrm{cth}(\lambda t) - t\right]\ , \tag{2.21}$$

$$\vec{\Phi}_1(\epsilon, r, \lambda) = \frac{\epsilon^2 \vec{r}}{8\pi} \int_0^\infty dt \, \left[\frac{\lambda}{\mathrm{sh}(\lambda t)}\right]^2 \exp\left[-\frac{\lambda \epsilon^2 r^2}{4} \mathrm{cth}(\lambda t) - t\right] . \tag{2.22}$$

Note that the $\bar{q}-q$ interaction enters Eqs. (2.18) and (2.19) via the parameter λ defined in (2.20). In the limit of vanishing interaction $\lambda \to 0$ (i.e. $Q^2 \to \infty$, α is fixed, $\alpha \neq 0$ or 1) Eqs. (2.18) - (2.19) produce the perturbative expressions of Eq. (2.8).

With the choice $a^2(\alpha) \propto \alpha(1-\alpha)$ the end-point behavior of the mean square interquark separation $\langle r^2 \rangle \propto 1/\alpha(1-\alpha)$ contradicts the idea of confinement. Following [30] we fix this problem via a simple modification of the LC potential,

$$a^2(\alpha) = a_0^2 + 4a_1^2 \, \alpha(1-\alpha) . \tag{2.23}$$

The parameters a_0 and a_1 were adjusted in [30] to data on total photoabsorption cross section [38, 39], diffractive photon dissociation and shadowing in nuclear photoabsorption reaction.

2.3. The meson wave function

The last ingredient in elastic production amplitude (2.1) is the vector meson wave function. We use a popular prescription [40] applying the Lorentz boost to the rest frame wave function assumed to be Gaussian which leads to radial parts of transversely (T) and longitudinally (L) polarized mesons in the form,

$$\Phi_V^{T,L}(\vec{r}, \alpha) = C^{T,L} \, \alpha(1-\alpha) \, f(\alpha) \exp\left[-\frac{\alpha(1-\alpha)\,\vec{r}^2}{2\,R^2}\right] \tag{2.24}$$

with a normalization defined below, and

$$f(\alpha) = \exp\left[-\frac{m_q^2 \, R^2}{2\,\alpha(1-\alpha)}\right] . \tag{2.25}$$

This procedure is ill motivated since the $\bar{q}q$ are not classical particles. Nevertheless, a detailed analysis of this problem [41] leads to the same form as Eq. (2.24) used in calculations with the parameters from [42].

We assume that the distribution amplitude of $\bar{q}q$ fluctuations for the vector meson and for the photon have a similar structure [42]. Then in analogy to Eqs. (2.18) – (2.19),

$$\Psi_V^T(\vec{r}, \alpha) = (A + \vec{B} \cdot \vec{\nabla}) \, \Phi_V^T(r, \alpha) ; \tag{2.26}$$

$$\Psi_V^L(\vec{r}, \alpha) = 2\, m_V \, \alpha(1-\alpha) \, (\bar{\chi} \, \vec{\sigma} \cdot \vec{n} \, \chi) \, \Phi_V^L(r, \alpha) . \tag{2.27}$$

Correspondingly, the normalization conditions for the transverse and longitudinal vector meson wave functions read,

$$N_C \int d^2r \int d\alpha \left\{ m_q^2 \left|\Phi_V^T(\vec{r}, \alpha)\right|^2 + \left[\alpha^2 + (1-\alpha)^2\right] \left|\partial_r \Phi_V^T(\vec{r}, \alpha)\right|^2 \right\} = 1 \tag{2.28}$$

$$4\, N_C \int d^2r \int d\alpha \, \alpha^2 \, (1-\alpha)^2 \, m_V^2 \left|\Phi_V^L(\vec{r}, \alpha)\right|^2 = 1 . \tag{2.29}$$

2.4. Model predictions vs. data

As the first test of the LC dipole approach we compared model predictions with data for for nucleon target. The forward production amplitude $\gamma^* N \to V N$ for transverse and longitudinal photons and vector mesons is calculated using the nonperturbative photon Eqs. (2.18), (2.19) and vector meson Eqs. (2.26), (2.27) wave functions. It has the following form [13, 21],

$$\mathcal{M}^T_{\gamma^* N\to VN}(s,Q^2)\Big|_{t=0} = N_C\, Z_q\, \sqrt{\alpha_{em}} \int d^2r\, \sigma_{\bar{q}q}(\vec{r},s) \int\limits_0^1 d\alpha \Big\{ m_q^2\, \Phi_0(\epsilon,\vec{r},\lambda) \Psi_V^T(\vec{r},\alpha) + \left[\alpha^2+(1-\alpha)^2\right] \vec{\Phi}_1(\epsilon,\vec{r},\lambda)\cdot\vec{\nabla}_r\, \Psi_V^T(\vec{r},\alpha)\Big\}\,; \tag{2.30}$$

$$\mathcal{M}^L_{\gamma^* N\to V\,N}(s,Q^2)\Big|_{t=0} = 4\, N_C\, Z_q\, \sqrt{\alpha_{em}}\, m_V\, Q \int d^2r\, \sigma_{\bar{q}q}(\vec{r},s) \times \int\limits_0^1 d\alpha\, \alpha^2\,(1-\alpha)^2\, \Phi_0(\epsilon,\vec{r},\lambda) \Psi_V^L(\vec{r},\alpha)\ . \tag{2.31}$$

These amplitudes are normalized as $|\mathcal{M}^{T,L}|^2 = 16\pi\, d\sigma_N^{T,L}/dt\Big|_{t=0}$. We included the real part of the amplitude according to the prescription described in Sect. 2.1. We calculated the cross sections $\sigma = \sigma^T + \epsilon\,\sigma^L$ assuming that the photon polarization is $\epsilon = 1$.

Now we can check the absolute value of the predicted cross section by comparing with data for elastic electroproduction $\gamma^* p \to V p$ for ρ and ϕ mesons [13]. Unfortunately, data are available only for the cross section integrated over t,

$$\sigma^{T,L}(\gamma^* N \to VN) = \frac{|\mathcal{M}^{T,L}|^2}{16\pi\, B_{\gamma^* N}}\ , \tag{2.32}$$

where $B_{\gamma^* N}$ is the t-slope parameter of the differential cross section fixed from available data.

Our predictions are plotted in Fig. 2.1 together with the data on the Q^2 dependence of the cross section from NMC, H1 and ZEUS [43, 44, 45, 46]).

We used the Q^2 dependent slope of the differential cross section $d\sigma(\gamma^* N \to VN)/dt \propto \exp\Big[B^V_{\gamma^* N}(Q^2)\, t\Big]$ parametrized as [47],

$$B_{\gamma^* N}(s,Q^2) = \beta_0^V(s) + \frac{\beta_1^V(s)}{Q^2+m_V^2} - \frac{1}{2}\,\ln\left(\frac{Q^2+m_V^2}{m_V^2}\right)\ . \tag{2.33}$$

We performed a fit [13] to the data [43, 48] from fixed target experiments for the Q^2 dependent slope in ρ production obtaining the parameters for $W \approx 10-15$ GeV, $\beta_0^\rho = (6.2 \pm 0.2)$ GeV^{-2}, $\beta_1^\rho = 1.5 \pm 0.2$. Using data from HERA [44, 45,

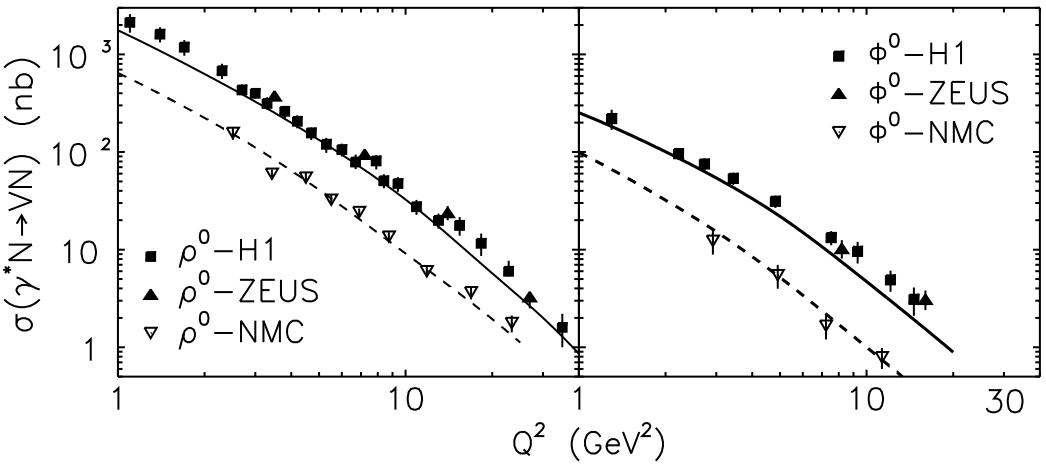

Figure 2.1.: *Q^2- dependence of the cross section for the reactions $\gamma^* p \to \rho p$ (left) and $\gamma^* p \to \phi p$ (right). The dashed and solid curves are compared with data at $W = 15$ GeV [43] and at 75 GeV ([44, 45] for ρ and [46] for ϕ), respectively. The figure is taken from [13].*

49, 50, 51, 52, 53] for ρ production at $W = 75$ GeV we get, $\beta_0^\rho = (7.1 \pm 0.1)$ GeV^{-2}, $\beta_1^\rho = 2.0 \pm 0.1$.

Repeating the same analysis for ϕ production we get at $W \approx 10 - 15$ GeV from data [43, 54], $\beta_0^\phi = (5.9 \pm 0.1)$ GeV^{-2}, $\beta_1^\phi = 0.5 \pm 0.1$. Data from HERA [55, 46] give, $\beta_0^\phi = (6.7 \pm 0.2)$ GeV^{-2}, $\beta_1^\phi = 1.0 \pm 0.1$. For calculations shown in Fig. 2.1 we use the central values of these parameters.

As the second test of our approach is a description of the low Q^2 region as well since the effects of the nonperturbative interaction between the q and $\bar{q}$ in the photon fluctuation are naturally incorporated in the Green function formalism. Comparison of the model with data [56, 57, 50, 51, 58] for the energy dependence of the cross section of real ρ photoproduction is presented in Fig. 2.2 [13]. Here we used the energy dependent slope parameter, $B_{\gamma N}^\rho = B_0^\rho + 2\alpha' \ln(s/s_0)$ with $\alpha' = 0.25$ GeV^{-2} and $B_0^\rho = 7.6$ GeV^{-2}, $s_0 = 20$ GeV^2 fitted to data [59, 56, 49, 51, 52]. The Pomeron part of the dipole cross section depicted by the dashed curve in Fig. 2.2 cannot explain the data at low energies, $W \lesssim 15$ GeV, while the addition of the Regge term (solid curve) leads to a good agreement for all energies.

Notice that the normalization of the cross section and its energy and Q^2 dependence are remarkably well reproduced in Figs. 2.1 – 2.2.

Variety of further predictions for the real and virtual photoproduction of different vector mesons and also their $2S$ radial excitations can be found in refs. [60, 61, 42, 62, 21, 13]

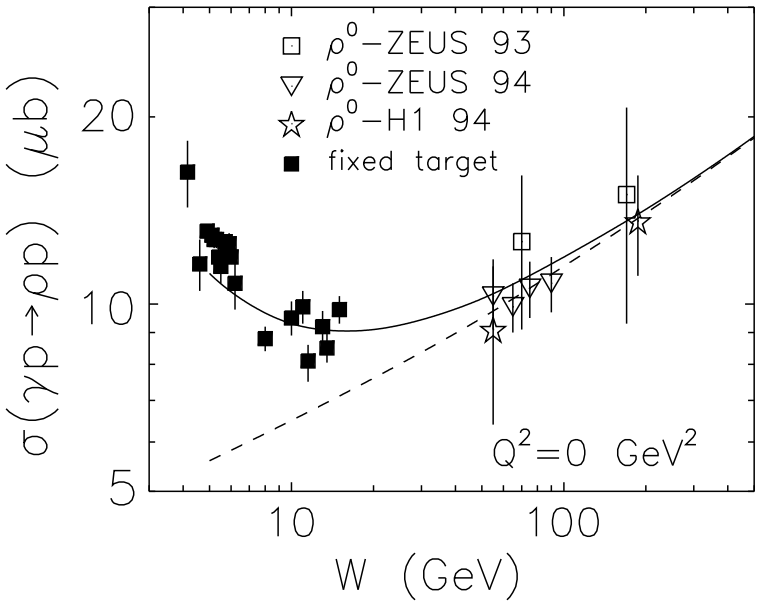

Figure 2.2.: *Energy dependence of the real photoproduction cross section on a nucleon, $\gamma\, p \to \rho^0\, p$. Our results (solid curve) are compared with data from the fixed target [56, 57], and collider HERA H1 [50] and ZEUS [51, 58] experiments. The dashed curve contains only the gluonic exchange in the t-channel. The figure is taken from ref. [13].*

2.5. Summary of the attached papers

2.5.1. Scanning the BFKL pomeron in elastic production of vector mesons at HERA

Physics Letters B **341** (1994) 228,
more than 100 citations
listed as A.1 on page 41.

In this article we demonstrated for the first time that the elastic production of vector mesons $\gamma^* N \to V N$ is the pomeron-exchange dominated diffractive reaction with much potential of probing the BFKL pomeron. We showed that the BFKL pomeron can be described in terms of the dipole cross section which is a solution of the generalized BFKL equation. For determination of the intercept of the BFKL pomeron is unavoidable to investigate the diffractive electroproduction of ρ^0 and J/Ψ mesons at large $Q^2 \sim (100 - 200)\mathrm{GeV}^2$ and/or the quasireal photoproduction of the Υ. We discussed for the first time that the energy and Q^2 dependence of elastic production of vector mesons at HERA allow scanning the dipole cross section as a function of dipole size r.

2.5.2. Color dipole systematics of diffractive photo- and electroproduction of vector mesons

Physics Letters B**374** (1996) 199
more than 50 citations
listed as A.2 on page 51.

In this paper we present the first evaluation of color dipole cross section from experimental data on diffractive photo- and electroproduction of vector mesons. The dipole-size and energy dependence of the found dipole cross section is consistent with expectations from the BFKL dynamics.

2.5.3. Color dipole phenomenology of diffractive electroproduction of light vector mesons at HERA

Zeitschrift fr Physik C**75** (1997) 71
more than 100 citations
listed as A.3 on page 57.

Here we developed for the first time the color dipole phenomenology of diffractive photo- and electroproduction $\gamma^* N \to V(V') N$ of light vector mesons ($V(1S) = \phi^0, \omega^0, \rho^0$) and their radial excitations ($V'(2S) = \phi', \omega', \rho'$). We have shown that the nodal structure of the radial wave function for the $2S$ states in conjunction with the energy dependence of the color dipole cross section lead to a strikingly different Q^2 and ν dependence of diffractive production of the $V(1S)$ and $V'(2S)$ vector mesons. We also discussed the restoration of flavor symmetry and universality properties in production of different vector mesons as a function of $Q^2+m_V^2$. We have found a good agreement of the color dipole model predictions for the ρ^0 and ϕ^0 production with available experimental data from the EMC, NMC, ZEUS and H1 collaborations.

2.5.4. Anomalous t-dependence in diffractive electroproduction of 2S radially excited light vector mesons at HERA

European Physical Journal C**18** (2001) 711
3 citations
listed as A.4 on page 75.

Within the color dipole gBFKL dynamics applied to the diffraction slope, we predict an anomalous t dependence of the differential cross section as a function of energy and Q^2 for production of radially excited $V'(2S)$ light vector mesons in contradiction with a well known standard monotonous t- behaviour for $V(1S)$ mesons. The origin of this phenomenon is based on the interplay of the nodal structure of $V'(2S)$ radial wave function with the energy- and dipole size dependence of the color dipole cross section and of the diffraction slope. We present

how a different position of the node in $V'(2S)$ wave function leads to a different form of anomalous t- behavior of the differential cross section and discuss a possibility how to determine this position from the low energy and HERA data.

3. Incoherent production of vector mesons off nuclei

Here and in the next Chapter 4 we present shortly the LC color dipole approach based on the rigorous Green function formalism and its corresponding generalization for nuclear targets developed in [13, 21] as a powerfull tool for description of incoherent and coherent electroproduction of vector mesons off nuclei.

The diffractive incoherent (quasielastic) production of vector mesons off nuclei, $\gamma^* A \to V X$, is associated with a break up of the nucleus, but without production of new particles. In another words, one sums over all final states of the target nucleus except those which contain particle (pion) creation. The observable usually studied experimentally is nuclear transparency defined as

$$Tr_A^{inc} = \frac{\sigma^{inc}_{\gamma^* A\to VX}}{A\,\sigma_{\gamma^* N\to VN}}\ . \tag{3.1}$$

The t-slope of the differential quasielastic cross section is the same as on a nucleon target. Therefore, instead of integrated cross sections one can also use nuclear transparency expressed in terms of the forward differential cross sections Eq. (2.2),

$$Tr_A^{inc} = \frac{1}{A}\left|\frac{\mathcal{M}_{\gamma^* A\to VX}(s,Q^2)}{\mathcal{M}_{\gamma^* N\to VN}(s,Q^2)}\right|^2\ . \tag{3.2}$$

3.1. The LC Green function approach

In the LC Green function approach [13] the physical photon $|\gamma^*\rangle$ can be decomposed into different Fock states, namely, the bare photon $|\gamma^*\rangle_0$, $|\bar{q}q\rangle$, $|\bar{q}qG\rangle$, etc. As we mentioned above the higher Fock states containing gluons describe the energy dependence of the photoproduction reaction on a nucleon. Besides, those Fock components also lead to gluon shadowing as far as nuclear effects are concerned. However, these fluctuations are heavier and have a shorter coherence time (lifetime) than the lowest $|\bar{q}q\rangle$ state. Consequently, gluon shadowing will be dominated at high energies. Detailed description and calculation of the gluon shadowing for the case of vector meson production off nuclei is presented in [13, 24] and will be discussed below in Chapter 5.

Propagation of an interacting $\bar{q}q$ pair in a nuclear medium is described by the Green function satisfying the evolution Eq. (2.13). However, the potential in this case acquires an imaginary part which represents absorption in the medium,

$$ImV_{\bar{q}q}(z_2,\vec{r},\alpha) = -\frac{\sigma_{\bar{q}q}(\vec{r},s)}{2}\,\rho_A(b,z_2)\,. \tag{3.3}$$

The evolution equation (2.13) with the potential $V_{\bar{q}q}(z_2, \vec{r}_2, \alpha)$ containing this imaginary part was used in [63, 23], and nuclear shadowing in deep-inelastic scattering was calculated in good agreement with data.

The analytical solution of Eq. (2.15) is only known for the harmonic oscillator potential $V(r) \propto r^2$. This corresponds to a quadratic approximation of the dipole cross section,

$$\sigma_{\bar{q}q}(r, s) = C(s)\, r^2 \ , \tag{3.4}$$

which allows to obtain the Green function in an analytical form. The energy dependent factor $C(s)$ was adjusted in [13].

Note, that in the limit $l_c \gg R_A$ (the so called "frozen" approximation) the Green function takes the simple form,

$$G_{\bar{q}q}(z_1, \vec{r}_1; z_2, \vec{r}_2) \Rightarrow \delta(\vec{r}_1 - \vec{r}_2)\, \exp\left[-\frac{1}{2}\, \sigma_{\bar{q}q}(r_1) \int\limits_{z_1}^{z_2} dz\, \rho_A(b, z)\right] \ . \tag{3.5}$$

With the potential Eqs. (3.3) – (3.4) the solution of Eq. (2.13) has the same form as Eq. (2.15), except that one should replace $\omega \Rightarrow \Omega$, where

$$\Omega = \frac{\sqrt{a^4(\alpha) - i\, \rho_A(b, z)\, \nu\, \alpha\, (1 - \alpha)\, C(s)}}{\nu\ \alpha(1 - \alpha)} \ . \tag{3.6}$$

Depending on the value of l_c one can distinguish several different regimes in incoherent production of vector mesons:

3.1.1. Short coherence lenght in light vector meson production

The CL is much shorter than the mean nucleon spacing in a nucleus ($l_c \to 0$). In this case $G(z_2, \vec{r}_2; z_1, \vec{r}_1) \to \delta(z_2 - z_1)$ since strong oscillations suppress propagation of the $\bar{q}q$ over longer distances. In the case according to Eq. (1.2) the formation time of the meson wave function is very short as well. Apparently, for light vector mesons $l_f \sim l_c$, so both must be short. In this case nuclear transparency is given by the simple formula Eq. (1.4) corresponding to the Glauber approximation

3.1.2. Short coherence lenght in heavy vector meson production

In the intermediate case $l_c \to 0$, but $l_f \sim R_A$, which can only be realized for heavy flavor quarkonia, the formation of the meson wave function is described by the Green function and the numerator of the nuclear transparency ratio Eq. (3.2) has the form [11],

$$\left|\mathcal{M}_{\gamma^* A \to VX}(s, Q^2)\right|^2_{l_c \to 0;\, l_f \sim R_A} = \int d^2b \int_{-\infty}^{\infty} dz\, \rho_A(b, z) \left|F_1(b, z)\right|^2 \ , \tag{3.7}$$

where

$$F_1(b,z) = \int_0^1 d\alpha \int d^2r_1\, d^2r_2\, \Psi_V^*(\vec{r}_2,\alpha)\, G(z',\vec{r}_2;z,\vec{r}_1)\, \sigma_{\bar{q}q}(r_1,s)\, \Psi_{\gamma^*}(\vec{r}_1,\alpha)\Big|_{z'\to\infty} \tag{3.8}$$

This expression is illustrated in Fig. 3.1a. The photon creates at the point z a

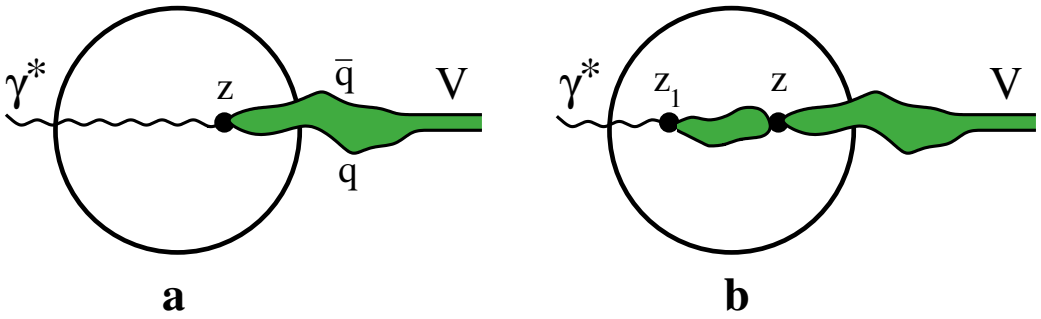

Figure 3.1.: *The incident virtual photon produces incoherently at the point z (quasielastic scattering) the colorless $\bar{q}q$ pair which then evolves propagating through the nucleus and forms the V-meson wave function (**a**). Alternatively, the photon can first produce diffractively and coherently at the point z_1 the colorless $\bar{q}q$ which then experiences quasielastic scattering at the point z (**b**). Propagation of the $\bar{q}q$ pair is described by the Green function (shaded areas). The figure is taken from [13].*

colorless $\bar{q}q$ pair with transverse separation $\vec{r}_1$. The quark and antiquark then propagate through the nucleus along different trajectories and end up with a separation $\vec{r}_2$. The contributions from different paths are summed up giving rise to the Green function $G(z',\vec{r}_2;z,\vec{r}_1)$ which is convoluted in (3.7) with the wave functions of γ^* and V. The corresponding path integral technique was suggested in [11] and developred in [13].

3.1.3. Long coherence lenght

In this case $l_c \gg R_A$ and $G(z_2,\vec{r}_2;z_1,\vec{r}_1) \to \delta(\vec{r}_2-\vec{r}_1)$, i.e. all fluctuations of the transverse $\bar{q}q$ separation are "frozen" by Lorentz time dilation. Then, the numerator on the r.h.s. of Eq. (3.2) takes the form [11],

$$\left|\mathcal{M}_{\gamma^*A\to VX}(s,Q^2)\right|^2_{l_c\gg R_A} = \int d^2b\, T_A(b) \left| \int d^2r \int_0^1 d\alpha \right.$$
$$\left. \times\, \Psi_V^*(\vec{r},\alpha)\, \sigma_{\bar{q}q}(r,s)\, \exp\left[-\frac{1}{2}\sigma_{\bar{q}q}(r,s)\, T_A(b)\right] \Psi_{\gamma^*}(\vec{r},\alpha,Q^2)\right|^2 . \tag{3.9}$$

In this case the $\bar{q}q$ attenuates with a constant absorption cross section like in the Glauber model, except that the whole exponential is averaged rather than just the cross section in the exponent. The difference between the results of the two prescriptions are well known as inelastic corrections of Gribov [5].

3.1.4. General formula for incoherent electroproduction amplitude

This new result has been developed and presented for the first time in [13]. It represents the general case with no restrictions for either l_c or l_f and can be applied to electroproduction of vector mesons beyond the limits discussed above in Sections 3.1.1, 3.1.2 and 3.1.3.

Within the VDM the corresponding Glauber model expression interpolating between the limiting cases of low [Sections 3.1.1, 3.1.2] and high [Section 3.1.3] energies was derived for the first time in [20]. We generalize that formalism to the LC dipole approach, and the incoherent photoproduction amplitude is represented as a sum of two terms [64] illustrated in Fig. 3.1b,

$$\left| \mathcal{M}_{\gamma^* A\to VX}(s,Q^2)\right|^2 = \int d^2b \int\limits_{-\infty}^{\infty} dz\, \rho_A(b,z) \left|F_1(b,z) - F_2(b,z)\right|^2 . \qquad (3.10)$$

The first term $F_1(b,z)$ introduced above in Eq. (3.8) is represented by Fig. 3.1a. Alone it would correspond to the short l_c limit as was presented in Section 3.1.2. The second term $F_2(b,z)$ in (3.10) corresponds to the situation illustrated in Fig. 3.1b when incident photon produces a $\bar{q}q$ pair diffractively and coherently at the point z_1 prior to incoherent quasielastic scattering at point z. The LC Green functions describe the evolution of the $\bar{q}q$ over the distance from z_1 to z and further on, up to the formation of the meson wave function. Correspondingly, this term has the form,

$$F_2(b,z) = \frac{1}{2} \int\limits_{-\infty}^{z} dz_1\, \rho_A(b,z_1) \int\limits_0^1 d\alpha \int d^2r_1\, d^2r_2\, d^2r\, \Psi_V^*(\vec{r}_2,\alpha)$$
$$\times G(z'\to\infty,\vec{r}_2;z,\vec{r})\, \sigma_{\bar{q}q}(\vec{r},s)\, G(z,\vec{r};z_1,\vec{r}_1)\, \sigma_{\bar{q}q}(\vec{r}_1,s)\, \Psi_{\gamma^*}(\vec{r}_1,\alpha)\,. \qquad (3.11)$$

Note that Eq. (3.10) correctly reproduces the limits presented in Sections 3.1.1, 3.1.2 and 3.1.3.

3.2. Color transparency vs. coherence length effects

In this section we will discuss how to discriminate between color transparency and coherence length effects. Exclusive incoherent electroproduction of vector mesons off nuclei was suggested already in [65] as a sensitive way to detect CT. Increasing

the photon virtuality Q^2 one squeezes the produced $\bar{q}q$ wave packet. The smaller is the transverse size of colorless system propagating through the nucleus the weaker is its attenuation. Here we assume that the energy is sufficiently high ($l_f \gg R_A$) and the fluctuations of the $\bar{q}q$ separation are frozen by Lorentz time dilation. Thus, a rise of nuclear transparency $Tr_A^{inc}(Q^2)$ with Q^2 should signal CT effects. Indeed, such a rise was observed in the E665 experiment at Fermilab for exclusive production of ρ^0 mesons off nuclei by a muon beam. This has been claimed in [66] to be a manifestation of CT.

However, we should check whether the expected signal for CT is mixed with the effect of coherence length [67, 20]. Indeed, if the coherence length varies from long to short compared to the nuclear size the nuclear transparency rises because the length of the path in nuclear matter becomes shorter and the vector meson (or $\bar{q}q$) attenuates less. This happens when Q^2 increases at fixed ν. One should carefully disentangle these two phenomena.

3.2.1. Long coherence length

It has been checked in [67] that the coherence length in the kinematic range corresponding to E665 experiment is sufficiently long allowing to use the "frozen" approximation, except of the highest values of $Q^2 \gtrsim 5$ GeV^2. We calculated nuclear transparency, Tr_A^{inc} for ρ^0 production using the exact Eq. (3.10) and the simplified "frozen" approximation Eqs. (3.5) – (3.9). The results are depicted in Fig. 3.2 by solid and dashed curves respectively.

One can see that fluctuations of the size of the $\bar{q}q$ pair become important only at high Q^2 causing a separation of the solid and dashed curves. At smaller Q^2 the observed variation of $Tr_A^{inc}(Q^2)$ is a net manifestation of CT. The agreement with our model is surprisingly good for calcium, while we underestimate the nuclear transparency at small Q^2 for lead. This may be a manifestation of large Coulomb corrections as found in [68], which are of the order $\alpha_{em}\, Z \approx 0.6$ for lead.

3.2.2. Medium long coherence length

At lower energies corresponding to HERMES experiment at HERA and at JLab one should carefully discriminate between the effects of CT and CL [67, 20]. A simple prescription [12] to eliminate the effect of CL from the data on the Q^2 dependence of nuclear transparency is to bin the data in a way which keeps $l_c = const$. It means that one should vary simultaneously ν and Q^2 maintaining the CL Eq. (1.3) constant,

$$\nu = \frac{1}{2}\, l_c\, (Q^2 + m_V^2)\ . \tag{3.12}$$

In this case the Glauber model predicts a Q^2 independent nuclear transparency, and any rise with Q^2 would signal CT [12].

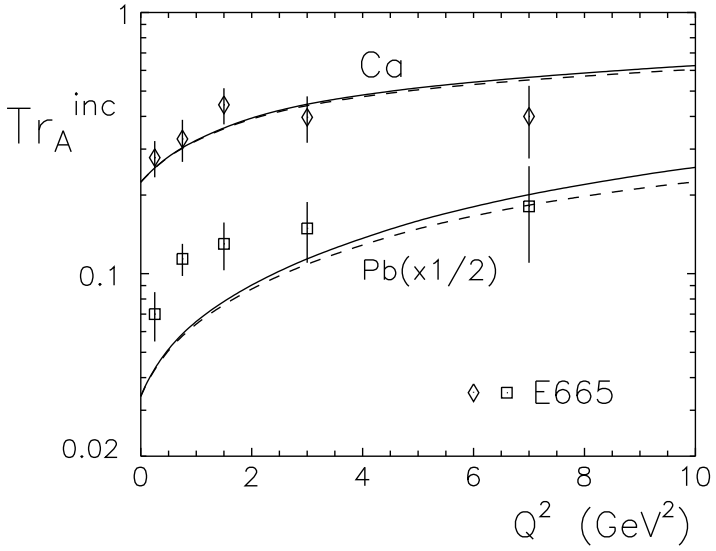

Figure 3.2.: Q^2- *dependence of nuclear transparency for lead and calcium* Tr_{Pb} *and* Tr_{Ca}*. The experimental points are from the E665 experiment [66]. Both the curves and data for lead are rescaled by the factor* 1/2*. Solid and dashed curves show our results using the LC Green function approach Eq. (3.10) and the "frozen" approximation Eq. (3.9) respectively. The figure is taken from [13].*

The LC Green function technique incorporates both the effects of coherence and formation. We performed calculations of $Tr_A^{inc}(Q^2)$ at fixed l_c starting from different minimal values of ν, which correspond to real photoproduction in Eq. (3.12),

$$\nu_{min} = \frac{1}{2}\, l_c\, m_V^2 \ . \tag{3.13}$$

The results for incoherent production of ρ and ϕ at $\nu_{min} = 0.9,\ 2,\ 5$ and 10 GeV ($l_c = 0.6 - 6.75$ fm) are presented in Fig. 3.3 for nitrogen, krypton and lead.

Variety of another predictions for the nuclear transparency in incoherent production of different vector mesons and their $2S$ radial excitations can be found in [69, 65, 70, 20, 13, 21, 71, 72]

3.3. Summary of the attached papers

3.3.1. Anomalous A-dependence of diffractive leptoproduction of the radial excitation $\rho'(2S)$

Physics Letters B**339** (1994) 194
15 citations
listed as A.5 on page 83

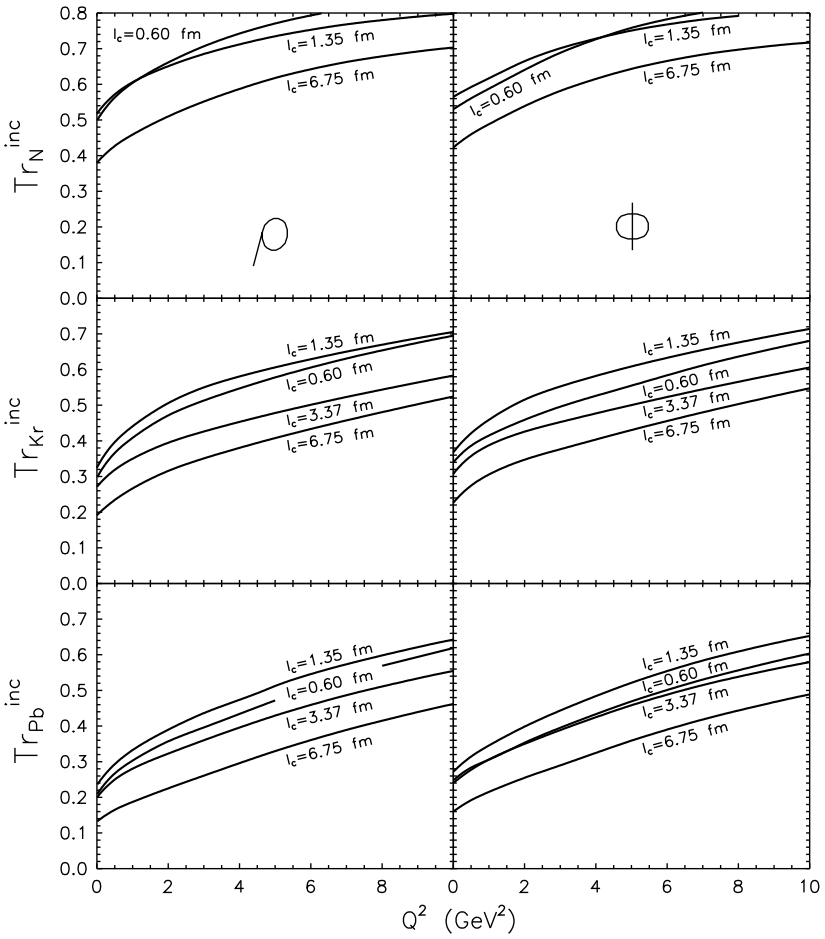

Figure 3.3.: *Q^2 dependence of the nuclear transparency Tr_A^{inc} for exclusive electroproduction of ρ (left) and ϕ (right) mesons on nuclear targets ^{14}N, ^{84}Kr and ^{207}Pb (from top to bottom). The CL is fixed at l_c = 0.60, 1.35, 3.37 and 6.75 fm. The figure is taken from [13].*

In this article we predicted a strikingly different A and Q^2 dependence of quasielastic leptoproduction of the $\rho^0(1S)$-meson and its radial excitation $\rho'(2S)$ on nuclei. Whereas for the ρ^0 production nuclear transparency T_A decreases monotonically with A, for the ρ' nuclear transparency T_A can have the counterintuitive nonmonotonic A-dependence, having the minimum for light nuclei, and increasing with A for medium and heavy nuclei. Strong enhancement of the ρ'/ρ^0 cross section ratio makes nuclear targets the ρ'-factory. The origin of the anomalous A-dependence is in the interplay of color transparency effects with the nodal structure of the ρ' wave function. The predicted effects take place at moderate $Q^2 \lesssim (2-3)\mathrm{GeV}^2$, which can be explored in high statistics experiments at CEBAF.

3.3.2. Incoherent production of charmonia off nuclei as a good tool for study of color transparency

Physical Review C**66** (2002) 045204
5 citations
listed as A.6 on page 91

This article si devoted to study of electroproduction of charmonia off nuclei within the light-cone QCD formalism which incorporates color transparency (CT), coherence length (CL) effects and gluon shadowing. We found a strong onset of CT effects in the range of $Q^2 \leq 20\,\mathrm{GeV}^2$ in contrast to production of light vector mesons (ρ^0, Φ^0) when at small and medium energies CT and the onset of CL effects are not easily separated. They are stronger at low than at high energies and can be easily identified by the planned future experiments. Our parameter-free model calculations explained well the NMC data for the Sn/C ratio of nuclear transparencies as function of the photon energy. We provided for the first time predictions for incoherent and coherent production of charmonia for future measurements.

4. Coherent production of vector mesons off nuclei

If electroproduction of a vector meson leaves the target intact the process is usually called coherent or elastic. The mesons produced at different longitudinal coordinates and impact parameters add up coherently. This fact considerably simplifies the expressions for the cross sections compared to the case of incoherent production presented in Chapter 3.

4.1. The formalism

Within the LC dipole formalism the integrated cross section has the form,

$$\sigma_A^{coh} \equiv \sigma^{coh}_{\gamma^* A\to VA} = \int d^2q \left| \int d^2b\, e^{i\vec{q}\cdot\vec{b}}\, \mathcal{M}^{coh}_{\gamma^* A\to VA}(b) \right|^2 = \int d^2\, b\, |\mathcal{M}^{coh}_{\gamma^* A\to VA}(b)\,|^2 \ , \tag{4.1}$$

where

$$\mathcal{M}^{coh}_{\gamma^* A\to VA}(b) = \int\limits_{-\infty}^{\infty} dz\, \rho_A(b,z)\, F_1(b,z) \ , \tag{4.2}$$

with the function $F_1(b,z)$ defined in (3.8).

One should not use Eq. (3.2) for nuclear transparency any more since the t-slopes of the differential cross sections for nucleon and nuclear targets are different and do not cancel in the ratio. Therefore, the nuclear transparency also includes the slope parameter $B_{\gamma^* N}$ for the process $\gamma^* N \to V N$,

$$Tr_A^{coh} = \frac{\sigma_A^{coh}}{A\,\sigma_N} = \frac{16\,\pi\, B_{\gamma^* N}\,\sigma_A^{coh}}{A\,|\mathcal{M}_{\gamma^* N\to VN}(s,Q^2)\,|^2} \tag{4.3}$$

One can also define a t-dependent transparency for coherent electroproduction of vector mesons,

$$Tr_A^{coh}(t) = \frac{d\sigma_A^{coh}/dt}{A^2\, d\sigma_N/dt|_{t=0}} \ , \tag{4.4}$$

where the differential cross section for coherent production $\gamma^* A \to V A$ reads

$$\frac{d\sigma_A^{coh}}{dt} = \frac{1}{16\,\pi} \left| \int d^2b\, e^{i\vec{b}\cdot\vec{q}} \int\limits_{-\infty}^{\infty} dz\, \rho_A(b,z)\, F_1(b,z) \right|^2 \tag{4.5}$$

with $F_1(b,z)$ defined in (3.8). This expression is simplified in the limit of long coherence time ($t=-q^2$),

$$\frac{d\sigma_A^{coh}}{dt}\Big|_{l_c\gg R_A} = \frac{1}{4\,\pi}\left|\int d^2b\, e^{i\vec{b}\cdot\vec{q}}\int d^2r\left\{1\;-\;\exp\left[-\,\frac{1}{2}\,\sigma_{\bar{q}q}(\vec{r},s)\,T(b)\right]\right\}\right. \times \left.\int\limits_0^1 d\alpha\,\Psi_V^*(\vec{r},\alpha)\,\Psi_{\gamma^*}(\vec{r},\alpha)\right|^2 , \tag{4.6}$$

a form which resembles its VDM analogue [14].

4.2. Predictions vs. data

Using Eq. (4.3) we can also calculate the normalized ratio of coherent cross sections on two nuclei $R_{coh}(A_1/A_2)=Tr_{A_1}^{coh}/Tr_{A_2}^{coh}$. The results of calculations for $R_{coh}(Pb/C)$ and $R_{coh}(Ca/C)$ are depicted by solid curves in Fig. 4.1 and compared with data from the E665 experiment [66] shown by squares and triangles, respectively. The calculations of Tr_A^{coh} were performed at mean photon energy

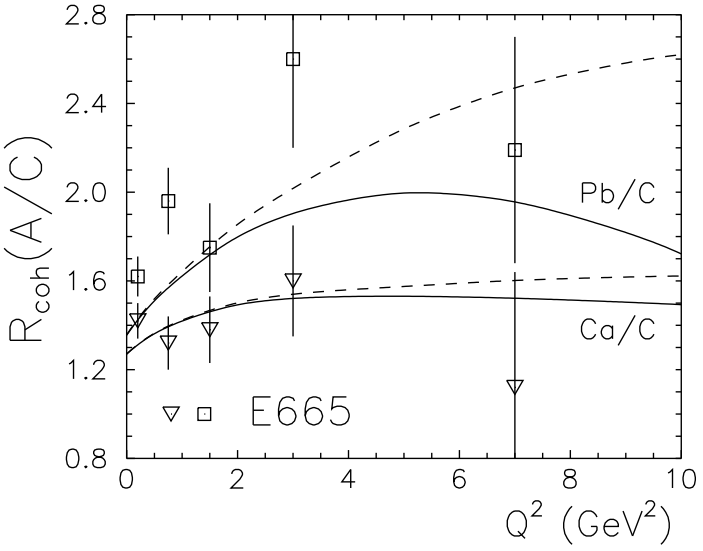

Figure 4.1.: *Q^2- dependence of the total cross section ratio $R_{coh}(A/C)=12\sigma_A^{coh}/A\sigma_C^{coh}$ for the coherent process $\gamma^*A\to\rho^0A$. Experimental points are from E665 [66] for Pb/C (squares) and Ca/C (triangles). Solid curves include the variation of l_c and l_f with Q^2. Dashed curves are calculated in the "frozen" approximation $l_c\gg R_A$. The figure is taken from [13].*

$\bar{\nu}=138$ GeV with the Q^2 dependent slope given by Eq. (2.33). All effects of CL and CT were included via the LC Green function formalism. In order to check

the onset of high energy limit, $l_c \gg R_A$, we presented also calculations in the "frozen" approximation and plotted the results as dashed curves in Fig. 4.1. One can see that the accuracy of this high energy approximation is rather good for calcium, while for lead it significantly deviates from the exact result already at $Q^2 \gtrsim 2$ GeV^2 since the approximation $l_c \gg R_A$ is less fulfilled for heavier nuclei.

We also see that the contraction of the CL with Q^2 causes an effect opposite to CT, namely nuclear transparency is suppressed rather than enhanced. Therefore, there is no danger that CL effects can mock CT, and one can conclude that this is an advantage of coherent compared to incoherent production [67]. However, at medium energy, when $l_c \lesssim R_A$, the suppression at short CL is so strong that no rise of nuclear transparency with Q^2 might be observable.

Note that in contrast to incoherent production where nuclear transparency is expected to saturate as $Tr_A^{inc}(Q^2) \to 1$ at large Q^2, for the coherent process nuclear transparency reaches a higher limit, $Tr_A^{coh}(Q^2) \to A^{1/3}$ (of course, $A^{1/3}$ is valid only for very large nuclei, otherwise it is an approximate number). The dashed curves in Fig. 4.1 nearly reach this upper limit at $Q^2 \sim 10$ GeV^2.

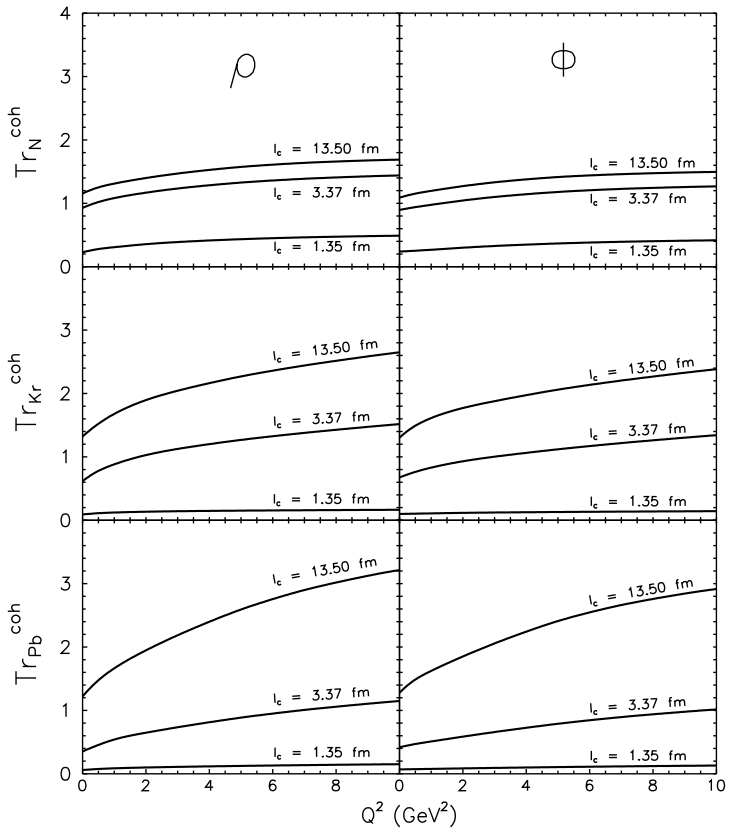

Figure 4.2.: *The same as in Fig. 3.3, but for coherent production of ρ and ϕ, $\gamma^* A \to V A$. The figure is taken from [13].*

One can eliminate the effects of CL and single out the net CT effect in a way

similar to what was suggested for incoherent reactions in Chapter 3 by selecting experimental events with $l_c = const$. We calculated nuclear transparency for the coherent reaction $\gamma^* A \to \rho(\phi) A$ at fixed values of l_c. The results for $l_c =$ 1.35, 3.37, 13.50 fm are depicted in Fig. 4.2 for several nuclei.

Variety of another predictions for the nuclear transparency in coherent production of different vector mesons and their $2S$ radial excitations can be found in [65, 13, 21, 71, 72].

4.3. Summary of the attached papers

4.3.1. Production of polarized vector mesons off nuclei

Physical Review C**76** (2007) 025210
5 citations
listed as A.7 on page 105

This article is devoted to investigation of color transparency (CT) and coherence length (CL) effects in electroproduction of longitudinally (L) and transversally (T) polarized vector mesons using the light-cone QCD dipole formalism. We predicted both the A and Q^2 dependence of the L/T- ratios, for ρ^0 mesons produced coherently and incoherently off nuclei in the kinematic region corresponding to HERMES experiment. We showed for the first time that for an incoherent reaction the CT and CL effects add up and result in a monotonic A dependence of the L/T-ratio at different values of Q^2. On the contrary, for a coherent process the contraction of the CL with Q^2 causes an effect opposite to that of CT and we expect quite a nontrivial A dependence, especially at large $Q^2 \gg m_V^2$.

5. Gluon shadowing

In the LC Green function approach [63, 23, 13, 21, 73, 74] the physical photon $|\gamma^*\rangle$ is decomposed into different Fock states, namely, the bare photon $|\gamma^*\rangle_0$, plus $|\bar{q}q\rangle$, $|\bar{q}qG\rangle$, etc. As we mentioned above in Chapter 2 the higher Fock states containing gluons describe the energy dependence of the photoabsorption cross section on a nucleon, and also lead to gluon shadowing (GS) in the nuclear case. However, these fluctuations are heavier and have a shorter coherence time (lifetime) than the lowest $|\bar{q}q\rangle$ state, and dominates at higher energies, i.e. at smaller values of Bjorken $x_{Bj} \lesssim 0.01$ [13, 21, 73, 74]. Since no data for GS are available one has to rely on theoretical calculations as will be discussed below.

The phenomenon of GS, just as for the case of nuclear shadowing discussed in Chapter 1, can be treated differently depending on the reference frame. In the infinite momentum frame this phenomenon looks similar to gluon-gluon fusion, corresponding to a nonlinear term in the evolution equation [75]. This effect should lead to a suppression of the small-x_{Bj} gluons also in a nucleon, and lead to a precocious onset of the saturation effects for heavy nuclei. Within such a parton model interpretation, in the infinite momentum frame of the nucleus the gluon clouds of nucleons which have the same impact parameter overlap at small x_{Bj} in the longitudinal direction. This allows gluons originated from different nucleons to fuse, leading to a gluon density which is not proportional to the density of nucleons any more. This is gluon shadowing.

The same phenomenon looks quite different in the rest frame of the nucleus. It corresponds to the process of gluon radiation and shadowing corrections, related to multiple interactions of the radiated gluons in the nuclear medium [22]. This is a coherence phenomenon known as the Landau-Pomeranchuk effect, namely the suppression of bremsstrahlung by interference of radiation from different scattering centers, demanding a sufficiently long coherence time of radiation, a condition equivalent to a small Bjorken x_{Bj} in the parton model.

Although these two different interpretations are not Lorentz invariant, they represent the same phenomenon, related to the Lorentz invariant Reggeon graphs. It was already discussed in detail in [13, 76] that the double-scattering correction to the cross section of gluon radiation can be expressed in Regge theory via the triple-Pomeron diagram. It is interpreted as a fusion of two Pomerons originated from different nucleons, $2\,\mathbb{P} \to \mathbb{P}$, which leads to a reduction of the nuclear gluon density G_A.

There are still very few numerical evaluations of gluon shadowing in the literature, all of them done in the rest frame of the nucleus, using the idea from ref. [22]. As was discussed in [13] gluon shadowing can be identified as the shad-

owing correction to the longitudinal cross section coming from the GG dipole representing the $|\bar{q}qG\rangle$ Fock component of the photon. An important point for the evaluation of GS is knowing about the transverse size of this GG dipole (radius of propagation of the LC gluons). This size has been extracted in [30] and found to be rather small, $r_0 \approx 0.3$ fm [77].

The small size of quark-gluon fluctuations has been incorporated into the LC dipole approach via nonperturbative LC potential describing the quark-gluon interaction. Such a potential was introduced into the Schrödinger equation for the LC Green function describing the propagation of a quark-gluon system [30, 23, 13, 21, 74].

We have improved in refs. [13, 21, 74] the calculations from [30] of the ratio of gluon densities in nuclei and nucleon,

$$R_G(x_{Bj},Q^2) = \frac{G_A(x_{Bj},Q^2)}{A\,G_N(x_{Bj},Q^2)} \approx 1 - \frac{\Delta\sigma(\bar{q}qG)}{\sigma_{tot}^{\gamma^* A}}\ , \tag{5.1}$$

where $\Delta\sigma(\bar{q}qG)$ is the inelastic correction to the total cross section $\sigma_{tot}^{\gamma^* A}$ related to the creation of a $\bar{q}qG$ intermediate state,

$$\Delta\sigma(\bar{q}qG) = \mathrm{Re}\int\limits_{-\infty}^{\infty} dz_2 \int\limits_{-\infty}^{z_2} dz_1\,\rho_A(b,z_1)\,\rho_A(b,z_2)\int d^2x_2\,d^2y_2\,d^2x_1\,d^2y_1\int d\alpha_q\,\frac{d\,\alpha_G}{\alpha_G}$$
$$\times F^{\dagger}_{\gamma^*\to\bar{q}qG}(\vec{x}_2,\vec{y}_2,\alpha_q,\alpha_G)\ G_{\bar{q}qG}(\vec{x}_2,\vec{y}_2,z_2;\vec{x}_1,\vec{y}_1,z_1)\ F_{\gamma^*\to\bar{q}qG}(\vec{x}_1,\vec{y}_1,\alpha_q,\alpha_G)\ . \tag{5.2}$$

Here $\vec{x}$ and $\vec{y}$ are the transverse distances from the gluon to the quark and antiquark, respectively, α_q is the fraction of the LC momentum of the $\bar{q}q$ carried by the quark, and α_G is the fraction of the photon momentum carried by the gluon. $F_{\gamma^*\to\bar{q}qG}$ is the amplitude of diffractive $\bar{q}qG$ production in a $\gamma^* N$ interaction [30], and it is given by

$$\begin{aligned} F_{\gamma^*\to\bar{q}qG}(\vec{x},\vec{y},\alpha_q,\alpha_G) &= \frac{9}{8}\,\Psi_{\bar{q}q}(\alpha_q,\vec{x}-\vec{y})\,\left[\Psi_{qG}\left(\frac{\alpha_G}{\alpha_q},\vec{x}\right) - \Psi_{\bar{q}G}\left(\frac{\alpha_G}{1-\alpha_q},\vec{y}\right)\right] \\ &\times \left[\sigma_{\bar{q}q}(x) + \sigma_{\bar{q}q}(y) - \sigma_{\bar{q}q}(\vec{x}-\vec{y})\right]\ , \end{aligned} \tag{5.3}$$

where $\Psi_{\bar{q}q}$ and $\Psi_{\bar{q}G}$ are the LC distribution functions of the $\bar{q}q$ fluctuations of a photon and qG fluctuations of a quark, respectively.

In the above equation $G_{\bar{q}qG}(\vec{x}_2,\vec{y}_2,z_2;\vec{x}_1,\vec{y}_1,z_1)$ is the LC Green function which describes the propagation of the $\bar{q}qG$ system from the initial state with longitudinal and transverse coordinates z_1 and $\vec{x}_1,\vec{y}_1$, respectively, to the final coordinates $(z_2,\vec{x}_2,\vec{y}_2)$. For the calculation of gluon shadowing one should suppress the intrinsic $\bar{q}q$ separation, i.e. assume $\vec{x}=\vec{y}$. In this case the Green function simplifies, and effectively describes the propagation of a gluon-gluon dipole through a medium.

Notice that calculations of GS [30, 23, 13, 21, 74] has been performed only for the lowest Fock component containing just one LC gluon. In terms of the parton model it reproduces the effects of fusion of many gluons to one gluon. Inclusion of higher multigluon Fock components is still a challenge. However, their effect can be essentially taken into account by the eikonalization of the calculated $R_G(x_{Bj}, Q^2)$, as was argued in [78]. In another words, the dipole cross section, should be renormalized everywhere, in the form

$$\sigma_{\bar{q}q} \Rightarrow R_G \, \sigma_{\bar{q}q} \ . \tag{5.4}$$

Such a procedure makes the nuclear medium more transparent. This could be expected since Gribov's inelastic shadowing is known to suppress the total hadron-nucleus cross sections, i.e. to make nuclei more transparent [5, 79].

As an illustration of not very strong onset of GS, here we present $R_G(x_{Bj}, Q^2)$, Eq. (5.1), for different nuclear thicknesses $T_A(b)$. Using an approximation of constant nuclear density (see Eq. (2.15)), $T_A(b) = \rho_0 \, L$, where $L = 2\sqrt{R_A^2 - b^2}$, the ratio $R_G(x_{Bj}, Q^2)$ is also implicitly a function of L. An example for the calculated L-dependence of $R_G(x_{Bj}, Q^2)$ at $Q^2 = 4$ GeV^2 is depicted in Fig. 5.1 for different values of x_{Bj}. As one should expect, the longer L, the stronger is

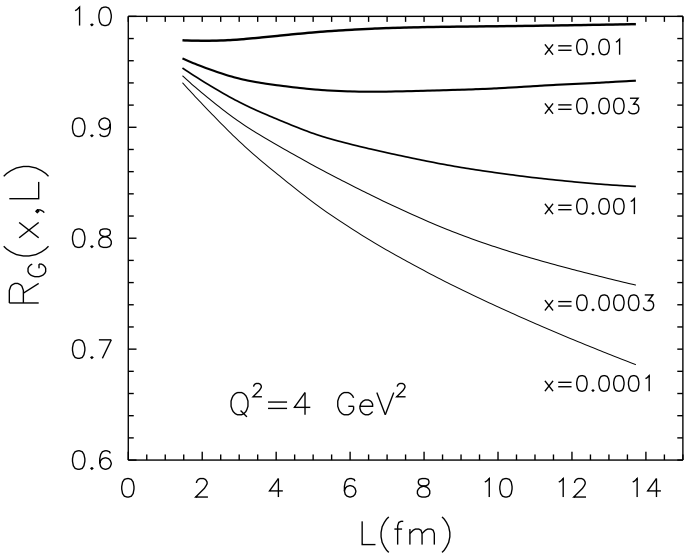

Figure 5.1.: *The ratio of nucleus to nucleon gluon densities as function of the thickness of the nucleus, $L = T(b)/\rho_0$, at $Q^2 = 4$ and different fixed values of x_{Bj}. The figure is taken from [13].*

gluon shadowing at small x_{Bj}. We have found [30, 23, 13, 21, 74] that at higher Q^2 the gluon shadowing slowly (logarithmically) decreases, in accordance with the expectations based on the evolution equation [80], which clearly demonstrates that GS is a leading-twist effect.

One can expect from Eq. (5.4) that GS should always diminish the nuclear cross sections of various processes in nuclear targets, and that the onset of GS

is stronger for heavier nuclei. However, this is not so for incoherent electroproduction of vector mesons, analyzed in [13]. Indeed, although the renormalization Eq. (5.4) suppresses the pre-exponential factor $\sigma_{\bar{q}q}(r,s)$ on the r.h.s. of Eq. (3.9), it simultaneously increases the exponential. These two effects essentially cancel. Consequently, the nuclear cross section for incoherent electroproduction of vector mesons is rather insensitive to GS as was demonstrated in [13]. Furthermore, the effect of GS is stronger for light than for heavy nuclear targets, in contradiction with the standard intuition. Moreover, for heavy nuclei the effect GS can lead even to a counterintuitive enhancement (antishadowing), as was analyzed in [13]. For the case of coherent vector meson production $\gamma^* A \to VA$ [13, 21], GS was shown to be a much stronger effect in comparison with incoherent production.

Similarly, it was analyzed in ref. [76, 81, 82] that multiple scattering of higher Fock states containing gluons leads to an additional suppression of the Drell-Yan cross section. In [74] we demonstrated that GS also suppresses the total photoabsorption cross section on a nucleus $\sigma_{tot}^{\gamma^* A}(x_{Bj}, Q^2)$. Here we predicted quite a strong effect of GS in the shadowing region of small $x_{Bj} \lesssim (0.01 \div 0.001)$, in the kinematic range of available data corresponding to small and medium values of $Q^2 \sim$ a few GeV^2.

5.1. Summary of the attached papers

5.1.1. Gluon Shadowing in DIS off Nuclei

Journal of Physics G**35** (2008) 115010
5 citations
listed as A.8 on page 127.

This paper is devoted to study of nuclear shadowing in deep-inelastic scattering at small Bjorken $x_{Bj} \lesssim 0.01$ within the light-cone QCD dipole formalism based on the Green function technique. We have performed calculations of the nuclear shadowing for the $\bar{q}q$ Fock component of the photon, which has been based on an exact numerical solution of the evolution equation for the Green function. We demonstrated unavoidability of this exact numerical solution for the range of Bjorken $x_{Bj} \gtrsim 10^{-4}$. The eikonal approximation, used so far in most of other models, can be applied only at high energies, when $x_{Bj} \lesssim 10^{-4}$ and the transverse size of the $\bar{q}q$ Fock component is "frozen" during propagation through the nuclear matter. The main emphasize has been devoted to study of gluon shadowing. At $x_{Bj} \leq 0.01$ we have found quite a large contribution of gluon suppression to nuclear shadowing, as a shadowing correction for the higher Fock states containing gluons. We have compared numerical results for nuclear shadowing with available data from the E665 and NMC collaborations. We have predicted also the magnitude of nuclear shadowing at very small x_{Bj} corresponding to LHC kinematical range. Finally, we have confronted our model predictions with the results obtained from other models.

6. Summary and conclusions

Electroproduction of vector mesons off nuclei is subject to an interplay between coherence (shadowing) and formation (color transparency) effects. We presented in Chapter 3 a rigorous quantum-mechanical approach based on the light-cone QCD Green function formalism [30, 13, 21], which naturally incorporates these interference effects. Our main results and observations are the following:

- In Chapters 2, 3 and 4 we presented a comprehensive model, based on the rigorous light-cone QCD Green function formalism, for theoretical description [30, 13] of exclusive electroproduction of vector mesons off nuclei. The original and pioneering result is represented by general formulas, Eq. (3.10) for incoherent production and Eq. (4.2) for coherent production, which interpolate between low and high energy limits, which are frequently used in the literature.

- Due to quark-hadron duality the Green function formalism under consideration is equivalent to a solution of the full multi-channel problem in the hadronic representation [12].

- In the incoherent electroproduction of vector mesons off nuclei (see Chapter 3) at medium and low energies, the onset of coherence effects (shadowing) can mimic the expected signal of CT. Then the observation of a rising nuclear transparency as function of Q^2 for fixed l_c would signal color transparency (see Fig. 3.3 and also [21]).

- Electroproduction of charmonia and bottomonia off nuclei is also very convenient for study of an interplay between coherence and formation effects [21]. A strong inequality $l_c < l_f$ (see Section 3.1.2) in all kinematic region of ν and Q^2 leads to a different scenario of CT-CL mixing as compared to light vector mesons (see Section 3.1.1). Consequently, at small and moderate photon energies, when $l_c \lesssim 1 \div 2$ fm, the problem of CT-CL separation is not so arisen.

- Predictions for the nucleus-to-nucleon ratio of electroproduction cross sections as a function of Q^2 at different fixed l_c shows rather strong onset of CT effects in incoherent production of charmonia [21]. Although the variation with Q^2 of nuclear transparency is predicted to be less strong than for production of light vector mesons [13], it is still rather significant to be investigated experimentally even in the range of $Q^2 \lesssim 20\,\mathrm{GeV}^2$.

- The successful experimental confirmation [83] of the predicted coherence length effects [20] seems to be an accidental consequence of the specific correlation between Q^2 and l_c in the HERMES data. The parameter-free rigorous calculations in [13] described well the observed variation of nuclear transparency with l_c as a result of a complicated interplay between the color transparency and coherence length effects.

- There are other effects, like the lowest order inelastic corrections and the finite lifetime of vector mesons [13], which cause a rise of nuclear transparency with Q^2 at $l_c = const$ mimicking thus a signal of CT. We found in [13] that both effects are too weak to be relevant.

- We have found in Chapter 4 that effects of CT in coherent production of light vector mesons are less pronounced (see Fig. 4.2). Although nuclear transparency decreases with Q^2 and does not mimic CT in this case, the CL effects significantly modify the Q^2 dependence and may completely eliminate any signal of CT at medium energies as is depicted in Fig. 4.1.

- The effects of CT in coherent production of charmonia [21] are found to be weak similarly as in production of light vector mesons [13]. A wider range of $Q^2 \leq 100\,\mathrm{GeV}^2$ and heavy nuclei gives higher chances for experimental investigation of CT.

- At small $x_{Bj} \lesssim 0.01$ we included the nuclear suppression of gluons, as was discussed in Chapter 5, within the same LC approach treating it as shadowing corrections for the higher Fock states containing gluons. The nonperturbative interaction of the LC gluons significantly reduces the predicted magnitude of gluon shadowing (see Fig. 5.1).

- Two main effects govern the magnitude of gluon shadowing: The amplitude of meson production off a bound nucleon is suppressed due to a reduced amount of gluons in the nucleus. On the other hand the same effect makes the nuclear medium more transparent and enhances the meson survival probability.

- For incoherent production of light vector mesons (ρ and Φ) these two effects nearly compensate each other for heavy nuclei as was demonstrated in [13]. The cross section for coherent production is less for more transparent nuclei, therefore the effect of gluon shadowing is more pronounced [13]. These corrections are not important in the kinematic range corresponding to HERMES or JLab energies, but are significant at higher energies starting from the RHIC kinematical region.

- The effects of gluon shadowing in electroproduction of charmonia were shown to be significant only at much higher energies than in production

of light vector mesons due to large mass of $\bar{c}c$ fluctuation. It was manifested in [21] that these corrections are quite small at medium energies dominant in searching for CT effects.

- For electroproduction of radially excited (2S) vector mesons, there is a strong correlation between a nontrivial and anomalous behavior of nuclear transparency as function of the mass number, photon energy and virtuality and the shape of the radial wave function with the corresponding position of the node. It gives a possibility to determine this position from data obtained in the future planned experiments.

A. Author's papers

ELSEVIER

29 December 1994

PHYSICS LETTERS B

Physics Letters B 341 (1994) 228–237

Scanning the BFKL pomeron in elastic production of vector mesons at HERA

J. Nemchik [a,b], N.N. Nikolaev [b,c], B.G. Zakharov [c]

[a] *Institute of Experimental Physics, Slovak Academy of Sciences, Watsonova 47, 04353 Kosice, Slovak Republic*

[b] *IKP (Theorie), KFA Jülich, 5170 Jülich, Germany*[1]

[c] *L.D. Landau Institute for Theoretical Physics, GSP-1, 117940, ul. Kosygina 2, Moscow 117334, Russia*

Received 26 May 1994; revised manuscript received 12 August 1994
Editor: P.V. Landshoff

Abstract

Elastic production of vector mesons $\gamma^* N \to V N$ is the pomeron-exchange dominated diffractive reaction with much potential of probing the BFKL pomeron. The BFKL pomeron can conveniently be described in terms of the dipole cross section which is a solution of the generalized BFKL equation. In this paper we discuss, how the energy and Q^2 dependence of elastic production of vector mesons at HERA will allow scanning the dipole cross section as a function of dipole size r. We show that determination of the intercept of the BFKL pomeron requires measuring the ρ^0 and J/Ψ production at $Q^2 \sim (100\text{–}200)$ GeV^2 and/or the quasireal photoproduction of the Y. We present predictions for the effective intercept in the kinematic range of the forthcoming HERA experiments, which can shed much light on the nonperturbative component of the pomeron.

Elastic real and virtual photoproduction of vector mesons

$$\gamma^* p \to V p\,, \quad V = \rho^0, \omega^0, \phi^0, J/\Psi, \Upsilon \ldots, \qquad (1)$$

is the typical diffractive reaction, dominated by pomeron exchange. Determination of parameters of the BFKL pomeron [1], in particular of its intercept $\Delta_{\mathbf{P}}$, is an outstanding problem for the HERA experiments on small x, and exploring the potential of reaction (1) is of great importance. In [2–4] we developed a novel approach to the BFKL pomeron in terms of the dipole cross section $\sigma(\xi, r)$ which satisfies the generalized BFKL equation. Here r is the size of the color dipole, $\xi = \log[2m_p\nu/(Q^2 + m_V^2)]$ is the rapidity, m_V is the vector meson mass, Q^2 is the virtuality of the photon and ν its energy in the proton rest frame. At very high ν and/or very small Bjorken variable x one expects

$$\sigma(\xi, r) = \sigma_{\mathbf{P}}(r) \exp(\Delta_{\mathbf{P}}\xi) \qquad (2)$$

and

$$F_2(x, Q^2) \propto \exp(\Delta_{\mathbf{P}}\xi) \sim \left(\frac{1}{x}\right)^{\Delta_{\mathbf{P}}} \qquad (3)$$

with the intercept $\Delta_{\mathbf{P}}$ which does not depend on Q^2, the real photoproduction $Q^2 = 0$ not excepted. Understanding the onset of the BFKL regime (2,3) is the most pressing issue, because experimentally a steep rise of $F_2(x, Q^2)$ at HERA [5] is accompanied by a much slower rise of the real photoabsorption cross section [6].

[1] E-mail: kph154@zam001.zam.kfa-juelich.de.

SSDI 0370-2693(94)01279-2

What makes reactions (1) exceptionally important is the scanning phenomenon discovered in [7–11], by which elastic production amplitude probes the dipole cross section at the scanning radius

$$r_S \approx \frac{C}{\sqrt{m_V^2 + Q^2}}. \tag{4}$$

The scale parameter C is rather large , and in [11] we gave an estimate $C \approx 6$. Changing Q^2 and the mass of the produced vector meson, one can probe $\sigma(\xi, r)$ and measure the effective intercept $\Delta_{\rm eff}(\xi, r) = \partial \log \sigma(\xi, r)/\partial \xi$ in a very broad range of dipole size r, from the nonperturbative regime of $r \gtrsim 1$ f down to the perturbative regime of $r \ll 1$ f. The HERA experiments are already amassing the data on production of vector mesons, and the purpose of this communication is to present the detailed predictions for reactions (1) from the approach to the BFKL pomeron developed in [2–4,12–15].

In order to set up the framework, we briefly review properties of the dipole cross section. In [3,4,12,13] we studied solutions of the generalized BFKL equation in the realistic model with the finite correlation radius R_c for perturbative gluons and the running QCD coupling $\alpha_S(r)$, which freezes at large distances $\alpha_S(r \geq R_f) = \alpha_S^{(\rm fr)} = 0.8$. With the $R_c = 0.3f$ as suggested by the lattice QCD studies, $\Delta_{\mathbf{P}} = 0.4$ [4,12]. The major findings are:

Firstly, the onset of the asymptotic behaviour (2,3) was found to be extremely slow. Namely, the effective intercept $\Delta_{\rm eff}(\xi, r)$ varies quite strongly in the range of r and ξ relevant to the HERA experiments on DIS. The usually discussed structure function $F_2(x, Q^2)$ receives contributions from a broad range of r and, for this reason, its x dependence does not allow a reliable experimental determination of the intercept $\Delta_{\mathbf{P}}$.

Secondly, by the diffusion property of the BFKL kernel [1,4,12], at asymptotic energies the behaviour (2) takes over at all values of r, including $r > R_c$, thus unifying the asymptotic energy dependence of the bare pomeron-exchange contribution to hadronic scattering, the real photoproduction and deep inelastic scattering. Furthermore, by the same diffusion property, the intercept $\Delta_{\mathbf{P}}$ is almost entirely controlled by the region of $r \sim R_c$ [4,12].

Thirdly, there happens to exist a "magic" size $r_\Delta \approx \frac{1}{2}R_c$, at which the precocious asymptotic behaviour $\Delta_{\rm eff}(\xi, r) \approx \Delta_{\mathbf{P}}$ will persist over the whole range of x at HERA. In [4,15] we showed how one can zoom at $r \sim r_\Delta$, measuring at HERA the charm structure function at $Q^2 \lesssim 10$ GeV^2, the longitudinal structure function $F_L(x, Q^2)$ at $Q^2 \sim$ (10–40) GeV^2 and the scaling violations $\partial F_T(x, Q^2)/\partial \log Q^2$ at $Q^2 \sim$ (2–10) GeV^2.

Fourthly, the BFKL pomeron describes the exchange by perturbative gluons with the typical interaction radius $\sim R_c$. At low energy and large dipole size $r \gg R_c$, the nonperturbative scattering mechanism can take over. The rise of the BFKL perturbative cross section is driven by the rising multiplicity of perturbative gluons in the high-energy photon (hadron), for the nonperturbative mechanism one can expect the (approximately) energy-independent contribution $\sigma^{(\rm npt)}(r)$ to the dipole cross section. A large contribution from the $\sigma^{(\rm npt)}(r)$ reconciles the steep rise of $F_2(x, Q^2)$ [5] with a much weaker energy dependence of the real photoabsorption cross section [6]. As we shall discuss below, the scanning phenomenon allows to study in much detail a transition between the nonperturbative and perturbative regimes, which makes reactions (1) particularly important.

The origin of the scanning phenomenon is as follows: In the dipole-cross section representation, the amplitude of the forward production $\gamma^* p \to V N$ of the (T) transverse and (L) longitudinally polarized vector mesons reads [7–11,16,17]

$$\begin{aligned}\mathcal{M}_T(\xi, Q^2) &= \frac{N_c C_V \sqrt{4\pi\alpha_{\rm em}}}{(2\pi)^2} \\ &\times \int d^2r \sigma(\xi, r) \int_0^1 \frac{dz}{z(1-z)} \{m_q^2 K_0(\varepsilon r)\phi(r, z) \\ &- [z^2 + (1-z)^2]\varepsilon K_1(\varepsilon r)\partial_r \phi(z, r)\} \\ &= \frac{1}{(m_V^2 + Q^2)^2} \int \frac{dr^2}{r^2} \frac{\sigma(\xi, r)}{r^2} W_T(Q^2, r^2) \end{aligned} \tag{5}$$

$$\begin{aligned}\mathcal{M}_L(\xi, Q^2) &= \frac{N_c C_V \sqrt{4\pi\alpha_{\rm em}}}{(2\pi)^2} \frac{2\sqrt{Q^2}}{m_V} \\ &\times \int d^2r \sigma(\xi, r) \int_0^1 dz \end{aligned}$$

$$\times \left\{ [m_q^2 + z(1-z)m_V^2] K_0(\varepsilon r)\phi(r,z) - \varepsilon K_1(\varepsilon r)\partial_r\phi(z,r) \right\} =$$

$$\frac{1}{(m_V^2+Q^2)^2}\frac{2\sqrt{Q^2}}{m_V}\int \frac{dr^2}{r^2}\frac{\sigma(\xi,r)}{r^2}W_L(Q^2,r^2). \quad (6)$$

Here $N_c = 3$ is the number of colours, $C_V = \frac{1}{\sqrt{2}}, \frac{1}{3\sqrt{2}}, \frac{1}{3}, \frac{2}{3}$ for the $\rho^0, \omega_0, \phi^0, J/\Psi$ production, respectively, $K_{0,1}(x)$ is the modified Bessel function,

$$\varepsilon^2 = m_q^2 + z(1-z)Q^2, \quad (7)$$

$\phi(z,r)$ is the lightcone wave function of the $q\bar{q}$ Fock state of the vector meson in the mixed $(z,\boldsymbol{r})$-representation, where $\boldsymbol{r}$ is the transverse separation of the quark and antiquark and z is a fraction of the lightcone momentum carried by the quark. The normalization of amplitudes is such that $d\sigma/dt|_{t=0} = |\mathcal{M}|^2/16\pi$, the wave functions are normalized by

$$\frac{N_c}{2\pi}\int d^2\boldsymbol{r}\int_0^1 \frac{dz}{z(1-z)}\{m_q^2\phi^2(r,z) + [z^2+(1-z)^2][\partial_r\phi(r,z)]^2\} = 1. \quad (8)$$

At very large Q^2 the scanning radius becomes small and the effects of short-distance interquark interaction by QCD gluon exchange in wave functions of vector mesons become important. We incorporate these "Coulomb" effects as follows [16]: Let the interquark potential be $V(\boldsymbol{R}) = V_c(R) - \frac{4}{3}\alpha_S(R)/R$, where $\boldsymbol{R}$ is the 3D separation of the q and $\bar{q}$ and $V_c(R)$ is the confining potential which is smooth at $R \to 0$, which we describe by the 3D harmonic oscillator. Treating the Coulomb interaction as a perturbation, the short-distance behaviour of the wave function can be written as

$$\Psi(\boldsymbol{R}) = \Psi_0(R) + \Psi_0(0)C\exp\left[-\frac{R}{2a(R)}\right], \quad (9)$$

where $\Psi_0(R)$ is a wave function in the confining potential and $a(R)$ is the "running Bohr radius"

$$a(R) = \frac{3C}{8m_q\alpha_s(R)}. \quad (10)$$

The parameter C can not be fixed in the first order in the Coulomb perturbation, the choice $C < 1$ is natural to have a steep decrease of the Coulomb correction in (9) at large R. If the $V\bar{q}q$ vertex is taken in the form $\Gamma\bar{q}\gamma_\mu q$, then the standard nonrelativistic relationship between the vertex function Γ and the Fourier transform $\Psi(\boldsymbol{p}) = \int d^3\boldsymbol{R}\Psi(\boldsymbol{R})\exp(-i\boldsymbol{pR})$ reads

$$\Psi(\boldsymbol{p}^2) \propto \frac{\Gamma(\boldsymbol{p}^2)}{4\boldsymbol{p}^2 + 4m_q^2 - m_V^2}, \quad (11)$$

the lightcone generalization of which is achieved by the substitution [18]

$$\boldsymbol{p}^2 = \tfrac{1}{4}(M^2 - 4m_q^2) = \frac{m_q^2 + \boldsymbol{k}^2}{4z(1-z)} - m_q^2, \quad (12)$$

where M is the invariant mass of the $q\bar{q}$ system. In terms of the p^2 of Eq. (12), for the ground state vector mesons this gives

$$\Psi(M^2) = N_0\left\{(2\pi)^{3/2}R_0^3\exp\left[-\tfrac{1}{2}R_0^2p^2\right] + C\frac{64\pi a^3(p^2)}{(1+4a^2(p^2)p^2)^2}\right\}, \quad (13)$$

where $a(p^2)$ is still given by Eq. (10) with the $\alpha_S(p^2)$ taken in the momentum representation. Notice, that the asymptotics of the Coulomb correction in (13) is $\propto \alpha_S(p^2)$ and does not depend on the parameter C. Finally, the lightcone wave function $\phi(r,z)$ in the mixed $(\boldsymbol{r},z)$ representation is given by

$$\phi(r,z) = \int \frac{d^2\boldsymbol{k}}{(2\pi)^2}\Psi(p^2)\exp(i\boldsymbol{kr}), \quad (14)$$

in which, finally, $a(p^2)$ is substituted for $a(r)$. The explicit form of $\phi(r,z)$ in terms of the modified Bessel functions [16] is too lengthy to be reproduced here. We fix the parameters C and R_0 so as to reproduce the width of the $V \to e^+e^-$ decay and the mean squared radius of the ground state. For the ρ^0 we assume the same charge radius as for the pion $\langle r^2\rangle = 0.97\ \mathrm{f}^2$, for the J/Ψ we take $\langle r^2\rangle = 0.15\ \mathrm{f}^2$ from the potential model analysis [19]. For the ρ_0, the resulting parameters are $C = 0.25$ and $R_0^2 = 0.76\ \mathrm{f}^2$ at $m_q = 0.15$ GeV, for the J/Ψ: $C = 0.5$, $R_0^2 = 0.16\ \mathrm{f}^2$ at $m_q = 1.3$ GeV. More detailed discussion of this relativization procedure and applications to the form factor calculations will be presented elsewhere [16].

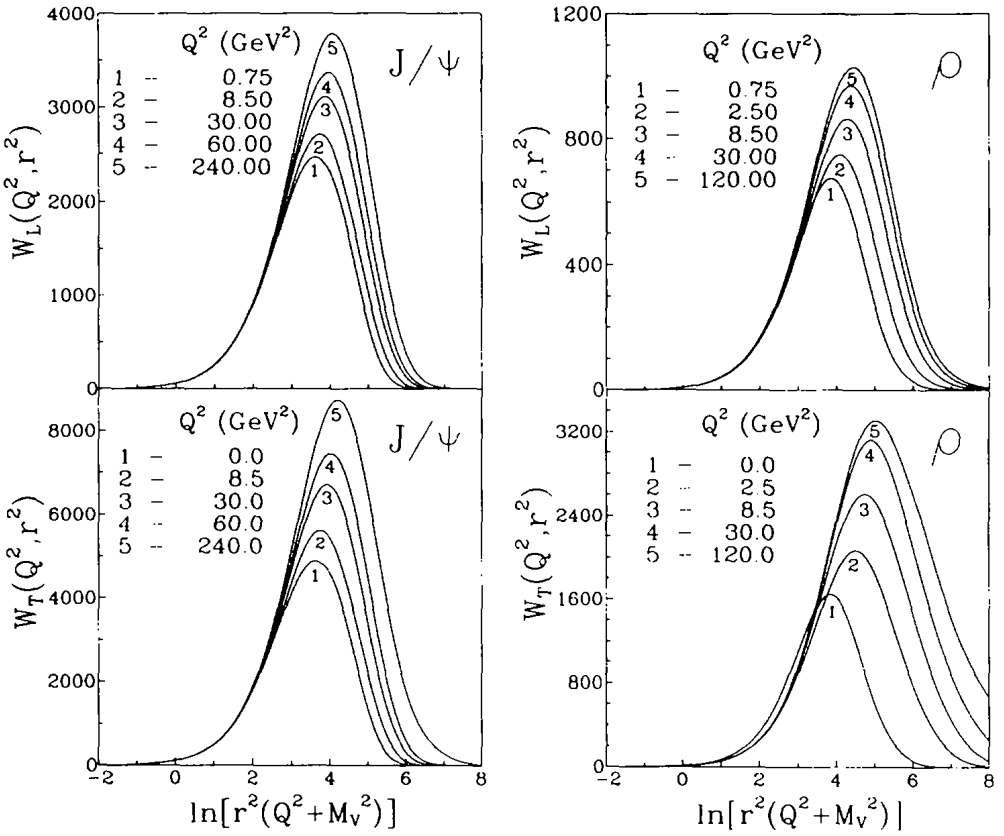

Fig. 1. Weight functions $W_{T,L}(Q^2, r^2)$ as a function of a variable $y = r^2(Q^2 + m_V^2)$.

The dipole cross section can be related to the gluon structure function of the target proton $G(x, q^2)$ [2,17,20,21]

$$\sigma(\xi, r) = \frac{\pi^2}{3} r^2 \alpha_S(r) G(x = \exp(\xi), q^2 = \frac{A}{r^2}) \propto r^2 \left[\frac{1}{\alpha_S(r)}\right]^{\gamma - 1} \exp(\Delta_{I\!P} \xi), \quad (15)$$

where $\gamma = 4/3\Delta_{I\!P}$ [14] and $A \approx 10$ (the emergence of this large numerical factor is explained in detail in [22]) The most important property of the dipole cross section is the color transparency driven dependence $\propto r^2$ at small r. Because $K_{0,1}(x) \propto \exp(-x)$ at large x, and the wave function of the vector meson is smooth, the amplitudes (5,6) will be dominated by the contribution from $r \approx 3/\varepsilon$, which in the nonrelativistic approximation of $m_V \sim 2m_q$ and $z \sim \frac{1}{2}$ leads to the scanning radius (4) and the estimate $C \approx 6$. When the scanning radius is small, $r_S \lesssim R_V$, where R_V is the vector meson radius, the amplitudes (6,7) can be evaluated as

$$M_T \propto r_S^2 \sigma(\xi, r_S) \propto \frac{1}{(m_V^2 + Q^2)^2}, \quad (16)$$

$$M_L \propto \frac{\sqrt{Q^2}}{m_V} r_S^2 \sigma(\xi, r_S) \propto \frac{\sqrt{Q^2}}{m_V} \frac{1}{(m_V^2 + Q^2)^2} \propto \frac{\sqrt{Q^2}}{m_V} M_T, \quad (17)$$

which must be contrasted to prediction of the vector dominance model $M_T \propto 1/(m_V^2 + Q^2)$. This departure from the vector dominance comes entirely from colour transparency property of the dipole cross section [11]. Production of the longitudinally polarized vector mesons dominates at $Q^2 \gg m_V^2$.

The scanning property is quantified by weight function $W_{T,L}(Q^2, r^2)$ in Eqs. (5), (6), which we introduced following [13]. The $W_{T,L}(Q^2, r^2)$ are sharply peaked (Fig. 1) and, because $\sigma(\xi, r)/r^2$ is a slow

function of r, see Eq. (15), the position of the peak gives the scanning radius r_S. At sufficiently large Q^2 such that $r_S \lesssim R_V$, which typically means $Q^2 \gg m_V^2$, the position of the peak in the variable $y = r^2(Q^2 + m_V^2)$ very weakly depends on Q^2. For production of the longitudinally polarized vector mesons, the peak corresponds to $C_L(J/\Psi) \sim 7$ and $C_L(\rho^0) \sim 8$. For the transversely polarized ρ^0 mesons, with rising Q^2 the peak is slowly drifting towards $C_T \sim 12$ at $Q^2 \sim 100$ GeV^2, which can be understood as follows [11]: At a fixed z, the scanning radius $r_S \approx 3/\varepsilon$. For the longitudinal photons, the wave function is peaked at $z \sim \frac{1}{2}$, hence the estimate $C \approx 6$ is rather accurate (for the related discussion of the longitudinal structure function see [2,17,22,23]). In the opposite to that, the transverse structure function receives significant contribution from the very asymmetric pairs with $z, (1-z) \sim m_q^2/Q^2$, which have a large, hadronic transverse size $r \sim 1/m_q$ [2,17]. Because of the contribution of such asymmetric pairs, the effective scanning radius for the transversely polarized vector mesons decreases with Q^2 less rapidly than given by the simple estimate (4), but the difference between C_T and C_L remains small even at $Q^2 \sim 100$ GeV^2. Notice, that because of very large numerical value of $C_{T,L}$, the scanning radius r_S Eq. (4) remains large, and the relativistic effects in wave functions are still marginal, in a very broad range of Q^2. For instance, for the J/Ψ we find $C_T \approx C_L$ and very close to the nonrelativistic estimate $C_{T,L} \approx 6$ even at $Q^2 \gg m_V^2$.

At small Q^2, the scanning radius r_S is large, and one probes the dipole cross section in the nonperturbative domain of r. In Fig. 2 we present the decomposition of the dipole cross section into the nonperturbative component $\sigma^{(npt)}(r)$ and the $\sigma^{(pt)}(\xi, r)$ which is a solution of the perturbative BFKL equation [2]:

$$\sigma(\xi, r) = \sigma^{(npt)}(r) + \sigma^{(pt)}(\xi, r) \qquad (18)$$

This additivity of the bare pomeron cross sections and/or of the eikonal functions when the unitarization is considered, is the simplest assumption [14], and more refined treatment will be necessary in an analysis of the future high-precision data. The shape of the

[2] This Fig. 2 updates Fig. 1 of Ref. [14], in which the mistake was made in plotting $\sigma^{(pt)}(\xi, r)$. This plotting mistake does not affect any of predictions made in [14], though. Our choice of $\sigma^{(npt)}(r)$ in this paper is slightly different from that in [14].

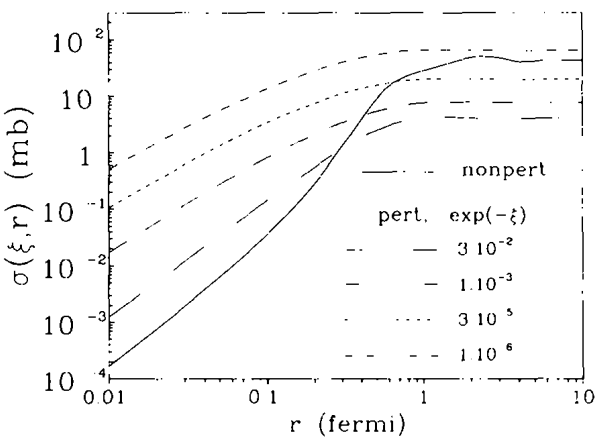

Fig. 2. Decomposition of the dipole cross section into the BFKL perturbative $\sigma^{(pt)}(\xi, r)$ and the nonperturbative $\sigma^{(npt)}(r)$ components. The growth of the BFKL cross section with energy (rapidity) is shown.

nonperturbative cross section is the largest unknown in the problem, and is mostly driven by our analysis of the Q^2 dependence of the photoproduction of vector mesons [8–11] and of structure functions at moderate Q^2 [18], which are well described by the dipole cross section calculated in [17]. Therefore, the $\sigma^{(npt)}(r)$ is tuned so as to reproduce the dipole cross section of Ref. [17] at $\xi = \xi_0 = -\log 0.03$, which we take as the starting point for the BFKL evolution. In terms of the relation (15), the $\sigma^{(npt)}(r)$ corresponds to the nonperturbative component of the gluon structure function $G(x, Q^2)$ which comes from the soft transverse momenta [14]. As such, this nonperturbative contribution is always implicitly present in the phenomenological gluon densities. In Fig. 2 we show how the $\sigma^{(pt)}(\xi, r)$ evolves with the rapidity ξ. At small r, the total dipole cross section is dominated by the BFKL cross section $\sigma^{(pt)}(\xi, r)$, and at sufficiently large ξ the $\sigma^{(pt)}(\xi, r)$ takes over the $\sigma^{(npt)}(r)$ also at large r. In this region, because of the so-called double logarithmic effects, the effective intercept $\Delta_{\text{eff}}(\xi, r) > \Delta_{\mathbf{P}}$ [3,4]. At large r, $\Delta_{\text{eff}}(\xi, r) \ll \Delta_{\mathbf{P}}$ because of the large contribution from the nonperturbative cross section $\sigma^{(npt)}(r)$. The analysis [4,13] has shown that there exists a magic radius $r \sim r_\Delta$, at which $\Delta_{\text{eff}}(\xi, r) \approx \Delta_{\mathbf{P}}$ starting already at moderate ξ. At this value of r, the nonperturbative cross section is small, and zooming at $r \sim r_\Delta$ shall allow direct measurement of $\Delta_{\mathbf{P}}$ at HERA.

The above discussion refers to the bare pomeron cross section. With the conventional Gaussian

parametrization of the elastic scattering peak, $d\sigma_{el}/dt \propto \exp(-B|t|)$, where $|t|$ is the momentum transfer squared, the profile function of elastic scattering takes the form

$$\Gamma(b) = \frac{\sigma_{tot}}{4\pi B} \exp\left(-\frac{b^2}{2B}\right), \tag{19}$$

where b is the impact parameter. The rise of the bare pomeron cross section will eventually conflict the s-channel unitarity bound $\Gamma(b) \leq 1$, and comments on the unitarity effects are in order. Unique solution of the unitarization problem is lacking; for the crude estimate we apply the $\mathcal{K}$-matrix unitraization

$$\Gamma(b) = \frac{\Gamma_0(b)}{1+\Gamma_0(b)}. \tag{20}$$

When the rising strength of the bare pomeron interaction $\Gamma_0(b) \gg 1$, the unitraized profile function tends to the black disc limit $\Gamma(b) \to 1$. The $\mathcal{K}$-matrix unitarization leads to a particularly simple form of the unitarized total cross section [2,21]

$$\sigma^{(U)}(\xi, r) = 4\pi B \log\left(1 + \frac{\sigma(\xi, r)}{4\pi B}\right). \tag{21}$$

For a crude evaluation of the unitarization effects, we take the energy-independent diffraction slope $B = 10$ GeV^{-2}. Evidently, the unitarization effects only become important when $\sigma(\xi, r) \gtrsim 4\pi B \sim 50$ mb, i.e., either at large r and/or at very high energy if r is small.

Our predictions for the energy dependence of different photoproduction observables are shown in Figs. 3, 4. In Fig. 3 we show the real photoabsorption cross section. It was calculated using the wave function of the photon derived in [17], assuming the effective quark mass $m_{u,d} = 0.15$ GeV, which is the sole parameter in the quark wave function. Only the nonperturbative contribution to $\sigma_{tot}(\gamma p)$ is sensitive to this parameter. For the comparison purposes, we also show our predictions for $\sigma_{tot}(\rho^0 p)$, which is close to $\sigma_{tot}(\pi N)$ and has a rise consistent with the observed trend of the hadronic total cross sections (for the recent review and high-energy extrapolations see [25]). We attribute the slow rise of $\sigma_{tot}(\gamma p)$ and $\sigma_{tot}(\rho^0 p)$ to the large contribution from the nonperturbative large-size cross section (for the early discussion of such a scenario see [26]). The effect of the unitarization slowly rises with energy. It predominantly affects the nonperturbative cross section and, given the uncertanty in the

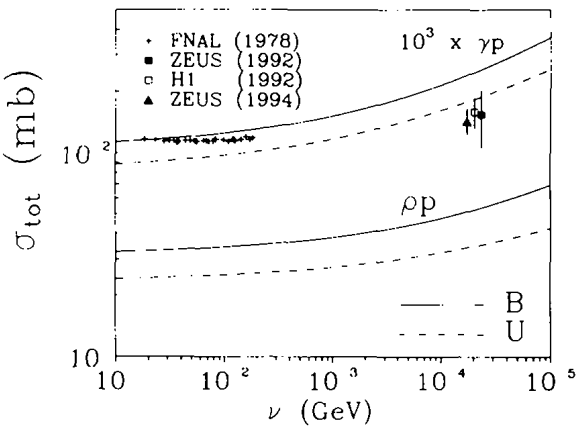

Fig. 3. The predicted energy dependence of the (B) bare and (U) unitarized total $\rho^0 p$ and real photoabsorption cross section. The data shown are from the HERA [6] and FNAL [21] experiments.

absolute normalization of the $\sigma^{(npt)}(r)$, at small energies it can be compensated for by upwards renormalization of the input $\sigma^{(npt)}(r)$. The energy dependent part of the unitarization correction is, however, the genuine effect and brings our results for $\sigma_{tot}(\gamma p)$ to a better agreement with the experiment [6]. The simple $\mathcal{K}$-matrix unitarization, as well as the eikonal unitarization, lacks the so-called triple-pomeron contribution, which enhances the effect of unitarization at high energies ([2,21] and references therein) and can tame the somewhat too rapid a growth of $\sigma_{tot}(\gamma p)$, a description of the low energy data [24] also can be augmented, by adding to the nonperturbative cross-section the Regge-behaving $\propto 1/\sqrt{\nu}$ terms [25]. However, the purpose of the present analysis is understanding the gross features of the BFKL phenomenology rather than fitting the low-Q^2 and low-energy experimental data. Recently, there was much discussion on the perturbative QCD contribution to the real photoabsorption cross section $\sigma_{tot}(\gamma p)$, in which the eikonal is evaluated with the BFKL cross section substituted for the inclusive minijet cross section ([27] and references therein) which is incorrect (for the related criticism see [28]).

In Fig. 4 we show how the unitarization affects the energy dependence of $d\sigma/dt|_{t=0}$ for the real photoproduction of the ρ^0 and J/Ψ. In the former case the scanning radius is large, $r_S \gtrsim 1$ f, in the latter case $r_S \sim 0.4$ f. We also show the unitarization effect for the virtual photoproduction of the longitudinally polarized ρ^0 meson at $Q^2 = 120$ GeV^2, appropriate for

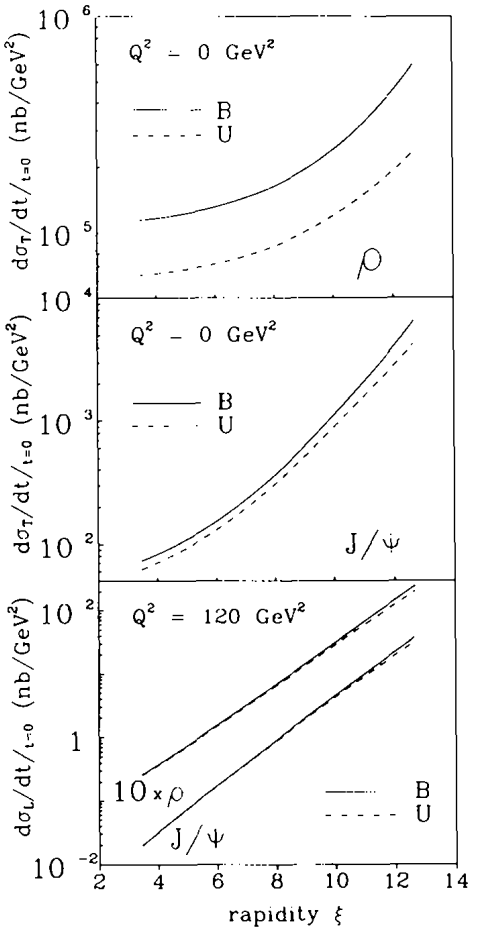

Fig. 4. The predicted energy (rapidity) dependence of the (B) bare and (U) unitarized differential cross section of forward real and virtual photoproduction of the ρ^0 and J/Ψ.

the scanning radius $r_S \sim r_\Delta \sim 0.15$ f. Notice a rapid decrease of the unitarization correction with the decrease of the scanning radius r_S.

For a crude estimate of elastic production cross section we can take $B(\rho^0) \approx 10$ GeV^2 [6] and $B(J/\Psi) \approx 4$ GeV^2 [28]. For the real photoproduction of the ρ^0 at $\sqrt{s} = \sqrt{2m_p\nu} = 200$ GeV, we find $\sigma(\gamma p \to \rho^0 p)/\sigma_{\rm tot}(\gamma p) = 0.085$ (for the bare, non-unitarized, cross sections this ratio equals 0.135), in good agreement with the ZEUS determination 0.1 ± 0.04 [6]. For the real photoproduction of the J/Ψ at $\nu = 150$ GeV we find $\sigma(\gamma p \to J/\Psi p) \sim 16$ nb, which agrees with the E687 result of 17.9 ± 4.0 nb at $\nu = 177$ GeV and 9.8 ± 2.9 nb at $\nu = 121$ GeV [29]. The rise of the J/Ψ production cross section with energy observed by E687 is also consistent with our prediction in Fig. 4. Our estimate for the real photoproduction of the J/Ψ at HERA at $\sqrt{s} = 200$ GeV, i.e., $\xi = 8.3$ is $\sigma_{\rm tot}(\gamma p \to J/\Psi p) \sim 90$ nb, i.e., we predict the five-fold increase from FNAL to HERA. Theoretical calculations of the forward production cross section are more straightforward and are free of uncertainties with the energy dependence of the diffraction slope, and it is very much desirable that the experimental data are presented in the form of $d\sigma/dt|_{t=0}$. More detailed comparison with the experiment will be presented elsewhere.

In Fig. 5 we present our predictions for the effective intercept

$$\Delta_{\rm eff}(\xi, Q^2) = \frac{1}{2}\frac{\partial \log(d\sigma/dt)|_{t=0})}{\partial \xi}$$

for the transverse and longitudinal polarizations of the J/Ψ and ρ^0. The rise of $\Delta_{\rm eff}(\xi, Q^2)$ with energy and Q^2 is an interplay of the BFKL perturbative and the nonperturbative cross section. On the other hand, for the J/Ψ and the longitudinally polarized ρ^0, at $Q^2 \approx C^2/r_\Delta^2 \sim (100\text{–}200)$ GeV^2 we predict the precocious BFKL behaviour $\Delta_{\rm eff}(\xi, Q^2) \approx \Delta_{I\!P}$. Such a behaviour of $\Delta_{\rm eff}(\xi, Q^2)$ is a very definitive prediction of our approach. Because of a large value of $C_T(\rho^0)$, in the transverse ρ^0 production the magic scanning radius $r_S \sim r_\Delta$ and $\Delta_{\rm eff}(\xi, Q^2) \approx \Delta_{I\!P}$ are not attainable even at $Q^2 \sim 200$ GeV^2. This prediction is difficult to test, though, because $\sigma_T \ll \sigma_L$. It is interesting that one has $r_S \sim r_\Delta$ also for the quasireal photoproduction of the $\Upsilon(1S)$, which reaction can even be favoured for the higher flux of quasireal photons. For the ρ^0 and J/Ψ production at large Q^2, the kinematical range of HERA corresponds to $\exp(-\xi) \approx x \gtrsim 10^{-5} \cdot (Q^2/\text{GeV}^2)$, in which region the unitarization effects can still be neglected. We emphasize that precisely the same approach with the same dipole cross section, gives a very good description of the HERA data on $F_2(x, Q^2)$ [14].

Within our lightcone formalism, the dipole cross section is a universal quantity, and all the dependence on the process is contained in wave functions of the initial and secondary particle. The point we wish to make is that once the different production processes $\gamma^* p \to V_i p$ are studied at values Q_i^2 so arranged as to have the same scanning radius r_S Eq. (4), then the production cross sections will exhibit identical energy

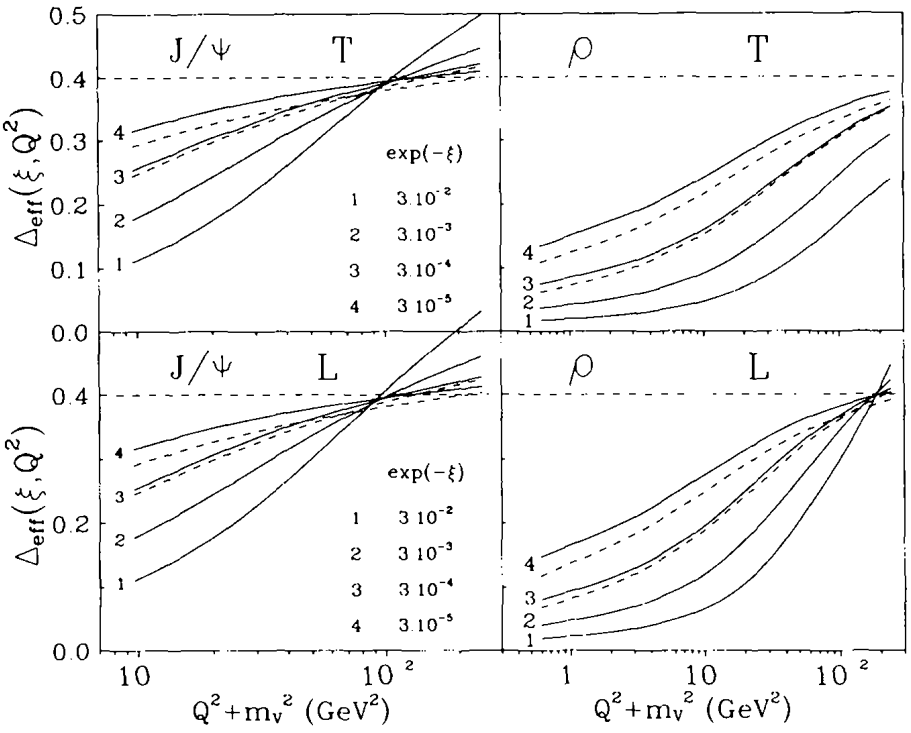

Fig. 5. The energy (rapidity) and Q^2 dependence of the effective intercept $\Delta_{\rm eff}(\xi, Q^2)$ for the forward production of the transverse and longitudinal ρ^0 and J/Ψ.

dependence. One must compare the cross sections at energy ν_i corresponding to the same rapidity ξ. For instance, we predict identical energy (ξ) dependence of the real photoproduction of the J/Ψ and of the virtual photoproduction of the longitudinal and transverse ρ^0 at $Q^2 \approx 20$ GeV^2 and $\approx$30 GeV^2, respectively. This rescaling from one vector meson to another constitutes an important cross-check of the whole formalism.

More predictions can be made, which are specific of the small gluon correlation radius $R_c = 0.3$ f. Namely for this reason, the perturbative BFKL cross section $\sigma^{(\rm pt)}(\xi, r)$ is concentrated at smaller r than the $\sigma^{(\rm npt)}(r)$, and the onset of the dominance of the BFKL cross section is followed by a change of the Q^2 dependence of the forward production cross section. In Fig. 6 we present our predictions for the energy dependence of

$$D_T = (m_V^2 + Q^2)^4 \cdot \left.\frac{d\sigma_T}{dt}\right|_{t=0},$$

$$D_L = (m_V^2 + Q^2)^4 \cdot \frac{m_V^2}{Q^2} \cdot \left.\frac{d\sigma_L}{dt}\right|_{t=0},$$

$$R = \frac{m_V^2}{Q^2}\frac{d\sigma(\gamma_L^* \to V_L)}{d\sigma(\gamma_T^* \to V_T)}.$$

The gradual rise of $D_{L,T}$ with Q^2 comes predominantly from the rising density of gluons, see Eq. (15). Notice, that the ratio $d\sigma_L/d\sigma_T$ rises much slower than Q^2/m_V^2 and exhibits a substantial energy dependence at fixed Q^2, which can be tested at HERA. We strongly advocate studying the Q^2 dependence at fixed rapidity ξ rather than the fixed energy ν.

Eqs. (15)–(17) show that the vector-meson production amplitude measures the dipole cross section $\sigma(\xi, r_S)$ and the gluon structure function of the proton. We wish to emphasize that this measurement is exceedingly sensitive to the $r_S - Q^2$ relationship. Typically, one will probe the gluon structure function $G(\xi, Q^2)$ at the factorization scale $q^2 \approx \tau(Q^2 + m_V^2)$, where

$$\tau_{T,L} \approx \frac{A}{C_{T,L}^2} \qquad (22)$$

In the range of $Q^2 \sim$ (10–100) GeV^2 of the practical interest, we find $\tau_{T,L}(J/\Psi) \sim 0.2$, $\tau_L(\rho^0) \sim 0.15$

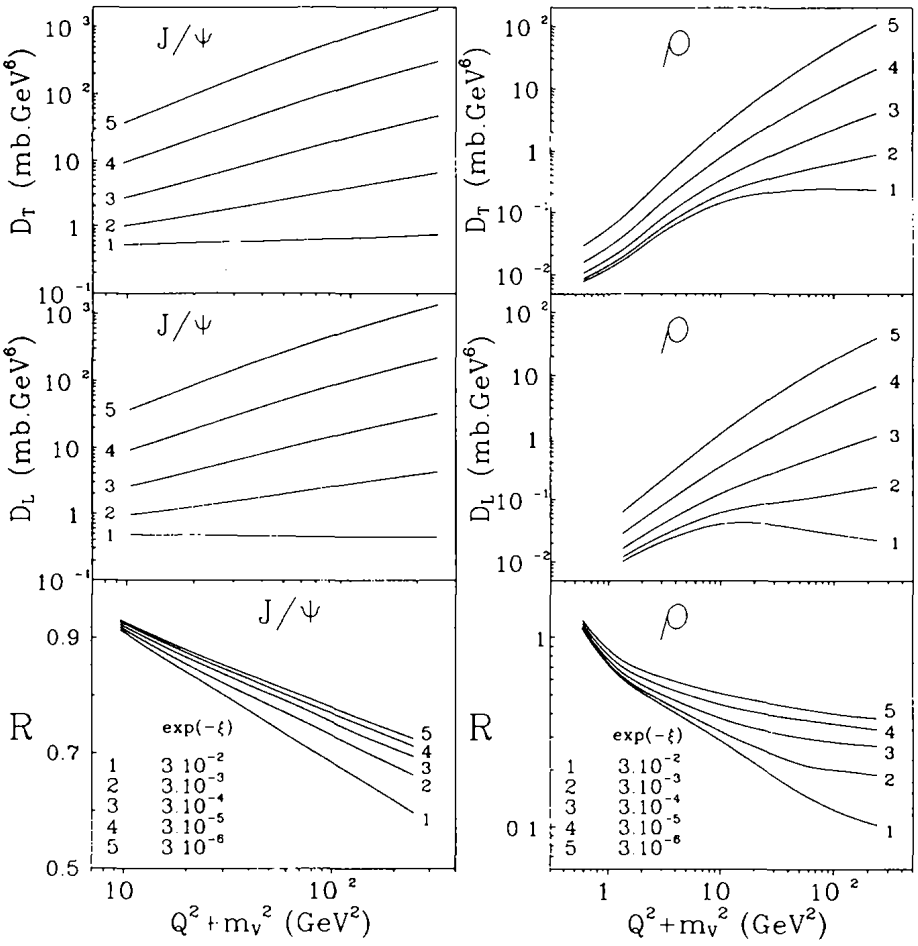

Fig. 6. Predictions for the Q^2 dependence of the differential cross section of forward production and the ratio of the longitudinal and transverse cross sections. Shown are the quantities $D_{T,L}$ and R defined in the text.

and $\tau_T(\rho^0) \sim (0.07\text{–}0.1)$. The emergence of such a dramatically small rescaling coefficients $\tau_{T,L}$ is a consequence of colour transparency. It was overlooked in [30], in which the proportionality of production amplitudes to the gluon density was discussed in a very different technique. We emphasize that the scale factor A in Eq. (15) is universal, only the scale factors $C_{T,L}$ depend on the amplitude and/or structure function calculated in terms of the dipole cross section [22].

A brief commment on the production of the $2S$ radial excitations ρ' and Ψ' is in order. The wave function of the $2S$ state has a node, because of which the corresponding weight function $W_{T,L}(Q^2, r^2)$ changes the sign at $r \sim R_V$. The resulting cancellations of the $r > R_V$ and $r < R_V$ contributions to the production amplitude (the node effect) lead to a strong suppression of the ρ'/ρ^0 and $\Psi'/(J/\Psi)$ production ratio [7–11]. With increasing energy and with the onset of the dominance of $\sigma^{(pt)}(\xi, r)$, which is concentrated at smaller r, the node effect will decrease. For instance, in the real photoproduction the $\Psi'/(J/\Psi)$ ratio is expected to increase by the factor $\sim$3 from the CERN/FNAL energies to the highest energies available at HERA [31]. The interesting possibility is that for the radially excited light mesons (ϕ', ω', ρ'), in the real photoproduction the V'/V ratio may exhibit the anomalous, nonmonotonic energy dependence, when this ratio first decreases with energy, and then starts increasing In the opposite to this, at large Q^2 such that $r_S \ll R_V$, the node effect disappears, and we expect $\rho'/\rho^0 \sim \Psi'/(J/\Psi) \sim 1$ over the whole

energy range.

Conclusions. The purpose of this paper was to examine how the dipole cross section $\sigma(\xi, r)$ is scanned in the virtual photoproduction of vector mesons. The BFKL dipole cross section, complemented by the nonperturbative dipole cross section at large r, gives the unified description of the photoproduction processes in the whole range of ν and Q^2, including the real photoproduction. The same dipole cross section gives a good description [14] of the proton structure function measured at HERA. Changing Q^2, one can probe the energy dependence of $\sigma(\xi, r)$ in a broad range of radii from the nonperturbative region of $r \sim 1$ f down to the perturbative domain of $r \ll 1$ f. One can zoom at the magic radius r_Δ and determine at HERA the pomeron intercept $\Delta_{\mathbf{P}}$, measuring the cross section of elastic $\rho^0, J/\Psi$ production at at $Q^2 \sim$ (100–200) GeV^2 and the quasireal photoproduction of the $\Upsilon(1S)$. We argued that this determination of $\Delta_{\mathbf{P}}$ is not affected by the unitarity corrections. We make a strong point that it is the dipole size r rather than the photon's virtuality Q^2, which controls the energy dependence of diffractive amplitudes: the value of Q^2 needed to scan the dipole cross section at the magic radius r_Δ strongly varies from the process to process, c.f. the discussion in [15]. We predict very specific variation with energy of the Q^2 dependence of elastic production cross section and of the L/T ratio, which derive from the small correlation radius for perturbative gluons $R_c \sim 0.3$ f. Elastic production is found to probe the gluon structure function of the proton at an anomalously small factorization scale.

References

[1] E.A. Kuraev, L.N. Lipatov and V.S. Fadin, Sov. Phys. JETP 44 (1976) 443; 45 (1977) 199;
Ya.Ya. Balitskii and L.N. Lipatov, Sov. J. Nucl. Phys. 28 (1978) 822;
L.N. Lipatov, Sov. Phys. JETP 63 (1986) 904; Pomeron in Quantum Chromodynamics. In: Perturbative Quantum Chromodynamics, editor A.H. Mueller, World Scientific, 1989.

[2] N. Nikolaev and B.G. Zakharov, JETP 78 (1994) 598; The triple-pomeron regime and the structure function of the pomeron in the diffractive deep inelastic scattering at very small x, Landau Inst. preprint Landau-16/93 and Jülich preprint KFA-IKP(Th)-1993-17, June 1993, to appear in Z. Phys. C (1994).

[3] N.N. Nikolaev, B.G. Zakharov and V.R. Zoller, JETP Letters 59 (1994) 8.

[4] N.N. Nikolaev, B.G. Zakharov and V.R. Zoller, The BFKL and GLDAP regimes for the perturbative QCD pomeron, Jülich preprint KFA-IKP(TH)-1994-02, January 1994; JETP 78(6) (1994) xxx.

[5] M. Derrick et al., ZEUS Collaboration, Phys. Lett. B (1993); I. Abt et al., H1 Collaboration, Nucl. Phys. B 407 (1993) 515.

[6] ZEUS Collaboration: M. Derrick et al., DESY 94-032 (1994); Phys. Lett. B 293 (1992) 465;
H1 Collaboration: T. Ahmed et al., Phys. Lett. B 299 (1993) 374.

[7] N.N. Nikolaev, Comments on Nucl. Part. Phys. 21 (1992) 41.

[8] B.Z. Kopeliovich and B.G. Zakharov, Phys. Rev. D 44 (1991) 3466.

[9] O. Benhar, B.Z. Kopeliovich, C. Mariotti, N.N. Nikolaev and B.G. Zakharov, Phys. Rev. Lett. 69 (1992) 1156.

[10] B.Z. Kopeliovich, J. Nemchik, N.N. Nikolaev and B.G. Zakharov, Phys. Lett. B 309 (1993) 179.

[11] B.Z. Kopeliovich, J. Nemchik, N.N. Nikolaev and B.G. Zakharov, Phys. Lett. B 324 (1994) 469.

[12] N.N. Nikolaev, B.G. Zakharov and V.R. Zoller, Phys. Lett. B 328 (1994) 486.

[13] N.N. Nikolaev and B.G. Zakharov, Phys. Lett. B 327 (1994) 157.

[14] N.N. Nikolaev and B.G. Zakharov, Phys. Lett. B 327 (1994) 149.

[15] N.N. Nikolaev and B.G. Zakharov, Phys. Lett. B 333 (1994) 250.

[16] J. Nemchik, N.N. Nikolaev and B.G. Zakharov, paper in preparation.

[17] N.N. Nikolaev and B.G. Zakharov, Z. Phys. C 49 (1991) 607; C 53 (1992) 331.

[18] M.V. Terentiev, Sov. J. Nucl. Phys. 24 (1976) 106.

[19] C. Quigg and J.L. Rosner, Phys. Rep. C 56 (1979) 167.

[20] V. Barone, M. Genovese, N.N. Nikolaev, E. Predazzi and B.G. Zakharov, Z. Phys. C 58 (1993) 541; Int. J. Mod. Phys. A 8 (1993) 2779.

[21] V. Barone, M. Genovese, N.N. Nikolaev, E. Predazzi and B.G. Zakharov, Phys. Lett. B 326 (1994) 161.

[22] N.N. Nikolaev and B.G. Zakharov, Phys. Lett. B 332 (1994) 184.

[23] V. Barone, M. Genovese, N.N. Nikolaev, E. Predazzi and B.G. Zakharov, Phys. Lett. B 304 (1993) 176.

[24] D.O. Caldwell et al., Phys. Rev. Lett. 40 (1978) 1222.

[25] A. Donnachie and P.V.L. Landshoff, Phys. Lett. B 296 (1992) 227.

[26] B.Z. Kopeliovich, N.N. Nikolaev and I.K. Potashnikova, Phys. Rev. D 39 (1989) 769.

[27] J.R. Forshaw and J.K. Storrow, Phys. Lett. B 321 (1994) 151.

[28] N.N. Nikolaev, Elastic and Diffractive Scattering: 3-d Blois Workshop, Nucl. Phys. B (Proc. Suppl.) 12 (1990) 93.

[29] P.L. Frabetti et al., Phys. Lett. B 316 (1993) 197.

[30] M.G. Ryskin, Z. Phys. C 57 (1993) 89;
S.J. Brodsky et al., SLAC-PUB-6412R (1994).

[31] J. Nemchik, N.N. Nikolaev and B.G. Zakharov, paper in preparation.

ELSEVIER

2 May 1996

PHYSICS LETTERS B

Physics Letters B 374 (1996) 199–204

Color dipole systematics of diffractive photo- and electroproduction of vector mesons

J. Nemchik [a,b,1], N.N. Nikolaev [c,d], E. Predazzi [a], B.G. Zakharov [a,d]

[a] *Dipartimento di Fisica Teorica, Università di Torino, and INFN, Sezione di Torino, I-10125, Torino, Italy*

[b] *Institute of Experimental Physics, Slovak Academy of Sciences, Watsonova 47, 04353 Kosice, Slovak Republik*

[c] *IKP(Theorie), KFA Jülich, 5170 Jülich, Germany*

[d] *L. D. Landau Institute for Theoretical Physics, GSP-1, 117940, ul. Kosygina 2, Moscow 117334, Russia*

Received 20 October 1995

Editor: R. Gatto

Abstract

We present the first evaluation of the color dipole cross section from experimental data on diffractive photo- and electroproduction of vector mesons. The dipole size and energy dependence of the found dipole cross section are consistent with expectations from the BFKL dynamics.

In the color dipole picture of high energy scattering [1–4] the dipole cross section is as fundamental a quantity as the low x gluon structure function of the proton in the conventional parton model. The diffractive electroproduction of vector mesons

$$\gamma^* p \to Vp\,, \qquad V = \rho^0, \omega^0, \phi^0, J/\Psi, \Upsilon \tag{1}$$

offers a unique window on the dipole cross section [5–7]. Here the crucial point is that for the shrinkage of the transverse size of the virtual photon with virtuality Q^2, the $1S$ vector meson production amplitude probes the dipole cross section at the dipole size $r \sim r_S$, where the scanning radius equals [8,9]

$$r_S = \frac{A}{\sqrt{m_V^2 + Q^2}} \tag{2}$$

with $A = 6$. Specifically, the amplitudes of production of the transversely (T) and longitudinally (L) polarized $1S$ vector mesons are of the form [8,9]

$$\mathcal{M}_T \propto r_S^2 \sigma(x_{\rm eff}, r_S), \quad \mathcal{M}_L \approx \frac{\sqrt{Q^2}}{m_V}\mathcal{M}_T,$$

and one can extract the dipole cross section from the vector meson production cross sections. For the alternative description of vector meson production at very large Q^2 in terms of the gluon structure function of the proton see [10,11].

In the present communication we report the results of the first evaluation of the color dipole cross section from the experimental data on real photoproduction and electroproduction of the ρ^0, ϕ^0 and J/Ψ from the fixed target and HERA collider experiments. A nice consistency with color blindness of the dipole cross section is found. When one takes the same value of the scanning radius, the ρ^0, ϕ^0 and J/Ψ production data yield close values of the dipole cross section. The

[1] E-mail: nemchik@to.infn.it.

PII 0370-2693(96)00153-0

results of the HERA experiments allow the first evaluation of energy dependence of the dipole cross section at different dipole sizes and confirm the prediction from BFKL dynamics that the smaller the dipole size, the faster the increase of the dipole cross section [3,12].

One needs the probability amplitudes to find color dipole of size r in the photon and vector meson. Here we use the formalism introduced in [1,5] and expounded in [9]. The spin independence of the dipole cross section leads to the s-channel helicity conservation. In terms of the light-cone "radial" wave function $\phi(r,z)$ of the $q\bar{q}$ Fock state of the vector meson and the color dipole cross section $\sigma(\nu,r)$, the imaginary part of the forward production amplitudes equals

$$\begin{aligned}
\mathrm{Im}\,\mathcal{M}_T(x_{\rm eff},Q^2) &= \frac{N_c C_V\sqrt{4\pi\alpha_{\rm em}}}{(2\pi)^2}\\
&\times\int d^2r\sigma(x_{\rm eff},r)\int_0^1\frac{dz}{z(1-z)}\\
&\times\Big\{m_q^2K_0(\varepsilon r)\phi(r,z)\\
&-[z^2+(1-z)^2]\varepsilon K_1(\varepsilon r)\partial_r\phi(r,z)\Big\}\\
&=\frac{1}{(m_V^2+Q^2)^2}\int\frac{dr^2}{r^2}\frac{\sigma(x_{\rm eff},r)}{r^2}W_T(Q^2,r^2)\\
&=g_T\sqrt{4\pi\alpha_{\rm em}}C_V\sigma(x_{\rm eff},r_S)\frac{m_V^2}{m_V^2+Q^2} \qquad (3)
\end{aligned}$$

$$\begin{aligned}
\mathrm{Im}\,\mathcal{M}_L(x_{\rm eff},Q^2) &= \frac{N_c C_V\sqrt{4\pi\alpha_{\rm em}}}{(2\pi)^2}\frac{2\sqrt{Q^2}}{m_V}\\
&\times\int d^2r\sigma(x_{\rm eff},r)\int_0^1 dz\\
&\times\Big\{[m_q^2+z(1-z)m_V^2]K_0(\varepsilon r)\phi(r,z)\\
&-\varepsilon K_1(\varepsilon r)\partial_r\phi(r,z)\Big\}\\
&=\frac{\sqrt{Q^2}}{m_V(m_V^2+Q^2)^2}\int\frac{dr^2}{r^2}\frac{\sigma(x_{\rm eff},r)}{r^2}W_L(Q^2,r^2)\\
&=g_L\sqrt{4\pi\alpha_{\rm em}}C_V\sigma(x_{\rm eff},r_S)\frac{\sqrt{Q^2}}{m_V}\frac{m_V^2}{m_V^2+Q^2}, \qquad (4)
\end{aligned}$$

where $\boldsymbol{r}$ is the transverse $q\bar{q}$ separation in the light-cone meson, i.e., the dipole size, z is the fraction of the momentum of the meson carried by the quark,

$$\varepsilon^2=m_q^2+z(1-z)Q^2, \qquad (5)$$

$N_c=3$ is the number of colors, $C_V=\frac{1}{\sqrt{2}},\frac{1}{3\sqrt{2}},\frac{1}{3},\frac{2}{3}$ for the ρ^0, ω^0, ϕ^0, J/Ψ production, respectively, $K_{0,1}(x)$ is the modified Bessel function. In (3), (4) the dipole cross section enters at an effective value of the Bjorken variable

$$x_{\rm eff}=\frac{Q^2+m_V^2}{2m_p\nu}. \qquad (6)$$

The normalization of production amplitudes is such that

$$\left.\frac{d\sigma}{dt}\right|_{t=0}=\frac{|\mathcal{M}|^2}{16\pi}. \qquad (7)$$

Eqs. (3), (4) give the imaginary part of production amplitudes, one can easily include small corrections for the real part by the substitution [13]

$$\begin{aligned}
\sigma(x_{\rm eff},r)&\Rightarrow\left(1-i\frac{\pi}{2}\frac{\partial}{\partial\log x_{\rm eff}}\right)\sigma(x_{\rm eff},r)\\
&=\Big[1-i\alpha_V(x_{\rm eff},r)\Big]\sigma(x_{\rm eff},r) \qquad (8)
\end{aligned}$$

Many gluon containing higher Fock states $q\bar{q}g...$ are very important at high energy ν. The crucial point is that in leading log $\frac{1}{x}$ their effect can be reabsorbed into the energy dependence of $\sigma(x,r)$, which satisfies the generalized BFKL equation ([2,3], for the related approach see also [4]). The color dipole factorization formulas (3), (4) follow from diagonalization of the scattering matrix in the $(\boldsymbol{r},z)$ representation. Clearly, this factorization holds even when the dipole size is large, beyond the perturbative region of small sizes. Only the wave function of the lowest $q\bar{q}$ Fock state enters the color dipole factorization (3), (4) formulas. At large dipole size r one can identify $\phi(r,z)$, which is the probability amplitude to find the dipole of size r, with the constituent quark wave function of the meson and to develop a viable phenomenology of diffractive scattering which is purely perturbative for small size mesons and allows a sensible interpolation between soft interactions for large dipoles and hard

Table 1
Values of the parameters R^2, C and m_q of the wave function of vector mesons [9]

Parameter	ρ^0	ϕ^0	J/Ψ	Υ
R^2 [fm^2]	1.370	0.690	0.135	0.015
C	0.360	0.530	1.130	1.990
m_q [GeV]	0.150	0.300	1.300	5.000

perturbative interactions of small dipoles. Here the key property is the flavour independence of the pomeron exchange dipole cross section. The detailed description of parameterization of $\phi(r,z)$, which incorporates the hard-QCD short distance behaviour, is given in [9]. The parameters of the wave function were constrained to reproduce the generally accepted radii of vector mesons and the width of leptonic decays $V \to e^+e^-$, they are listed in Table 1.

Eqs. (3), (4) describe the pure pomeron exchange, which dominates at large values of the Regge parameter $\omega = 1/x_{\rm eff}$. At moderate values of $\omega = 1/x_{\rm eff}$ a substantial part of the γp total cross section is due to the non-vacuum Reggeon exchange contribution. For instance, the Regge fit to the γp total cross section can be cast in the form [14]

$$\sigma_{\rm tot}(\gamma p) = \sigma_{I\!P}(\gamma p)\left(1+\frac{A}{\omega^{\Delta}}\right) \qquad (9)$$

where the term A/ω^{Δ} in the factor $f = 1 + A/\omega^{\Delta}$ represents the non-vacuum Reggeon exchange contribution, the Donnachie-Landshoff fit gives $A = 2.332$ and $\Delta = 0.533$. The similar Regge correction emerges also in real ρ^0 photoproduction amplitude. We do not know how large this non-vacuum contribution to the ρ^0 production is at large Q^2, for the crude estimation we assume that the Reggeon/pomeron ratio scales with ω, which is not inconsistent with the known decomposition of the proton structure function into the valence (non-vacuum Reggeon) and sea (pomeron) contributions. Then, for the NMC kinematics we find $f = 1.25$ at $\omega \simeq 70$ relevant to $Q^2 = 3\,{\rm GeV}^2$ and $f = 1.8$ at $\omega \simeq 9$ relevant to $Q^2 = 20\,{\rm GeV}^2$. For the HERA energy range the non-vacuum Reggeon exchange contribution can be neglected due to a large value of the Regge parameter ω. In practical terms, we calculate the quantity

$$d\sigma(\gamma^* \to V)/dt|_{t=0} = f^2 d\sigma_{I\!P}(\gamma^* \to V)/dt|_{t=0}.$$

For the Zweig rule, one expects $f = 1$ for the $\phi^0, J/\Psi, \Upsilon$ production.

In the final form of amplitudes in (3), (4) we separated out the rapid dependence on Q^2 and/or scanning radius r_S, and the so introduced coefficient functions $g_{T,L}$ are smooth functions of Q^2. The possibility of such a local relationship between the production amplitude and the dipole cross section at a well defined dipole size r_S is based on two observations:

i) the weight functions $W_{T,L}(Q^2,r^2)$ have a sharp peak at $r = A_{T,L}/\sqrt{Q^2+m_V^2}$ with $A_{T,L} \sim 6$ [9],

ii) the ratio $\sigma(x_{\rm eff},r)/r^2$ is a smooth function of the radius [3,12].

For these reasons, the coefficient functions $g_{T,L}$ have only a weak sensitivity to the detailed shape of the dipole cross section. The gross features of $\sigma(x_{\rm eff},r)$ are well understood and in [15] good quantitative description of the small-x structure function of the proton was obtained in the color dipole BFKL dynamics. The model dependence of $g_{T,L}$ can be evaluated using the low-energy and high-energy forms of $\sigma(x_{\rm eff},r)$ described in [15,9], which have a markedly different r dependence. In Fig. 1 we present the Q^2 dependence of $g_{T,L}$ for different production processes at $W = 15\,{\rm GeV}$ and $W = 150\,{\rm GeV}$ (values of interest for the fixed target and HERA experiments respectively). The variation of the resulting coefficient functions $g_{T,L}$ from small to large W does not exceed 15%, which is a conservative estimate of the theoretical uncertainty of the above procedure. The residual smooth Q^2 dependence of $g_{T,L}$ mostly reflects the smooth and well understood Q^2 dependence of the scale factors $A_{T,L}$ which enter the relationship between the position $A_{T,L}/\sqrt{Q^2+m_V^2}$ of the peak of $W_{T,L}(Q^2,r^2)$ and r_S as given by Eq. (2) (see also the discussion in [9]). In (3), (4), the $g_{T,L}$ are so defined as to relate the amplitude to $\sigma(x_{\rm eff},r_S)$ at the well defined scanning radius (2), reabsorbing the effect of small departure of $A_{T,L}$ from 6 into $g_{T,L}$.

The experimentally measured forward cross production section section equals

$$\frac{d\sigma(\gamma^* \to V)}{dt}|_{t=0} = \frac{f^2}{16\pi}\left[(1+\alpha_{V,T}^2)\mathcal{M}_T^2 + \epsilon(1+\alpha_{V,L}^2)\mathcal{M}_L^2\right] \qquad (10)$$

The difference between $\alpha_{V,L}$ and $\alpha_{V,T}$ for the longitudinal and transverse cross sections and the overall ef-

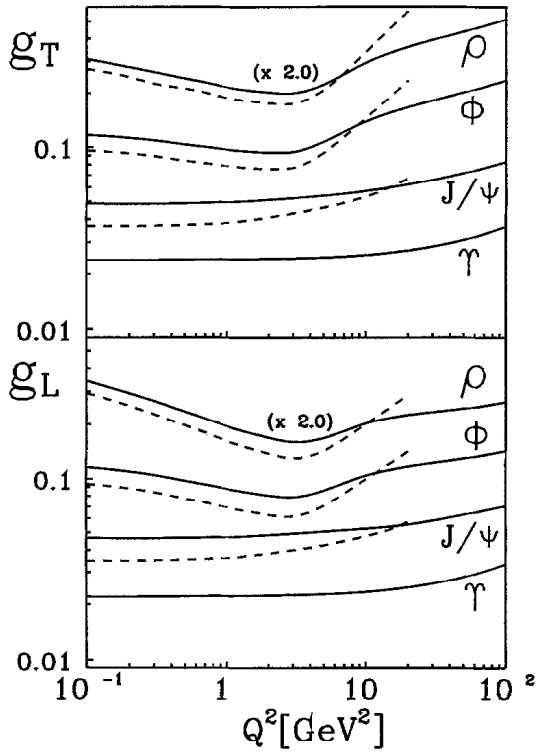

Fig. 1. The Q^2 dependence of the coefficient functions $g_{T,L}$ at $W = 15$ GeV (dashed curve) and $W = 150$ GeV (solid curve).

fect of the real part is marginal and can safely be neglected compared to other uncertainties. Then, making use of the so determined $g_{T,L}$, in terms of the experimentally measured forward production cross section we can write using Eq. (3), (4), (7) and (10)

$$\sigma(x_{\rm eff}, r_S) = \frac{1}{f}\frac{1}{C_V}\frac{Q^2+m_V^2}{m_V^2}\frac{2}{\sqrt{\alpha_{\rm em}}} \times \left(g_T^2 + \epsilon\, g_L^2 \frac{Q^2}{M_V^2}\right)^{-1/2} \times \left(1+\alpha_V^2\right)^{-1/2} \sqrt{\left.\frac{d\sigma(\gamma^* \to V)}{dt}\right|_{t=0}} \qquad (11)$$

Here ϵ is the longitudinal polarization of the photon, the values of which are taken from the corresponding experimental publications. In (11) f is the above discussed factor which accounts for the non-vacuum Reggeon contribution to the ρ^0 production, for the ϕ^0 and J/Ψ production, $f \equiv 1$. In the case that the experimental data are presented in the form of the t-integrated cross section, we evaluate

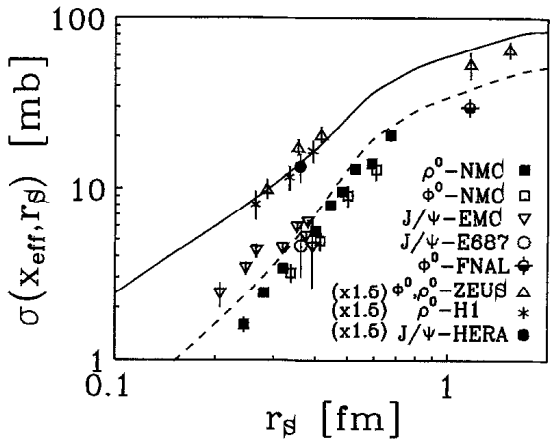

Fig. 2. The dipole size dependence of the dipole cross section extracted from the experimental data on photoproduction and electroproduction of vector mesons: the NMC data on ϕ^0 and ρ^0 production [18], the EMC data on J/Ψ production [23,25], the E687 data on J/Ψ production [24], the FNAL data on ρ^0 production [16], the ZEUS data on ρ^0 production [20–22], the ZEUS data on ϕ^0 production [17], the H1 data on ρ^0 production [19] and the average of the H1 and ZEUS data on J/Ψ production [26,27]. The dashed and solid curve show the dipole cross section of the model [15,9] evaluated for the c.m.s. energy $W = 15$ and $W = 70$ GeV respectively. The data points at HERA energies and the corresponding solid curve are multiplied by the factor 1.5.

$$\left.\frac{d\sigma(\gamma^* \to V)}{dt}\right|_{t=0} = B\sigma_{\rm tot}(\gamma^* \to V)$$

using the diffraction slope B as cited in the same publication. In Fig. 2 we show the results of such analysis of the low energy [16] and ZEUS [17] data on real photoproduction of the ϕ^0, the NMC data [18] on electroproduction of the ρ^0 and ϕ^0, the HERA results on real and virtual photoproduction of the ρ^0 (H1 [19], ZEUS [20–22]), fixed target data on real photoproduction [23,24] and electroproduction [25] of the J/Ψ and HERA results on real photoproduction of the J/Ψ (H1 [26], ZEUS [27]). The error bars shown here correspond to the error bars in the measured cross sections as cited in the experimental publications. The experimental data on vector meson production fall into the two broad categories: the fixed target data taken at typical center of mass energy $W \sim$(10–15) GeV and the HERA collider data taken at $W \sim$(70–150) GeV. The color dipole cross section is flavour blind, there is only kinematical dependence on the vector meson through the definition of $x_{\rm eff}$. However, if different reactions are compared at the same value of the scanning radius r_S, i.e., at the same value of $Q^2 + m_V^2$, then at

the fixed energy ν the corresponding values of $x_{\rm eff}$ are equal. Consequently, we expect that within each data group, the procedure (11) applied to different vector mesons will yield the same value of $\sigma(x_{\rm eff}, r_S)$ at the same value of r_S. This is an important consistency check. The experimental data on the vector meson production give a solid evidence for the decrease of the dipole cross section towards small dipole size r_S. The fixed target data exhibit a decrease of $\sigma(x_{\rm eff}, r_S)$ by one order in the magnitude from $r_S \approx 1.2$ fm in real photoproduction of the ϕ^0 down to $r_S \approx 0.24$ fm in electroproduction of the ρ^0 at $Q^2 = 23\,{\rm GeV}^2$ and of the J/Ψ at $Q^2 = 13\,{\rm GeV}^2$. In the region of overlapping values of r_S there is a remarkable consistency between the dipole size dependence and also absolute values of the dipole cross section determined from the data on the ρ^0, ϕ^0 and J/Ψ production, in agreement with the flavour independence of the dipole cross section.

The high energy data from HERA exhibit a decrease of the dipole cross section by the factor ~6–7 from $r_S = 1.5$ fm in real photoproduction of the ρ^0 down to $r_S = 0.26$ fm in electroproduction of the ρ^0 at $Q^2 = 19.5\,{\rm GeV}^2$. A comparison of the fixed-target and HERA data on real photoproduction and electroproduction confirms the prediction [3,12,9] of faster growth of the dipole cross section at smaller dipole size, although the error bars are still large.

The above determination of $\sigma(x_{\rm eff}, r_S)$ is rather crude for the several reasons.

i) First, the early EMC data on vector meson production are well known to have been plagued by a background from the inelastic process $\gamma^* p \to VX$. A comparison of the more recent NMC [18] and the EMC data [28] on the ρ^0 production suggests that the inelastic admixture could have enhanced the observed cross section by as large factor as ~ 3 at $Q^2 = 17\,{\rm GeV}^2$. Such an uncertainty would have resulted in overestimation of $\sigma(x_{\rm eff}, r_S)$ by the factor ~ 1.8. This may be an origin of slightly larger values of $\sigma(x_{\rm eff}, r_S)$ deduced from the EMC data [25] on the J/Ψ electroproduction. Also the scattering of the measured J/Ψ photoproduction cross sections is quite large, $\sim 50\%$. Still, this factor of 2 uncertainty is much smaller than the more than one order in magnitude variation of $\sigma(x_{\rm eff}, r_S)$ over the considered span in r_S. In the recent NMC data [18] a special care has been taken to eliminate an inelastic background and the values of $\sigma(x_{\rm eff}, r_S)$ from the ρ^0 and ϕ^0 production data are consistent within the experimental error bars.

ii) There are further uncertainties with the value of the diffraction slope B. At large Q^2, the values of B could have been underestimated due to the same inelastic background. Even in the better quality data, there are uncertainties with extrapolation down to $t = 0$. Because of the curvature of the diffraction cone, one may somewhat underestimate the forward cross section. The experimental situation with the diffraction slopes is quite unsatisfactory, in the case of the J/Ψ and at large Q^2 for light vector mesons even the $\sim 50\%$ uncertainty cannot be excluded at the moment. However, this uncertainty in the diffraction slope corresponds to $\lesssim 25\%$ uncertainty in our evaluation of $\sigma(x_{\rm eff}, r_S)$, which is sufficient for the purposes of the present exploratory evaluation of $\sigma(x_{\rm eff}, r_S)$.

iii) There is also the above evaluated conservative $\lesssim 15\%$ theoretical inaccuracy of our procedure.

iv) Finally, there is a residual uncertainty with the wave function of light vector mesons. As a matter of fact, if the dipole cross section were known, then diffractive $\gamma^* p \to Vp$ must be regarded as a local probe of the wave function of vector mesons at $r \approx r_S$ [7], which may eventually become one of applications of vector meson production. To this end, the consistency of $\sigma(x_{\rm eff}, r)$ determined from different reactions indicates that wave functions of vector mesons are reasonably constrained by the leptonic width. Here we only wish to notice that at high Q^2 and small scanning radius, the vector meson production cross section is $\propto \Gamma(V \to e^+e^-)$ and even the factor 2 uncertainty in this quantity corresponds to only $\lesssim 40\%$ uncertainty in the determination of the dipole cross section.

To summarize, within the above stated uncertainties of our simple procedure and the experimental error bars, there is a consistency between the dipole cross section determined from the ρ^0 ϕ^0 and J/Ψ production data. This is the first direct determination of the dipole cross section from the experimental data and our main conclusions on properties of the dipole cross section are not affected by the above cited uncertainties.

In Fig. 2 we show also the dipole cross section from the BFKL analysis [15,9], which gives a good quantitative description of structure function of the photon at small x. We conclude that the color dipole BFKL dynamics provides a unified description of the experimental data on diffractive production of vector mesons and on the proton structure function.

Conclusions. We presented the first determination of the dipole cross section from the experimental data on diffractive production of vector mesons. We evaluated the color dipole cross section $\sigma(x_{\rm eff}, r_S)$ at dipole size r_S down to $r_S \approx 0.2$ fm and confirmed the theoretically expected rapid decrease of $\sigma(x_{\rm eff}, r_S)$ towards small r_S. We found a remarkable consistency between the absolute value and the dipole size and energy dependence of the dipole cross section extracted from the data on different vector mesons. This constitutes an important cross-check of the color dipole picture of the QCD pomeron. The found pattern of the energy dependence of the dipole cross section is consistent with the flavour independence and with expectations from the BFKL dynamics.

This work was partly supported by the INTAS grant No. 93-239.

References

[1] N.N. Nikolaev and B.G. Zakharov, Z. Phys. C 49 (1991) 607; C 53 (1992) 331.
[2] N. Nikolaev and B.G. Zakharov, JETP 78 (1994) 598; Z. Phys. C 64 (1994) 631.
[3] N.N. Nikolaev, B.G. Zakharov and V.R. Zoller, JETP Lett. 59 (1994) 8; JETP 78 (1994) 866; Phys. Lett. B 328 (1994) 486.
[4] A.E. Mueller and H. Patel, Nucl. Phys. B 425 (1994) 471.
[5] B.Z. Kopeliovich and B.G. Zakharov, Phys. Rev. D 44 (1991) 3466.
[6] N.N. Nikolaev, Comments on Nucl. Part. Phys. 21 (1992) 41.
[7] B.Z. Kopeliovich, J. Nemchik, N.N. Nikolaev and B.G. Zakharov, Phys. Lett. B 309 (1993) 179.
[8] B.Z. Kopeliovich, J. Nemchik, N.N. Nikolaev and B.G. Zakharov, Phys. Lett. B 324 (1994) 469.
[9] J. Nemchik, N.N. Nikolaev and B.G. Zakharov, Phys. Lett. B 341 (1994) 228.
[10] M.G. Ryskin, Z. Phys. C 57 (1993) 89.
[11] S.J. Brodsky et al., Phys. Rev. D 50 (1994) 3134.
[12] N.N. Nikolaev and B.G. Zakharov, Phys. Lett. B 327 (1994) 157.
[13] V.N. Gribov, A.A. Migdal, Sov. J. Nucl. Phys. 8 (1969) 703.
[14] A. Donnachie and P.V.L. Landshoff, Phys. Lett. B 296 (1992) 227; B 348 (1995) 213.
[15] N.N. Nikolaev and B.G. Zakharov, Phys. Lett. B 327 (1994) 149.
[16] J. Busenitz et al., Phys. Rev. D 40 (1989) 40 and references therein.
[17] ZEUS Collab., M. Derrick et al., Elastic Photoproduction of ω, ϕ and ρ' mesons at HERA, presented on Int. Europhys. Conf. on HEP, Brussels, July 27–August 2, 1995, paper EPS-0389.
[18] NMC Collab., M. Arneodo, et al., Nucl. Phys. B 429 (1994) 503.
[19] H1 Collab., T. Ahmed et al., Exclusive ρ^0 Production in Deep-inelastic Scattering Events at HERA, presented on Int. Europhys. Conf. on HEP, Brussels, July 27–August 2, 1995, paper EPS-0490.
[20] ZEUS Collab., M. Derrick et al., Z. Phys. C 63 (1994) 391.
[21] ZEUS Collab., M. Derrick et al., DESY 95-143, submitted to Z. Phys. C (1995).
[22] ZEUS Collab., M. Derrick et al., Phys. Lett. B 356 (1995) 601.
[23] EMC Collab., J.J. Aubert et al., Phys. Lett. B 89 (1980) 267.
[24] L. Frabetti et al., Phys. Lett. B 316 (1993) 197.
[25] EMC Collab., J.J. Aubert et al., Nucl. Phys. B 213 (1983) 1; J. Ashman et al.,Z. Phys. C 39 (1988) 169.
[26] H1 Collab., T. Ahmed et al., Phys. Lett. B 338 (1994) 507.
[27] ZEUS Collab., M. Derrick et al., Phys. Lett. B 350 (1995) 120.
[28] EMC Collab., J.J. Aubert et al., Phys. Lett. B 161 (1985) 203.

Z. Phys. C 75, 71–87 (1997)

ZEITSCHRIFT
FÜR PHYSIK C

Color dipole phenomenology of diffractive electroproduction of light vector mesons at HERA

J. Nemchik[1,2], N.N. Nikolaev[3,4], E. Predazzi[1], B.G. Zakharov[1,4]

[1] Dipartimento di Fisica Teorica, Università di Torino, and INFN, Sezione di Torino, I-10125 Torino, Italy (e-mail: nemchik@to.infn.it; predazzi@to.infn.it)
[2] Institute of Experimental Physics, Slovak Academy of Sciences, Watsonova 47, 04353 Kosice, Slovak Republik
[3] IKP(Theorie), KFA Jülich, D-5170 Jülich, Germany (e-mail: kph154@aix.sp.kfa-juelich.de)
[4] L. D. Landau Institute for Theoretical Physics, GSP-1, 117940, ul. Kosygina 2, Moscow 117334, Russia (e-mail: bgz@landau.ac.ru)

Received: 18 November 1995 / Revised version: 22 April 1996

Abstract. We develop the color dipole phenomenology of diffractive photo- and electroproduction $\gamma^* N \to V(V')N$ of light vector mesons ($V(1S) = \phi^0, \omega^0, \rho^0$) and their radial excitations ($V'(2S) = \phi', \omega', \rho'$). The node of the radial wave function of the $2S$ states in conjunction with the energy dependence of the color dipole cross section is shown to lead to a strikingly different Q^2 and ν dependence of diffractive production of the $V(1S)$ and $V'(2S)$ vector mesons. We discuss the restoration of flavor symmetry and universality properties of production of different vector mesons as a function of $Q^2 + m_V^2$. The color dipole model predictions for the ρ^0 and ϕ^0 production are in good agreement with the experimental data from the EMC, NMC, ZEUS and H1 collaborations. We present the first direct evaluation of the dipole cross section from these data.

1 Introduction

Diffractive electroproduction of vector mesons

$$\gamma^* p \to Vp\,, \qquad V = \rho^0,\, \omega^0,\, \phi^0,\, J/\Psi,\, \Upsilon \tag{1}$$

at high energy ν offers a unique possibility of studying the pomeron exchange at high energies [1–8]. Particularly important is the observation that the transverse size of the photon shrinks with the increase of its virtuality Q^2. This property can conveniently be quantified in the mixed $(\mathbf{r}, z)$ light-cone technique [9, 10], in which the high energy hadrons and photons are described as systems of color dipoles with the transverse size $\mathbf{r}$ frozen during the interaction process. The interaction of color dipoles with the target nucleon is quantified by the color dipole cross section $\sigma(\nu, r)$ whose evolution with the energy ν is described by the generalized BFKL equation [10, 11] (for a related approach see also [12]). The shrinkage of the photon with Q^2 together with the small-size behavior of the dipole cross section ($\sim r^2$) leads to what has come to be known as the *scanning phenomenon* [4–6]: the $V(1S)$ vector meson production amplitude is dominated by the contribution from the dipole cross section at the dipole size $r \sim r_S$, where r_S is the scanning radius

$$r_S \approx \frac{A}{\sqrt{m_V^2 + Q^2}}\,. \tag{2}$$

This scanning property makes the vector meson production an ideal laboratory for testing the generalized BFKL dynamics [gBFKL hereafter]. At large Q^2 and/or for heavy vector mesons, the amplitude of reaction (1) becomes short-distance dominated and is perturbatively calculable in terms of the short-distance behavior of the vector mesons wave function. However, the asymptotic short distance formulas [3, 7] are not yet applicable at the moderate $Q^2 \lesssim 20\,\mathrm{GeV}^2$ of interest in the present fixed target and HERA experiments where the scanning radius r_S is still large due to a large scale parameter $A \approx 6$ in (2) as derived in [6]. For this reason, the onset of the short-distance dominance is very slow and there emerges a unique possibility of studying the transition between the soft and hard interaction regimes in a well controlled manner. Furthermore, the scanning phenomenon allows to directly test the steeper subasymptotic energy dependence of the dipole cross section at smaller dipole size r, which is one interesting consequence of the color dipole gBFKL dynamics [11, 13].

The scanning phenomenon has particularly interesting implications for the diffractive production of the $2S$ radially excited vector mesons

$$\gamma^* p \to V'p\,, \qquad V'(2S) = \rho',\, \omega',\, \phi',\, \Psi',\, \Upsilon'\,.. \tag{3}$$

Here one encounters the node effect: a tricky and strong cancellation between the large and the small size contributions to the production amplitude i.e., those above and below the node position r_n in the $2S$ radial wave function [2, 14, 15] respectively. The node effect is the only dynamical mechanism that gives a strong natural suppression of the photoproduction of excited vector mesons $V'(2S)$ vs. $V(1S)$ mesons. For instance, it correctly predicted [2, 14] the strong suppression of real photoproduction of the Ψ' compared to the J/Ψ observed in the NMC experiment [16] and confirmed recently in the high statistics E687 experiment [17]. In anticipation of the new experimental data on real and virtual V' photoproduction from HERA, it is important to further explore the salient features of the node effect in the framework of the color dipole gBFKL dynamics. At moderate Q^2, the scanning radius r_S is comparable to r_n. First, for

this reason even a slight variation of r_S with Q^2 leads to a strong change of the cancellation pattern in the $V'(2S)$ production amplitude and to an anomalous Q^2 dependence for the electroproduction of the radially excited vector mesons [2, 14, 15]. Second, the cancellation pattern is sensitive also to the dipole-size dependence of the color dipole cross section $\sigma(\nu, r)$ which in the gBFKL dynamics changes which ν leading to an anomalous energy dependence for producing the $V'(2S)$ vector mesons as compared to a smooth energy dependence for the $V(1S)$ ground state vector mesons. This anomalous Q^2 and energy dependence of the $V'(2S)$ production offers a unique signature of the $2S$ radial excitation vs. the D-wave state. Third, at very small Q^2, the $V'(2S)$ production amplitude can be of opposite sign with respect to that of the $V(1S)$ production amplitude (the overcompensation scenario of [15]) to then conform to the same sign at larger Q^2 (the undercompensation scenario of [15]). Here we wish to emphasize that the relative sign of the V' and V production amplitudes is experimentally measurable using the so-called Söding-Pumplin effect ([18, 19], see also [20]).

In this paper we develop the color dipole phenomenology of diffractive photo- and electroproduction of the $1S$ ground state and of the $2S$ radially excited vector mesons. As stated above, for a large scanning radius, the large distance contribution to the production amplitude is not yet negligibly small in the so far experimentally studied region of Q^2, in particular in the $2S$ meson production. In this paper we show that the Q^2 and energy dependence of the diffractive production of vector mesons offers a unique possibility of studying how the color dipole cross section changes from the large nonperturbative to the small perturbative dipole size. The problem can be attacked both ways. First, we present detailed predictions using the color dipole cross section [21, 6], which gives a very good quantitative description of the proton structure function from very small to large Q^2. Second, we can invert the problem and evaluate the color dipole cross section from the corresponding experimental data. Such an evaluation of the dipole cross section is presented here for the first time.

The paper is organized as follows. In Sect. 2 we formulate the color dipole factorization for vector meson production amplitudes. In Sect. 3 we present our numerical results. We find good agreement with the experimental data from the fixed target and HERA collider experiments. The subject of Sect. 4 is the anomalous Q^2 and energy dependence of electroproduction of $2S$ radially excited vector mesons. In Sect. 5 we discuss the scaling relations between production cross sections for different vector mesons and the restoration of flavor symmetry in the variable $Q^2+m_V^2$. We comment on how the scanning phenomenon enables a direct comparison of the spatial wave functions of the ρ^0 and ω^0 mesons. The first evaluation of the dipole cross section from the experimental data is presented in Sect. 6. In Sect. 7 we summarize our main results and conclusions. In the Appendix we describe the lightcone parameterization of the wave functions of the $V(1S)$ and $V(2S)$ vector mesons used in our analysis.

2 Color dipole factorization for vector meson production

The Fock state expansion for relativistic mesons starts with the quark-antiquark state which can be considered as a color dipole. The relevant variables are the dipole moment **r** which is the transverse separation (with respect to the collision axis) of the quark and antiquark and z - the fraction of the lightcone momentum of the meson carried by a quark. The interaction of the relativistic color dipole with the target nucleon is described by the energy dependent color dipole cross section $\sigma(\nu, r)$. The many gluon contributions of higher Fock states $q\bar{q}g...$ become very important at high energy ν. The crucial point is that in the leading $\log\frac{1}{x}$ the effect of higher Fock states can be reabsorbed into the energy dependence of $\sigma(\nu, r)$, which satisfies the generalized BFKL equation ([10, 11]). The flavor blind (one should really say *flavor tasteless*) dipole cross section unifies the description of various diffractive processes. To apply the color dipole formalism to deep inelastic and quarkonium scattering and diffractive production of vector mesons one needs the probability amplitudes $\Psi_{\gamma^*}(\mathbf{r}, z)$ and $\Psi_V(\mathbf{r}, z)$ to find the color dipole of size r in the photon and quarkonium (vector meson), respectively. The color dipole distribution in (virtual) photons was derived in [9, 10]. In terms of these probability amplitudes, the imaginary part of the virtual photoproduction of vector mesons in the forward direction ($t = 0$) reads

$$\mathrm{Im}\mathcal{M} = \langle V|\sigma(\nu, r)|\gamma^*\rangle = \int_0^1 dz \int d^2\mathbf{r}\, \sigma(\nu, r) \cdot \Psi_V^*(\mathbf{r}, z)\Psi_{\gamma^*}(\mathbf{r}, z) \tag{4}$$

whose normalization is $d\sigma/dt|_{t=0} = |\mathcal{M}|^2/16\pi$. For small size heavy quarkonium the probability amplitude $\Psi_V(\mathbf{r}, z)$ can safely be identified with the constituent quark-antiquark quarkonium wave function. The color dipole factorization (4) takes advantage of the diagonalization of the scattering matrix in the $(\mathbf{r}, z)$ representation, which clearly holds even when the dipole size **r** is large, i.e. beyond the perturbative region of short distances. Due to this property and to the fact that in leading $\log\frac{1}{x}$ the effect of higher Fock states is reabsorbed in the energy dependence of the dipole cross section $\sigma(\nu, r)$, as a starting approximation we can identify the probability amplitude $\Psi_V(\mathbf{r}, z)$ for large size dipoles in light vector mesons with the constituent quark wave function of the meson. This provides a viable phenomenology of diffractive scattering which is purely perturbative for small size mesons and/or large Q^2 and small scanning radius r_S and allows a sensible interpolation between soft interactions for large dipoles and hard perturbative interactions of small dipoles. For light quarkonia and small Q^2, this implies the assumption that small-size constituent quarks are the relevant degrees of freedom and the spatial separation of constituent quarks is a major dynamical variable in the scattering process.[1] The large-r contribution to the production amplitude (6) depends on both the dipole cross section for large-size dipoles and the distribution amplitudes of large-size color dipoles and/or on the nonperturbative wave func-

[1] See also earlier works on the color dipole analysis of hadronic diffractive interactions which used constituent quark wave functions for the color dipole distribution amplitudes [22]

tions of light vector mesons at large r, both of which are poorly known at the moment. Still, testing the predictions from such a minimal model is interesting for its own sake and can shed light on the transition between the soft and hard scattering regimes which is still far from understood. An analysis of the sensitivity to models for the nonperturbative wave functions of vector mesons and to how one can disentangle the effects of large r behavior of the wave function and of the dipole cross section, goes beyond the scope of the present exploratory study.

The energy dependence of the dipole cross section is quantified in terms of the dimensionless rapidity ξ, which in deep inelastic scattering equals $\xi = \log\frac{1}{x}$. Consideration of the intermediate masses in diagrams for exclusive production of vector mesons shows that to the leading $\log\frac{1}{x}$ approximation one must take $\xi = \log\frac{1}{x_{eff}}$, where

$$x_{eff} = \frac{Q^2 + m_V^2}{2m_p\nu}\,, \tag{5}$$

and m_V is a mass of the vector meson. The pomeron exchange dominance holds when the Regge parameter is large,

$$\omega = \frac{1}{x_{eff}} = \frac{2m_p\nu}{(Q^2 + m_V^2)} \gg 1\,. \tag{6}$$

Hereafter, we write the amplitudes in terms of $\sigma(x_{eff}, r)$. The spin independence of the dipole cross section $\sigma(x_{eff}, r)$ in (4) leads to the s-channel helicity conservation: the transversely polarized photons produce transversely polarized vector mesons and the longitudinally polarized vector mesons are produced by longitudinal photons. More explicitly, the form of the forward production amplitudes for the transversely (T) and the longitudinally (L) polarized vector mesons in terms of the lightcone radial wave function $\phi(r, z)$ of the $q\bar{q}$ Fock state of the vector meson reads [6]

$$\begin{aligned}\mathrm{Im}\mathscr{M}_T(x_{eff}, Q^2) &= \frac{N_c C_V\sqrt{4\pi\alpha_{em}}}{(2\pi)^2}\int d^2\mathbf{r}\sigma(x_{eff}, r)\\ &\cdot\int_0^1\frac{dz}{z(1-z)}\left\{m_q^2 K_0(\varepsilon r)\phi(r,z)\right.\\ &\left.-[z^2+(1-z)^2]\varepsilon K_1(\varepsilon r)\partial_r\phi(r,z)\right\}\\ &= \frac{1}{(m_V^2+Q^2)^2}\int\frac{dr^2}{r^2}\frac{\sigma(x_{eff}, r)}{r^2}W_T(Q^2, r^2)\end{aligned} \tag{7}$$

$$\begin{aligned}\mathrm{Im}\mathscr{M}_L(x_{eff}, Q^2) &= \frac{N_c C_V\sqrt{4\pi\alpha_{em}}}{(2\pi)^2}\frac{2\sqrt{Q^2}}{m_V}\int d^2\mathbf{r}\sigma(x_{eff}, r)\\ &\cdot\int_0^1 dz\left\{[m_q^2 + z(1-z)m_V^2]K_0(\varepsilon r)\phi(r,z)\right.\\ &\left.-\varepsilon K_1(\varepsilon r)\partial_r\phi(r,z)\right\}\\ &= \frac{1}{(m_V^2+Q^2)^2}\frac{2\sqrt{Q^2}}{m_V}\int\frac{dr^2}{r^2}\frac{\sigma(x_{eff}, r)}{r^2}W_L(Q^2, r^2)\end{aligned} \tag{8}$$

where

$$\varepsilon^2 = m_q^2 + z(1-z)Q^2\,, \tag{9}$$

α_{em} is the fine structure constant, $N_c = 3$ is the number of colors, $C_V = \frac{1}{\sqrt{2}}, \frac{1}{3\sqrt{2}}, \frac{1}{3}, \frac{2}{3}$ for ρ^0, ω^0, ϕ^0, J/Ψ production, respectively and $K_{0,1}(x)$ are the modified Bessel functions. The detailed discussion and parameterization of $\phi(r, z)$ is given in the Appendix, here we only mention that the form of $\phi(r, z)$ we use has the hard-QCD driven short distance behavior and gives the electromagnetic form factor of mesons with the correct QCD asymptotic behavior. At large r we follow the conventional spectroscopic models [23] and constrain the parameters of the wave functions by the widths of the leptonic decays $V, V' \to e^+e^-$, the radii of the vector mesons and the 2S-1S mass splitting. The terms $\propto \phi(r,z)K_0(\varepsilon r)$ and $\propto \partial_r\phi(r,z)\varepsilon K_1(\varepsilon r)$, i.e., $\partial_r\phi(r,z)\partial_r K_0(\varepsilon r)$, in the integrands of (7) and (8) derive from the helicity conserving and helicity nonconserving transitions $\gamma^* \to q\bar{q}$ and $V \to q\bar{q}$ in the $A_\mu\Psi\gamma_\mu\Psi$ and $V_\mu\Psi\gamma_\mu\Psi$ vertices (see Bjorken et al. [24] and [9]; the technique of calculation of traces in the spinorial representation of the relevant Feynman amplitudes is given in [9] and need not be repeated here; for the related Melosh transformation analysis see [25]). For the heavy quarkonium the nonrelativistic approximation [2] has a rather high accuracy, the relativistic corrections become important only at large Q^2 and for the production of light vector mesons. Equations (7),(8) give the imaginary part of the production amplitudes; one can easily include small corrections for the real part by performing the substitution [26],

$$\begin{aligned}\sigma(x_{eff}, r) &\Rightarrow \left(1 - i\cdot\frac{\pi}{2}\cdot\frac{\partial}{\partial\,\log\,x_{eff}}\right)\sigma(x_{eff}, r)\\ &= \left[1 - i\cdot\alpha_V(x_{eff}, r)\right]\sigma(x_{eff}, r)\end{aligned} \tag{10}$$

For brevity, in the subsequent discussion we suppress the real part of the production amplitude; it is consistently included in all the numerical calculations.

The color dipole cross section is flavor blind. The only kinematical sensitivity to the vector meson produced comes via the rapidity variable, see (5). For small r, in the leading $\log\frac{1}{x}$ and leading $\log\frac{1}{r^2}$, i.e., leading $\log Q^2$, the dipole cross section can be related [27] to the gluon structure function $G(x, \bar{Q}^2)$ of the target nucleon through

$$\sigma(x, r) = \frac{\pi^2}{3}r^2\alpha_s(r)G(x, \bar{Q}^2)\,, \tag{11}$$

where the gluon structure function enters at the factorization scale $\bar{Q}^2 \sim \frac{B}{r^2}$ (for the origin of the large scale factor $B \sim 10$, see [28]). The integrands of (7),(8) are smooth at small r and decrease exponentially at $r > 1/\epsilon$ due to the exponential decrease of the modified Bessel functions. Together with the $\propto r^2$ behavior of the color dipole cross section (11), this implies that the amplitudes (7),(8) receive their dominant contribution from $r \approx r_S$. (Equation (2) assumes that the scanning radius r_S is substantially smaller than the radius R_V of the vector meson.) Then, a simple evaluation gives [5]

$$\begin{aligned}\mathrm{Im}\mathscr{M}_T &\propto r_S^2\sigma(x_{eff}, r_S) \propto \frac{1}{Q^2 + m_V^2}\sigma(x_{eff}, r_S)\\ &\propto \frac{1}{(Q^2 + m_V^2)^2}\end{aligned} \tag{12}$$

and

$$\mathrm{Im}\mathscr{M}_L \approx \frac{\sqrt{Q^2}}{m_V}\mathscr{M}_T \propto \frac{\sqrt{Q^2}}{m_V}r_S^2\sigma(x_{eff}, r_S)$$

$$\propto \frac{\sqrt{Q^2}}{m_V}\frac{1}{(Q^2+m_V^2)^2} \qquad (13)$$

respectively.[2] The prediction of the dominance of the longitudinal cross section at large Q^2 is shared by all the models of diffractive leptoproduction, starting with the vector dominance model ([3, 5, 7], for an excellent review of early work on photo- and electroproduction of vector mesons and on vector dominance model see Bauer et al. [29]) and is confirmed by all the experiments on leptoproduction of the ρ^0 at large Q^2 [30–33]. The first factor $\propto r_S^2 \propto 1/(Q^2+m_V^2)$ in (12) comes from the overlap of wave function of the shrinking photon and that of the vector meson. The familiar vector dominance model (VDM) prediction is $M_T \propto \frac{1}{(m_V^2+Q^2)}\sigma_{tot}(\rho N)$, whereas in our QCD approach a small $\sigma(x_{eff}, r_S) \propto r_S^2 \propto 1/(Q^2+m_V^2)$ enters instead of $\sigma_{tot}(VN)$. In (12),(13) we show only the leading Q^2 dependence, suppressing the phenomenologically important departure form the law $\sigma(x,r) \propto r^2$, whose large Q^2 dependence can be related to scaling violations in the gluon density (see (11) and the discussion below). We recall that the shrinkage of the virtual photons and/or the decrease of the scanning radius r_S with Q^2 is the origin of color transparency effects in diffractive leptoproduction of vector mesons off nuclei [2, 4, 5, 34]. The important confirmation of the quantitative predictions [4, 5] of color transparency effects based on the same technique as used here came from the E665 experiment [35].

A more accurate analysis of the scanning phenomenon can be performed in terms of the weight functions $W_{T,L}(Q^2, r^2)$ which are sharply peaked at $r \approx A_{T,L}/\sqrt{Q^2+m_V^2}$; in the relevant variable $\log r$ the width of the peak in $W_L(Q^2, r^2)$ at half maximum equals $\Delta \log r \approx 1.2$ for J/Ψ production and $\Delta \log r \approx 1.3$ for ρ^0 production and varies little with Q^2 [6]. The values of the scale parameter $A_{T,L}$ turn out to be close to $A \sim 6$, which follows from $r_S = 3/\varepsilon$ with the nonrelativistic choice $z = 0.5$; in general $A_{T,L} \geq 6$ and increases slowly with Q^2. This Q^2 dependence of $A_{T,L}$ comes from the large-size asymmetric $q\bar{q}$ configurations when, for instance, the antiquark and the quark in the photon and in the vector mesons carry a very large and a very small fraction of the meson momentum respectively (or the other way around). A comparison of the integrands in (7) and (8) shows that the latter contains an extra factor $z(1-z)$ which makes considerably smaller the contribution from asymmetric configurations to the longitudinal meson production. For completeness, we quote the results of [6]: $A_{T,L}(J/\Psi; Q^2 = 0) \approx 6$, $A_{T,L}(J/\Psi; Q^2 = 100\,\mathrm{GeV}^2) \approx 7$, $A_L(\rho^0; Q^2 = 0) \approx 6.5$, $A_L(\rho^0; Q^2 = 100\,\mathrm{GeV}^2) \approx 10$, $A_T(\rho^0; Q^2 = 0) \approx 7$, $A_T(\rho^0, Q^2 = 100\,\mathrm{GeV}^2) \approx 12$.

An alternative formulation of the slow onset of the purely perturbative regime can be seen as follows: at very large Q^2 when the scanning radius is very small, the dipole cross section $\sigma(x_{eff}, r)$ and the vector meson production amplitudes are proportional to the gluon density $G(x_{eff}, \bar{Q}^2)$ at the factorization scale $\bar{Q}^2 = \tau(Q^2+m_V^2)$ (see also [3, 7] which use momentum-space wave functions, related to the color dipole factorization by the Fourier-Bessel transform; the detailed comparison with the work of Brodsky et al. [7] will be presented below in Sect. 6). The large values of $A_{T,L}$ previously quoted, reflect into very small values of τ [6]: in the interesting region of $Q^2 \gtrsim 10\,GeV^2$ one finds $\tau_{T,L}(J/\Psi) \approx 0.2$, $\tau_L(\rho^0) \approx 0.15$ and $\tau_T(\rho^0) \approx$0.07-0.1, which is different and substantially smaller than the values $\tau = 0.25$ suggested in [3] and $\tau = 1$ suggested in [7]. Very large Q^2 values are needed for reaching the perturbatively large $\bar{Q}^2$ and for the applicability of the pQCD relationship (11).

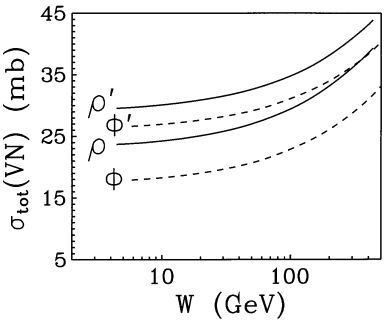

Fig. 1. The color dipole model predictions for the total cross section $\sigma_{tot}(VN)$ for the interaction of the light vector mesons ρ, ρ', ϕ and ϕ' with the nucleon target as a function of c.m.s. energy W

Consequently, for the domain presently under experimental study, $Q^2+m_V^2 \lesssim$10-20 GeV^2, the production amplitudes receive substantial contribution from semiperturbative and nonperturbative r. In [21, 6] this contribution was modeled by the energy independent soft cross section $\sigma^{(npt)}(r)$. The particular form of this cross section successfully predicted [21] the proton structure function at very small Q^2 recently measured by the E665 collaboration [36] and also gave a good description of real photoabsorption [6]. As an example, in Fig. 1 we present an evaluation of the vector meson-nucleon total cross section

$$\sigma_{tot}(VN) = \frac{N_c}{2\pi}\int_0^1 \frac{dz}{z^2(1-z)^2}\int d^2\mathbf{r}\ \left\{m_q^2\phi(r,z)^2 + [z^2+(1-z)^2][\partial_r\phi(r,z)]^2\right\}\sigma(x_{eff}, r)\,. \qquad (14)$$

The total cross section $\sigma_{tot}(\rho^0 N)$ so found, is close to $\sigma_{tot}(\pi N)$, and the rise of $\sigma_{tot}(VN)$ with the c.m.s energy W is consistent with the observed trend of the hadronic total cross sections [37]. In the color dipole picture the smaller values of $\sigma_{tot}(\phi N)$ and $\sigma_{tot}(\phi' N)$ derive from the smaller radius of the $s\bar{s}$ quarkonium. In the simple model [21, 6] the rise of $\sigma_{tot}(VN)$ is entirely due to the gBFKL rise of the perturbative component $\sigma^{(pt)}(x_{eff}, r)$ of the dipole cross section. The rate of rise is small for two reasons: i) at moderate energy, $\sigma^{(pt)}(x_{eff}, r)$ at large r is much smaller than the soft cross section $\sigma^{(npt)}(r)$, ii) at large r the subasymptotic effective intercept of the gBFKL pomeron is small [11, 13]. The detailed description of the dipole cross section used in the present analysis is given in [21, 6] and will not be repeated here. It is partly shown below in Fig. 16. The reason why we focus here on this particular model is that its success in phenomenological applications makes it a realistic tool for the interpolation between soft and hard scattering regions.

[2] Unless otherwise specified, for each flavor, m_V will always be the mass of the ground state 1S vector meson

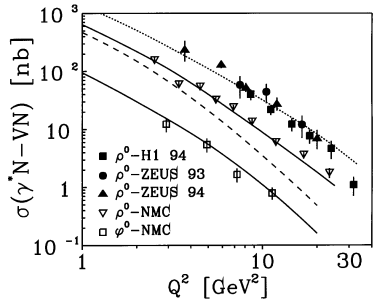

Fig. 2. The color dipole model predictions for the Q^2 dependence of the observed cross section $\sigma(\gamma^* \to V) = \sigma_T(\gamma^* \to V) + \epsilon\sigma_L(\gamma^* \to V)$ of exclusive ρ^0 and ϕ^0 production vs. the low-energy NMC [31] and high-energy ZEUS [32, 38] and H1 [33] data. The top curve is a prediction for the ρ^0 production at $W = 70\,\mathrm{GeV}$, the lower curves are for the ρ^0, ϕ^0 production at $W = 15\,\mathrm{GeV}$. The *dashed curve* for the ρ^0 shows the pure pomeron contribution $\sigma_{\mathbb{P}}(\gamma^* \to \rho^0)$, the *solid curve* for the ρ^0 shows the effect of correcting for the non-vacuum Reggeon exchange as described in the text

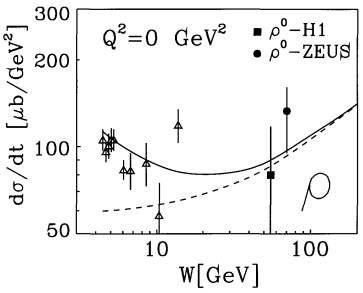

Fig. 3. The color dipole model energy dependence predictions for forward real photoproduction of ρ^0 mesons compared with fixed target data [39] and high energy data from the ZEUS [40, 41] and H1 [43] experiments at HERA collider. The dashed curve is the pure pomeron exchange contribution, the solid curve shows the correction for the the non-vacuum Reggeon exchange as described in the text

Once the vector mesons wave functions are fixed from their spectroscopic and decay properties, all the results for diffractive real and virtual photoproduction of vector mesons to be reported here do not contain any adjustable parameters.

3 Diffractive ρ^0 and ϕ^0 production: predictions and comparison with experiment

The most interesting prediction from the color dipole dynamics is a rapid decrease of production amplitudes (12),(13) at large Q^2. The broadest region of Q^2 was covered in the recent NMC experiment [31] where special care was taken to minimize the inelastic production background which plagued earlier data on ρ^0 and J/Ψ production. In Fig. 2 we compare our predictions for ρ^0 and ϕ^0 production with the NMC data and the data from the HERA experiments [32, 38, 33]. Shown here is the observed polarization-unseparated cross section $\sigma(\gamma^* \to V) = \sigma_T(\gamma^* \to V) + \epsilon\sigma_L(\gamma^* \to V)$ for the value of the longitudinal polarization ϵ of the virtual photon taken from the corresponding experimental paper (typically, $\epsilon \sim 1$). The quantity which is best predicted theoretically is $d\sigma(\gamma^* \to V)/dt|_{t=0}$; in our evaluation of the total production cross section $\sigma(\gamma^* \to V) = B(\gamma^* \to V)d\sigma(\gamma^* \to V)/dt|_{t=0}$ we use the diffraction slope $B(\gamma^* \to V)$ given in the corresponding experimental paper.

Equations (7),(8) describe the pure pomeron exchange contribution to the production amplitude. While at HERA energies secondary Reggeon exchanges can be neglected since the Regge parameter ω is very large, at the lower energy of the NMC experiment, $\langle\nu\rangle$ =(90-140) GeV, the Regge parameter ω is small and non-vacuum Reggeon exchange cannot be neglected. The fit to $\sigma_{tot}(\gamma p)$ can, for instance, be cast in the form

$$\sigma_{tot}(\gamma p) = \sigma_{\mathbb{P}}(\gamma p) \cdot \left(1 + \frac{A}{\omega^{\Delta}}\right) \qquad (15)$$

where the term A/ω^{Δ} in the factor $f = 1 + A/\omega^{\Delta}$ represents the non-vacuum Reggeon exchange contribution. The Donnachie-Landshoff fit gives $A = 2.332$ and $\Delta = 0.533$ [37]. We do not know how large this non-vacuum contribution to ρ^0 production is at large Q^2; for a crude estimation we assume the Reggeon/pomeron ratio to scale with ω, which is not inconsistent with the known decomposition of the proton structure function into the valence (non-vacuum Reggeon) and sea (pomeron) contributions. Then, for the NMC kinematics we find $f = 1.25$ at $\omega \simeq 70, Q^2 = 3\,\mathrm{GeV}^2$ and $f = 1.8$ at $\omega \simeq 9, Q^2 = 20\,\mathrm{GeV}^2$. This departure of f from unity provides a conservative scale for the theoretical uncertainties at moderate values of ω. Anyway, the Q^2 dependence of the Reggeon correction factor f is weak compared with the very rapid variations of $\mathscr{M}_T$ and $\mathscr{M}_L$ with Q^2. The correction for the secondary exchanges, $\sigma(\gamma^* \to \rho^0) = f^2\sigma_{\mathbb{P}}(\gamma^* \to \rho^0)$, brings the theory to a better agreement with the NMC data. The dipole cross section of [21, 6] correctly describes the variation of the ρ^0 production cross section over 3 orders of magnitude from $Q^2 = 0$ to $Q^2 = 16.5\,\mathrm{GeV}^2$. For ϕ^0 production, $f \equiv 1$ due to the Zweig rule and the pure pomeron contribution correctly reproduces the magnitude of $\sigma(\gamma^* \to \phi^0)$ and its variation over nearly three orders of magnitude from $Q^2 = 0$ to $Q^2 = 11.3\,\mathrm{GeV}^2$.

The specific prediction from the gBFKL dynamics is a steeper subasymptotic growth with energy of the dipole cross section $\sigma(\nu, r)$ at smaller dipole size r, which by virtue of the scanning phenomenon translates into a steeper rise of $\sigma(\gamma^* \to V)$ at higher Q^2 and/or for heavy quarkonia. This consequence of the color dipole dynamics was first explored in [6]; the ρ^0 wave function parameters used in [6] are slightly different from those used here but the difference in $\sigma(\gamma^* \to \rho^0)$ is marginal. The agreement of our high-energy results with the HERA data is good for both $Q^2 = 0$ (Fig. 3) and large Q^2 (Fig. 2) and confirms the growth of the dipole cross section with energy expected from the gBFKL dynamics.

The above high-Q^2 data are dominated by the longitudinal cross section; real photoproduction ($Q^2 = 0$) measures the purely transverse cross section. In Fig. 3 we present our results with and without secondary Reggeon corrections ($d\sigma_{\mathbb{P}}(\gamma \to \rho^0)/dt|_{t=0}$ and $d\sigma(\gamma \to \rho^0)/dt|_{t=0} = f^2 d\sigma_{\mathbb{P}}(\gamma \to \rho^0)/dt|_{t=0}$ respectively) as a function of energy. The Reggeon correction factor f^2 brings the theory to a better agreement with the low energy ρ^0 production data [39]. Real photoproduction of ρ^0 is dominated by the soft

Table 1. The parameters R^2, C, m_q and α of the vector mesons wave function and some of the observables evaluated with these wave functions: the r.m.s. R_V, the leptonic width $\Gamma(e^+e^-)$ and the $V'(2S)-V(1S)$ mass splitting. The values of $\Gamma(e^+e^-)$ from the Particle Data Tables [50] is shown for the comparison

Parameter	ρ^0	ρ'	ϕ^0	ϕ'	J/Ψ	Ψ'	Υ	Υ'
R^2 [fm^2]	1.37	1.39	0.69	0.83	0.135	0.248	0.015	0.047
C	0.36	0.28	0.53	0.44	1.13	0.99	1.99	1.72
m_q [GeV]	0.15	0.15	0.30	0.30	1.30	1.30	5.00	5.00
α		0.86		0.94		1.20		1.53
R_V [fm]	1.30	2.28	0.91	1.68	0.41	0.83	0.19	0.42
$\Delta m(2S-1S)$ [GeV]		0.73		0.64		0.60		0.55
$\Gamma(e^+e^-)$ [keV]	6.29	2.62	1.23	0.47	5.06	1.78	1.20	0.54
$\Gamma^{exp}(e^+e^-)$ [keV]	6.77		1.37	0.48	5.36	2.14	1.34	0.56
	± 0.32		± 0.05	± 0.14	± 0.29	± 0.21	± 0.04	± 0.140

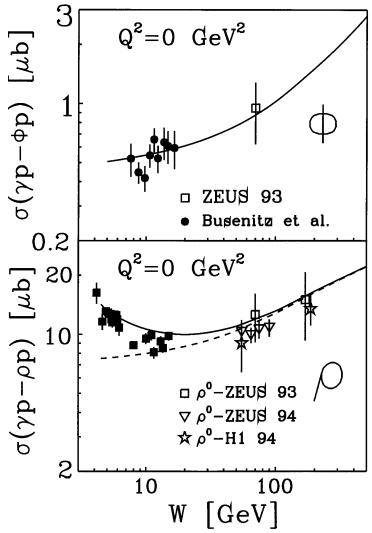

Fig. 4. The color dipole model predictions for the energy dependence of real photoproduction of the ϕ^0 mesons compared with fixed target [44] and high energy ZEUS data [45] (*open square* in the top box). The color dipole model predictions for the energy dependence of real photoproduction of the ρ^0 mesons compared with fixed target [39] and high energy ZEUS [40–42] (*open squares* and *triangles* in the bottom box) and H1 data [43] (*stars* in the bottom box)

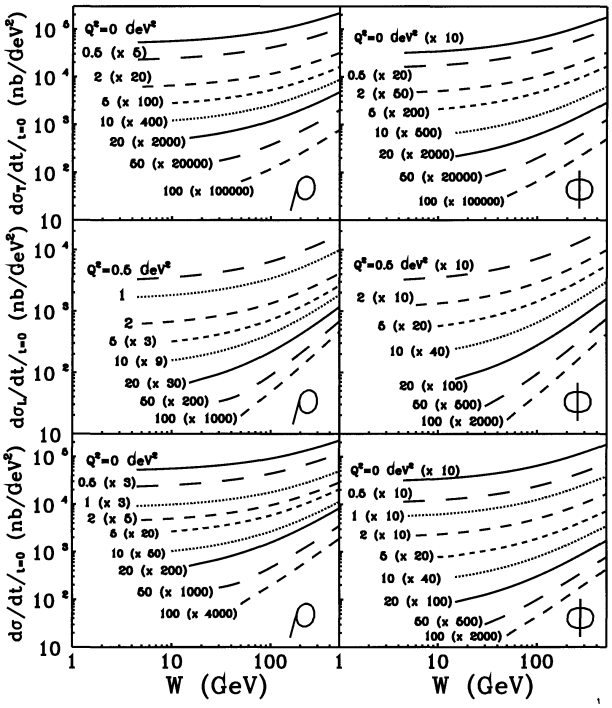

Fig. 5. The color dipole model predictions of the forward differential cross sections $d\sigma_{L,T}(\gamma^* \to V)/dt|_{t=0}$ for transversely (T) (*top boxes*) and longitudinally (L) (*middle boxes*) polarized ρ^0 and ϕ^0 and for the polarization-unseparated $d\sigma(\gamma^* \to V)/dt|_{t=0} = d\sigma_T(\gamma^* \to V)/dt|_{t=0} + \epsilon d\sigma_L(\gamma^* \to V)/dt|_{t=0}$ (*bottom boxes*) for $\epsilon = 1$ as a function of the c.m.s. energy W at different values of Q^2

contribution, the growth of the production cross section is driven by the rising gBFKL component of the dipole cross section. Our predictions for high energy agree well with the recent ZEUS [40–42] and H1 [43] data. The ϕ^0 production is pomeron dominated which implies $f \equiv 1$. We find good agreement with the fixed target [44] and ZEUS [45] data on real photoproduction of the ϕ^0, although the error bars are large (Fig. 4). Because in ϕ^0 photoproduction the relevant dipole sizes are smaller than in the ρ^0 case, (see the radii of ρ^0 and ϕ^0 in Table 1), we predict a steep energy dependence of the ϕ^0 production forward cross section: $d\sigma(\gamma \to \phi^0)/dt|_{t=0}$ is predicted to grow by a factor ≈ 2.5 from $3.75\,\mu b/GeV^2$ at $\nu = 175\,GeV$, i.e., $W = 18\,GeV$, up to $\sim 8.84\,\mu b/GeV^2$ at $W = 170\,GeV$ at HERA. At $W = 70$ GeV we have $\sigma(\gamma \to \phi^0) = 0.87 \mu b$ which agrees with the first ZEUS measurement $\sigma(\gamma \to \phi^0) = 0.96 \pm 0.27\,\mu b$ [45]. More detailed predictions for the energy and Q^2 dependence of $d\sigma(\gamma^* \to V)/dt|_{t=0}$ are presented in Fig. 5 and clearly show a steeper rise with energy at larger Q^2 (see also [6]).

In Fig. 6 we show our predictions for

$$R_{LT} = \frac{m_V^2}{Q^2}\,\frac{d\sigma_L(\gamma^* \to V)}{d\sigma_T(\gamma^* \to V)}\,. \tag{16}$$

The steady decrease of R_{LT} with Q^2 which implies a diminution of the dominance of the longitudinal cross section is a very specific prediction of the color dipole approach. It follows from a larger contribution from large size dipoles to the production amplitude for the transversely polarized vector mesons and larger value of the average scanning radius, i.e., $A_T \gtrsim A_L$ [6]. This prediction can be checked with the higher precision data from HERA; the available experimental data [30–33] agree with $R_{LT} < 1$ but have still large error bars.

The Q^2 dependence of the observed polarization-unseparated cross section depends on the longitudinal polarization

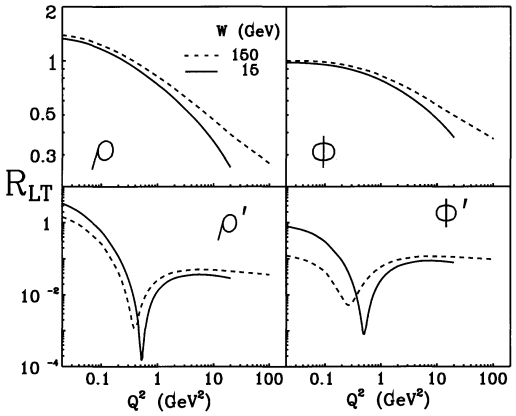

Fig. 6. The color dipole model predictions for the Q^2 and W dependence of the ratio of the longitudinal and transverse differential cross sections in the form of the quantity $R_{LT} = \frac{m_V^2}{Q^2}\frac{d\sigma_L(\gamma^* \to V)}{d\sigma_T(\gamma^* \to V)}$, where m_V is the mass of the vector meson. The *solid* and *dashed curves* are for $W = 15\,GeV$ and $W = 150\,GeV$

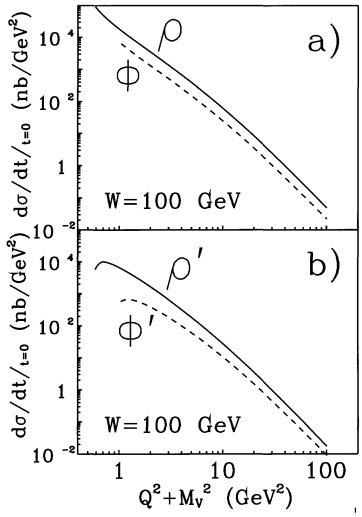

Fig. 7. The color dipole model predictions for the dependence on the scaling variable $Q^2 + m_V^2$ of the polarization-unseparated $d\sigma(\gamma^* \to V)/dt|_{t=0} = d\sigma_T(\gamma^* \to V)/dt|_{t=0} + \epsilon d\sigma_L(\gamma^* \to V)/dt|_{t=0}$ for $\epsilon = 1$ at the HERA energy $W = 100\,GeV$

ϵ of the virtual photon. To a crude approximation the color dipole dynamics predicts

$$\sigma(\gamma^* \to V) = \sigma_T(\gamma^* \to V) + \epsilon\sigma_L(\gamma^* \to V) \propto \frac{1}{(Q^2 + m_V^2)^4}\left(1 + \epsilon R_{LT}\frac{Q^2}{m_V^2}\right) \quad (17)$$

If one approximates (17) by the $(Q^2 + m_V^2)^{-n}$ behavior, one finds $n \sim 3$ vs. $n \sim 1$ in the naive VDM. In (17) we suppressed the extra Q^2 dependence which at large Q^2 comes from the scaling violations in the gluon density factor $\propto G^2(x, \tau(Q^2 + m_V^2))$, see (11). For these scaling violations, at fixed x_{eff} and asymptotically large Q^2 we expect $n \lesssim 3$. In Fig. 7a we present our predictions for ρ^0 and ϕ^0 production at $W = 100\,GeV$ as a function of $Q^2 + m_V^2$ assuming for the longitudinal polarization $\epsilon = 1$ as in the ZEUS [32, 46] and H1 [33, 47] kinematics. These cross sections can be roughly approximated by the $\propto (Q^2 + m_V^2)^{-n}$ law with the exponent $n \approx 2.4$ for the semiperturbative r_S region $1 \lesssim Q^2 \lesssim 10$ GeV^2. At fixed W, x_{eff} varies with Q^2 and for the x_{eff} dependence of $\sigma(x_{eff}, Q^2)$ we predict $n \approx 3.2$ for the perturbative $15 \lesssim Q^2 \lesssim 100\,\text{GeV}^2$ where r_S is small. We strongly urge a careful analysis of the Q^2 dependence in terms of the natural variable $Q^2 + m_V^2$ (for more discussion see Sect. 5 below). For the sake of completeness, in Fig. 5 we present also our predictions for the energy dependence of the polarization-unseparated production cross section $\sigma = \sigma_T + \epsilon\sigma_L$ for the typical $\epsilon = 1$.

4 Anomalies in electroproduction of $2S$ radially excited vector mesons

Here the keyword is the node effect - the Q^2 and energy dependent cancellations from the soft (large size) and hard (small size) contributions to the production amplitude of the $V'(2S)$ radially excited vector mesons. When the value of the scanning radius r_S is close to the node $r_n \sim R_V$, these cancellations must exhibit a strong dependence on both Q^2 and energy due to the different energy dependence of the dipole cross section at small ($r < R_V$) and large ($r > R_V$) dipole sizes. It must be made clear from the very beginning that when strong cancellations of the large and small region contributions are involved, the predictive power becomes very weak and the results strongly model dependent. Our predictions for the production of the $V'(2S)$ radial excitations which we report here serve mostly as an illustration of the unusual Q^2 and energy dependence possible in these reactions. (Manifestations of the node effect in electroproduction on nuclei were discussed earlier, see [15] and [48])

In the nonrelativistic limit of heavy quarkonia, the node effect will not depend on the polarization of the virtual photon and of the produced vector meson. Not so for light vector mesons. The wave functions of the transversely and longitudinally polarized photons are different, the regions of z which contribute to the $\mathscr{M}_T$ and $\mathscr{M}_L$ are different, and the Q^2 and energy dependence of the node effect in production of the transverse and longitudinally polarized $V'(2S)$ vector mesons will be different.

Let us start with the transverse amplitude. Two cases can occur [15], the undercompensation and the overcompensation scenario. In the undercompensation case, the production amplitude $\langle 2S|\sigma(x_{eff}, r)|\gamma^*\rangle$ is dominated by the positive contribution coming from $r \lesssim r_n$ and the $V(1S)$ and $V'(2S)$ photoproduction amplitudes have the same sign. With our model wave functions this scenario is realized for transversely polarized ρ' and ϕ' (we can not, however, exclude the overcompensation scenario). As discussed in [15], in the undercompensation scenario a decrease of of the scanning radius with Q^2 leads to a rapid decrease of the negative contribution coming from large $r \gtrsim r_n$ and to a rapid rise of the $V'(2S)/V(1S)$ production ratio with Q^2. The stronger the suppression of the real photoproduction of the $V'(2S)$ state, the steeper the Q^2 dependence of the $V'(2S)/V(1S)$ production ratio expected at small Q^2. With our model wave functions, the $\rho'(2S)/\rho^0$ and $\phi'(2S)/\phi^0$ production ratios

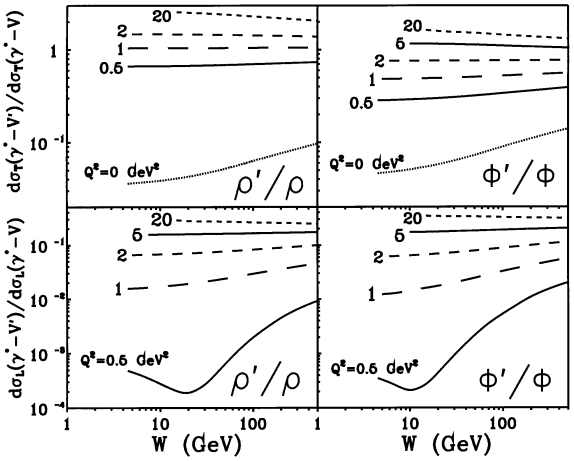

Fig. 8. The color dipole model predictions for the Q^2 and W dependence of the ratios $\sigma(\gamma^* \to \rho'(2S))/\sigma(\gamma^* \to \rho^0)$ and $\sigma(\gamma^* \to \phi'(2S))/\sigma(\gamma^* \to \phi^0)$ for the (T) and (L) polarization of the vector mesons

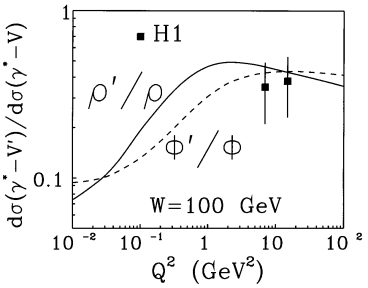

Fig. 9. The color dipole model predictions for the Q^2 dependence of the ratio of the polarization-unseparated forward production cross sections $d\sigma(\gamma^* \to \rho'(2S))/d\sigma(\gamma^* \to \rho^0)$ and $d\sigma(\gamma^* \to \phi'(2S))/d\sigma(\gamma^* \to \phi^0)$ for the polarization of the virtual photon $\epsilon = 1$ at the HERA energy $W = 100\,GeV$ vs. H1 data [52] for the ρ'/ρ production ratio

for the transverse polarization are predicted to rise by more than one order of magnitude in the range $Q^2 \lesssim 0.5\,\mathrm{GeV}^2$, see Fig. 8; the $V(2S)$ and $V(1S)$ production cross sections become comparable at $Q^2 \gtrsim 1\,\mathrm{GeV}^2$, when the production amplitudes are dominated by dipole sizes $r \ll r_n$ [15, 6].

For the longitudinally polarized $\rho'(2S)$ and $\phi'(2S)$ mesons, our model wave functions predict overcompensation; at $Q^2 = 0\,GeV^2$ the amplitude is dominated by the negative contribution from $r \gtrsim r_n$. Consequently, with the increase of Q^2, i.e. with the decrease of the scanning radius r_S, one encounters the *exact* cancellation of the large and small distance contributions. Our model wave functions lead to this exact node effect in the dominant imaginary part of the production amplitude at some value $Q_n^2 \sim 0.5\,\mathrm{GeV}^2$ for both the $\rho'_L(2S)$ and $\phi'_L(2S)$ production (see Fig. 6). The value of Q_n^2 is slightly different for the imaginary and the real part of the production amplitude but the real part is typically very small and this difference will be hard to observe experimentally. Here we can not insist on the precise value of Q_n^2 which is subject to the soft-hard cancellations, our emphasis is on the likely scenario with the exact node effect at a finite Q_n^2.

We wish to emphasize that only the experiment will be able to decide between the overcompensation and undercompensation scenarios. For instance, let the ρ^0 and $\rho'(2S)$ be observed in the $\pi\pi$ photoproduction channel. The Söding-Pumplin effect of interference between the direct, non-resonant $\gamma p \to \pi\pi p$ production and the resonant $\gamma p \to \rho^0(\rho')p \to \pi\pi p$ production amplitudes leads to the skewed ρ^0 and ρ' mass spectrum. The asymmetry of the $\rho^0(\rho')$ mass spectrum depends on the sign of the $\rho^0(\rho')$ production amplitudes ([18], the detailed theory has been worked out in [19]). The Söding-Pumplin technique has already been applied to the $\rho'(1600)$ mass region in $\gamma p \to \pi^+\pi^- p$ at 20 GeV studied in the SLAC experiment [20]. Their fit to the $\rho'(1600)$ mass spectrum requires that the sign of the ρ' production amplitude be negative relative to that of the ρ. Although the interpretation of this result is not clear at the moment, because there are two $\rho'(1450)$ and $\rho'(1700)$ states which were not resolved in this experiment, the Söding-Pumplin technique seems promising.

With the further increase of Q^2 and decrease of the scanning radius one enters the above described undercompensation scenario. Although the radii of the $s\bar{s}$ and $u\bar{u}, d\bar{d}$ vector mesons are different, the Q^2 dependence of $\rho'(2S)/\rho^0$ and $\phi'(2S)/\phi^0$ production cross section ratios will exhibit a similar pattern. For both the transverse and longitudinally polarized photons, these ratios rise steeply with Q^2 on the scale $Q^2 \sim 0.5\,\mathrm{GeV}^2$. At large Q^2 where the production of longitudinally polarized mesons dominates, the $\rho'(2S)/\rho^0$ and $\phi'(2S)/\phi^0$ cross section ratios level off at ~ 0.3 (see Fig. 8). This large-Q^2 limiting value of the $\rho'(2S)/\rho^0$ and $\phi'(2S)/\phi^0$ cross section ratios depend on the ratio of $V'(2S)$ and $V(1S)$ wave functions at the origin, which in potential models is subject to the detailed form of the confining potential [23]. It is interesting that due to the different node effect for the T and L polarizations, we find $R_{LT}(2S) \ll R_{LT}(1S)$, see Fig. 6.

In Fig. 7b we present our predictions for the Q^2 dependence of the polarization-unseparated cross section $\sigma(\gamma^* \to V'(2S)) = \sigma_T(\gamma^* \to V'(2S)) + \epsilon\sigma_L(\gamma^* \to V'(2S))$ at the HERA energy $W = 100\,GeV$ assuming $\epsilon = 1$. In Fig. 9 we show the Q^2 dependence of the polarization-unseparated forward cross section ratios $d\sigma(\gamma^* \to \rho'(2S))/d\sigma(\gamma^* \to \rho^0)$ and $d\sigma(\gamma^* \to \phi'(2S))/d\sigma(\gamma^* \to \phi^0)$ at $W = 100\,\mathrm{GeV}$. Due to its smallness, the anomalous properties of $\sigma_L(2S)$ at small Q^2 are essentially invisible in the polarization-unseparated $V'(2S)$ production cross section shown in Figs. 7b, 9 and 10. In contrast to $\sigma(\gamma^* \to V(1S))$, which falls monotonically and steeply from $Q^2 = 0\,GeV^2$ on, the $\sigma(\gamma^* \to V'(2S))$ shown in Fig. 7b exhibits a weak rise at small Q^2. At Q^2 large enough that the scanning radius $r_S < R_V$ and the node effect becomes negligible, we predict very similar dependence on $Q^2 + m_V^2$ of the $V'(2S)$ and $V(1S)$ production.

Color dipole dynamics uniquely is the source of such a tricky Q^2 dependence of the $V'(2S)/V(1S)$ production ratio. We already mentioned the experimental confirmation [16, 17] of the node effect predicted in Ψ' production [2]. Further experimental confirmations of the node effect, in particular of the unique overcompensation scenario which is possible for light vector mesons, would be extremely interesting. The available experimental data on real photoproduction of radially excited light $V'(2S)$ mesons con-

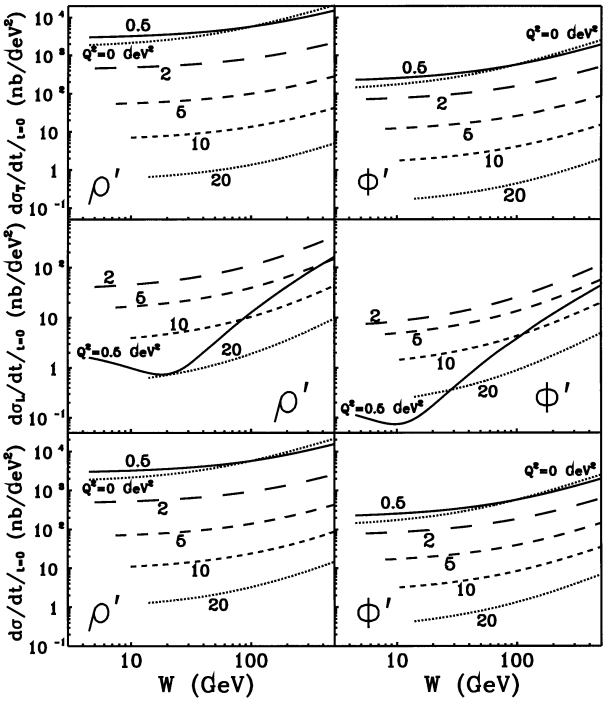

Fig. 10. The color dipole model predictions of the forward differential cross sections $d\sigma_{L,T}(\gamma^* \to V')/dt|_{t=0}$ for transversely(T) (*top boxes*) and longitudinally (L) (*middle boxes*) polarized radially excited vector mesons $\rho'(2S)$ and $\phi'(2S)$ and for the polarization-unseparated $d\sigma(\gamma^* \to V')/dt|_{t=0} = d\sigma_T(\gamma^* \to V')/dt|_{t=0} + \epsilon d\sigma_L(\gamma^* \to V')/dt|_{t=0}$ for $\epsilon = 1$ (*bottom boxes*) as a function of the c.m.s. energy W at different values of Q^2

firm $\sigma(\gamma \to V'(2S))/\sigma(\gamma \to V(1S)) \ll 1$, but are still of a poor quality and the branching ratios of the V' decays are not yet established (for a review see [49] and the Review of Particle Properties [50]). For instance, the FNAL E401 experiment at $\nu \approx 100$ GeV found [44] $\sigma(\gamma \to \phi'(1700, K^+K^-)) = 8.0 \pm 2.7(stat) \pm 1.4(syst)$ nb to be compared with $\sigma(\gamma \to \phi) \approx 0.55\,\mu$b (see Fig. 4). In the ρ family, the very spectroscopy of the ρ' mesons is not yet conclusive [49, 50]. There are two ρ' states, $\rho'(1450)$ and $\rho'(1600)$, the $2S$ and D-wave assignment for these states is not yet clear. The first high energy data on the $\rho'(1450)$ and $\rho'(1700)$ leptoproduction were reported by the E665 collaboration [51]. These E665 data refer to the coherent production on Ca target. For the $\rho'(1700)$, they exhibit a strong rise of $R_{21} = \sigma(\rho' \to 4\pi)/\sigma(\rho \to 2\pi)$ with Q^2 by more than one order of magnitude from (0.004 ± 0.004) at $Q^2 = 0.15\,GeV^2$ to (0.15 ± 0.07) at $Q^2 = 4.5\,GeV^2$. Such a steep Q^2 dependence is perfectly consistent with our expectations for the production of radially excited 2S light vector mesons. For the $\rho'(1450)$ there is a weak evidence of a nonmonotonic Q^2 dependence: $R_{21} = (0.035 \pm 0.011)$ at $Q^2 = 0.15\,GeV^2$ followed by decrease down to $R_{21} = (0.012 \pm 0.004)$ at $Q^2 = 0.3\,GeV^2$ and then to an increase and leveling off to $R_{21} = (0.08 \pm 0.04)$ at larger $Q^2 \geq 2\,GeV^2$. Such a Q^2 dependence of R_{21} would be natural for a D-wave state which has a nodeless radial wave function. If these E665 observations will be confirmed in higher statistics experiments, then the color dipole interpretation of the Q^2 dependence would strongly suggest the 2S and D-wave state assignments for the $\rho'(1700)$ and $\rho'(1450)$, respectively. We remind the reader that, for a quantitative comparison with the predictions of our model (shown in Fig. 10), the E665 results for R_{21} must be corrected for the branching ratio $B(\rho' \to 4\pi)$, which is still experimentally unknown [50].

Recently the new data on elastic ρ' electroproduction were presented from the H1 collaboration [52]. The observed signal can be interpreted in terms of the production of a single resonance with mass 1.57 ± 0.02 GeV and width 0.18 ± 0.09 GeV, which can be analysed in terms of interfering production of $\rho'(1450)$ and $\rho'(1700)$. They found the ratio $R_{21} = 0.35 \pm 0.09 \pm 0.11$ and $R_{21} = 0.38 \pm 0.10 \pm 0.11$ for $< Q^2 >= 7$ and 15 GeV^2 in a broad energy range from $W = 60$ to 110 GeV. These values of R_{21} are consistent with our color dipole predictions (see Fig. 9).

The energy dependence of the $\rho'(2S), \phi'(2S)$ real photoproduction is shown in Fig. 10 and has its own peculiarities. In the color dipole gBFKL dynamics, the negative contribution to the $2S$ production amplitude coming from large size dipoles, $r \gtrsim r_n$, has a slower growth with energy than the positive contribution coming from the small size dipoles $r \lesssim r_n$. For this reason, in the undercompensation regime the destructive interference of the two contributions becomes weaker at higher energy and we predict a growth of the $V'(2S)/V(1S)$ cross section ratios with energy. Taking only the pure pomeron contributions into account, we find for the forward cross section ratio $d\sigma(\gamma \to \rho'(2S)/d\sigma(\gamma \to \rho^0) = 0.041$ at $W = 15$ GeV, which at HERA energies increases to 0.063 and 0.071 at $W = 100$ GeV and $W = 150$ GeV, respectively. Whereas in ρ and ρ' production one must be aware of the non-vacuum Reggeon exchange contributions at lower energy, in the pomeron dominated ϕ', ϕ real photoproduction we find a somewhat faster rise of $d\sigma(\gamma \to \phi'(2S)/d\sigma(\gamma \to \phi^0)$ with energy from 0.054 at $W = 15$ GeV to 0.089 and 0.099 at $W = 100$ GeV and $W = 150$ GeV, respectively.

If the leptoproduction of the longitudinally polarized $V'_L(2S)$ will be separated experimentally, we will have a chance of studying the Q^2 and energy dependence in the overcompensation scenario. Start with the moderate energy and consider Q^2 very close to Q^2_n but still $\lesssim Q^2_n$. In this case the negative contribution from $r \gtrsim r_n$ takes over in the $V'_L(2S)$ production amplitude. With increasing energy, the positive contribution to the production amplitude rises faster and ultimately takes over. At some intermediate energy, there will be an exact cancellation of the two contributions to the production amplitude and the longitudinal $V'_L(2S)$ production cross section shall exhibit a minimum at this energy (the minimum will partly be filled because cancellations in the real and imaginary part of the production amplitude are not simultaneous). With our model wave functions, we find a nonmonotonic energy dependence of the $\rho'_L(2S)$ and $\phi'_L(2S)$ production at $Q^2 \approx 0.5$ GeV^2, which is shown in Figs. 8 and 10. At higher Q^2 and smaller scanning radii r_S the energy dependence of $V'_L(2S)/V_L(1S)$ production ratio becomes very weak.

Finally, a brief comment on the t-dependence of the differential cross sections is in order. For the 1S vector mesons

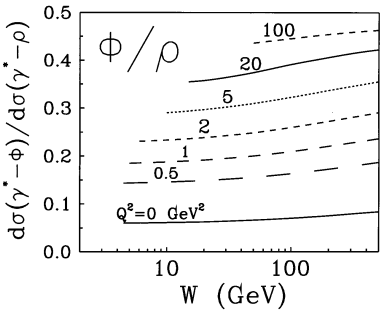

Fig. 11. The color dipole model predictions for the energy dependence of the ratio of the polarization-unseparated forward production cross sections $d\sigma(\gamma^* \to \phi^0)/d\sigma(\gamma^* \to \rho^0)$ for the polarization of the virtual photon $\epsilon = 1$ at different values of Q^2

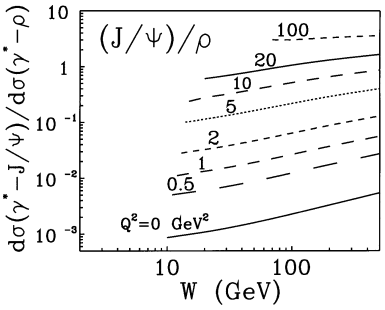

Fig. 12. The color dipole model predictions for the energy dependence of the ratio of the polarization-unseparated forward production cross sections $d\sigma(\gamma^* \to J/\Psi)/d\sigma(\gamma^* \to \rho^0)$ for the polarization of the virtual photon $\epsilon = 1$ at different values of Q^2

we expect the conventional diffractive peak with smooth and gentle energy dependence. For the radially excited vector mesons the t-dependence can be anomalous. The point is that the large size contribution to the $V'(2S)$ meson production amplitude has steeper t-dependence that the small size contribution. The destructive interference of these two amplitudes can lead to two effects: i) the diffraction slope in the $V'(2S)$ meson production will be smaller than in the $V(1S)$ meson production, ii) the effective diffraction slope for the $V'(2S)$ meson production decreases towards small t contrary to the familiar increase for the $V(1S)$ meson production. High statistics data on the ρ', ϕ' production at HERA are needed to test these predictions. More detailed discussion of the diffraction slope will be presented elsewhere.

5 Scaling relations for the production of different vector mesons

The color dipole cross section is flavor blind and only depends on the dipole size. The results (12),(13) for the production amplitudes strongly suggest restoration of flavor symmetry, i.e., a similarity between the production of different vector mesons when compared at the same value of the scanning radius r_S and/or the same value of $Q^2 + m_V^2$.[3] Such a comparison must be performed at the same energy, which also provides the equality of x_{eff} at equal $Q^2 + m_V^2$. Evidently, the value of Q^2 must be large enough so that the scanning radius r_S is smaller than the radii of vector mesons compared.

In order to illustrate the above point we present in Figs. 11 and 12 the ratio of forward production cross sections $R((J/\Psi)/\rho^0; Q^2) = d\sigma(\gamma^* \to J/\Psi)/d\sigma(\gamma^* \to \rho^0)$ and $R(\phi^0/\rho^0; Q^2) = d\sigma(\gamma^* \to \phi^0)/d\sigma(\gamma^* \to \rho^0)$ as a function of the c.m.s energy W at different Q^2 (here we use for the J/Ψ production cross section the values obtained from a recent calculation [54], which practically coincide with those of [6], the slight difference being due to a somewhat different J/Ψ wave function). Here we compare the polarization-unseparated cross sections $\sigma = \sigma_T + \epsilon\sigma_L$, taking for definiteness $\epsilon = 1$ which is typical of the HERA kinematics.

[3] For the first considerations of the restoration of flavor symmetry in diffractive production of vector mesons off nuclei see [5], the scaling relations between diffraction slopes for $\gamma^* p \to Vp$ are discussed in [53]

These ratios exhibit quite a strong Q^2 dependence, which predominantly comes from the Q^2 dependence of the factor

$$\left(\frac{Q^2 + m_{V_1}^2}{Q^2 + m_{V_2}^2}\right)^n ,$$

which changes rapidly when the two vector mesons have different masses. The energy dependence of the cross section ratios taken at the same Q^2 derives from the different energy dependence of the dipole cross section which enters at different radii $r_{Si} \approx \frac{6}{\sqrt{Q^2+m_{Vi}^2}}$ in the numerator and denominator of the V_1/V_2 cross section ratio,

$$R(V_1/V_2; Q^2) = \frac{\sigma(\gamma^* \to V_1)}{\sigma(\gamma^* \to V_2)} \propto \frac{\sigma^2(\nu, r_{S1})}{\sigma^2(\nu, r_{S2})} .$$

In the HERA energy range we predict $R((J/\Psi)/\rho^0; Q^2 = 0) = \sigma(\gamma \to J/\Psi)/\sigma(\gamma \to \rho^0) = 0.0022$ at $W = 70\,\mathrm{GeV}$ and 0.0032 at $W = 150\,\mathrm{GeV}$, which agrees with the experimentally observed ratio 0.0041 ± 0.0016 at $W \sim 70\,\mathrm{GeV}$ and 0.0054 ± 0.0017 at $W \sim 150\,\mathrm{GeV}$ of H1 [55, 43] and with the ratio 0.0035 ± 0.0012 at $W \sim 70\,\mathrm{GeV}$ and 0.0045 ± 0.0023 at $W \sim 150\,\mathrm{GeV}$ of ZEUS [40, 41, 56]. Notice the rise of $R((J/\Psi)/\rho^0; Q^2)$ by more than 3 orders in the magnitude from $Q^2 = 0$ to $Q^2 = 100\,\mathrm{GeV}^2$. Our result for the ratio $R(\phi^0/\rho^0; Q^2 = 0) = d\sigma(\gamma \to \phi^0)/d\sigma_{\mathbb{P}}(\gamma \to \rho^0)$ shown in Fig. 11 is substantially smaller than the factor $2/9$ expected from the naive VDM, in a very good agreement with the experiment ([44] and references therein). This suppression is a natural consequence of the color dipole approach and derives from the smaller radius of the $s\bar{s}$ quarkonium and smaller transverse size of the $s\bar{s}$ Fock state of the photon as compared to the radius of the ρ^0 and size of the $u\bar{u}, d\bar{d}$ Fock states of the photon, respectively, cf. Table 1. For increasing Q^2s, the ratio $R(\phi^0/\rho^0; Q^2)$ overshoots the VDM ratio $2/9$ and rises by one order of magnitude from $Q^2 = 0$ to $Q^2 = 100\,\mathrm{GeV}^2$. In Figs. 11 and 12 we compare only pure pomeron contributions to the production cross section; at smaller values of the energy and of the Regge parameter ω, the ϕ^0/ρ^0 and $(J/\Psi)/\rho^0$ production ratios will be further suppressed by the factor f^2.

The remarkable restoration of flavor symmetry in the natural scaling variable $Q^2 + m_V^2$ is demonstrated in Figs. 13 and 14, where we present a ratio $R(i/k; Q^2 + m_V^2)$ of the

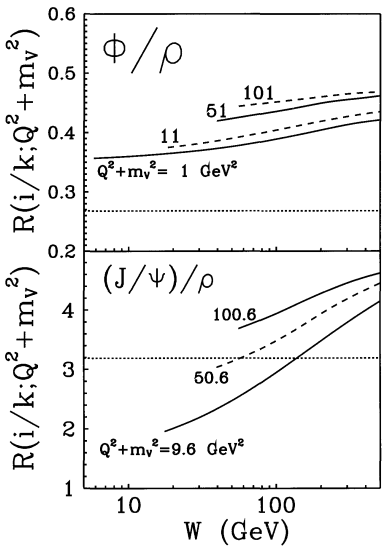

Fig. 13. Approximate scaling in the variable $Q^2 + m_V^2$ for the ratio of the polarization-unseparated forward production cross sections $d\sigma(\gamma^* \to \phi^0)/d\sigma(\gamma^* \to \rho^0)$ and $d\sigma(\gamma^* \to J/\Psi)/d\sigma(\gamma^* \to \rho^0)$ for the polarization of the virtual photon $\epsilon = 1$. The horizontal dotted straight lines show the ratio corresponding to (18)

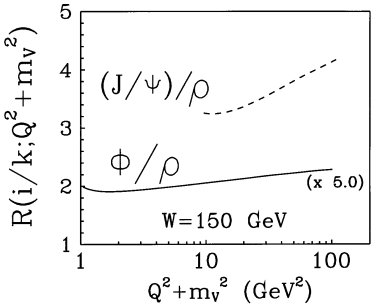

Fig. 14. Approximate scaling in the variable $Q^2 + m_V^2$ for the ratio of the polarization-unseparated forward production cross sectionsf $d\sigma(\gamma^* \to \phi^0)/d\sigma(\gamma^* \to \rho^0)$ and $d\sigma(\gamma^* \to J/\Psi)/d\sigma(\gamma^* \to \rho^0)$. at c.m.s. energy $W = 150\,\mathrm{GeV}$ (the polarization of the virtual photon $\epsilon = 1$)

same cross sections taken at equal $Q^2 + m_V^2$ rather than equal Q^2. A marginal variation of the $R((J/\Psi)/\rho^0; Q^2 + m_V^2)$ and $R(\phi^0/\rho^0; Q^2 + m_V^2)$ in this scaling variable must be contrasted with the variation of the $R((J/\Psi)/\rho^0; Q^2 = 0)$ and $R(\phi^0/\rho^0; Q^2 = 0)$ by the three and one orders in the magnitude previously mentioned, respectively, over the same span of Q^2 values $0 < Q^2 < 100\,\mathrm{GeV}^2$. The origin of the slight departures from exact scaling in the variable $Q^2 + m_V^2$ comes from a well understood difference between the scales $A_{T,L}$ and $\tau_{T,L}$ for production of different vector mesons. The same difference of $A_{T,L}$ and $\tau_{T,L}$ brings in the energy dependence of $R(i/k; Q^2 + m_V^2)$. This is a specific prediction from the preasymptotic gBFKL dynamics. The radii of the ϕ^0 and ρ^0 mesons do not differ much and for this reason we find a precocious scaling in $Q^2 + m_V^2$. The energy dependence of the ϕ^0/ρ^0 ratio also turns out very weak. The radii of the ρ^0 and J/Ψ differ much more strongly and the ratio $R((J/\Psi)/\rho^0; Q^2 + m_V^2)$ exhibits a somewhat stronger dependence on energy and $Q^2 + m_V^2$. For the same reason,

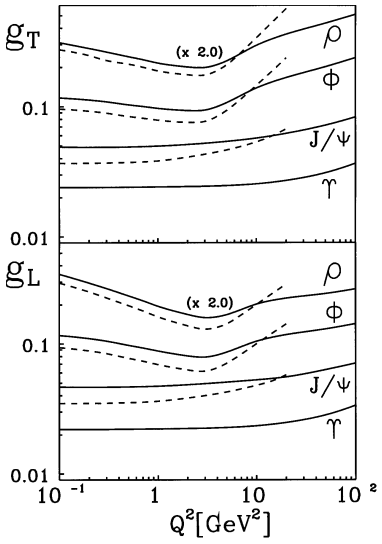

Fig. 15. The Q^2 dependence of the coefficient functions $g_{T,L}$ at $W = 15\,GeV$ (*dashed curve*) and $W = 150\,GeV$ (*solid curve*)

we predict a substantial departure of $R(i/k; Q^2 + m_V^2)$ from the short-distance formula

$$R(i/k; Q^2 + m_V^2) = \frac{m_i \Gamma_i(e^+e^-)}{m_k \Gamma_k(e^+e^-)}\,, \tag{18}$$

which is shown in Fig. 13 by horizontal lines. The formula (18) can readily be derived generalizing the asymptotic-Q^2 considerations [3] (for further discussion of the crucial rôle of the scaling variable $Q^2 + m_V^2$ in this comparison see below Sect. 6).

The case of the ω^0, ω' virtual photoproduction is very interesting. Is the $\rho^0 - \omega^0$ mass degeneracy accidental? Does it imply also similar spatial wave functions in the ρ and ω families? The scanning property of diffractive production allows a direct comparison of spatial wave functions of the ρ^0 and ω^0. If the $\omega^0 - \rho^0$ degeneracy extends also to the spatial wave functions, then we predict

$$\frac{\sigma(\gamma^* \to \omega^0)}{\sigma(\gamma^* \to \rho^0)} = \frac{1}{9} \tag{19}$$

independent of energy and Q^2. On the other hand, if the radii of the ρ^0 and ω^0 are different, for instance $R_\omega < R_\rho$, then the ω^0/ρ^0 production ratio must exhibit the Q^2 dependence reminiscent of the ϕ^0/ρ^0 ratio. Similarly, a comparison of the ω' and ρ' production can shed light on the isospin dependence of interquark forces in vector mesons.

6 Determination of color dipole cross section from vector meson production data

Inverting (12),(13) one can evaluate $\sigma(x_{eff}, r)$ from the vector meson production data. It is convenient to cast (12),(13) in the form

$$\mathrm{Im}\mathscr{M}_T = g_T \sqrt{4\pi\alpha_{em}} C_V \sigma(x_{eff}, r_S) \frac{m_v^2}{m_V^2 + Q^2} \tag{20}$$

$$\mathrm{Im}\mathcal{M}_L = g_L\sqrt{4\pi\alpha_{em}}C_V\sigma(x_{eff},r_S)\frac{\sqrt{Q^2}}{m_V}\cdot\frac{m_v^2}{m_V^2+Q^2} \quad (21)$$

In (20),(21) the coefficient functions $g_{T,L}$ are defined so as to relate the amplitude to $\sigma(r_S)$ at the well defined scanning radius (2) with $A \equiv 6$. The major point of this decomposition is that at large Q^2 and/or small $r_S \lesssim R_V$, the coefficients $g_{T,L}$ will be very smooth functions of Q^2 and energy. The smooth Q^2 and energy dependence of $g_{T,L}$ mostly reflects the smooth and well understood Q^2 dependence of the scale factors $A_{T,L}$. Such a procedure is somewhat crude and the $\mathrm{Im}\mathcal{M}_{T,L} - \sigma(x_{eff},r_S)$ relationship is sensitive to the assumed r dependence of the dipole cross section $\sigma(x_{eff},r)$. Using the dipole cross section [6] the shape of which changes significantly from $\omega = \frac{1}{x_{eff}} = 30$ up to $\omega = 3\cdot 10^6$, we have checked that this sensitivity is weak. In Fig. 15 we present the Q^2 dependence of $g_{T,L}$ for different production processes at $W = 15\,\mathrm{GeV}$ and $W = 150\,\mathrm{GeV}$. The variation of the resulting coefficient functions $g_{T,L}$ from small to large W does not exceed 15%, which is a conservative estimate of the theoretical uncertainty of the above procedure.

The experimentally measured forward cross production section section equals

$$\frac{d\sigma(\gamma^*\to V)}{dt}\Big|_{t=0} = \frac{f^2}{16\pi}\cdot\left[(1+\alpha_{V,T}^2)\mathcal{M}_T^2 + \epsilon(1+\alpha_{V,L}^2)\mathcal{M}_L^2\right] \quad (22)$$

The difference between $\alpha_{V,L}$ and $\alpha_{V,T}$ for the longitudinal and transverse cross sections and the overall effect of the real part is marginal and can safely be neglected compared to other uncertainties. Then, making use of the above determined $g_{T,L}$ and combining (20), (21) and (22), we obtain

$$\sigma(x_{eff},r_S) = \frac{1}{f}\cdot\frac{1}{C_V}\cdot\frac{Q^2+m_V^2}{m_V^2}\cdot\frac{2}{\sqrt{\alpha_{em}}}\cdot\left(g_T^2+\epsilon\,g_L^2\cdot\frac{Q^2}{M_V^2}\right)^{-1/2}\cdot\left(1+\alpha_V^2\right)^{-1/2}\sqrt{\frac{d\sigma(\gamma^*\to V)}{dt}\Big|_{t=0}} \quad (23)$$

Here ϵ is the longitudinal polarization of the photon the values of which are taken from the corresponding experimental publications. In (22),(23) f is the above discussed factor which accounts for the non-vacuum Reggeon contribution to ρ^0 production; for ϕ^0 and J/Ψ production, $f \equiv 1$. In the case the experimental data are presented in the form of the t-integrated cross section, we evaluate $\frac{d\sigma(\gamma^*\to V)}{dt}\Big|_{t=0} = B\sigma_{tot}(\gamma^*\to V)$ using the diffraction slope B as cited in the same experimental publication.

In Fig. 16 we show the results of such an analysis on the low energy [44] and ZEUS [45] ϕ^0 real photoproduction data, on the ρ^0 and ϕ^0 NMC electroproduction data [31], on the ρ^0 HERA real and virtual photoproduction (H1 [33], ZEUS [40, 41, 32]), on the fixed target data on real photoproduction (EMC [57], E687 [58]), on the EMC J/Ψ electroproduction data ([59]) and on the HERA real photoproduction J/Ψ data (H1 [55], ZEUS [56]). The error bars

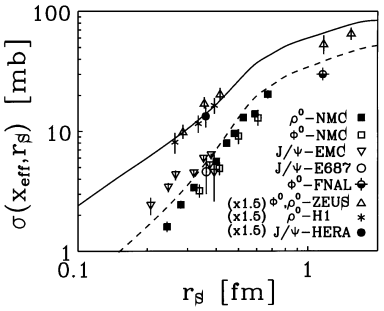

Fig. 16. The dipole size dependence of the dipole cross section extracted from the experimental data on photoproduction and electroproduction of vector mesons: the NMC data on ϕ^0 and ρ^0 production [31], the EMC data on J/Ψ production [57, 59], the E687 data on J/Ψ production [58], the FNAL data on ρ^0 production [44], the ZEUS data on ϕ^0 production [45], the ZEUS data on ρ^0 production [40, 41, 32], the H1 data on ρ^0 production [33] and the average of the H1 and ZEUS data on J/Ψ production [55, 56]. The *dashed* and *solid curve* show the dipole cross section of the model [21, 6] evaluated for the c.m.s. energy $W = 15$ and $W = 70$ GeV respectively. The data points at HERA energies and the corresponding *solid curve* are multiplied by the factor 1.5

are the error bars in the measured cross sections as cited in the experimental publications. The experimental data on the vector meson production give a solid evidence for a decrease of $\sigma(x_{eff},r_S)$ by one order of magnitude from $r_S \approx 1.2$ fm in ϕ^0 real photoproduction down to $r_S \approx 0.24$ fm in the electroproduction of ρ^0 at $Q^2 = 23\,\mathrm{GeV}^2$ and of J/Ψ at $Q^2 = 13\,\mathrm{GeV}^2$. In the region of overlapping values of r_S there is a remarkable consistency between the dipole size dependence and the absolute values of the dipole cross section determined from the data on the ρ^0, ϕ^0 and J/Ψ production, in agreement with the flavor independence of the dipole cross section. A comparison of determinations of $\sigma(x_{eff},r)$ at fixed-target and HERA energy confirms the prediction [11, 13, 6] of faster growth of the dipole cross section at smaller dipole size, although the error bars are still large.

The above determination of $\sigma(x_{eff},r_S)$ is rather crude for several reasons.

i) First, a comparison of the NMC [31] and early EMC data [60] on ρ^0 production suggests that the admixture of inelastic process $\gamma^* p \to VX$ could have enhanced the EMC cross section by as large a factor as ~ 3 at $Q^2 = 17\,GeV^2$. The value of $\sigma(\gamma^*\to V)$ thus overestimated, leads to $\sigma(x_{eff},r_S)$ overestimated by the factor $\sim\sqrt{3}$, which may be a reason why the EMC J/Ψ electroproduction data [59] lead consistently to somewhat larger values of $\sigma(x_{eff},r_S)$. Still, even this factor of $\sim\sqrt{3}$ uncertainty is much smaller than the more than one order of magnitude by which $\sigma(x_{eff},r_S)$ varies over the considered span of r_S. In the recent NMC data [31] a special care has been taken to eliminate an inelastic background and the values of $\sigma(x_{eff},r_S)$ from the ρ^0 and ϕ^0 production data are consistent within the experimental error bars.

ii) There are further uncertainties with the value of the diffraction slope $B(\gamma^*\to V)$ and the curvature of the diffraction cone which affect the extrapolation down to $t = 0$. The experimental situation with the diffraction slopes is quite

unsatisfactory; in the case of the J/Ψ and of the light vector mesons at large Q^2, one can not exclude even a $\sim 50\%$ uncertainty in the value of $B(\gamma^* \to V)$. However, this uncertainty in $B(\gamma^* \to V)$ corresponds to $\lesssim 25\%$ uncertainty in our evaluation of $\sigma(x_{eff}, r_S)$, which is sufficient for the purposes of the present exploratory study.
iii) In addition, there is also the above evaluated conservative $\lesssim 15\%$ theoretical inaccuracy of our procedure.
iv) Finally, there is a residual uncertainty concerning the wave function of light vector mesons. As a matter of fact, if the dipole cross section were known, the diffractive production $\gamma^* p \to Vp$ would be a unique local probe of the vector meson wave function at $r \approx r_S$ [4]; this may well become one of the major applications of vector meson production. To this aim, the consistency of $\sigma(x_{eff}, r)$ determined from different reactions indicates that the wave functions of vector mesons are reasonably constrained by modern spectroscopic models and by the leptonic width.

This is the first direct determination of the dipole cross section from the experimental data and our main conclusions on the properties of the dipole cross section are not affected by the above cited uncertainties. In Fig. 16 we show also the dipole cross section from the gBFKL analysis [21, 6], which gives a good quantitative description of the photon structure function at small x. We conclude that the color dipole gBFKL dynamics provides a unified description of diffractive production of vector mesons and of the proton structure function.

Finally, a comparison of the color dipole analysis of diffractive electroproduction [4, 5, 6] with the related momentum space analysis of [3, 7] is in order. At a very large Q^2 and/or very short scanning radius, $r_S \ll R_V$, electroproduction probes the wave function of vector mesons and/or the z-distribution amplitude at a vanishing transverse size, integrated over z with the z-dependent factor which emerges in (7),(8). The wave function at the vanishing 3-dimensional separation of the quark and antiquark can be related to the width of the leptonic decay, $V \to e^+e^-$. The form of the z-dependent factor is mostly dictated by $r_S^2 \sim 1/(4z(1-z)Q^2+m_V^2)$ which emerges in the integrands of (7),(8) after the r integration, and for the asymptotical Q^2 when $4z(1-z)Q^2 \gg m_V^2$, Brodsky et al. [7] introduced the moment of the longitudinal distribution amplitude

$$\eta_V = \frac{\int_0^1 dz \frac{1}{2z(1-z)} \Psi_V(r=0,z)}{\int_0^1 dz \Psi_V(r=0,z)} \,. \tag{24}$$

One must be careful with the interpretation of η_V , though, because for the very asymmetric $q\bar{q}$ configurations, $z(1-z) \lesssim M_V^2/Q^2$, the scanning radius stays large even for $Q^2 \to \infty$; for instance, precisely these asymmetric configurations dominate the cross section of the diffraction dissociation of photons, $\gamma^* p \to Xp$, into the continuum states X [9, 10]. With these reservations, we can combine the representations (20),(21), the pQCD relationship (11) and the formula (2) for the scanning radius, and cast the production amplitude in the form (here we focus on the dominant longitudinal amplitude)

$$\mathscr{M}_L = \frac{8\pi^2}{3} f_V \sqrt{4\pi\alpha_{em}} \eta_V m_V \frac{\sqrt{Q^2}}{m_V} \frac{1}{(Q^2+m_V^2)^2}$$

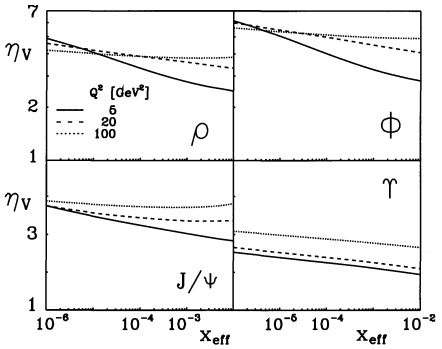

Fig. 17. The Q^2 dependence of the parameter η_V in the representation (25) for the amplitude of leptoproduction of different vector mesons at fixed energy W = 150 GeV

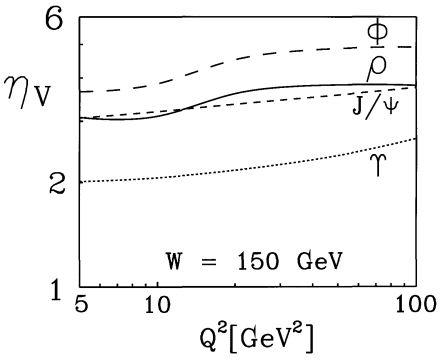

Fig. 18. The x_{eff} dependence of the parameter η_V in the representation (25) for the amplitude of leptoproduction of different vector mesons at several values of Q^2

$$\cdot\alpha_S(\bar{Q}^2) G(x,\bar{Q}^2) = \frac{2 f_V e \eta_V m_V}{9} \frac{\sqrt{\bar{Q}^2}}{m_V} \left(\frac{6}{A}\right)^2 r_S^2 \sigma(r_S) \,, \tag{25}$$

where

$$f_V^2 = \frac{3}{8\pi\alpha_{em}^2} \Gamma(V \to e^+e^-) m_V \,. \tag{26}$$

Then, we can present our results for $\mathscr{M}_L$ in terms of this parameter η_V. The first line of (25) gives the asymptotic-Q^2 form of $\mathscr{M}_L$ in terms of the gluon structure function of the proton, the second line is equivalent to it at large pQCD factorization scale $\bar{Q}^2$ and serves as a working definition of η_V at moderately large Q^2 and/or moderately small scanning radius r_S. The above finding that $g_{T,L}$ only weakly depend on Q^2 and energy, already suggests that η_V defined by the second line of (25) will be approximately constant, and now we show that this is indeed the case.

Evidently, the resulting values of η_V will depend on the pQCD factorization scale $\bar{Q}^2$. The scale parameter τ in the pQCD factorization scale $\bar{Q}^2 = \tau(Q^2+m_V^2)$ was evaluated in [6]. It is related to the scale parameter $B \approx 10$ in the pQCD formula (11) and the scale parameter A in the scanning radius (2) as $\tau \sim B/A^2$, for production of the longitudinal vector mesons in DIS [6] finds $\tau_L(J/\Psi) \approx 0.2$ and $\tau_L(\rho^0) \approx 0.15$. Reference [7] cites the asymptotic leading twist form of (25), with m_V^2 neglected in the denomina-

tor compared to Q^2 and with the pQCD factorization scale $\bar{Q}^2 = Q^2$, besides the more accurate definition of the pQCD scale $\bar{Q}^2$ we differ from [7] also by the factor 2 in (11). The scale A in the scanning radius is given by the position of the peak in $W_L(Q^2, r^2)$, it varies slightly with Q^2; bringing in the slight variation of the scale factors $A_{T,L}$, at large Q^2 it is reasonable to take $A_L(J/\Psi) = 6$ and $A_L(\rho^0, \phi^0) = 8$ [6]. With this choice of A_L, our results for the production amplitude $\mathscr{M}_L$ correspond to the values of η_V shown in Figs. 17 and 18. For the nonrelativistic quarkonium, in which $z \approx \frac{1}{2}$, (24) gives $\eta_V \approx 2$. The Υ is a good approximation to the nonrelativistic quarkonium and we indeed find $\eta_V \approx 2$. Taking a fixed scale A, we neglected the slight variation of τ with Q^2, which propagates into the slight variation of η_V with Q^2. Because the shape of the color dipole cross section varies with x_{eff}, the scale parameter A varies also with x slightly. Taking the x-independent A, we cause the slight mismatch of the x-dependence of the r.h.s. and l.h.s. of (24), which propagates into the weak x_{eff} dependence of η_V. In Fig. 17 we show η_V for the fixed energy $W = 150\,\mathrm{GeV}$ relevant to the HERA experiments, here the combined Q^2 and x_{eff} dependence of the scale parameter A contribute to the variation of η_V. The issue of the Q^2 and x dependence of the pQCD factorization scale $\bar{Q}^2$ in (24) deserves a dedicated analysis, here we wish to focus only on the fact that the so determined η_V exhibits a remarkably weak variation with Q^2 and x_{eff}. Furthermore, Fig. 18 shows that the x_{eff}-dependence of η_V becomes substantially weaker at larger Q^2. This testifies the importance of $Q^2+m_V^2$ as a relevant scaling variable, which absorbs major mass corrections to the Q^2 dependence of the production amplitude (see also the discussion of the flavor symmetry restoration in Sect. 5). To this end we wish to notice that the expansion

$$\frac{1}{(Q^2+m_V^2)^2} = \frac{1}{Q^4}\left(1 + \frac{2m_V^2}{Q^2} - ...\right) \tag{27}$$

corresponds to the abnormally large scale $2m_V^2$ for the higher twist correction to the leading twist production amplitude. For the light vector mesons, Brodsky et al. estimate η_V = 3–5; our results in Figs. 17 and 18 are very close to these estimates, as it must be expected because the momentum-space technique of Brodsky et al. and our color dipole factorization technique are related by the Fourier-Bessel transform. With the present poor knowledge of the large dipole distributions in vector mesons and/or the wave functions of vector mesons, the variations of η_V in Figs. 17 and 18 and the range of estimates for η_V in [7] indicate the range of uncertainty in the predictions of leptoproduction amplitudes.

7 Conclusions

The purpose of this paper is the phenomenology of diffractive photoproduction and electroproduction of ground state ($1S$) and radially excited ($2S$) light vector mesons in the framework of the color dipole picture of the QCD pomeron. In this picture, the Q^2 dependence of production of the $1S$ vector mesons is controlled by the shrinkage of the transverse size of the virtual photon and the small dipole size dependence of the color dipole cross section. Taking the same color dipole cross section as used in the previous successful prediction of the low x structure function of the proton, we have obtained a good quantitative description of the experimental data on diffractive photoproduction and electroproduction of $1S$ vector mesons ρ^0, ϕ^0 and J/Ψ. We have presented the first determination of the dipole cross section from these data and found a remarkable consistency between the absolute value and the dipole size and energy dependence of the dipole cross section extracted from the data on different vector mesons. This represents an important cross-check of the color dipole picture. The pattern we found for the energy dependence of the dipole cross section is consistent with flavor independence and with expectations from the gBFKL dynamics. The color dipole picture leads to the restoration of flavor symmetry and to novel scaling relations between the production of different vector mesons when compared at the same $Q^2 + m_V^2$. Such relations are borne out by the available data and will be further tested when the higher precision data from HERA will become available. Regarding this $(Q^2+m_V^2)$-scaling, perhaps still more interesting are the deviations from scaling, which originate from a substantial contribution of the large size dipoles even at very large Q^2s.

The second class of predictions concerns the rich pattern of an anomalous Q^2 and energy dependence of the production of the $V'(2S)$ radially excited vector mesons, which depends entirely on the quantum mechanical fact that the $2S$ wave function has a node which makes these anomalies an unavoidable effect. We find a very strong suppression of the $V'(2S)/V(1S)$ production ratio in the real photoproduction limit of very small Q^2. For the longitudinally polarized $2S$ mesons we find a plausible overcompensation scenario leading to a sharp dip of the longitudinal cross section $\sigma_L(2S)$ at some finite $Q^2 = Q_n^2 \sim 0.5\,\mathrm{GeV}^2$. The position Q_n^2 of this dip depends on the energy and leads to a nonmonotonic energy dependence of $\sigma_L(2S)$ at fixed Q^2. Regarding the experimental choice between the overcompensation and undercompensation scenarios in the HERA experiments, the situation looks quite favorable because the sign of the ρ' production amplitude relative to that of the ρ^0 can be measured directly by the Söding-Pumplin method. At larger Q^2, the scanning radius becomes shorter, and we predict a steep rise of the $2S/1S$ cross section ratio, typically by one order of magnitude on the very short scale $Q^2 \lesssim 0.5\,GeV^2$ in agreement with the present indications from the E665 data. The flattening of this $2S/1S$ ratio at large Q^2 is a non-negotiable prediction from the color dipole dynamics. Remarkably, the Q^2 dependence of the V' production offers a unique possibility of distinguishing between $2S$ radially excited and D-wave vector mesons.

Finally, in the color dipole framework, a comparison of the Q^2 dependence of the diffractive production of the ρ^0 and ω^0 constitutes a direct comparison of the spatial wave functions of the two mesons. A comparison of the Q^2 dependence of the ω' and ρ' production can shed light on the isospin dependence of the interquark forces in vector mesons.

Acknowledgements. The stay of B.G.Z. at Institut f. Kernphysik, KFA Jülich was supported by DFG. The support by the INTAS grand 93-238 is acknowledged.

Note added in proof: Since the paper was submitted for publication (in 1995), to the time it was accepted, many new data have appeared from the ZEUS and H1 collaborations. As a consequence, quite a few references have been added (following the advice of the referee) and a number of data points have been correspondingly added in some of the figures (Figs. 2, 3, 4 and 9). Also, an explicative sentence concerning ρ' production has been added in Sect. 4.

Appendix

Here we present the parameterization of the wave functions of vector mesons in the lightcone mixed $(\mathbf{r}, z)$ representation. Due to the fact that small size $q\bar{q}$ configurations become important at large Q^2, one needs to include the short distance hard QCD gluon exchange effects to make the electromagnetic form factors consistent with the QCD predictions. Here we follow a simple procedure suggested in [6], which uses the relativization technique of [61, 62]. We are perfectly aware of the fact that the wave functions of light vector mesons are still unknown; in the present exploratory study our major concern is to have a parameterization which is consistent with the size of vector mesons as suggested by the conventional spectroscopic models and has the short distance behavior driven by the hard QCD gluon exchange [62].

Let the $Vq\bar{q}$ vertex be $\Gamma\bar{q}V_\mu\gamma_\mu q$ where the vertex function Γ is a function of the lightcone invariant variable [61]

$$\mathbf{p^2} = \frac{1}{4}(M^2 - 4m_q^2) \tag{28}$$

where M is the invariant mass of the $q\bar{q}$ system

$$M^2 = \frac{m_q^2 + \mathbf{k}^2}{z(1-z)}\,, \tag{29}$$

$\mathbf{k}$ and m_q are the transverse momentum and quark mass, and z is the fraction of lightcone momentum of the meson carried by the quark ($0 < z < 1$). In the nonrelativistic limit $\mathbf{p}$ is the 3-momentum of the quark and we have the familiar relationship between the vertex function and the momentum space wave function

$$\Psi(\mathbf{p}^2) \propto \frac{\Gamma(\mathbf{p}^2)}{4\mathbf{p}^2 + 4m_q^2 - m_V^2}\,. \tag{30}$$

The hard gluon exchange Coulomb interaction $\frac{4}{3}\frac{\alpha_S(d)}{d}$, where $\mathbf{d}$ is the 3-dimensional quark-antiquark separation and $\alpha_S(d)$ is the running QCD coupling in the coordinate representation, is singular at the origin, $\mathbf{d} \to 0$, but becomes important only at short distances d, much smaller than the radius R_V of the vector meson. For this reason, the hard gluon Coulomb interaction can be treated perturbatively. Namely, let $\Psi_{soft}(\mathbf{d})$ be the wave function of the vector meson in the soft, non-singular potential. Solving the Schrödinger equation at small $\mathbf{d}$ to the first order in Coulomb interaction, one readily finds the Coulomb-corrected wave function of the form

$$\Psi(\mathbf{d}) = \Psi_{soft}(\mathbf{d}) + \Psi_{soft}(0)C\exp\left(-\frac{d}{2Ca(d)}\right). \tag{31}$$

Here $a(d)$ is the "running Bohr radius" equal to

$$a(d) = \frac{3}{8m\alpha_s(d)} \tag{32}$$

where $m = m_q/2$ is the reduced quark mass. The parameter C is controlled by the transition between the hard Coulomb and the soft confining interaction; we treat it as a variational parameter. (Similar analysis of the correction to the momentum space wave function for the short distance Coulomb interaction is reviewed in [62]). The 3-dimensional Fourier transform of the Coulomb-corrected wave function (31) reads

$$\Psi(\mathbf{p}) = N_0\left\{(2\pi R^2)^{3/2}\exp\left[-\frac{1}{2}p^2R^2\right] + C^4\,\frac{64a^3(p^2)\pi}{(1+4C^2a^2(p^2)p^2)^2}\right\}, \tag{33}$$

where $a(p^2)$ is still given by (32) with the running $\alpha_S(p^2)$ evaluated in the momentum representation.

The relativistic lightcone wave function $\Psi(z, \mathbf{k})$ is obtained from $\Psi(\mathbf{p})$ by the standard substitution of the light cone expression (28, 29) for the nonrelativistic $\mathbf{p^2}$ in (33) [61, 62]. The relativistic wave function thus obtained gives the correct QCD asymptotics $\propto \alpha_S(Q^2)/Q^2$ of the vector meson form factor, in perfect correspondence to the familiar hard QCD mechanism (for the review see [62]; the more detailed analysis of form factors will be presented elsewhere). Then, the lightcone radial wave function is the Fourier transform

$$\phi(r, z) = \int \frac{d^2\mathbf{k}}{(2\pi)^2}\,\Psi(z, \mathbf{k})\exp(i\mathbf{kr})\,. \tag{34}$$

With the conventional harmonic oscillator form of $\Psi_{soft}(\mathbf{d})$ we obtain the simple analytical formula

$$\phi_{1S}(r, z) = \Psi_0(1S)\left\{4z(1-z)\sqrt{2\pi R_{1S}^2}\exp\left[-\frac{m_q^2R_{1S}^2}{8z(1-z)}\right]\cdot\exp\left[-\frac{2z(1-z)r^2}{R_{1S}^2}\right]\exp\left[\frac{m_q^2R_{1S}^2}{2}\right] + C^4\,\frac{16a^3(r)}{AB^3}rK_1(\beta r)\right\} \tag{35}$$

where $a(r)$ is given by (32), $\beta = A/B$, and

$$A^2 = 1 + \frac{C^2a^2(r)m_q^2}{z(1-z)} - 4C^2a^2(r)m_q^2 \tag{36}$$

$$B^2 = \frac{C^2a^2(r)}{z(1-z)} \tag{37}$$

For the $1S$ ground state vector mesons we determine the parameters R_{1S}^2 and C by the standard variational procedure using the conventional linear+Coulomb potential models [23]. We check that the resulting wave function are consistent with the experimentally measured width of the $V \to e^+e^-$ decay (see Tab. 1). This is one of the major constraints because at very large Q^2 and/or $r_S \ll R_V$, the electroproduction amplitude is controlled by the wave function at the vanishing transverse size. For the heavy quarkonia, we

check that the radii of the $1S$ states are close to the results of more sophisticated solution of the Schrödinger equation [23]. The radius of the ρ^0 meson given by our wave function is consistent with the charge radius of the pion. Still another cross check is provided by $\sigma_{tot}(\rho^0 N)$ discussed in Sect. 3, which comes out very close to the pion-nucleon total cross section.

The node of the radial wave function of the $V'(2S)$ is expected at $r_n \sim R_V$ far beyond the Coulomb region. For this reason, we only modify the soft component of the wave function and take the same functional form of the Coulomb correction as for the $1S$ state:

$$\phi_{2S}(r,z) = \Psi_0(2S)\Bigg\{4z(1-z)\sqrt{2\pi R_{2S}^2}\exp\left[-\frac{m_q^2 R_{2S}^2}{8z(1-z)}\right]$$
$$\cdot\exp\left[-\frac{2z(1-z)r^2}{R_{2S}^2}\right]\exp\left[\frac{m_q^2 R_{2S}^2}{2}\right]$$
$$\cdot\Big\{1-\alpha\Big[1+m_q^2R_{2S}^2-\frac{m_q^2R_{2S}^2}{4z(1-z)}+\frac{4z(1-z)}{R_{2S}^2}r^2\Big]\Big\}$$
$$+C^4\,\frac{16a^3(r)}{AB^3}rK_1\beta r)\Bigg\}\Bigg\}. \qquad (38)$$

The new parameter α controls the position r_n of the node. The two parameters α and R_{2S} are determined from the orthogonality condition

$$\frac{N_c}{2\pi}\int_0^1\frac{dz}{z^2(1-z)^2}\int d^2\mathbf{r}\left\{m_q^2\phi_i(r,z)\phi_k(r,z)+[z^2\right.$$
$$\left.+(1-z)^2][\partial_r\phi_i(r,z)][\partial_r\phi_k(r,z)]\right\}=\delta_{ik} \qquad (39)$$

and from the $2S-1S$ mass splitting evaluated with the same linear+Coulomb potential. For the heavy quarkonia, we can check the resulting $V'(2S)$ wave function against the accurate data on the width of the $V'(2S)\to e^+e^-$ decay, the agreement in all the cases is good. The so determined parameters, the quark masses used and some comparisons with the experiment are summarized in Table 1. It is $Ca(r)$ which defines at which radii the interaction is important. A posteriori, for light vector mesons C is found small, the radius $Ca(r)$ is indeed small and the resulting parameters are consistent with the assumption that the Coulomb interaction is a short-distance perturbation. Furthermore, for the light vector mesons we find $R_{1S}\approx R_{2S}$. For heavier mesons C is larger and Coulomb effects are becoming more important and $R_{2S}>R_{1S}$ closer to the one for the Coulomb system (see Table 1). Because our Ansatz for the relativistic wave function has the correct short-distance QCD behavior and gives a reasonable description of soft cross sections, we believe it provides a reasonable interpolation between the soft and hard regimes in the electroproduction of vector mesons.

References

1. A.Donnachie and P.V.Landshoff, Phys. Lett. **B185** (1987) 403; J.R.Cuddell, Nucl. Phys. **B336** (1990) 1.
2. B.Z.Kopeliovich and B.G.Zakharov, Phys. Rev. **D44** (1991) 3466.
3. M.G.Ryskin, Z. Phys. **C57** (1993) 89.
4. B.Z.Kopeliovich, J.Nemchik, N.N.Nikolaev and B.G.Zakharov, Phys. Lett. **B309** (1993) 179.
5. B.Z.Kopeliovich, J.Nemchik, N.N.Nikolaev and B.G.Zakharov, Phys.Lett. **B324** (1994) 469.
6. J.Nemchik, N.N.Nikolaev and B.G.Zakharov, Phys.Lett. **B341** (1994) 228.
7. S.J.Brodsky et al., Phys. Rev. **D50** (1994) 3134.
8. J.R.Forshaw and M.G.Ryskin, Z. Phys. **C** (1995) to be published
9. N.N. Nikolaev and B.G. Zakharov, *Z. Phys.* **C49** (1991) 607; *Z. Phys.* **C53** (1992) 331.
10. N.Nikolaev and B.G.Zakharov, JETP **78** (1994) 598; Z. Phys. **C64** (1994)631.
11. N.N.Nikolaev, B.G.Zakharov and V.R.Zoller, JETP Letters **59** (1994) 8; JETP **78** (1994) 866; Phys. Lett. **B328** (1994) 486.
12. A.E.Mueller, Nucl. Phys. **B415** (1994) 373; A.E.Mueller and H.Patel, Nucl. Phys. **B425** (1994) 471; Z.Chen and A.E.Mueller, Nucl. Phys. **B451** (1995) 579.
13. N.N.Nikolaev and B.G.Zakharov, Phys. Lett. **B327** (1994) 157.
14. N.N.Nikolaev, Comments on Nucl. Part. Phys. **21** (1992) 41.
15. J.Nemchik, N.N.Nikolaev and B.G.Zakharov, Phys.Lett. **B339** (1994) 194.
16. NMC Collab., P.Amaudruz, et al., Nuc. Phys. **B 371** (1992) 3.
17. P.Frabetti et al., presented on Int. Europhys. Conf. on HEP, Brussels, July 27 - August 2, 1995.
18. P.Söding, Phys. Lett. **19** (1966) 702.
19. J.Pumplin, Phys. Rev. **D2** (1970) 1859.
20. K.Abe et al., Phys. Rev. Lett. **53** (1984) 751.
21. N.N.Nikolaev and B.G.Zakharov, Phys. Lett. **B327** (1994) 149.
22. F.E.Low, Phys. Rev. **D12** (1975) 163; J.F.Gunion and D.E.Soper, Phys. Rev. **D.15** (1977) 2617; A.B.Zamolodchikov, B.Z.Kopeliovich and L.I.Lapidus, JETP Letters **33** (1981) 612; G.Bertsch, S.Brodsky, A.S.Goldhaber and J.F.Gunion, Phys. Rev. Lett. **47** (1981) 297.
23. W.Buchmüller, S.-H.H.Tye, Phys. Rev. **D24** (1981) 132.
24. J.D.Bjorken, J.B.Kogut and D.E.Soper, Phys. Rev. **D3** (1971) 1382.
25. S.R.Gevorkyan and A.V.Tarasov, Dubna preprint **E2-94-465** (1994).
26. V.N.Gribov, A.A.Migdal, Sov. J. Nucl. Phys. **8** (1969) 703.
27. V.Barone, M.Genovese, N.N.Nikolaev, E.Predazzi and B.G.Zakharov, Z. Phys. **C58** (1993) 541; Int.J.Mod.Phys A, **8** (1993) 2779.
28. N.N.Nikolaev and B.G.Zakharov, Phys. Lett. **B332** (1994) 184.
29. T.H.Bauer, R.D.Spital, D.R.Yennie and F.M.Pipkin, Rev. Mod. Phys. **50** (1978) 261.
30. E665 Collab., M.R.Adams et al., Phys. Rev. Lett. **74** (1995) 1525.
31. NMC Collab., M.Arneodo, et al., Nucl.Phys. **B 429** (1994) 503.
32. ZEUS Collab., M.Derrick et al., Phys. lett. **B356** (1995) 601.
33. H1 Collab., T.Ahmed et al., Nucl. Phys. **B468** (1996) 3.
34. S.J.Brodsky and A.H.Mueller, Phys. Lett. **B206** (1988) 685.
35. M.R.Adams et al., Phys. Rev. Lett. **74** (1995) 1525.
36. H.Schellman, Blois Workshop on Diffractive and Elastic Scattering, Blois, June 1995
37. A.Donnachie and P.V.L.Landshoff, Phys. Lett. **B296** (1992) 227; Phys. Lett. **B348** (1995) 213.
38. ZEUS Collab., M.Derrick et al., High Q^2 Exclusive Vector Meson Production at HERA, paper **pa02-028**, submitted to the 28th International Conference on High Energy Physics, 25-31 July, 1996, Warsaw, Poland
39. OMEGA Collab., D.Aston et al. Nucl. Phys. **B209** (1982) 56; J.Park et al. Nucl. Phys. **B36** (1972) 404; R.M.Egloff et al. Phys. Rev. Lett. **43** (1979) 657.
40. ZEUS Collab., M.Derrick et al., Z. Phys. **C63** (1994) 391.
41. ZEUS Collab., M.Derrick et al., Z. Phys. **C69** (1995) 39.
42. ZEUS Collab., M.Derrick et al., Measurement of ρ^0 Photoproduction at HERA, paper **pa02-050**, submitted to the 28th International Conference on High Energy Physics, 25-31 July, 1996, Warsaw, Poland
43. H1 Collab., S.Aid et al., Nucl. Phys. **B463** (1996) 3.
44. J. Busenitz et al., Phys. Rev. **D40** (1989) 40 and refrences therein.
45. ZEUS Collab., M.Derrick et al., Phys. Lett. **B377** (1996) 259.
46. ZEUS Collab., M.Derrick et al., Measurement of the Reaction $\gamma^* p\to\phi p$ in Deep Inelastic Scattering at HERA, **DESY 96-067** (April 1996), accepted in Phys. Lett. **B**
47. H1 Collab., S.Aid et al., Elastic Electroproduction of ϕ Mesons at Large Q^2 at HERA, paper **pa02-064**, submitted to the 28th International Conference on High Energy Physics, 25-31 July, 1996, Warsaw, Poland

48. O.Benhar, B.G.Zakharov, N.N.Nikolaev and S.Fantoni, Phys. Rev. Lett. **74** (1995) 3565.
49. A.Donnachie and A.B.Clegg, Z. Phys. **C42** (1989) 663 and references therein.
50. Review of Particle Properties, Phys. Rev. **D50** (1994) 1177.
51. E665 Collab., C.Salgado, Workshop on CT at CEBAF, May, 1995
52. H1 Collab., S.Aid et al., Elastic ρ' Electroproduction at High Q^2 , paper **pa01-088**, submitted to the 28th International Conference on High Energy Physics, 25-31 July, 1996, Warsaw, Poland
53. N.N.Nikolaev, B.G.Zakharov and V.R.Zoller, Phys. Lett. **B366** (1996) 337.
54. J.Nemchik, N.N.Nikolaev, E.Predazzi and B.G.Zakharov, BFKL pomeron and diffractive electroproduction of heavy vector mesons at HERA, paper in preparation
55. H1 Collab., S.Aid et al., Nucl. Phys. **B472** (1996) 3.
56. ZEUS Collab., M.Derrick et al., Phys. Lett. **B350** (1995) 120.
57. EMC Collab., J.J.Aubert et al., Phys. Lett. **B89** (1980) 267.
58. L.Frabetti et al., Phys. Lett. **B316** (1993) 197.
59. EMC Collab., J.J.Aubert et al., Nucl. Phys. **B213** (1983) 1; J.Ashman et al.,Z. Phys. **C39** (1988) 169.
60. EMC Collab., J.J.Aubert et al., Phys. Lett. **B161** (1985) 203.
61. M.V.Terentiev, Sov. J. Nucl. Phys. **24** (1976) 106.
62. S.J.Brodsky and G.P.Lepage, in Perturbative Quantum Chromodynamics, editor A.H.Mueller, World Scientific, Singapore, 1989.

Eur. Phys. J. C 18, 711–718 (2001)
Digital Object Identifier (DOI) 10.1007/s100520100572

THE EUROPEAN PHYSICAL JOURNAL C

Anomalous t-dependence in diffractive electroproduction of $2S$ radially excited light vector mesons at HERA

J. Nemchik

Institute of Experimental Physics, Slovak Academy of Sciences, Watsonova 47, 04353 Košice, Slovakia

Received: 5 September 2000 / Revised version: 24 November 2000 /
Published online: 23 January 2001 – © Springer-Verlag 2001

Abstract. Within the color dipole gBFKL phenomenology of the diffraction slope we predict an anomalous t-dependence of the differential cross section $\mathrm{d}\sigma/\mathrm{d}t$ as a function of energy and Q^2 for the production of radially excited $V'(2S)$ light vector mesons. The pattern we found for the t-dependence for $\mathrm{d}\sigma/\mathrm{d}t$ is in contradiction with the well-known standard monotonical t-behavior for the $V(1S)$ vector mesons. The origin of this phenomenon lies in the interplay of the nodal structure of the $V'(2S)$ radial wave function and the energy and dipole size dependence of the color dipole cross section and the diffraction slope. We show how a different position of the node in the $V'(2S)$ wave function leads to a different pattern of anomalous t-behavior of $\mathrm{d}\sigma/\mathrm{d}t$ and discuss the possibility to determine this position from the low energy and HERA data.

1 Introduction

The diffractive photo- and electroproduction of ground state ($V(1S)$) and radially excited ($V'(2S)$) vector mesons,

$$\gamma^* p \to V(V')p \quad V = \rho, \Phi, \omega, J/\Psi, \Upsilon \cdots \\ (V' = \rho', \Phi', \omega', \Psi', \Upsilon' \cdots), \qquad (1)$$

at high c.m.s. energy $W = s^{1/2}$, intensively studied by the recent experiments at HERA, represents one of the main sources for the further development of pomeron physics. Pomeron exchange in the diffractive leptoproduction of vector mesons at high energies has been intensively studied [1–9] within the framework of perturbative QCD (pQCD).

The standard approach to pQCD is based on the BFKL equation [10–12], which represents the integral equation for the leading-log s (LLs) evolution of the gluon distribution, formulated in the scaling approximation of the infinite gluon correlation radius $R_{\rm c} \to \infty$ (massless gluons) and of the fixed running coupling $\alpha_{\rm S} = $ const. Later, however, a novel s-channel approach to the LLs BFKL equation (the running gBFKL approach) has been developed [13,14] in terms of the color dipole cross section $\sigma(\xi, r)$ (hereafter r is the transverse size of the color dipole, $\xi = \log(W^2 + Q^2)/(m_V^2 + Q^2)$ is the rapidity variable) which consistently incorporates the asymptotic freedom (AF) (i.e. the running QCD coupling $\alpha_{\rm S}(r)$) and the finite propagation radius $R_{\rm c}$ of perturbative gluons. The freezing of $\alpha_{\rm S}(r)$, $\alpha_{\rm S}(r) \leq \alpha_{\rm S}^{\rm fr}$, and the gluon correlation radius $R_{\rm c}$ represent the nonperturbative parameters, which describe the transition from the soft (nonperturbative, infrared) to the hard (perturbative) region.

The details of the gBFKL phenomenology of diffractive electroproduction of light vector mesons are presented in [15]. The color dipole phenomenology of the diffraction slope for photo- and electroproduction of heavy vector mesons has been developed in [16]. The analysis of the diffractive production of light [6,15] and heavy [16] vector mesons at $t = 0$ within the gBFKL phenomenology shows that the $V(1S)$ vector meson production amplitude probes the color dipole cross section at the dipole size $r \sim r_S$ (*scanning phenomenon* [17,4–6]), where the scanning radius can be expressed through the scale parameter A:

$$r_{\rm S} \approx \frac{A}{\sqrt{m_V^2 + Q^2}}, \qquad (2)$$

where Q^2 is the photon virtuality, m_V is the vector meson mass and $A \approx 6$. Consequently, changing Q^2 and the mass of the produced vector meson one can probe the dipole cross section $\sigma(\xi, r)$ and the dipole diffraction slope $B(\xi, r)$ and thus measure the effective intercept $\Delta_{\rm eff}(\xi, r) = \partial \log \sigma(\xi, r)/\partial\xi$ and the local Regge slope $\alpha'_{\rm eff}(\xi, r) = (1/2)\partial B(\xi, r)/\partial\xi$ in a very broad range of the dipole size r. This fact allows one to study the transition from large nonperturbative dipole size $r_{\rm S} \gg R_{\rm c}$ to the perturbative region of very short $r_{\rm S} \ll R_{\rm c}$.

The experimental investigation of the electroproduction of radially excited $V'(2S)$ vector mesons can provide additional information on the dipole cross section and the dipole diffraction slope.

The presence of the node in the $V'(2S)$ radial wave function leads to a strong cancellation of dipole size contributions to the production amplitude from the region above and below the node position $r_{\rm n}$ (the node effect [2,17,4, 18,15,16]). For this reason the amplitudes for the electroproduction of the $V(1S)$ and $V'(2S)$ vector mesons probe $\sigma(\xi,r)$ and $B(\xi,r)$ in a different way. The onset of a strong node effect has been demonstrated in [15], where the study of the electroproduction of $V'(2S)$ light vector mesons has shown a very spectacular pattern of anomalous Q^2 and energy dependence for the production cross section. For the electroproduction of $V'(2S)$ heavy vector mesons the node effect becomes much weaker but still leads to a slightly different Q^2- and energy dependence of the production cross section for Ψ' versus J/Ψ and to a nonmonotonical Q^2-dependence of the diffraction slope at small $Q^2 \lesssim 5\,{\rm GeV}^2$ for Ψ' production [16]. Another manifestation of the node effect experimentally confirmed at HERA (and at fixed target experiments as well) in J/Ψ and Ψ' photoproduction is a strong suppression of the diffractive production of $V'(2S)$ versus $V(1S)$. The stronger the node effect, the smaller is the $V'(2S)/V(1S)$ ratio of the production cross sections. The node effect also leads to a counterintuitive inequality, $B(\gamma^*\to\Psi') \lesssim B(\gamma^*\to J/\Psi)$ [16], which can be tested at HERA. Therefore, it is very important to further explore the salient features of the node effect in conjunction with the emerging gBFKL phenomenology of the diffraction slope [19,20,16], especially in the production of $V'(2S)$ light vector mesons where the node effect is expected to be very strong. An anomalous energy and Q^2-dependence of the diffraction slope for the production of $V'(2S)$ light vector mesons has recently been studied in [21]. We found a correspondence between a specific nonmonotonic Q^2 and energy behavior of the diffraction slope and the position of the node in the $V'(2S)$ radial wave function. Moreover, we demonstrated that the above counterintuitive inequality found for the production of heavy vector mesons is not always valid for the production of light vector mesons.

In the present paper we concentrate on the model predictions for the differential cross sections ${\rm d}\sigma(\gamma^*\to V(1S))/{\rm d}t$ and ${\rm d}\sigma(\gamma^*\to V'(2S))/{\rm d}t$ at different energies and Q^2 and discuss for the first time how the explicit pattern of anomalous t behavior of ${\rm d}\sigma(\gamma^*\to V'(2S))/{\rm d}t$ is connected with the position of the node in the radial wave function. We predict a strikingly different t-dependence of the differential cross section at different energies and Q^2 for the production of $V'(2S)$ versus $V(1S)$ vector mesons. The pattern we found for the anomalous t-behavior for ${\rm d}\sigma(\gamma^*\to V'(2S))/{\rm d}t$ can be tested at HERA.

This paper is organized as follows. In Sect. 2 we present a very short description of the color dipole phenomenology of diffractive photo- and electroproduction of vector mesons and the main results of the gBFKL phenomenology of the diffraction slope. In Sect. 3 we present the model predictions for the differential cross sections ${\rm d}\sigma(\gamma^*\to V(1S))/{\rm d}t$ and ${\rm d}\sigma(\gamma^*\to V'(2S))/{\rm d}t$ at different Q^2 and energies, and we discuss how the position of the node in the $V'(2S)$ radial wave function can be extracted from the data. The summary and conclusions are presented in Sect. 4.

2 Short review of the color dipole phenomenology for vector meson production and the diffraction slope

In the mixed $(\mathbf{r},z)$-representation the high energy meson is considered as a system of a color dipole described by the distribution of the transverse separation $\mathbf{r}$ of the quark and antiquark given by the $q\bar q$ wave function $\Psi(\mathbf{r},z)$, where z is the fraction of the meson's light-cone momentum carried by a quark. The Fock state expansion for the relativistic meson starts with the $q\bar q$ state, and the higher Fock states $q\bar qg\cdots$ become very important at high energy. The interaction of the relativistic color dipole of the dipole size $\mathbf{r}$ with the target nucleon is quantified by the energy dependent color dipole cross section $\sigma(\xi,r)$ satisfying the gBFKL equation [13,14] for the energy evolution. This reflects the fact that in the leading-$\log 1/x$ approximation the effect of higher Fock states can be reabsorbed into the energy dependence of $\sigma(\xi,r)$. The dipole cross section is flavor independent and represents the universal function of r which describes various diffractive processes in unified form. At high energy when the transverse separation $\mathbf{r}$ of the quark and antiquark is frozen during the interaction process, the scattering matrix describing the $q\bar q$–nucleon interaction becomes diagonal in the mixed $(\mathbf{r},z)$-representation (z is known also as the Sudakov light-cone variable). This diagonalization property exists even when the dipole size $\mathbf{r}$ is large, i.e. beyond the perturbative region of short distances. The detailed discussion of the space-time pattern of diffractive electroproduction of vector mesons is presented in [16,15].

Following the advantage of the $(\mathbf{r},z)$-diagonalization of the $q\bar q$–N scattering matrix, the imaginary part of the production amplitude for the real (virtual) photoproduction of vector mesons with momentum transfer $\mathbf{q}$ can be represented in the factorized form

$$\begin{aligned}{\rm Im}\mathcal{M}(\gamma^*\to V,\xi,Q^2,\mathbf{q}) &= \langle V|\sigma(\xi,r,z,\mathbf{q})|\gamma^*\rangle \\ &= \int\limits_0^1 {\rm d}z\int {\rm d}^2\mathbf{r}\sigma(\xi,r,z,\mathbf{q})\Psi_V^*(\mathbf{r},z)\Psi_{\gamma^*}(\mathbf{r},z) \quad (3)\end{aligned}$$

the normalization of which is ${\rm d}\sigma/{\rm d}t|_{t=0} = |\mathcal{M}|^2/16\pi$. In (3), $\Psi_{\gamma^*}(\mathbf{r},z)$ and $\Psi_V(\mathbf{r},z)$ represent the probability amplitudes to find a color dipole of size r in the photon and quarkonium (vector meson), respectively. The color dipole distribution in (virtual) photons was derived in [22,13]. $\sigma(\xi,r,z,\mathbf{q})$ is the scattering matrix for the $q\bar q$–N interaction and represents the above mentioned color dipole cross section for $\mathbf{q}=0$. The color dipole cross section $\sigma(\xi,r)$ depends only on the dipole size r. For small $\mathbf{q}$, as considered in this paper, one can safely neglect the z-dependence of $\sigma(\xi,r,z,\mathbf{q})$ for light and heavy vector meson production and set $z=1/2$. This follows partially from the analysis

within a double gluon exchange approximation [22] leading to a slow z-dependence of the dipole cross section.

The energy dependence of the dipole cross section is quantified in terms of the dimensionless rapidity $\xi = \log 1/x_{\rm eff}$; $x_{\rm eff}$ is the effective value of the Bjorken variable

$$x_{\rm eff} = \frac{Q^2 + m_V^2}{Q^2 + W^2} \approx \frac{m_V^2 + Q^2}{2\nu m_p}, \tag{4}$$

where m_p and m_V is the proton mass and mass of the vector meson, respectively. Hereafter, we will write the energy dependence of the dipole cross section in both variables, either in ξ or in $x_{\rm eff}$ whatever seems convenient.

The production amplitudes for the transversely (T) and the longitudinally (L) polarized vector mesons with small momentum transfer $\mathbf{q}$ can be written in more explicit form [6,16]:

$$\begin{aligned}
&{\rm Im}\mathcal{M}_{\rm T}(x_{\rm eff}, Q^2, \mathbf{q}) \\
&= \frac{N_c C_V \sqrt{4\pi\alpha_{\rm em}}}{(2\pi)^2} \int {\rm d}^2\mathbf{r}\sigma(x_{\rm eff}, r, \mathbf{q}) \\
&\quad \times \int_0^1 \frac{{\rm d}z}{z(1-z)} \left\{ m_q^2 K_0(\varepsilon r)\phi(r,z) - [z^2 + (1-z)^2] \right. \\
&\quad \left. \times \varepsilon K_1(\varepsilon r)\partial_r\phi(r,z) \right\} \\
&= \frac{1}{(m_V^2 + Q^2)^2} \int \frac{{\rm d}r^2}{r^2} \frac{\sigma(x_{\rm eff}, r, \mathbf{q})}{r^2} W_{\rm T}(Q^2, r^2)
\end{aligned} \tag{5}$$

$$\begin{aligned}
&{\rm Im}\mathcal{M}_{\rm L}(x_{\rm eff}, Q^2, \mathbf{q}) \\
&= \frac{N_c C_V \sqrt{4\pi\alpha_{\rm em}}}{(2\pi)^2} \frac{2\sqrt{Q^2}}{m_V} \int {\rm d}^2\mathbf{r}\sigma(x_{\rm eff}, r, \mathbf{q}) \int_0^1 {\rm d}z \\
&\quad \times \left\{ [m_q^2 + z(1-z)m_V^2] K_0(\varepsilon r)\phi(r,z) - \partial_r^2\phi(r,z) \right\} \\
&= \frac{1}{(m_V^2 + Q^2)^2} \frac{2\sqrt{Q^2}}{m_V} \int \frac{{\rm d}r^2}{r^2} \frac{\sigma(x_{\rm eff}, r, \mathbf{q})}{r^2} W_{\rm L}(Q^2, r^2),
\end{aligned} \tag{6}$$

where

$$\varepsilon^2 = m_q^2 + z(1-z)Q^2; \tag{7}$$

$\alpha_{\rm em}$ is the fine structure constant, $N_c = 3$ is the number of colors, $C_V = 1/2^{1/2}$, $1/(3\sqrt{2})$, $1/3$, $2/3$, $1/3$ for ρ^0, ω^0, ϕ^0, $J/\Psi, \Upsilon$ production, respectively, and the $K_{0,1}(x)$ are the modified Bessel functions. The detailed discussion and parameterization of the light-cone radial wave function $\phi(r,z)$ of the $q\bar{q}$ Fock state of the vector meson is given in [15].

The terms $\propto \epsilon K_1(\epsilon r)\partial_r\phi(\mathbf{r},z)$ for (T) polarization and $\propto K_0(\epsilon r)\partial_r^2\Phi(\mathbf{r},z)$ for (L) polarization in the integrands of (5) and (6) represent the relativistic corrections; these become important at large Q^2 and for the production of light vector mesons. For the production of heavy quarkonia, the nonrelativistic approximation can be used with a rather high accuracy [2].

For small dipole size and $\mathbf{q} = 0$ in the leading-$\log 1/x$ approximation the dipole cross section can be related to the gluon structure function $G(x,q^2)$ of the target nucleon through

$$\sigma(x,r) = \frac{\pi^2}{3} r^2 \alpha_s(r) G(x,q^2), \tag{8}$$

where the gluon structure function enters at the factorization scale $q^2 \sim B/r^2$ [23] with the parameter $B \sim 10$ [24].

The weight functions $W_{\rm T}(Q^2,r^2)$ and $W_{\rm L}(Q^2,r^2)$ introduced in (5) and (6) have a smooth Q^2-behavior [6] and are very convenient for the analysis of the scanning phenomenon. They are sharply peaked at $r \approx A_{\rm T,L}/(Q^2 + m_V^2)^{1/2}$. At small Q^2 the values of the scale parameter $A_{\rm T,L}$ are close to $A \sim 6$, which follows from $r_{\rm S} = 3/\varepsilon$ with the nonrelativistic choice $z = 1/2$. In general, $A_{\rm T,L} \geq 6$ and increases slowly with Q^2 [6]. For the production of light vector mesons the relativistic corrections play an important role, especially at large $Q^2 \gg m_V^2$, and they lead to a Q^2-dependence of $A_{\rm L,T}$ coming from the large size asymmetric $q\bar{q}$-configurations $A_{\rm L}(\rho^0; Q^2 = 0) \approx 6.5$, $A_{\rm L}(\rho^0; Q^2 = 100\,{\rm GeV}^2) \approx 10$, $A_{\rm T}(\rho^0; Q^2 = 0) \approx 7$, $A_{\rm T}(\rho^0, Q^2 = 100\,{\rm GeV}^2) \approx 12$ [6]. Due to an extra factor $z(1-z)$ in the integrand of (6) in comparison with (5) the contribution from asymmetric $q\bar{q}$-configurations to the longitudinal meson production is considerably smaller.

The integrands in (5) and (6) contain the dipole cross section $\sigma(\xi, r, \mathbf{q})$. As was already mentioned, due to a very slow onset of the pure perturbative region (see (2)) one can easily anticipate a contribution to the production amplitude coming from the semiperturbative and nonperturbative $r \gtrsim R_{\rm c}$. Following the simplest assumption about the additive property of the perturbative and nonperturbative mechanism of interaction we can represent the contribution of the bare pomeron exchange to $\sigma(\xi, r, \mathbf{q})$ as a sum of the perturbative and nonperturbative components[1]:

$$\sigma(\xi, r, \mathbf{q}) = \sigma_{\rm pt}(\xi, r, \mathbf{q}) + \sigma_{\rm npt}(\xi, r, \mathbf{q}), \tag{9}$$

with the parameterization of both components at small $\mathbf{q}$

$$\begin{aligned}
&\sigma_{\rm pt,npt}(\xi, r, \mathbf{q}) = \\
&\sigma_{\rm pt,npt}(\xi, r, \mathbf{q} = 0) \exp\left(-\frac{1}{2} B_{\rm pt,npt}(\xi, r)\mathbf{q^2} \right).
\end{aligned} \tag{10}$$

Here $\sigma_{\rm pt,npt}(\xi, r, \mathbf{q} = 0) = \sigma_{\rm pt,npt}(\xi, r)$ represent the contributions of the perturbative and nonperturbative mechanisms to the $q\bar{q}$–nucleon interaction cross section, respectively; $B_{\rm pt}(\xi, r)$ and $B_{\rm npt}(\xi, r)$ are the corresponding dipole diffraction slopes.

The small real part of the production amplitudes can be taken in the form [25]

$${\rm Re}\mathcal{M}(\xi, r) = \frac{\pi}{2} \frac{\partial}{\partial\xi} {\rm Im}\mathcal{M}(\xi, r), \tag{11}$$

and can easily be included in the production amplitudes (5) and (6) using the substitution

$$\begin{aligned}
\sigma(x_{\rm eff}, r, \mathbf{q}) &\to \left(1 - {\rm i}\frac{\pi}{2} \frac{\partial}{\partial \log x_{\rm eff}} \right) \sigma(x_{\rm eff}, r) \\
&= [1 - {\rm i}\alpha_V(x_{\rm eff}, r)]\sigma(x_{\rm eff}, r, \mathbf{q}).
\end{aligned} \tag{12}$$

[1] The additive property of such a decomposition of the dipole cross section has been already discussed in [15,16]

The formalism for the calculation of $\sigma_{\rm pt}(\xi,r)$ in the leading-log s approximation was developed in [22,13,14]. The contribution $\sigma_{\rm npt}(\xi,r)$ to the dipole cross section was used in [26,6,15,16], where we assumed that this soft nonperturbative component of the pomeron is a simple Regge pole with intercept $\Delta_{\rm npt}=0$. The particular form together with the assumption of the energy independent $\sigma_{\rm npt}(\xi=\xi_0,r)=\sigma_{\rm npt}(r)$ (ξ_0 corresponds to the boundary condition for the gBFKL evolution: $\xi_0=\log(1/x_0)$, $x_0=0.03$) allows one to successfully describe the proton structure function at very small Q^2 [26], the real photoabsorption [6] and the diffractive real and virtual photoproduction of light [15] and heavy [16] vector mesons. A larger contribution of the nonperturbative pomeron exchange to $\sigma_{\rm tot}(\gamma p)$ versus $\sigma_{\rm tot}(\gamma^* p)$ can, for example, explain the much slower rise with energy of the real photoabsorption cross section $\sigma_{\rm tot}(\gamma p)$ in comparison with $F_2(x,Q^2)\propto\sigma_{\rm tot}(\gamma^* p)$ observed at HERA [27,28]. Besides, the reasonable form of $\sigma_{\rm npt}(r)$ was confirmed in the process of the first determination of the dipole cross section from the data on vector meson electroproduction [29]. The energy and dipole size dependence of the extracted $\sigma(\xi,r)$ is in a good agreement with the dipole cross section obtained from the gBFKL dynamics [6,26]. The nonperturbative component of the pomeron exchange plays a dominant role at low NMC energies in the production of the light vector mesons, where the scanning radius $r_{\rm S}$, see (2), is large. However, the perturbative component of the pomeron becomes more important with the rise of energy also in the nonperturbative region of the dipole size.

If one starts with the familiar impact-parameter representation for the amplitude of elastic scattering of the color dipole,

$$\mathrm{Im}\mathcal{M}(\xi,r,\mathbf{q})=2\int \mathrm{d}^2\mathbf{b}\,\exp(-\mathrm{i}\mathbf{q}\mathbf{b})\Gamma(\xi,\mathbf{r},\mathbf{b}),\qquad(13)$$

then the diffraction slope $B=-2\mathrm{d}\log\mathrm{Im}\mathcal{M}/\mathrm{d}q^2|_{q=0}$ equals

$$B(\xi,r)=\frac{1}{2}\langle\mathbf{b}^{\,2}\rangle=\lambda(\xi,r)/\sigma(\xi,r),\qquad(14)$$

where

$$\lambda(\xi,r)=\int \mathrm{d}^2\mathbf{b}\mathbf{b}^2\Gamma(\xi,\mathbf{r},\mathbf{b}).\qquad(15)$$

The generalization of the color dipole factorization formula (3) to the diffraction slope of the reaction $\gamma^* p\to Vp$ reads

$$B(\gamma^*\to V,\xi,Q^2)\mathrm{Im}\mathcal{M}(\gamma^*\to V,\xi,Q^2,\mathbf{q}=0)$$
$$=\int\limits_0^1\mathrm{d}z\int\mathrm{d}^2\mathbf{r}\lambda(\xi,r)\Psi_V^*(r,z)\Psi_{\gamma^*}(r,z).\qquad(16)$$

The diffraction cone in the color dipole gBFKL approach for the production of vector mesons has been studied in detail in [16]. Here we only present the salient feature of the color diffraction slope emphasizing the presence of the geometrical contribution from the beam dipole, $r^2/8$, and the contribution from the target proton size, $R_N^2/3$:

$$B(\xi,r)=\frac{1}{8}r^2+\frac{1}{3}R_N^2+2\alpha'_{I\!P}(\xi-\xi_0)+\mathcal{O}(R_{\rm c}^2),\qquad(17)$$

where R_N is the radius of the proton. For the electroproduction of light vector mesons the scanning radius is larger than the correlation one, $r\gtrsim R_{\rm c}$, even for $Q^2\lesssim 50\,\mathrm{GeV}^2$, and one recovers a sort of additive quark model, in which the uncorrelated gluonic clouds build up around the beam and target quarks and antiquarks and the term $2\alpha'_{I\!P}(\xi-\xi_0)$ describes the familiar Regge growth of the diffraction slope for the quark–quark scattering. The geometrical contribution to the diffraction slope from the target proton size $(1/3)R_N^2$ persists for all the dipole sizes $r\gtrsim R_{\rm c}$ and $r\lesssim R_{\rm c}$. The last term in (17) is also associated with the proton size and is negligibly small.

The soft pomeron and diffractive scattering of a large color dipole have also been studied in detail in [16]. Here we assume the conventional Regge rise of the diffraction slope for the soft pomeron [16]

$$B_{\rm npt}(\xi,r)=\Delta B_{\rm d}(r)+\Delta B_N+2\alpha'_{\rm npt}(\xi-\xi_0),\qquad(18)$$

where $\Delta B_{\rm d}(r)$ and ΔB_N stand for the contribution from the beam dipole and target nucleon size. As a guidance we take the experimental data on the pion–nucleon scattering [30], which suggest $\alpha'_{\rm npt}=0.15\,\mathrm{GeV}^{-2}$. In (18) the proton size contribution is

$$\Delta B_N=\frac{1}{3}R_N^2,\qquad(19)$$

and the beam dipole contribution has been proposed to have the form [16]

$$\Delta B_{\rm d}(r)=\frac{r^2}{8}\frac{r^2+aR_N^2}{3r^2+aR_N^2},\qquad(20)$$

where a is a phenomenological parameter, $a\sim 1$. We take $\Delta B_N=4.8\,\mathrm{GeV}^{-2}$. Then the pion–nucleon diffraction slope is reproduced with a reasonable value of the parameter a in (20): $a=0.9$ for $\alpha'_{\rm npt}=0.15\,\mathrm{GeV}^{-2}$.

Following the simple geometrical properties of the gBFKL diffraction slope $B(\xi,r)$ (see (17) and [19]) one can express its energy dependence through the energy dependent effective Regge slope $\alpha'_{\rm eff}(\xi,r)$

$$B_{\rm pt}(\xi,r)\approx\frac{1}{3}\langle R_N^2\rangle+\frac{1}{8}r^2+2\alpha'_{\rm eff}(\xi,r)(\xi-\xi_0).\qquad(21)$$

The effective Regge slope $\alpha'_{\rm eff}(\xi,r)$ varies with energy differently at different dipole sizes [19]. At fixed scanning radius and/or $Q^2+m_V^2$, it decreases with energy. At fixed rapidity ξ and/or $x_{\rm eff}$, see (4), $\alpha'_{\rm eff}(\xi,r)$ rises with $r\lesssim 1.5\,\mathrm{fm}$. At fixed energy it is a flat function of the scanning radius. At asymptotically large ξ (W), $\alpha'_{\rm eff}(\xi,r)\to\alpha'_{I\!P}=0.072\,\mathrm{GeV}^{-2}$. At lower and HERA energies the subasymptotic $\alpha'_{\rm eff}(\xi,r)\sim(0.15\text{–}0.20)\,\mathrm{GeV}^{-2}$ and is very close to $\alpha'_{\rm soft}$ known from the Regge phenomenology of soft scattering. This means that the gBKFL dynamics predicts

a substantial rise with the energy and dipole size of the diffraction slope $B(\xi,r)$ in accordance with the energy and dipole size dependence of the effective Regge slope $\alpha'_{\rm eff}(\xi,r)$ and due to the presence of the geometrical components $\propto r^2$ in (17) and $\Delta B_{\rm d}(r) \propto r^{1.7}$ in (18) (see also (20))[2]. The overall dipole diffraction slope contains contributions from both $B_{\rm npt}(\xi,r)$ and $B_{\rm pt}(\xi,r)$ and the corresponding geometrical component has r^α-behavior with $1.7 < \alpha \lesssim 2.0$. Therefore, for discussions on the qualitative level in the subsequent section we assume (with a quite reasonable accuracy) an approximate r^2-dependence of the geometrical component contribution to the dipole diffraction slope.

Using the expressions (5) and (6) for the (T) and (L) production amplitudes in conjunction with (9), (10), (18) and (21) we can calculate the differential cross section of the vector meson electroproduction as a function of t.

3 Anomalous t-dependence of the differential cross section for the production of $V'(2S)$ vector mesons

The most important feature for $V'(2S)$ vector meson production is the node effect – the Q^2- and energy dependent cancellations from the soft (large size) and hard (small size) contributions (i.e. from the region above and below the node position, $r_{\rm n}$) to the $V'(2S)$ production amplitude. The strong Q^2-dependence of these cancellations comes from the scanning phenomenon (2) when the scanning radius $r_{\rm S}$ for some value of Q^2 is close to $r_{\rm n} \sim R_V$ (R_V is the vector meson radius). The energy dependence of the node effect is due to a different energy dependence of the dipole cross section at small ($r < R_V$) and large ($r > R_V$) dipole sizes. We would like to emphasize from the very beginning that in the region of energy and Q^2 where the exact node effect is encountered the predictive power becomes weak and the predictions are strongly model dependent. The model predictions for $V'(2S)$ vector mesons presented in this section serve mostly as an illustration of a possible anomalous Q^2 and energy dependence[3].

There are several reasons to expect that for the production of $V'(2S)$ light vector mesons the node effect depends on the polarization of the virtual photon and of the produced vector meson [15]. First, the wave functions of (T) and (L) polarized (virtual) photons are different. Second, different regions of z contribute to $\mathcal{M}_{\rm T}$ and $\mathcal{M}_{\rm L}$. Third, different scanning radii for the production of (T) and (L) polarized vector mesons and the different energy dependence of $\sigma(\xi,r)$ at these scanning radii lead to a different Q^2 and energy dependence of the node effect in the production of (T) and (L) polarized $V'(2S)$ vector mesons. Not so for the nonrelativistic limit of heavy quarkonia, where the node effect is very weak and is approximately polarization independent. There is only a weak polarization dependence of the node effect for Ψ' production [16]. For Υ' production the node effect is negligibly small and is almost polarization independent.

There are two possible scenarios for the node effect which can occur in the $V'(2S)$ production amplitude: the undercompensation and the overcompensation scenario [18].

In the undercompensation scenario, the $V'(2S)$ production amplitude $\langle V'(2S)|\sigma(\xi,r)|\gamma^*\rangle$ is dominated by the positive contribution coming from small dipole sizes, $r \lesssim r_{\rm n}$, and the $V(1S)$ and $V'(2S)$ photoproduction amplitudes have the same sign. This scenario corresponds namely to the production of $V'(2S)$ heavy vector mesons $\Psi'(2S)$ and $\Upsilon'(2S)$. In the overcompensation scenario, the $V'(2S)$ production amplitude is dominated by the negative contribution coming from large dipole sizes, $r \gtrsim r_{\rm n}$, and the $V(1S)$ and $V'(2S)$ photoproduction amplitudes have opposite sign[4].

The anomalous properties of the diffraction slope were recently studied in [21] and come from the expression (16), which can be rewritten as the ratio of two matrix elements:

$$B(\gamma^*\to V(V'),\xi,Q^2) = \frac{\int\limits_0^1 {\rm d}z \int {\rm d}^2\mathbf{r}\Psi^*_{V(V')}(r,z)\sigma(\xi,r)B(\xi,r)\Psi_{\gamma^*}(r,z)}{\int\limits_0^1 {\rm d}z \int {\rm d}^2\mathbf{r}\Psi^*_{V(V')}(r,z)\sigma(\xi,r)\Psi_{\gamma^*}(r,z)}. \quad (22)$$

The production amplitude in the denominator of (22) is dominated by the contribution from the dipole size corresponding to the scanning radius $r_{\rm S}$ (2). However, due to the approximately $\propto r^2$ behavior of the dipole diffraction slope (see the discussion in Sect. 2), the integrand of the matrix element in the numerator of (22), is peaked by $r = r_B \sim 5/3 r_{\rm S} > r_{\rm S}$.

Let us discuss now the possible peculiarities in the t-dependence of the differential cross section ${\rm d}\sigma/{\rm d}t$ for the $V'(2S)$ production. Because of an approximate $\propto r^2$ behavior of the geometrical contribution to the diffraction slope, the large size negative contribution to the production amplitude from the region above the node position corresponds to a larger value of the diffraction slope than the small size contribution from the region below the node position. This means that the negative contribution to the $V'(2S)$ production amplitude has a steeper t-dependence than the positive contribution. This can be understood in a somewhat demonstrative form when the t-dependent production amplitude reads

[2] The dipole size behavior of $\Delta B_{\rm d}(r)$ (20) representing the geometrical contribution to the dipole diffraction slope $B_{\rm npt}(\xi,r)$ (18) for diffractive scattering of a large color dipole has the standard r^2-dependence at small, $r^2 \ll aR_N^2$, and large, $r^2 \gg aR_N^2$, values of the dipole size, respectively. In the intermediate region, $r^2 \sim aR_N^2$, which corresponds to the production of $V(1S)$ and $V'(2S)$ light vector mesons, the dipole size dependence of $\Delta B_{\rm d}(r)$ can be parameterized by the power function r^α with $\alpha \sim 1.7$

[3] Manifestations of the node effect in electroproduction on nuclei were discussed in [18,31]

[4] A discussion of the experimental determination of the relative sign of the $V'(2S)$ and $V(1S)$ production amplitudes using the so-called Söding–Pumplin effect [32,33] is presented in [15]

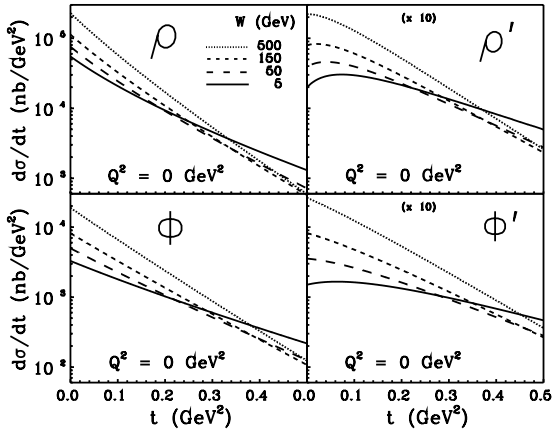

Fig. 1. The color dipole model predictions for the differential cross sections $\mathrm{d}\sigma(\gamma^* \to V(V'))/\mathrm{d}t$ for the real photoproduction ($Q^2 = 0$) of $\rho^0, \rho'(2S), \phi^0$ and $\phi'(2S)$ at different values of the c.m.s. energy W

$$\mathcal{M}(t) = \alpha \exp\left(-\frac{1}{2}B_1 t\right) - \beta \exp\left(-\frac{1}{2}B_2 t\right), \qquad (23)$$

where α and β represent the contributions to the matrix element from the region below and above the node position with the corresponding effective diffraction slopes B_1 and B_2, respectively ($B_1 < B_2$). Consequently, the inequality $\alpha > \beta$ corresponds to the undercompensation whereas $\alpha < \beta$ is associated with the overcompensation regime. The destructive interference of these two contributions results in a decrease of the effective diffraction slope for the $V'(2S)$ meson production towards small t, contrary to the familiar increase for the $V(1S)$ meson production. Such a situation is shown in Fig. 1, where we present the model predictions for the differential cross section $\mathrm{d}\sigma(\gamma^* \to V(V'))/\mathrm{d}t$ for the production of the $V(1S)$ and $V'(2S)$ mesons at different c.m.s. energies W and at $Q^2 = 0$. The real photoproduction measures the purely transverse cross section. Using the vector meson wave functions from [15] the forward production amplitude (3) is in the undercompensation regime (positive value). However, the matrix element in the numerator of (22) is safely in the overcompensation regime (negative value) (at $W \lesssim 150\,\mathrm{GeV}$ for $\rho'(2S)$ production and at $W \lesssim 30\,\mathrm{GeV}$ for $\phi'(2S)$ production) because of $r_B > r_S$. As the result, we predict the negative value diffraction slope at $t = 0$ and $Q^2 = 0$. At $t > 0$ the node effect becomes weaker. The higher t, the weaker is the node effect as a consequence of the destructive interference discussed above. Consequently, the differential cross section first rises with t, and flattens off at $t \in (0.0\text{–}0.2)\,\mathrm{GeV}^2$, having a broad maximum. At large t, the node effect is weak and $\mathrm{d}\sigma(\gamma^* \to V'(2S))/\mathrm{d}t$ decreases with t monotonically as for $V(1S)$ production. The position of the maximum can be roughly evaluated from (23) and reads

$$t_{\max} \sim \frac{1}{B-A} \log\left[\frac{\beta^2}{\alpha^2}\frac{B^2}{A^2}\right], \qquad (24)$$

with the supplementary condition

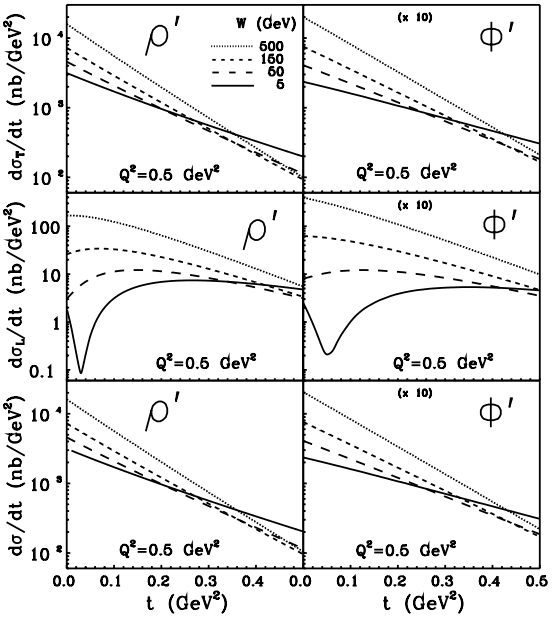

Fig. 2. The color dipole model predictions for the differential cross sections $\mathrm{d}\sigma_{\mathrm{L,T}}(\gamma^* \to V'(2S))/\mathrm{d}t$ for transversely (T) (top boxes) and longitudinally (L) (middle boxes) polarized radially excited $\rho'(2S)$, $\phi'(2S)$ and for the polarization-unseparated $\mathrm{d}\sigma(\gamma^* \to V')/\mathrm{d}t = \mathrm{d}\sigma_{\mathrm{T}}(\gamma^* \to V'(2S))/\mathrm{d}t + \epsilon \mathrm{d}\sigma_{\mathrm{L}}(\gamma^* \to V'(2S))/\mathrm{d}t$ for $\epsilon = 1$ (bottom boxes) at $Q^2 = 0.5\,\mathrm{GeV}^2$ and different values of the c.m.s. energy W

$$\frac{\beta}{\alpha} > \frac{A}{B}, \qquad (25)$$

where $A = 2B_1$ and $B = 2B_2$, $A < B$. If the condition (25) is not fulfilled, $\mathrm{d}\sigma(\gamma^* \to V'(2S))/\mathrm{d}t$ has no maximum and exhibits a standard monotonical t-behavior as for the production of $V(1S)$ mesons.

The predicted nonmonotonic t-behavior of the differential cross section for $\rho'(2S)$ and $\phi'(2S)$ production in the photoproduction limit is strikingly different, especially at smaller energies, from the familiar decrease with t of $\mathrm{d}\sigma(\gamma \to \rho^0(1S))/\mathrm{d}t$ and $\mathrm{d}\sigma(\gamma \to \phi^0(1S))/\mathrm{d}t$ (see Fig. 1). Here we cannot insist on the precise form of the t-dependence of the differential cross sections; the main emphasis is on the likely pattern of the t-dependence coming from the node effect.

At larger energies, $W \gtrsim 150\,\mathrm{GeV}$ for the $\rho'(2S)$ photoproduction and $W \gtrsim 30\,\mathrm{GeV}$ for $\phi'(2S)$ photoproduction, the node effect becomes weaker and we predict the positive value diffraction slope at $t = 0$ because both the matrix elements in (22) are positive valued. For this reason, the nonmonotonic t-dependence of the differential cross section is exchanged for the monotonic one, but still the effective diffraction slope decreases slightly towards small t (see Fig. 1).

Because of a possible overcompensation scenario for $\rho'_{\mathrm{L}}(2S)$ and $\phi'_{\mathrm{L}}(2S)$ mesons in the forward direction ($t = 0$) and at small Q^2 (see [15]), we present in Fig. 2 the model predictions for $\mathrm{d}\sigma(\gamma^* \to V'(2S))/\mathrm{d}t$ at different energies W and at fixed $Q^2 = 0.5\,\mathrm{GeV}^2$ for the produc-

tion of (T), (L) polarized and polarization-unseparated $\rho'(2S)$ and $\phi'(2S)$ mesons. As was mentioned above, at $Q^2 = 0.5\,\mathrm{GeV}^2$, the node effect becomes weaker, the amplitudes for both $\rho'_{\mathrm{T}}(2S)$ and $\phi'_{\mathrm{T}}(2S)$ production at $t = 0$ are in the undercompensation regime and the corresponding slope parameters $B(\rho'_{\mathrm{T}}(2S))$ and $B(\phi'_{\mathrm{T}}(2S))$ have a positive value. For this reason, we predict the familiar t-dependence of $\mathrm{d}\sigma(\gamma^* \to V'_{\mathrm{T}}(2S))/\mathrm{d}t$ (see bottom boxes in Fig. 2). The above mentioned maximum of $\mathrm{d}\sigma/\mathrm{d}t$ is absent because of a weaker node effect and consequently the condition (25) is not fulfilled.

However, at $Q^2 \lesssim 0.5\,\mathrm{GeV}^2$, the production amplitude for $\rho'_{\mathrm{L}}(2S)$ and $\phi'_{\mathrm{L}}(2S)$ in the forward direction (and the matrix element $\langle V'_{\mathrm{L}}(2S)|\sigma(\xi,r)B(\xi,r)|\gamma^*\rangle$ as well) is still in the overcompensation regime and the corresponding diffraction slope $B(V'_{\mathrm{L}}(2S))$ has a positive value at small energies, $W \lesssim 20\,\mathrm{GeV}$. This results in the very spectacular pattern of anomalous t-dependence for $\mathrm{d}\sigma(\gamma^* \to V'_{\mathrm{L}}(2S))/\mathrm{d}t$ shown in Fig. 2 (middle boxes). With rising t due to the above described destructive interference of two contributions to the production amplitude with different t-dependences (see (23)), one encounters the exact node effect at some $t \sim t_{\min}$. Consequently, the differential cross section first falls rapidly with t, having a minimum at $t \sim t_{\min}$. At still larger t, when the overcompensation scenario of the t-dependent production amplitude is changed for the undercompensation one and the slope parameter becomes negatively valued, $\mathrm{d}\sigma(\gamma^* \to V'_{\mathrm{L}}(2S))/\mathrm{d}t$ rises with t and the further pattern of the t-behavior is analogous to that for $V'_{\mathrm{T}}(2S)$ production (see Fig. 1).

The position of the minimum in the differential cross section is model dependent and can be roughly estimated from (23):

$$t_{\min} \sim \frac{1}{B-A}\log\left[\frac{\beta^2}{\alpha^2}\right]. \qquad (26)$$

The gBFKL model predictions give $t_{\min} \sim 0.03\,\mathrm{GeV}^2$ for $\rho'_{\mathrm{L}}(2S)$ production and $t_{\min} \sim 0.05\,\mathrm{GeV}^2$ for $\phi'_{\mathrm{L}}(2S)$ production at $Q^2 = 0.5\,\mathrm{GeV}^2$ and at $W = 5\,\mathrm{GeV}$. However, we cannot exclude the possibility that this minimum will be placed at other values of t. At $Q^2 < 0.5\,\mathrm{GeV}^2$, $t_{\min}$ reaches larger values of t. At higher energy, the position of $t_{\min}$ is shifted to a smaller value of t unless the exact node effect is reached at $t = 0$. At still larger energy, when the $V'_{\mathrm{L}}(2S)$ production amplitude is in the undercompensation regime, this minimum disappears and we predict the pattern of t-behavior for $\mathrm{d}\sigma(\gamma^* \to V'_{\mathrm{L}}(2S))/\mathrm{d}t$ analogous to that for $\mathrm{d}\sigma(\gamma \to V'_{\mathrm{T}}(2S))/\mathrm{d}t$ in the photoproduction limit described in Fig. 1. These predicted anomalies can be tested at HERA measuring the diffractive electroproduction of $V'(2S)$ light vector mesons in the separate (T) and (L) polarizations.

4 Conclusions

We study the diffractive photo- and electroproduction of the ground state $V(1S)$ and radially excited $V'(2S)$ vector mesons within the color dipole gBFKL dynamics with the main emphasis on the differential cross section $\mathrm{d}\sigma/\mathrm{d}t$. There are two main consequences of vector meson production coming from the gBFKL dynamics.

First, the energy dependence of the $V(1S)$ vector meson production is controlled by the energy dependence of the dipole cross section which is steeper for smaller dipole sizes. The energy dependence of the diffraction slope for $V(1S)$ production is given by the effective Regge slope with a small variation with energy.

Second, the Q^2-dependence of the $V(1S)$ vector meson production is controlled by the shrinkage of the transverse size of the virtual photon and the small dipole size dependence of the color dipole cross section. The Q^2-behavior of the diffraction slope is given by the geometrical contribution with an approximate $\sim r^2$ behavior coming from the color dipole gBFKL phenomenology of the slope parameter.

As a consequence of the node in the $V'(2S)$ radial wave function, we predict a strikingly different t-dependence of the differential cross section for the production of $V'(2S)$ versus $V(1S)$ vector mesons. The origin of this is in the destructive interference of the large distance negative contribution to the production amplitude from the region above the node position with a steeper t-dependence and the small distance positive contribution to the production amplitude from the region below the node position with a weaker t-dependence. As a result, we predict at $Q^2 = 0$ a nonmonotonic t-dependence of $\mathrm{d}\sigma(\gamma \to V'_{\mathrm{T}}(2S))/\mathrm{d}t$ and a decreasing diffraction slope for $V'_{\mathrm{T}}(2S)$ mesons towards small values of t in contrast with the familiar increase for the $V(1S)$ mesons. The differential cross section $\mathrm{d}\sigma(\gamma \to V'_{\mathrm{T}}(2S))/\mathrm{d}t$ first rises with t, having a broad maximum at $t \sim t_{\max}$ as given by (24). The position of the maximum is model dependent and is shifted to smaller values of t with rising energy and Q^2 due to a weaker node effect. At larger t when the node effect is still weaker, $\mathrm{d}\sigma(\gamma \to V'_{\mathrm{T}}(2S))/\mathrm{d}t$ has the standard monotonic t-behavior as for the production of $V(1S)$ vector mesons. This pattern of the anomalous t-dependence of $\mathrm{d}\sigma(\gamma \to V'_{\mathrm{T}}(2S))/\mathrm{d}t$ corresponds to the undercompensation scenario for the production amplitude.

For the production of (L) polarized $V'_{\mathrm{L}}(2S)$ mesons, there is overcompensation at $t = 0$ leading to an exact cancellation of the positive contribution from large size dipoles and the negative contribution from small size dipoles to the production amplitude and to a minimum of the differential cross section at some value of $t \sim t_{\min}$. The position of $t_{\min}$ is given by (25), is energy dependent, and leads to a complicated pattern of anomalous t-dependence for $\mathrm{d}\sigma(\gamma^* \to V'_{\mathrm{L}}(2S))/\mathrm{d}t$ at fixed Q^2. Consequently, $\mathrm{d}\sigma(\gamma^* \to V'_{\mathrm{L}}(2S))/\mathrm{d}t$ first falls with t having a minimum at $t \sim t_{\min}$ when the overcompensation scenario is changed for the undercompensation one. The following pattern of t-behavior is then analogous to $\mathrm{d}\sigma(\gamma \to V'_{\mathrm{T}}(2S))/\mathrm{d}t$ at $Q^2 = 0$. These anomalies are also energy and Q^2-dependent and can be tested at HERA.

The experimental investigation of the t-dependent differential cross section for real photoproduction ($Q^2 = 0$) of $V'(2S)$ vector mesons at fixed target and HERA exper-

iments offers an unique possibility to make a choice between the undercompensation and overcompensation scenarios. The presence of the minimum in $\mathrm{d}\sigma(\gamma \to V'(2S))/\mathrm{d}t$ for a broad energy range corresponds to the overcompensation scenario. Otherwise, the $V'(2S)$ production amplitude is in the undercompensation scenario.

The position of the node in the radial $V'(2S)$ wave function can be tested also by the vector meson data with the separate (L) and (T) polarizations at $Q^2 > 0$. The existence of a dip (minimum) (for a broad energy range) in the t-dependent differential cross section is connected again with the overcompensation scenario in the $V'(2S)$ production amplitude. The broad maximum and/or the standard monotonic t-behavior of $\mathrm{d}\sigma/\mathrm{d}t$ leads one to prefer the undercompensation scenario.

References

1. A. Donnachie, P.V. Landshoff, Phys. Lett. B **185**, 403 (1987); J.R. Cuddell, Nucl. Phys. B **336**, 1 (1990)
2. B.Z. Kopeliovich, B.G. Zakharov, Phys. Rev. D **44**, 3466 (1991)
3. M.G. Ryskin, Z. Phys. C **57**, 89 (1993)
4. B.Z. Kopeliovich, J. Nemchik, N.N. Nikolaev, B.G. Zakharov, Phys. Lett. B **309**, 179 (1993)
5. B.Z. Kopeliovich, J. Nemchik, N.N. Nikolaev, B.G. Zakharov, Phys. Lett. B **324**, 469 (1994)
6. J. Nemchik, N.N. Nikolaev, B.G. Zakharov, Phys. Lett. B **341**, 228 (1994)
7. S.J. Brodsky et al., Phys. Rev. D **50**, 3134 (1994)
8. J.R. Forshaw, M.G. Ryskin, Z. Phys. C **68**, 137 (1995)
9. E. Gotsman, E.M. Levin, U. Maor, Nucl. Phys. B **464**, 251 (1996)
10. E.A. Kuraev, L.N. Lipatov, S.V. Fadin, Sov. Phys. JETP **44**, 443 (1976); **45**, 199 (1977)
11. Yu.Yu.Balitsky, L.N. Lipatov, Sov. J. Nucl. Phys. **28**, 822 (1978)
12. L.N. Lipatov, Sov. Phys. JETP **63**, 904 (1986); L.N. Lipatov, in: Perturbative Quantum Chromodynamics, edited by A.H. Mueller (World Scientific 1989)
13. N. Nikolaev, B.G. Zakharov, JETP **78**, 598 (1994); Z. Phys. C **64**, 631 (1994)
14. N.N. Nikolaev, B.G. Zakharov, V.R. Zoller, JETP Letters **59**, 6 (1994); JETP **78**, 866 (1994); Phys. Lett. B **328**, 486 (1994)
15. J. Nemchik, N.N. Nikolaev, E. Predazzi, B.G. Zakharov, Z. Phys C **75**, 71 (1997)
16. J. Nemchik, N.N. Nikolaev, E. Predazzi, B.G. Zakharov, V.R. Zoller, JETP **86**, 1054 (1998)
17. N.N. Nikolaev, Comments on Nucl. Part. Phys. **21**, 41 (1992)
18. J. Nemchik, N.N. Nikolaev, B.G. Zakharov, Phys. Lett. B **339**, 194 (1994)
19. N.N. Nikolaev, B.G. Zakharov, V.R. Zoller, Phys. Lett. B **366**, 337 (1996)
20. N.N. Nikolaev, B.G. Zakharov, V.R. Zoller, JETP Lett. **60**, 694 (1994)
21. J. Nemchik, The wave function of $2S$ radially excited vector mesons from data for diffraction slope, hep-ph 0003245, submitted to Phys. Rev. D
22. N.N. Nikolaev, B.G. Zakharov, Z. Phys. C **49**, 607 (1991); Z. Phys. C **53**, 331 (1992)
23. V. Barone, M. Genovese, N.N. Nikolaev, E. Predazzi, B.G. Zakharov, Z. Phys. C **58**, 541 (1993); Int. J. Mod. Phys. A **8**, 2779 (1993)
24. N.N. Nikolaev, B.G. Zakharov, Phys. Lett. B **332**, 184 (1994)
25. V.N. Gribov, A.A. Migdal, Sov. J. Nucl. Phys. **8**, 703 (1969)
26. N.N. Nikolaev, B.G. Zakharov, Phys. Lett. B **327**, 149 (1994)
27. H1 Collab., I. Abt et al., Nucl. Phys. B **407**, 515 (1993)
28. ZEUS Collab., M. Derrick et al., Phys. Lett. (1993)
29. J. Nemchik, N.N. Nikolaev, E. Predazzi, B.G. Zakharov, Phys. Lett. B **374**, 199 (1996)
30. A. Schiz et al., Phys. Rev. D **24**, 26 (1981); J.P. Burq et al., Phys. Lett. B **109**, 111 (1982)
31. O. Benhar, B.G. Zakharov, N.N. Nikolaev et al., Phys. Rev. Lett. **74**, 3565 (1995); O. Benhar, S. Fantoni, N.N. Nikolaev et al., Zh. Exp. Teor. Fiz. **111**, 769 (1997)
32. P. Söding, Phys. Lett. **19**, 702 (1966)
33. J. Pumplin, Phys. Rev. D **2**, 1859 (1970)

ELSEVIER

10 November 1994

PHYSICS LETTERS B

Physics Letters B 339 (1994) 194–200

Anomalous A-dependence of diffractive leptoproduction of the radial excitation $\rho'(2S)$

J. Nemchik [a,c], N.N. Nikolaev [b,c], B.G. Zakharov [b]

[a] *Institute of Experimental Physics, Slovak Academy of Sciences, Watsonova 47, 043 53 Kosice, Slovak Republic*
[b] *L.D. Landau Institute for Theoretical Physics, GSP-1, ul.Kosygina 2, V-334, 117940 Moscow, Russia*
[c] *IKP (Theorie), KFA Jülich, D-52425 Jülich, Germany*

Received 31 May 1994; revised manuscript received 12 August 1994
Editor: P.V. Landshoff

Abstract

We predict a strikingly different A- and Q^2-dependence of quasielastic leptoproduction of the $\rho^0(1S)$-meson and its radial excitation $\rho'(2S)$ on nuclei. Whereas for ρ^0 production the nuclear transparency T_A decreases monotonically with A, for the ρ' nuclear transparency T_A can have the counterintuitive nonmonotonic A-dependence, having a minimum for light nuclei, and increasing with A for medium and heavy nuclei. Strong enhancement of the ρ'/ρ^0 cross section ratio makes nuclear targets of the ρ'-factory. The origin of the anomalous A-dependence is in the interplay of color transparency effects with the nodal structure of the ρ' wave function. The predicted effects take place at moderate $Q^2 \lesssim (2-3)$ GeV^2, which can be explored in high statistics experiments at CEBAF.

1. Introduction

The recent FNAL E665 experiment [1] on the exclusive virtual photoproduction of the ρ^0-mesons on nuclei confirmed the long anticipated effect of color transparency (CT): decrease of nuclear attenuation of the produced ρ^0-mesons with increasing virtuality Q^2 of photons [2,3]. Regarding the accuracy of the data, the potential of the CERN and FNAL muon scattering experiments is nearly exhausted. Fortunately, very high statistics experiments can be performed at CEBAF upgraded to the $(8-12)$ GeV energy range [4]. (For discussion of the vector meson physics as the case for $(10-20)$ GeV electron facility see [5], high energy aspects of leptoproduction of vector mesons are discussed in [3,6], for the recent review on CT see [7].) Apart from the much more detailed studies of the onset of CT in ρ^0 production, the CEBAF experiments can open an entirely new window on CT, as due to high luminosity and excellent CLAS facility, an accurate measurement of production of the radially excited ρ'-meson becomes possible for the first time. As we shall demonstrate below, CT leads to a spectacular pattern of anomalous A- and Q^2-dependence of ρ' production.

The crucial observation is that the very mechanism of CT leads to a novel phenomenon of scanning the wave function of vector mesons [2,8,9]. Specifically, the amplitude of the forward production $\gamma_T^* p \to V_T N$ of the transverse polarized vector mesons can be written as

0370-2693/94/$07.00
SSDI 0370-2693(94)01200-8

$$\mathcal{M}_N = \frac{N_c C_\rho \sqrt{4\pi\alpha_{em}}}{(2\pi)^2} \times \int d^2\boldsymbol{r}\sigma(r) \int_0^1 \frac{dz}{z(1-z)} m_q^2 K_0(\varepsilon r)\phi(r,z). \quad (1)$$

Here $C_\rho = 1/\sqrt{2}$, $N_c = 3$ is the number of colours, $K_{0,1}(x)$ is the modified Bessel function,

$$\varepsilon^2 = m_q^2 + z(1-z)Q^2, \quad (2)$$

$m_q = 0.3$ GeV is the quark mass, $\phi(z,r)$ is the lightcone wave function of the $q\bar{q}$ Fock state of the vector meson in the mixed $(z,\boldsymbol{r})$-representation, where $\boldsymbol{r}$ is the transverse separation of the quark and antiquark and z is a fraction of the lightcone momentum carried by the quark. In Eq. (2), we used the explicit form $\phi_{\gamma^*}(z,r) \propto K_0(\varepsilon r)$ for the photon wavefunction [8,10]. The normalization of amplitudes is such that $d\sigma/dt|_{t=0} = |\mathcal{M}|^2/16\pi$, the wave functions are normalized by

$$\frac{N_c}{2\pi}\int d^2\boldsymbol{r}\int_0^1 \frac{dz}{z(1-z)} m_q^2\phi^2(r,z) = 1. \quad (3)$$

If the $V\bar{q}q$ vertex is taken in the form $\Gamma\bar{q}\gamma_\mu q$, then the standard nonrelativistic relationship between the vertex function Γ and the Fourier transform $\Psi(\boldsymbol{p}) = \int d^3\boldsymbol{R}\Psi(\boldsymbol{R})\exp(-i\boldsymbol{pR})$ of the wavefunction reads

$$\Psi(\boldsymbol{p}^2) \propto \frac{\Gamma(\boldsymbol{p}^2)}{4\boldsymbol{p}^2 + 4m_q^2 - m_V^2}, \quad (4)$$

the lightcone generalization of which is achieved by the substitution [11]

$$4\boldsymbol{p}^2 + 4m_q^2 = M^2 = \frac{m_q^2 + \boldsymbol{k}^2}{z(1-z)}. \quad (5)$$

For the $\rho^0(1S)$ and the $\rho'(2S)$ we use the wave functions of the harmonic oscillator type

$$\Psi_1(M^2) = N_1\exp(-\tfrac{1}{2}R_1^2M^2), \quad (6)$$

$$\Psi_2(M^2) = N_2\left\{1 - \alpha\left[3 - R_2^2(\tfrac{1}{4}M^2 - m_q^2)\right]\right\} \times \exp(-\tfrac{1}{2}R_2^2M^2), \quad (7)$$

The lightcone wave function $\phi(r,z)$ in the mixed $(\boldsymbol{r},z)$ representation is given by

$$\phi(r,z) = \int \frac{d^2\boldsymbol{k}}{(2\pi)^2}\Psi(M^2)\exp(i\boldsymbol{kr}). \quad (8)$$

The parameter $R_1^2 = 1.078$ fm^2 was chosen to have $\langle\boldsymbol{r}^2\rangle_{\rho^0} = 1.2$ fm^2, which corresponds to the similar charge radii of the ρ^+ and π^+-mesons and leads to $\sigma_{tot}(\rho^0 N) = 23$ mb. For the ρ'-meson, we assume a harmonic oscillator model motivated size, $\langle\boldsymbol{r}^2\rangle_{\rho'} = 2.5\langle\boldsymbol{r}^2\rangle_{\rho^0}$, and impose the orthogonality of the $1S$ and $2S$ wavefunctions, which gives $R_2^2 = 0.807$ fm^2, $\alpha = 0.725$ and, for purpose of reference, $\sigma_{tot}(\rho' N) = 28$ mb. In this paper we only are interested in the region of small Q^2, in which the relativistic corrections coming from the lower components of the quark wave functions can be neglected; full relativistic treatment demonstrates a very slow onset of relativistic effects with increasing Q^2 [12].

In Eq. (1), $\sigma(r)$ is the cross section for interaction with the nucleon of the $q\bar{q}$ color dipole of size r. We use $\sigma(r)$ calculated in [12]. By virtue of CT, for the small-size color dipole [10,13]

$$\sigma(r) \propto r^2, \quad (9)$$

and the production amplitude (1) receives the dominant contribution from ([3] and see below)

$$r \sim r_S = \frac{6}{\sqrt{m_V^2 + Q^2}}. \quad (10)$$

The wave function of the radial excitation $\rho'(2S)$ has a node. For this reason, in the ρ' production amplitude there is the node efffect – cancellations between the contributions from r below, and above, the node, which depends on the scanning radius r_S. If the node effect is strong, even slight variations of r_S lead to an anomalously rapid variation of the ρ' production amplitude, which must be contrasted to the smooth Q^2- and r_S-dependence of the $\rho^0(1S)$ production amplitude. The point which we wish to make in this communication is that apart from changing Q^2, one can also vary the effective scanning radius employing the CT property of stronger nuclear attenuation of the large-r states. We predict a strikingly different, and often counterintuitive, A- (and Q^2)-dependence of ρ' and ρ^0 production on nuclei, the experimental observation

of which will shed new light on our understanding of the mechanism of CT.

2. Scanning the wave function of the ρ'-meson

We start with the derivation of the scanning radius r_S Eq. (10). The most important feature of the photon wave function $\phi_{\gamma^*}(r,z)$ is an exponential decrease at large distances [2,3,8-10]

$$\phi_{\gamma^*}(r,z) \propto K_0(\varepsilon r) \propto \exp(-\varepsilon r)\,. \tag{11}$$

In the nonrelativistic quarkonium $z \sim 1/2$ and, by virtue of Eqs. (11) and (2), the relevant $q\bar{q}$ fluctuations have a size

$$r \sim r_Q = \frac{1}{\sqrt{m_q^2 + \frac{1}{4}Q^2}} \approx \frac{2}{\sqrt{m_V^2 + Q^2}}\,. \tag{12}$$

The wave function of the vector meson is smooth at small r. Then, because of CT property Eq. (9), the integrand in Eq. (1) will be peaked at $r \sim r_S \approx 3r_Q$ as it is stated in Eq. (10). The product $\sigma(r)\Psi_{\gamma^*}(z,r)$ acts as a distribution which probes the wave function of the vector meson at the scanning radius $r \sim r_S$ [2,9]. The large numerical factor on the r.h.s. of Eq. (10) stretches the large-size dominance, and the simple nonrelativistic approximation $z \sim 1/2$ remains viable in a broad range of $Q^2 \lesssim (3-5)$ GeV^2 of interest at CEBAF.

For Ψ' and Υ' production, the node effect is perturbatively tractable even for the real photoproduction $Q^2 = 0$. The prediction [8] of $\sigma(\gamma N \to \Psi' N)/\sigma(\gamma N \to J/\Psi N) = 0.17$ is in excellent agreement with the NMC result $0.20 \pm 0.05(\text{stat}) \pm 0.07(\text{syst})$ for this ratio [14]. In this case the node effect is relatively weak. For the light mesons the scanning radius r_S is larger and, at small Q^2, the node effect is much stronger. With the above described harmonic oscillator wave function, we find the Q^2-dependence of the ρ'/ρ^0 production ratio shown in Fig. 1. It corresponds to the *overcompensation* scenario when, at $Q^2 = 0$, the ρ' production amplitude is dominated by the contribution from r above the node. As Q^2 increases and the scanning radius r_S decreases, we encounter the exact node effect, the ρ'/ρ^0 production ratio has a dip at finite Q^2, and with the further increase of Q^2 and decrease of r_S, we have

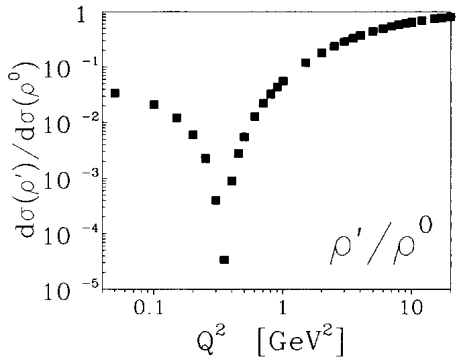

Fig. 1. The Q^2-dependence of the $\rho'(2S)/\rho^0(1S)$ ratio of forward production cross sections.

the *undercompensation* regime – the free-nucleon amplitude will be dominated by the contribution from r below the node. The node effect will decrease with rising Q^2 and the ρ'/ρ^0 ratio will rise with Q^2.

At small Q^2 the scanning radius is large, and we are not in the domain of the perturbative QCD. What, then, are our firm predictions? Firstly, the strong node effect and the strong suppression of the real photoproduction of the ρ' is not negotiable, and this prediction is consistent with the meagre experimental information (for the review see [15]). Secondly, the wave functions of the $\rho^0(1S)$ and $\rho'(2S)$ at the origin are approximately equal. Therefore, at very large Q^2 when r_S is very small, we have a firm prediction that $d\sigma_{\rho'} \sim d\sigma_{\rho^0}$. In the above overcompensation scenario, the ρ'/ρ^0 ratio has a dip at finite Q^2. The position of this dip is model dependent, but the prediction of the steep rise of the ρ'/ρ^0 in the region of $Q^2 \lesssim (2-3)\text{GeV}^2$ is a firm consequence of the Q^2-dependence of the scanning radius, which is driven by CT. This is precisely the region where the high statistics data can be taken at CEBAF, and the experimental observation of such a dramatic large-distance manifestation of CT will be very important contribution to our understanding of the onset of CT.

3. The two possible scenarios for the node effect in ρ' production on nuclei

ρ' production on nuclei is indispensable for testing the node affect, as nuclear attenuation gives still another handle on the scanning radius. For the sake of definiteness, we discuss quasielastic (incoherent) ρ'

production on nuclei, extension to the coherent production is straightforward and will be presented elsewhere.

At high energy ν, the (virtual) photon forms its $q\bar{q}$ Fock state at a distance (the coherence length) in front of the target nucleus (nucleon)

$$l_c = \frac{2\nu}{Q^2 + m_V^2}. \tag{13}$$

After interaction with the target, the $q\bar{q}$ pair recombines into the observed vector meson V with the formation (recombination) length

$$l_f = \frac{\nu}{m_V \Delta m}, \tag{14}$$

where Δm is the typical level splitting in the quarkonium. At low energy and $l_f \ll R_A$, where R_A is a radius of the target nucleus, recombination of the $q\bar{q}$ pair into the vector meson takes place well inside the nucleus, nuclear attenuation will be given by the free-nucleon VN cross section and the CT effect disappears. The condition $l_f \gtrsim R_A$ is crucial for the onset of CT, and for the ρ^0, ρ' system it requires

$$\nu \gtrsim (3-4) \cdot A^{1/3}\,\mathrm{GeV}, \tag{15}$$

which for light and medium nuclei is well within the reach of the (8 – 12) GeV upgrade of CEBAF. (In this energy range we can also limit ourselves to the contribution from the lowest $q\bar{q}$ Fock states of the photon and vector meson.) In the opposite to that, the condition $l_c \gtrsim R_A$ is not imperative for the onset of CT. Nuclear attenuation effects only increase somewhat when l_c increases from $l_c \ll R_A$ to $l_c \gtrsim R_A$ [2,16]. The finite-energy effects can easily be incorporated using the path integral technique developed in [8,2]. For the sake of simplicity, in this paper we concentrate on the high-energy limit of $f_f, l_c \gtrsim R_A$, when the nuclear transparency $T_A = d\sigma_A/A\sigma_N$ equals [2,9,16]

$$\mathrm{Tr}_A = \frac{1}{A}\int d^2\boldsymbol{b}T(b) \times \frac{\langle V|\sigma(r)\exp\left[-\frac{1}{2}\sigma(r)T(b)\right]|\gamma^*\rangle^2}{\langle V|\sigma(r)|\gamma^*\rangle^2}. \tag{16}$$

Here $T(b) = \int dz n_A(b,z)$ is the optical thickness of a nucleus, where $n_A(b,z)$ is the nuclear matter density (For the compilation of the nuclear density parameters see [17]). The A-dependence of the node effect comes from the nuclear attenuation factor $\exp[-\frac{1}{2}\sigma(r)T(b)]$ in the nuclear matrix element $\mathcal{M}_A(T) = \langle V|\sigma(r)\exp\left[-\frac{1}{2}\sigma(r)T(b)\right]|\gamma^*\rangle$.

Firstly, consider the value of Q^2, at which the cross section for ρ' production on the free nucleon takes its minimal value because of the exact node effect. Because of the r-dependence of the attenuation factor, in the nuclear amplitude the node effect will be incomplete. Consequently, as a function of Q^2, the nuclear transparency T_A will have a spike $T_A \gg 1$ at a finite value of Q^2 [2].

Secondly, consider ρ' production on nuclei at a fixed value of Q^2 such that the free nucleon amplitude is still in the overcompensation regime. Increasing A and enhancing the importance of the attenuation factor $\exp[-\frac{1}{2}\sigma(r)T(b)]$, we shall bring the nuclear amplitude to the nearly exact compensation regime. Therefore, the ρ'/ρ^0 production ratio, as well as the nuclear transparency for ρ' production, will decrease with A and take a minimum value at a certain finite A. With the further increase of A, the undercompensation regime takes over, and we encounter a very counterintuitive situation: the nuclear transparency for the ρ' is larger for the strongly absorbing nuclei! This situation is illustrated in Fig. 2a and must be contrasted with the smooth and uneventful decrease of transparency for ρ^0 production on heavy nuclei.

Evidently, the possibility of the perfect node effect in $\mathcal{M}_A(T)$ depends on the optical thickness $T(b)$. This is shown in Fig. 3, in which we present the relative nuclear matrix element

$$R(T) = \frac{\langle\rho'|\sigma(r)\exp[-\frac{1}{2}\sigma(r)T(b)]|\gamma^*\rangle}{\langle\rho'|\sigma(r)|\gamma^*\rangle}. \tag{17}$$

At large impact parameter b, at the periphery of the nucleus, the optical thickness of the nucleus is small, the overcompensation in the nuclear matrix element is the same as for the free nucleon, and we have $R(T) = 1$. At smaller impact parameters, one encounters the exact node effect: $R(T) = 0$. At still smaller impact parameters, the overcompensation changes for the undercompensation and $R(T) < 0$. Here the breaking of the compensation and the overall attenuation start competing. For very heavy nuclei and small impact parameters, the overall attenuation takes over and $R(T)$ starts decreasing again. For the particular case of real

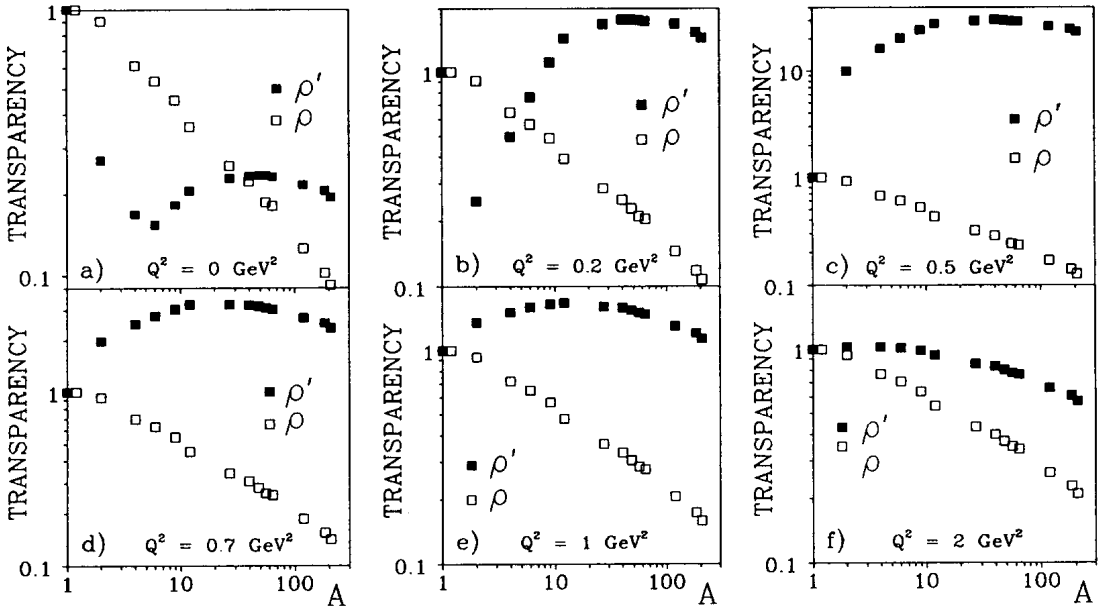

Fig. 2. The Q^2- and A-dependence of the nuclear transparency for $\rho^0(1S)$ and $\rho'(2S)$ electroproduction on nuclei.

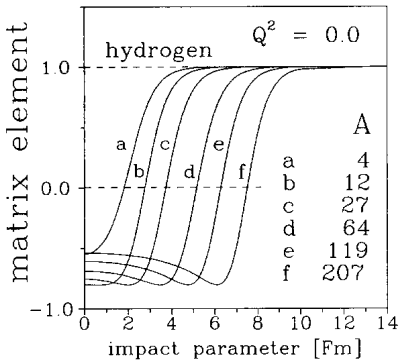

Fig. 3. The impact parameter dependence of the reduced nuclear matrix element $R(T)$ for the real photoproduction of the $\rho'(2S)$.

photoproduction, and for the specific wave function of the ρ'-meson, in the undercompensation domain we have $|R(T)| \leq 1$. The resulting A-dependence of the nuclear transparency T_A is shown in Fig. 2a. It takes the minimum value for the ^7Li target, then increases with A, flattens and starts decreasing for very heavy nuclei.

In Fig. 2 we show how the nuclear transparency for the ρ' varies with Q^2. The slight increase of Q^2 up to $Q^2 = 0.2$ GeV^2 and the slight change of the scanning radius enhance the node effect in the free nucleon amplitude, see Fig. 1. In this case, we find an almost exact node effect for the ^{4}He target, which is followed by the dominant undercompensation regime for heavier nuclei (Fig. 2b). Also, in this case the undercompensation regime for heavy nuclei is followed by $|R(T)| > 1$, which leads to significant antishadowing $T_A > 1$.

With the further increase of Q^2 one enters the pure undercompensation regime for all the targets. Nuclear suppression of the node effect enhances $\mathcal{M}_A$ and nuclear transparency T_A, whereas the overall attenuation factor $\exp[-\frac{1}{2}\sigma(r)T(b)]$ decreases T_A. Of these two competing effects, the former remains stronger and we find antishadowing of ρ' production in a broad range of A and Q^2, see Figs. 2c–2e. Typically, we find a nuclear enhancement of the ρ'/ρ^0 production ratio on heavy targets by one order in magnitude with respect to the free nucleon target. This enables leptoproduction on nuclei of the ρ' factory, and the ρ' production experiments at CEBAF can contribute much to the poorly understood spectroscopy of the radially excited vector mesons. Only at a relatively large $Q^2 \gtrsim 2$ GeV^2, the attenuation effect takes over, and nuclear transparency for ρ' production will start decreasing monotonically with A (Fig. 2f). Still, this decrease is much weaker than for the ρ^0-meson. At very large Q^2, when the node effect disappears because of the

small scanning radius r_S, the nuclear transparency for ρ^0 and ρ' production will become identical. This pattern repeats qualitatively the one studied in [2,8] for the J/Ψ- and Ψ'-mesons.

Notice, that for ρ^0 production, the nuclear transparency is a very slow function of Q^2. For instance, for the lead target $T_{Pb}(Q^2 = 0) \approx 0.1$ and $T_{Pb}(Q^2 = 2\ \mathrm{GeV}^2) \approx 0.23$. The reason for this slow onset of color transparency is that because of the large numerical factor on the r.h.s of Eq. (10), even at $Q^2 = 2$ GeV^2 the scanning radius is still large, $r_S \sim 0.8$ fm. Furthermore, a more detailed analysis [3] has shown that nuclear shadowing is controlled by a still larger $r \sim 5r_Q$. Our numerical predictions [2,3] for the Q^2-dependence of incoherent and coherent ρ^0 production on nuclei are in excellent agreement with the E665 data.

The above presented results refer to the production of the transversely polarized ρ^0- and ρ'-mesons. Accurate separation of production of the transverse and longitudinal cross section can easily be done in the high statistics CEBAF experiments. Here we only wish to mention the interesting possibility that for the longitudinally polarized ρ'-mesons, the exact node effect can take place at a value of Q^2 different from that for the transversely polarized ρ'-mesons, and polarization of the produced ρ' can exhibit very rapid change with Q^2.

4. Discussion of the results and conclusions

We presented the strong case for the anomalous Q^2- and A-dependence of incoherent production of the ρ'-meson on nuclear targets. The origin of the effect is in the Q^2-dependence of the scanning radius r_S, which follows from the color transparency property in QCD. At the relatively small values of Q^2 discussed in this paper, the scanning radius is rather large, of the order of the size of the ρ^0-meson. For this reason, the ρ' production amplitude proves to be extremely sensitive to the nodal structure of the ρ' wave function. Specifically, the node effect leads to a strong suppression of the ρ'/ρ^0 ratio in real photoproduction, which is consistent with the meagre experimental information on the production of radially excited vector mesons.

In the overcompensation scenario suggested by the lightcone generalization of the simple oscillator model, the most striking effect is the nonmonotonic A-dependence of the nuclear transparency shown in Fig. 2. The numerical predictions are very sensitive to the position of the node in the wave function of $2S$ states. It is quite possible that the dip of nuclear transparency T_A will take place for targets much heavier than in Figs. 2a, 2b, and the disappearance of the node effect and the onset of the more conventional nuclear shadowing $T_A < 1$ for ρ' production like in Fig. 2f only will take place at much larger Q^2. Also, the possibility of the undercompensation at $Q^2 = 0$ can not be excluded. However, the strikingly different A-dependence of incoherent ρ^0 and ρ' production on nuclei persists in such a broad range of Q^2 and scanning radius r_S, that the existence of the phenomenon of anomalous A- and Q^2-dependence of ρ' production cannot be denied. It is a direct manifestation of the color-transparency driven Q^2-dependence of the scanning radius and, as such, deserves a dedicated experimental study.

For the sake of simplicity, here we concentrated on the high energy limit in which the theoretical treatment of nuclear production is greatly simplified. One can easily go beyond the frozen-size approximation employing the path-integral technique [2,8]. The detailed analysis performed in [2] shows that at energies of the virtual photon $\sim (6 - 10)$ GeV, the subasymptotic corrections do not change much the predictions for nuclear transparency. This is the energy range wich can be reached at CEBAF after the energy upgrade.

A few more comments about the possibilities of CEBAF are worthwhile. Because of the strong suppression of the ρ'/ρ^0 production ratio, the high luminosity of CEBAF is absolutely crucial for high-statistics experiments on ρ' production. Notice, that the most interesting anomalies in the A- and Q^2-dependence take place near the minimum of the ρ' production cross section. Furthermore, the observation of ρ' production requires detection of its 4-pion decays, and here one can take advantage of the CLAS multiparticle spectrometer available at CEBAF. Finally, similar effects must persist also for ω' and ϕ' production, and also in the coherent production of the radially excited mesons.

Acknowledgement

One of the authors (J.N.) is grateful to J. Speth for the hospitality at the Institut für Kernphysik, KFA Jülich, where this work was completed. N.N.N. thanks R. Holt and N. Isgur for discussions during the workshop on CEBAF at Higher Energies.

References

[1] E665 Collab., M.R. Adams et al., preprint FERMILAB-PUB-94/233-E, submitted to Phys. Rev. Lett..
[2] B.Z. Kopeliovich, J. Nemchik, N.N. Nikolaev and B.G. Zakharov, Phys. Lett. B 309 (1993) 179.
[3] B.Z. Kopeliovich, J. Nemchik, N.N. Nikolaev and B.G. Zakharov, Phys. Lett. B 324 (1993) 469.
[4] G. Fang, M. Kossov, S. Brodsky, A. Mueller and N.N. Nikolaev, talks Workshop on CEBAF at Higher Energies (CEBAF, Newport News, VA, 14–16 April 1994);
N.N. Nikolaev and B.G. Zakharov, Color transparency after the NE18 and E665 experiments: Outlook and perspectives at CEBAF. Jülich preprint KFA-IKP(Th)-1994-20, in: Proc. Workshop at CEBAF at Higher Energies, to be published.
[5] N.N. Nikolaev and J. Speth, The ELFE Project: an Electron Laboratory for Europe, eds. J. Arvieux and E. De Sanctis (Editrice Compositori, Bologna, 1993) pp. 179-212.
[6] S.J. Brodsky et al., preprint SLAC-PUB-6412R (1994).
[7] N.N. Nikolaev and B.G. Zakharov, Proc. Workshop on Electron Nucleus Scattering (Marciana Marina, Elba, 5–10 July 1993), eds. O. Benhar, A. Fabrocini and R. Schiavilla (World Scientific, Singapore, 1994) p. 323.
[8] B.Z. Kopeliovich and B.G. Zakharov, Phys. Rev. D 44 (1991) 3466.
[9] N.N. Nikolaev, Comm. Nucl. Part. Phys. 21 (1992) 41.
[10] N.N. Nikolaev and B.G. Zakharov, Z. Phys. C 49 (1991) 607; C 53 (1992) 331.
[11] M.V. Terentiev, Sov. J. Nucl. Phys. 24 (1976) 106.
[12] J. Nemchik, N.N. Nikolaev and B.G. Zakharov, Scanning the BFKL pomeron in elastic production of vector mesons at HERA, Jülich preprint KFA-IKP(Th)-1994-17, submitted for publication in Phys. Lett. B.
[13] A.B. Zamolodchikov, B.Z. Kopeliovich and L.I. Lapidus, JETP Lett. 33 (1981) 595;
G. Bertsch, S.J. Brodsky, A.S. Goldhaber and J.R. Gunion, Phys. Rev. Lett. 47 (1981) 267.
[14] P. Amaudruz et al., Nucl. Phys. B 371 (1992) 3.
[15] T.H. Bauer et al., Rev. Mod. Phys. 50 (1978) 261;
A. Donnachie and H. Mirzaie, Z. Phys. C 33 (1987) 407;
A. Donnachie and A.B. Clegg, Z. Phys. C 34 (1987) 257; C 40 (1980) 313; C 42 (1989) 663; C 45 (1990) 677.
[16] O. Benhar, B.Z. Kopeliovich, Ch. Mariotti, N.N. Nikolaev and B.G. Zakharov, Phys. Rev. Lett. 69 (1992) 1156.
[17] H. de Vries, C.W. de Jager and C. de Vries, At. Data Nucl. Data Tables 36 (1987) 495.

Incoherent production of charmonia off nuclei as a good tool for the study of color transparency

J. Nemchik
Institute of Experimental Physics, Slovak Academy of Sciences, Watsonova 47, 04353 Kosice, Slovakia
(Received 17 June 2002; published 17 October 2002)

Within a light-cone QCD formalism incorporating color transparency, coherence length effects, and gluon shadowing, we study electroproduction of J/Ψ off nuclei. In contrast to light vector meson production when at small and medium energies color transparency and coherence length effects are not easily separated, in charmonium production color transparency effects dominate. We found rather large color transparency effects in the range of $Q^2 \leqslant 20$ GeV^2. They are stronger at low than at high energies and can be easily identified by the planned future experiments. Model calculations explain well the data of the New Muon Collaboration on the Sn/C ratio of nuclear transparencies as a function of the photon energy. We provide predictions for incoherent and coherent charmonium production for future measurements.

DOI: 10.1103/PhysRevC.66.045204 PACS number(s): 13.60.Le, 25.30.Rw, 25.20.Lj

I. INTRODUCTION: SPACE-TIME PATTERN OF CHARMONIUM PRODUCTION

The dynamics of charmonium production has been a hot topic evolved intensively during almost the last three decades. Discovery of J/Ψ in 1973 confirmed the idea of charm quark and gave a basis for its further investigations, affected also by further experiments carried out at new accelerators using more powerful electronics. Later, at the beginning of 1990's the experiments with relativistic heavy-ion collisions [1] stimulated the enhanced interest about charmonium suppression as a possible indication of the quark-gluon plasma formation. This fact became a motive power in investigation of space-time pattern of charmonium production and opened new possibilities to analyze various consequent phenomena.

One of the fundamental phenomena coming from QCD is color transparency (CT), studied intensively for almost the last two decades. This phenomenon can be treated either in the hadronic or in the quark basis. The former approach leads to Gribov's inelastic corrections [2], the latter one manifests itself as a result of color screening [3,4]. Although these two approaches are complementary, the quark-gluon interpretation is more intuitive and straightforward. Colorless hadrons can interact only because color is distributed inside them. If the hadron transverse size r tends to zero then the interaction cross section $\sigma(r)$ vanishes as r^2 [3]. As a result, the nuclear medium is more transparent for smaller transverse size of the hadron. Besides, this fact naturally explains the correlation between the cross sections of hadrons and their sizes [5–7].

Investigation of diffractive electroproduction of vector mesons off nuclei is very effective and sensitive for the study of CT. A photon of high virtuality Q^2 is expected to produce a pair with a small $\sim 1/Q^2$ transverse separation.[1] Then CT manifests itself as a vanishing absorption of the small sized colorless $\bar{q}q$ wave packet during propagation through the nucleus. Dynamical evolution of the small sized $\bar{q}q$ pair to a normal sized vector meson is controlled by the time scale, called formation time. Due to the uncertainty principle, one needs a time interval to resolve different levels V (the ground state) or V' (the next excited state) in the final state. In the rest frame of the nucleus this formation time is Lorentz dilated,

$$t_f = \frac{2\nu}{m_{V'}{}^2 - m_V^2}, \tag{1}$$

where ν is the photon energy. A rigorous quantum-mechanical description of the pair evolution was suggested in Ref. [8] and is based on the light-cone Green function technique. A complementary description of the same process in the hadronic basis is presented in Ref. [9].

Another phenomenon known to cause nuclear suppression is the effect of quantum coherence. It results from destructive interference of the amplitudes for which the interaction takes place on different bound nucleons. It reflects the distance from the absorption point when the pointlike photon becomes the hadronlike $\bar{q}q$ pair. This may also be interpreted as a lifetime of $\bar{q}q$ fluctuation providing the time scale which controls the shadowing. Again, it can be estimated by relying on the uncertainty principle and Lorentz time dilation as

$$t_c = \frac{2\nu}{Q^2 + m_V^2}. \tag{2}$$

It is usually called coherence time, but we will also use the term coherence length (CL), since light-cone kinematics is assumed, $l_c = t_c$ (similarly, for formation length $l_f = t_f$). CL is related to the longitudinal momentum transfer $q_c = 1/l_c$ in $\gamma^* N \to VN$, which controls the interference of the production amplitudes from different nucleons.

Exclusive production of vector mesons at high energies is controlled by the small-x_{Bj} (x_{Bj} is the Bjorken variable) physics, and gluon shadowing becomes an important phe-

[1]For production of light vector mesons (ρ^0, Φ^0) very asymmetric pairs can be possible when either q or $\bar{q}$ carries almost the whole photon momentum. As a result, the $\bar{q}q$ pair can have a large separation, see Sec. II and Eq. (17). However, it is not so for the production of charmonia, where mainly symmetric $\bar{q}q$ pairs (either q or $\bar{q}$ carries one half of the whole photon momentum) dominate.

nomenon [10]. It was shown in Ref. [11] that for electroproduction of charmonia off nuclei the gluon shadowing starts to be important at center-of-mass system (c.m.s.) energies $\sqrt{s}\geqslant 30$–60 GeV, depending on nuclear target and Q^2. Although the gluon shadowing is quite small in the kinematic range important for investigation of CT and discussed in the present paper, we include it in all calculations.

In electroproduction of vector mesons off nuclei one needs to disentangle CT (absorption) and CL (shadowing) as the two sources of nuclear suppression. Detailed analysis of the CT and CL effects in electroproduction of vector mesons off nuclei showed [10] that one can easily identify the difference of the nuclear suppression corresponding to absorption and shadowing in two limiting cases which can be illustrated for the example of vector dominance model (VDM).

(i) In the limit of small l_c, shorter than the mean internucleon spacing ~ 2 fm, only final state absorption matters. The ratio of the quasielastic (or incoherent) $\gamma^* A\to VX$ and $\gamma^* N\to VX$ cross sections, usually called nuclear transparency (Tr), reads [8]

$$\begin{aligned}\mathrm{Tr}_A^{inc}|_{l_c\ll R_A}&\equiv\frac{\sigma_V^{\gamma^* A}}{A\sigma_V^{\gamma^* N}}=\frac{1}{A}\int d^2b\int_{-\infty}^{\infty}dz\,\rho_A(b,z)\\&\times\exp\left[-\sigma_{in}^{VN}\int_z^{\infty}dz'\rho_A(b,z')\right]\\&=\frac{1}{A\sigma_{in}^{VN}}\int d^2b\{1-\exp[-\sigma_{in}^{VN}T(b)]\}\\&=\frac{\sigma_{in}^{VA}}{A\sigma_{in}^{VN}}.\end{aligned}\tag{3}$$

Here z is the longitudinal coordinate and $\vec{b}$ is the impact parameter of the production point of vector meson. In Eq. (3) $\rho_A(b,z)$ is the nuclear density and σ_{in}^{VN} is the inelastic V-N cross section.

(ii) In the limit of long l_c the expression for nuclear transparency takes a different form,

$$\mathrm{Tr}_A^{inc}|_{l_c\gg R_A}=\int d^2b\,T_A(b)\exp[-\sigma_{in}^{VN}T_A(b)],\tag{4}$$

where we assume $\sigma_{el}^{VN}\ll\sigma_{in}^{VN}$ for the sake of simplicity. $T_A(b)$ is the nuclear thickness function

$$T_A(b)=\int_{-\infty}^{\infty}dz\,\rho_A(b,z).\tag{5}$$

The exact expression that interpolates between the two regimes, Eqs. (3) and (4), can be found in Ref. [12].

The problem of CT-CL separation arises especially in production of light vector mesons (ρ^0, Φ^0) [10]. In this case the coherence and formation lengths are comparable starting from the photoproduction limit up to $Q^2\sim 1$–2 GeV^2. In charmonium production, however, there is a strong inequality $l_f>l_c$ independent of Q^2 and ν. It leads to a different scenario of CT-CL mixing compared to light vector meson production. This fact gives a motivation for separate study of J/Ψ production presented in this paper using light-cone dipole approach generalized for the case of a finite coherence length and developed in Ref. [10]. Another reason is supported by the recent paper [11], where charmonium production was calculated in the approximation of long coherence length $l_c\gg R_A$ using realistic charmonium wave functions from Ref. [13] and corrections for finite values of l_c. It gives very interesting possibility to compare the predictions of the present paper with the results obtained from Ref. [11] for enhancement of reliability of theoretical predictions as a realistic basis for planned future electron-nucleus collisions.

The paper is organized as follows. In Sec. II we present a short review of the light-cone (LC) approach to diffractive electroproduction of vector mesons in the rest frame of the nucleon target. Here we also present the following individual ingredients contained in the production amplitude.

(i) The dipole cross section characterizing the universal interaction cross section for a colorless quark-antiquark dipole and a nucleon.

(ii) The LC wave function for a quark-antiquark fluctuation of the virtual photon.

(iii) The LC wave function of charmonia.

As the first test of the model we calculate in Sec. III the cross section of elastic electroproduction of J/Ψ off a nucleon target. Model calculations reproduce both energy and Q^2 dependence remarkably well, including the absolute normalization.

Section IV is devoted to incoherent production of J/Ψ off nuclei. Model predictions are compared with the data of the New Muon Collaboration (NMC) on the Sn/C ratio of nuclear transparencies as a function of the photon energy. We find a different scenario of an interplay between coherence and formation length effects from that occurring in light vector meson production. Because a variation of l_c with Q^2 can mimic CT at medium and low energies, one can map experimental events in Q^2 and ν in such a way as to keep $l_c=\mathrm{const}$. The LC dipole formalism predicts rather large effect of CT in the range of $Q^2\leqslant 20$ GeV^2. This fact makes it feasible to find a clear signal of CT effects also in exclusive production of J/Ψ in the planned future experiments.

Coherent production of vector mesons off nuclei leaving the nucleus intact is studied in Sec. V. The detailed calculations show that the effect of CT on the Q^2 dependence of nuclear transparency at $l_c=\mathrm{const}$ is weaker than in the case of incoherent production and is difficult to be detected at low energies since the cross section is small.

We show that the gluon shadowing suppresses electroproduction of charmonia at high energies. However, it is not very significant in the energy range important for search of CT effects. Despite this fact, we include the gluon shadowing effects in all calculations for nuclear transparency.

The results of the paper are summarized and discussed in Sec. VI. An optimistic prognosis for discovery of CT in electroproduction of charmonia is made for the future experiments.

II. A SHORT REVIEW OF THE LIGHT-CONE DIPOLE PHENOMENOLOGY FOR ELASTIC ELECTROPRODUCTION OF CHARMONIA $\gamma^* N \to J/\Psi\ N$

The LC dipole approach for elastic electroproduction $\gamma^* N \to VN$ was already used in Ref. [13] to study the exclusive photo- and electroproduction of charmonia and in Ref. [10] for elastic virtual photoproduction of light vector mesons ρ^0 and Φ^0. Therefore, we present only a short review of this LC phenomenology with the main emphasis on elastic electroproduction of charmonia. Here a diffractive process is treated as elastic scattering of a $\bar{q}q$ fluctuation ($\bar{c}c$ fluctuation for the case of charmonium production) of the incident particle. The elastic amplitude is given by convolution of the universal flavor independent dipole cross section for the $\bar{q}q$ interaction with a nucleon, $\sigma_{\bar{q}q}^{-}$, [3] and the initial and final wave functions. For the exclusive photo- or electroproduction of charmonia $\gamma^* N \to J/\Psi\ N$ the forward production amplitude is represented in the quantum-mechanical form,

$$\mathcal{M}_{\gamma^* N \to J/\Psi N}(s,Q^2) = \langle J/\Psi | \sigma_{qq}^{N}(\vec{r},s) | \gamma^* \rangle = \int_0^1 d\alpha \int d^2 r \Psi_{J/\Psi}^{*}(\vec{r},\alpha) \times \sigma_{\bar{q}q}^{-}(\vec{r},s) \Psi_{\bar{c}c}^{-}(\vec{r},\alpha,Q^2), \quad (6)$$

with the normalization

$$\left.\frac{d\sigma}{dt}\right|_{t=0} = \frac{|\mathcal{M}|^2}{16\pi}. \quad (7)$$

In order to calculate the photoproduction amplitude one needs to know the following ingredients of Eq. (6).

(i) The dipole cross section $\sigma_{\bar{q}q}^{-}(\vec{r},s)$ which depends on the $\bar{q}q$ transverse separation $\vec{r}$ and the c.m. energy squared s.

(ii) The LC wave function of the $\bar{c}c$ Fock component of the photon $\Psi_{\bar{c}c}^{-}(\vec{r},\alpha,Q^2)$, which also depends on the photon virtuality Q^2 and the relative share α of the photon momentum carried by the quark.

(iii) The LC wave function $\Psi_{J/\Psi}(\vec{r},\alpha)$ of J/Ψ.

Note that in the LC formalism the photon and meson wave functions contain also higher Fock states $|\bar{q}q\rangle$, $|\bar{q}qG\rangle$, $|\bar{q}q2G\rangle$, etc. The effects of higher Fock states are implicitly incorporated into the energy dependence of the dipole cross section $\sigma_{\bar{q}q}^{-}(\vec{r},s)$ as is given in Eq. (6).

The dipole cross section $\sigma_{\bar{q}q}^{-}(\vec{r},s)$ represents the interaction of a $\bar{q}q$ dipole of transverse separation $\vec{r}$ with a nucleon [3]. It is a flavor independent universal function of $\vec{r}$ and energy and allows to describe various high-energy processes in an uniform way. It is known to vanish quadratically $\sigma_{\bar{q}q}^{-}(r,s) \propto r^2$ as $r \to 0$ due to color screening (CT property) and cannot be predicted reliably because of poorly known higher-order perturbative QCD (pQCD) corrections and nonperturbative effects. A detailed discussion about the dipole cross section $\sigma_{\bar{q}q}^{-}(\vec{r},s)$ with an emphasis on the production of light vector mesons is presented in Ref. [10]. In electroproduction of charmonia the corresponding transverse separations of $\bar{c}c$ dipole reach the values $\leqslant 0.4$ fm (semiperturbative region). It means that nonperturbative effects are sufficiently smaller as compared to light vector mesons. Similarly, the relativistic corrections are also small enough and the nonrelativistic limit $\alpha = 0.5$ can be safely used with rather high accuracy [8].

There are two popular parametrizations of $\sigma_{\bar{q}q}^{-}(\vec{r},s)$. The first one suggested in Ref. [14] reflects the fact that at small separations the dipole cross section should be a function of r and $x_{Bj} \sim 1/(r^2 s)$ to reproduce Bjorken scaling. It describes well the data for deep-inelastic scattering (DIS) at small x_{Bj} and medium and high Q^2. However, at small Q^2 it cannot be correct since it predicts energy independent hadronic cross sections. Besides, x_{Bj} is not anymore a proper variable at small Q^2 and should be replaced by energy. This defect is removed by the second parametrization suggested in Ref. [15], which is similar to the one in Ref. [14], but contains an explicit energy dependence. It is valid down to the limit of real photoproduction. Since we want to study CT effects starting from $Q^2 = 0$, we choose the second parametrization, which has the following form:

$$\sigma_{\bar{q}q}^{-}(r,s) = \sigma_0(s)[1 - e^{-r^2/r_0^2(s)}], \quad (8)$$

where

$$\sigma_0(s) = \sigma_{tot}^{\pi p}(s)\left[1 + \frac{3}{8}\frac{r_0^2(s)}{\langle r_{ch}^2 \rangle}\right] \text{ mb} \quad (9)$$

and

$$r_0(s) = 0.88\left(\frac{s}{s_0}\right)^{-0.14} \text{ fm}. \quad (10)$$

Here $\langle r_{ch}^2 \rangle = 0.44$ fm^2 is the mean pion charge radius squared; $s_0 = 1000$ GeV^2. The cross section $\sigma_{tot}^{\pi p}(s)$ was fitted to data in Refs. [16,17],

$$\sigma_{tot}^{\pi p}(s) = 23.6\left(\frac{s}{s_0}\right)^{0.079} \text{ mb}. \quad (11)$$

The dipole cross section, Eqs. (8)–(11), provides the imaginary part of the elastic amplitude. It is known, however, that the energy dependence of the total cross section generates also a real part [18],

$$\sigma_{\bar{q}q}^{-}(r,s) \Rightarrow \left(1 - i\frac{\pi}{2}\frac{\partial}{\partial \ln(s)}\right)\sigma_{\bar{q}q}^{-}(r,s). \quad (12)$$

The energy dependence of the dipole cross section Eq. (8) is rather steep at small r, leading to a large real part which should not be neglected. For instance, the photoproduction amplitude of the process $\gamma N \to J/\Psi N$ rises $\propto s^{0.2}$ and the real-to-imaginary part ratio is over 30%.

Although the calculations of DIS using parametrization of the dipole cross section, Eq. (8), successfully describe the data at small x_{Bj} up to $Q^2 \approx 10$ GeV^2, we prefer this parametrization for study of charmonium electroproduction. The

reason is that we want to study CT effects predominantly in the range of $Q^2 \leqslant 20$ GeV^2 and, in addition, parametrization Eq. (8) describes the transition toward photoproduction limit better than the parametrization presented in Ref. [14]. Besides, in the paper [13] it was shown by studying electroproduction of charmonia off nucleons that the difference between the predictions using both parametrizations [14] and Eq. (8) is rather small and can be taken as a measure of the theoretical uncertainty.

The perturbative distribution amplitude ("wave function") of the $\bar{q}q$ ($\bar{c}c$ for J/Ψ production) Fock component of the photon has the following form for transversely (T) and longitudinally (L) polarized photons [19–21]:

$$\Psi_{\bar{q}q}^{T,L}(\vec{r},\alpha)=\frac{\sqrt{N_C\alpha_{em}}}{2\pi}Z_q\bar{\chi}\hat{O}^{T,L}\chi K_0(\epsilon r), \tag{13}$$

where χ and $\bar{\chi}$ are the spinors of the quark and antiquark, respectively; Z_q is the quark charge, $Z_q=Z_c=2/3$ for J/Ψ production; $N_C=3$ is the number of colors. $K_0(\epsilon r)$ is a modified Bessel function with

$$\epsilon^2=\alpha(1-\alpha)Q^2+m_c^2, \tag{14}$$

where $m_c=1.5$ GeV is mass of the c quark, and α is the fraction of the LC momentum of the photon carried by the quark. The operators $\hat{O}^{T,L}$ read

$$\hat{O}^T=m_c\vec{\sigma}\cdot\vec{e}+i(1-2\alpha)(\vec{\sigma}\cdot\vec{n})(\vec{e}\cdot\vec{\nabla}_r)+(\vec{\sigma}\times\vec{e})\cdot\vec{\nabla}_r, \tag{15}$$

$$\hat{O}^L=2Q\alpha(1-\alpha)(\vec{\sigma}\cdot\vec{n}). \tag{16}$$

Here $\vec{\nabla}_r$ acts on transverse coordinate $\vec{r}$; $\vec{e}$ is the polarization vector of the photon, $\vec{n}$ is a unit vector parallel to the photon momentum, and $\vec{\sigma}$ is the three vector of the Pauli spin matrices.

In general, the transverse $\bar{q}q$ separation is controlled by the distribution amplitude, Eq. (13), with the mean value

$$\langle r\rangle\sim\frac{1}{\epsilon}=\frac{1}{\sqrt{Q^2\alpha(1-\alpha)+m_q^2}}. \tag{17}$$

For production of light vector meson very asymmetric $\bar{q}q$ pairs with α or $(1-\alpha)\leqslant m_q^2/Q^2$ become possible. Consequently, the mean transverse separation $\langle r\rangle\sim 1/m_q$ becomes huge since one must use current quark masses within PQCD. However, that is not the case in charmonium production because of a large quark mass $m_c=1.5$ GeV. Therefore, we are out of the problem how to include nonperturbative interaction effects between c and $\bar{c}$ because they are rather small. Despite this fact, for completeness we include these nonperturbative interaction effects in all calculations to avoid small but supplementary uncertainties in predictions. We take from Ref. [15] the corresponding phenomenology including the interaction between c and $\bar{c}$ based on the light-cone Green function approach.

The Green function $G_{\bar{q}q}^{-}(z_1,\vec{r}_1;z_2,\vec{r}_2)$ describes the propagation of an interacting qq pair (cc pair for the case of J/Ψ production) between points with longitudinal coordinates z_1 and z_2 and with initial and final separations $\vec{r}_1$ and $\vec{r}_2$. This Green function satisfies the two-dimensional Schrödinger equation,

$$\begin{aligned} i\frac{d}{dz_2}G_{\bar{q}q}^{-}(z_1,\vec{r}_1;z_2,\vec{r}_2) &= \left[\frac{\epsilon^2-\Delta_{r_2}}{2\nu\alpha(1-\alpha)}+V_{\bar{q}q}^{-}(z_2,\vec{r}_2,\alpha)\right] \\ &\times G_{\bar{q}q}^{-}(z_1,\vec{r}_1;z_2,\vec{r}_2). \end{aligned} \tag{18}$$

Here ν is the photon energy. The Laplacian Δ_r acts on the coordinate r.

The imaginary part of the LC potential $V_{\bar{q}q}^{-}(z_2,\vec{r}_2,\alpha)$ in Eq. (18) is responsible for attenuation of the qq in the medium, while the real part represents the interaction between q and $\bar{q}$. This potential is supposed to provide the correct LC wave functions of vector mesons. For the sake of simplicity we use the oscillator form of the potential,

$$\mathrm{Re}\,V_{\bar{q}q}^{-}(z_2,\vec{r}_2,\alpha)=\frac{a^4(\alpha)\vec{r}_2^2}{2\nu\alpha(1-\alpha)}, \tag{19}$$

which leads to a Gaussian r dependence of the LC wave function of the meson ground state. The shape of the function $a(\alpha)$ will be discussed below.

In this case, Eq. (18) has an analytical solution, the harmonic oscillator Green function [22],

$$\begin{aligned} G_{\bar{q}q}^{-}(z_1,\vec{r}_1;z_2,\vec{r}_2) &= \frac{a^2(\alpha)}{2\pi i\sin(\omega\Delta z)}\exp\left\{\frac{ia^2(\alpha)}{\sin(\omega\Delta z)}[(r_1^2+r_2^2)\cos(\omega\Delta z)\right. \\ &\left.-2\vec{r}_1\cdot\vec{r}_2]\right\}\exp\left[-\frac{i\epsilon^2\Delta z}{2\nu\alpha(1-\alpha)}\right], \end{aligned} \tag{20}$$

where $\Delta z=z_2-z_1$ and

$$\omega=\frac{a^2(\alpha)}{\nu\alpha(1-\alpha)}. \tag{21}$$

The boundary condition is $G_{\bar{q}q}^{-}(z_1,\vec{r}_1;z_2,\vec{r}_2)|_{z_2=z_1}=\delta^2(\vec{r}_1-\vec{r}_2)$.

The probability amplitude to find the $\bar{q}q$ fluctuation of a photon at the point z_2 with separation $\vec{r}$ is given by an integral over the point z_1, where the $\bar{q}q$ is created by the photon with initial zero separation,

$$\Psi^{T,L}_{qq}(\vec{r},\alpha)=\frac{iZ_q\sqrt{\alpha_{em}}}{4\pi\nu\alpha(1-\alpha)}\int_{-\infty}^{z_2}dz_1 \times(\bar{\chi}\hat{O}^{T,L}\chi)G^{-}_{qq}(z_1,\vec{r}_1;z_2,\vec{r})|_{r_1=0}. \quad (22)$$

The operators $\hat{O}^{T,L}$ are defined in Eqs. (15) and (16). Here they act on the coordinate $\vec{r}_1$.

If we write the transverse part as

$$\bar{\chi}\hat{O}^T\chi=\bar{\chi}m_c\vec{\sigma}\cdot\vec{e}\chi+\bar{\chi}[i(1-2\alpha)(\vec{\sigma}\cdot\vec{n})\vec{e} +(\vec{\sigma}\times\vec{e})]\chi\cdot\vec{\nabla}_r =E+\vec{F}\cdot\vec{\nabla}_r, \quad (23)$$

then the distribution functions read

$$\Psi^{T}_{qq}(\vec{r},\alpha)=Z_q\sqrt{\alpha_{em}}[E\Phi_0(\epsilon,r,\lambda)+\vec{F}\cdot\vec{\Phi}_1(\epsilon,r,\lambda)], \quad (24)$$

$$\Psi^{L}_{qq}(\vec{r},\alpha)=2Z_q\sqrt{\alpha_{em}}Q\alpha(1-\alpha)\bar{\chi}\vec{\sigma}\cdot\vec{n}\chi\Phi_0(\epsilon,r,\lambda), \quad (25)$$

where

$$\lambda=\frac{2a^2(\alpha)}{\epsilon^2}. \quad (26)$$

The functions $\Phi_{0,1}$ in Eqs. (24) and (25) are defined as

$$\Phi_0(\epsilon,r,\lambda)=\frac{1}{4\pi}\int_0^\infty dt\frac{\lambda}{\mathrm{sh}(\lambda t)}\exp\left[-\frac{\lambda\epsilon^2r^2}{4}\mathrm{cth}(\lambda t)-t\right], \quad (27)$$

$$\vec{\Phi}_1(\epsilon,r,\lambda)=\frac{\epsilon^2\vec{r}}{8\pi}\int_0^\infty dt\left[\frac{\lambda}{\mathrm{sh}(\lambda t)}\right]^2\exp\left[-\frac{\lambda\epsilon^2r^2}{4}\mathrm{cth}(\lambda t)-t\right], \quad (28)$$

where $\mathrm{sh}(x)$ and $\mathrm{cth}(x)$ is the hyperbolic sine and hyperbolic cotangent, respectively. Note that the $\bar{q}$-q interaction enters Eqs. (24) and (25) via the parameter λ defined in Eq. (26). In the limit of vanishing interaction $\lambda\to 0$ (i.e., $Q^2\to\infty$, α is fixed, $\alpha\neq 0$ or 1) Eqs. (24) and (25) produce the perturbative expressions of Eq. (13). As mentioned above, for charmonium production nonperturbative interaction effects are quite weak. Consequently, the parameter λ (26) is rather small due to a large mass of the c quark.

With the choice $a^2(\alpha)\propto\alpha(1-\alpha)$ the end-point behavior of the mean square interquark separation $\langle r^2\rangle\propto 1/\alpha(1-\alpha)$ contradicts the idea of confinement. Following Ref. [15] we fix this problem via a simple modification of the LC potential,

$$a^2(\alpha)=a_0^2+4a_1^2\alpha(1-\alpha). \quad (29)$$

The parameters a_0 and a_1 were adjusted in Ref. [15] to the data on total photoabsorption cross section [23,24], diffractive photon dissociation, and shadowing in nuclear photoabsorption reaction. The results of our calculations vary within 1% only when a_0 and a_1 satisfy the relation

$$a_0^2=v^{1.15}(0.112)^2\ \ \mathrm{GeV}^2,$$
$$a_1^2=(1-v)^{1.15}(0.165)^2\ \ \mathrm{GeV}^2, \quad (30)$$

where v takes any value $0\leqslant v\leqslant 1$. In the view of this insensitivity of the observables we fix the parameters at $v=1/2$. We checked that this choice does not affect our results beyond a few percent uncertainty.

The last ingredient in elastic production amplitude (6) is the charmonium wave function. We use a popular prescription [25] applying the Lorentz boost to the rest frame wave function assumed to be Gaussian, which leads to radial parts of transversely and longitudinally polarized mesons in the form

$$\Phi^{T,L}_{J/\Psi}(\vec{r},\alpha)=C^{T,L}_{J/\Psi}\alpha(1-\alpha)f(\alpha)\exp\left[-\frac{\alpha(1-\alpha)r^2}{2R^2}\right] \quad (31)$$

with a normalization defined below, and

$$f(\alpha)=\exp\left[-\frac{m_c^2R^2}{2\alpha(1-\alpha)}\right] \quad (32)$$

with the parameters from Ref. [26], $R=0.183$ fm and $m_c=1.5$ GeV. A detailed analysis of various problems in this relativization procedure [27] leads to the same form as Eq. (31).

We assume that the distribution amplitudes of $\bar{c}c$ fluctuations for J/Ψ and for the photon have a similar structure [26]. Then in analogy to Eqs. (24) and (25),

$$\Psi^{T}_{J/\Psi}(\vec{r},\alpha)=(E+\vec{F}\cdot\vec{\nabla}_r)\Phi^{T}_{J/\Psi}(\vec{r},\alpha), \quad (33)$$

$$\Psi^{L}_{J/\Psi}(\vec{r},\alpha)=2m_{J/\Psi}\alpha(1-\alpha)(\bar{\chi}\vec{\sigma}\cdot\vec{n}\chi)\Phi^{L}_{J/\Psi}(\vec{r},\alpha). \quad (34)$$

Correspondingly, the normalization conditions for the transverse and longitudinal charmonium wave functions read

$$N_C\int d^2r\int d\alpha\{m_c^2|\Phi^T_{J/\Psi}(\vec{r},\alpha)|^2 +[\alpha^2+(1-\alpha)^2]|\partial_r\Phi^T_{J/\Psi}(\vec{r},\alpha)|^2\} =1, \quad (35)$$

$$4N_C\int d^2r\int d\alpha\,\alpha^2(1-\alpha)^2m^2_{J/\Psi}|\Phi^L_{J/\Psi}(\vec{r},\alpha)|^2=1. \quad (36)$$

III. ELECTROPRODUCTION OF J/Ψ ON A NUCLEON, COMPARISON WITH DATA

In this section we verify first the LC approach by comparing with data for nucleon target. The forward production amplitude $\gamma^*N\to J/\Psi N$ for transverse and longitudinal pho-

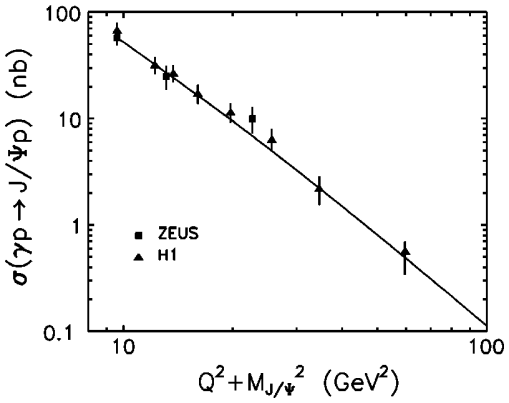

FIG. 1. $Q^2+m_{J/\Psi}^2$ dependence of the integrated cross section for the reactions $\gamma^* p \to J/\Psi p$. The model calculations are compared with H1 [29] and ZEUS [30] data at energy $W=90$ GeV.

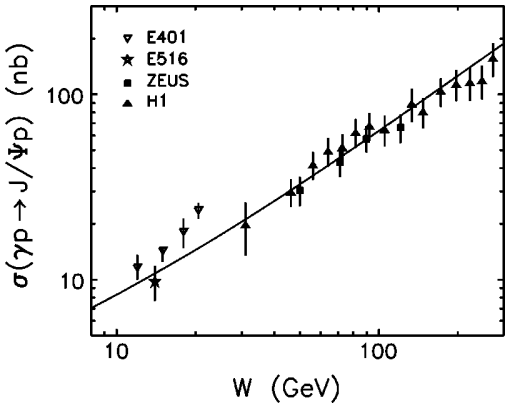

FIG. 2. Energy dependence of the real photoproduction cross section on a nucleon, $\gamma p \to J/\Psi p$. Our results are compared with data from the fixed target E401 [31], E516 [32], and collider HERA H1 [28] and ZEUS [33] experiments.

tons and charmonium is calculated using the nonperturbative photon, Eqs. (24) and (25), and vector meson, Eqs. (33), (34), wave functions and has the following form:

$$\mathcal{M}^T_{\gamma^* N\to J/\Psi N}(s,Q^2)|_{t=0} = N_C Z_c \sqrt{2\ \alpha_{em}} \int d^2r \sigma^-_{qq}(\vec{r},s) \times \int_0^1 d\alpha \{ m_c^2 \Phi_0(\epsilon,\vec{r},\lambda)\Phi^T_{J/\Psi}(\vec{r},\alpha) - [\alpha^2+(1-\alpha)^2]\vec{\Phi}_1(\epsilon,\vec{r},\lambda)\cdot\vec{\nabla}_r \Phi^T_{J/\Psi}(\vec{r},\alpha)\}, \tag{37}$$

$$\mathcal{M}^L_{\gamma^* N\to J/\Psi N}(s,Q^2)|_{t=0} = 4N_C Z_c \sqrt{2\ \alpha_{em}} m_{J/\Psi} Q \int d^2r \sigma^-_{qq}(\vec{r},s) \int_0^1 d\alpha\, \alpha^2 \times (1-\alpha)^2 \Phi_0(\epsilon,\vec{r},\lambda)\Phi^L_{J/\Psi}(\vec{r},\alpha). \tag{38}$$

These amplitudes are normalized as $|\mathcal{M}^{T,L}|^2 = 16\pi d\sigma_N^{T,L}/dt|_{t=0}$. The real part of the amplitude is included according to the prescription described in the preceding section. We calculate the cross sections $\sigma=\sigma^T+\epsilon'\sigma^L$ assuming that the photon polarization is $\epsilon'=1$.

Now we can check the absolute value of the production cross section by comparing with data for elastic charmonium electroproduction $\gamma^* p \to J/\Psi p$. Unfortunately, data are available only for the cross section integrated over t,

$$\sigma^{T,L}(\gamma^* N\to J/\Psi\ N) = \frac{|\mathcal{M}^{T,L}|^2}{16\pi B_{J/\Psi}}, \tag{39}$$

where $B_{J/\Psi}$ is the slope parameter in reaction $\gamma^* N \to J/\Psi N$. We use the experimental value [28] $B_{J/\Psi}=4.7\ \mathrm{GeV}^{-2}$.

Our predictions are plotted in Fig. 1, together with the data on the $Q^2+m_{J/\Psi}^2$ dependence of the cross section from H1 [29] and ZEUS [30].

The second test of our approach is a description of the real J/Ψ photoproduction. As we discussed in the preceding section, we include for completeness into calculations the nonperturbative interaction effects between c and $\bar{c}$ although they are rather small. Comparison of the model with data [31,32,28,33] for the energy dependence of the cross section of real J/Ψ photoproduction is presented in Fig. 2.

The normalization of the cross section and its energy and Q^2 dependence are remarkably well reproduced in Figs. 1 and 2. This is an important achievement since the absolute normalization is usually much more difficult to reproduce the production cross sections than nuclear effects. For instance, the similar, but simplified calculations in Ref. [8] underestimate the J/Ψ photoproduction cross section on protons by an order of magnitude.

As a cross check for the choice of the J/Ψ wave function in Eqs. (31) and (32) we also calculated the total J/Ψ nucleon cross section, which was already estimated in Ref. [13] using the charmonium wave functions calculated with several realistic $\bar{q}q$ potentials. The J/Ψ nucleon total cross section has the form

$$\sigma_{tot}^{J/\Psi-N} = N_C \int d^2r \int d\alpha \{ m_c^2 |\Phi^T_{J/\Psi}(\vec{r},\alpha)|^2 + [\alpha^2+(1-\alpha)^2]|\partial_r \Phi^T_{J/\Psi}(\vec{r},\alpha)|^2\} \sigma^-_{qq}(\vec{r},s). \tag{40}$$

We calculated $\sigma_{tot}^{J/\Psi-N}$ with the charmonium wave function in the form (31) (corresponding to quadratic $\bar{q}$-q potential) with the parameters described in the preceding section. For the dipole cross section we adopt the parametrization (8) which is designed to describe low-Q^2 data. Then, at $\sqrt{s}=10$ GeV we obtain $\sigma_{tot}^{J/\Psi-N}=4.2$ mb, which is not in contradiction with $\sigma_{tot}^{J/\Psi-N}=3.6\pm0.1$ mb evaluated in Ref. [13] using more realistic $\bar{q}$-q potentials and/or charmonium wave functions.

IV. INCOHERENT PRODUCTION OF CHARMONIA OFF NUCLEI

A. The *LC* Green function formalism

In this section we present a short review of the LC Green function formalism for incoherent production of an arbitrary vector meson. For the case of charmonium production one should replace $V\to J/\Psi$ and $\bar{q}q\to\bar{c}c$. In general, the diffractive incoherent (quasielastic) production of vector mesons off nuclei, $\gamma^*A\to VX$, is associated with a breakup of the nucleus, but without production of new particles. In other words, one sums over all final states of the target nucleus except those which contain particle (pion) creation. The observable usually studied experimentally is nuclear transparency defined as

$$\mathrm{Tr}_A^{inc}=\frac{\sigma^{inc}_{\gamma^*A\to VX}}{A\sigma_{\gamma^*N\to VN}}. \tag{41}$$

The t slope of the differential quasielastic cross section is the same as on a nucleon target. Therefore, instead of integrated cross sections one can also use nuclear transparency expressed via the forward differential cross sections Eq. (7),

$$\mathrm{Tr}_A^{inc}=\frac{1}{A}\left|\frac{\mathcal{M}_{\gamma^*A\to VX}(s,Q^2)}{\mathcal{M}_{\gamma^*N\to VN}(s,Q^2)}\right|^2. \tag{42}$$

In the LC Green function approach [10] the physical photon $|\gamma^*\rangle$ is decomposed into different Fock states, namely, the bare photon $|\gamma^*\rangle_0$, $|\bar{q}q\rangle$, $|\bar{q}qG\rangle$, etc. As we mentioned above, the higher Fock states containing gluons describe the energy dependence of the photoproduction reaction on a nucleon. Besides, those Fock components also lead to gluon shadowing as far as nuclear effects are concerned. However, these fluctuations are heavier and have a shorter coherence time (lifetime) than the lowest $|\bar{q}q\rangle$ state. Therefore, at medium energies only $|\bar{q}q\rangle$ fluctuations of the photon matter. Consequently, gluon shadowing related to the higher Fock states will be dominated at high energies. Detailed description and calculation of gluon shadowing for the case of vector meson production off nuclei is presented in Refs. [10,11]. Although the gluon shadowing effects are rather small in the kinematic range important for study of CT effects in elastic and quasielastic charmonium production off nuclei, we include them in all calculations.

Propagation of an interacting $\bar{q}q$ pair in a nuclear medium is also described by the Green function satisfying the evolution Eq. (18). However, the potential in this case acquires an imaginary part which represents absorption in the medium,

$$\mathrm{Im}\,V^-_{qq}(z_2,\vec{r},\alpha)=-\frac{\sigma^-_{qq}(\vec{r},s)}{2}\rho_A(b,z_2), \tag{43}$$

where $\rho_A(b,z_2)$ is the nuclear density function defined at the point with longitudinal coordinate z_2 and impact parameter $\vec{b}$. The evolution equation (18) with the potential $V^-_{qq}(z_2,\vec{r}_2,\alpha)$ containing this imaginary part was used in Refs. [34,35], and nuclear shadowing in deep-inelastic scattering was calculated in good agreement with data.

The analytical solution of Eq. (20) is only known for the harmonic oscillator potential $V(r)\propto r^2$. To keep the calculations reasonably simple we are forced to use the dipole approximation,

$$\sigma^-_{qq}(r,s)=C(s)r^2, \tag{44}$$

which allows to obtain the Green function in an analytical form.

The energy dependent factor $C(s)$ in Eq. (44) is adjusted by demanding that calculations employing the approximation Eq. (44) reproduce correctly the results based on the realistic cross section Eq. (8) in the limit $l_c\gg R_A$ (the so called ''frozen'' approximation) when the Green function takes the simple form,

$$G^-_{qq}(z_1,\vec{r}_1;z_2,\vec{r}_2)\Rightarrow\delta(\vec{r}_1-\vec{r}_2)\exp\left[-\frac{1}{2}\sigma^-_{qq}(r_1)\int_{z_1}^{z_2}dz\,\rho_A(b,z)\right], \tag{45}$$

where the dependence of the Green function on impact parameter is dropped. Thus, for incoherent production of vector mesons, the factor $C(s)$ is fixed by the relation

$$\frac{\int d^2bT_A(b)\left|\int d^2rr^2\exp\left[-\frac{1}{2}C(s)r^2T_A(b)\right]\int d\alpha\Psi_V^{*T,L}(\vec{r},\alpha)\Psi^{T,L}_{qq}(\vec{r},\alpha)\right|^2}{\left|\int d^2r\,r^2\int d\alpha\Psi_V^{*T,L}(\vec{r},\alpha)\Psi^{T,L}_{qq}(\vec{r},\alpha)\right|^2}$$
$$=\frac{\int d^2bT_A(b)\left|\int d^2r\,\sigma^-_{qq}(r,s)\exp\left[-\frac{1}{2}\sigma^-_{qq}(r,s)T_A(b)\right]\int d\alpha\Psi_V^{*T,L}(\vec{r},\alpha)\Psi^{T,L}_{qq}(\vec{r},\alpha)\right|^2}{\left|\int d^2r\,\sigma^-_{qq}(r,s)\int d\alpha\,\Psi_V^{*T,L}(\vec{r},\alpha)\Psi^{T,L}_{qq}(\vec{r},\alpha)\right|^2} \tag{46}$$

To take advantage of the analytical form of the Green function which is known only for the LC potential Eq. (43) with a constant nuclear density, we use the approximation $\rho_A(b,z)=\rho_0\Theta(R_A^2-b^2-z^2)$. Therefore we have to use this form for Eq. (46) as well. The value of the mean nuclear density ρ_0 was determined using the relation

$$\int d^2b[1-\exp(-\sigma_0\rho_0\sqrt{R_A^2-b^2})] = \int d^2b\left[1-\exp\left(-\frac{\sigma_0}{2}T(b)\right)\right], \quad (47)$$

where the nuclear thickness function $T_A(b)$ is calculated with the realistic Woods-Saxon form of the nuclear density. The value of ρ_0 turns out to be practically independent of the cross section σ_0 in the range from 1 to 50 mb.

With the potential Eqs. (43) and (44) the solution of Eq. (18) has the same form as Eq. (20), except that one should replace $\omega\Rightarrow\Omega$ and $a^2(\alpha)\Rightarrow b(\alpha)$, where

$$\Omega=\frac{b(\alpha)}{\nu\alpha(1-\alpha)}=\frac{\sqrt{a^4(\alpha)-i\rho_A(b,z)\nu\alpha(1-\alpha)C(s)}}{\nu\alpha(1-\alpha)}. \quad (48)$$

As we discussed in Ref. [10] the value of l_c can distinguish different regimes of vector meson production.

(i) The CL is much shorter than the mean nucleon spacing in a nucleus ($l_c\to 0$). In this case $G(z_2,\vec{r}_2;z_1,\vec{r}_1)\to\delta(z_2-z_1)$. Correspondingly, the formation time of the meson wave function is very short as well as given in Eq. (1). For light vector mesons $l_f\sim l_c$ and since formation and coherence lengths are proportional to photon energy both must be short. Consequently, nuclear transparency is given by the simple formula Eq. (3) corresponding to the Glauber approximation.

(ii) In production of charmonia and other heavy flavor quarkonii there is a strong inequality $l_c<l_f$ and the intermediate case $l_c\to 0$, but $l_f\sim R_A$ can be realized. Then the formation of the meson wave function is described by the Green function and the numerator of the nuclear transparency ratio Eq. (42) has the form [8],

$$|\mathcal{M}_{\gamma^*A\to VX}(s,Q^2)|^2_{l_c\to 0;l_f\sim R_A} = \int d^2b\int_{-\infty}^{\infty}dz\,\rho_A(b,z)|F_1(b,z)|^2, \quad (49)$$

where

$$F_1(b,z)=\int_0^1 d\alpha\int d^2r_1d^2r_2\Psi_V^*(\vec{r}_2,\alpha)G(z',\vec{r}_2;z,\vec{r}_1) \times\sigma_{qq}^-(r_1,s)\Psi_{qq}^-(\vec{r}_1,\alpha)|_{z'\to\infty}. \quad (50)$$

(iii) In the high-energy limit $l_c\gg R_A$ (in fact, it is more correct to compare with the mean free path of the $\bar{q}q$ in a nuclear medium if the latter is shorter than the nuclear radius). In this case $G(z_2,\vec{r}_2;z_1,\vec{r}_1)\to\delta(\vec{r}_2-\vec{r}_1)$, i.e., all fluctuations of the transverse $\bar{q}q$ separation are "frozen" by Lorentz time dilation. Then, the numerator on the right-hand side of Eq. (42) takes the form [8],

$$|\mathcal{M}_{\gamma^*A\to VX}(s,Q^2)|^2_{l_c\gg R_A} = \int d^2b\,T_A(b)\left|\int d^2r\int_0^1 d\alpha\Psi_V^*(\vec{r},\alpha)\sigma_{qq}^-(r,s) \times\exp\left[-\frac{1}{2}\sigma_{qq}^-(r,s)T_A(b)\right]\Psi_{qq}^-(\vec{r},\alpha,Q^2)\right|^2. \quad (51)$$

In this case the $\bar{q}q$ attenuates with a constant absorption cross section like in the Glauber model, except that the whole exponential is averaged rather than just the cross section in the exponent. The difference between the results of the two prescriptions are the well known inelastic corrections of Gribov [3].

(iv) This regime reflects the general case when there is no restrictions for either l_c or l_f. The corresponding theoretical tool has been developed for the first time only recently in Ref. [10] and applied to electroproduction of light vector mesons at medium and high energies. Even within the VDM the Glauber model expression interpolating between the limiting cases of low [(i), (ii)] and high [(iii)] energies has been derived only recently [12] as well. In this general case the incoherent photoproduction amplitude is represented as a sum of two terms [36],

$$|\mathcal{M}_{\gamma^*A\to VX}(s,Q^2)|^2 = \int d^2b\int_{-\infty}^{\infty}dz\,\rho_A(b,z)|F_1(b,z)-F_2(b,z)|^2. \quad (52)$$

The first term $F_1(b,z)$ introduced above in Eq. (50) alone would correspond to the short l_c limit (ii). The second term $F_2(b,z)$ in Eq. (52) corresponds to the situation when the incident photon produces a $\bar{q}q$ pair diffractively and coherently at the point z_1 prior to incoherent quasielastic scattering at point z. The LC Green functions describe the evolution of the $\bar{q}q$ over the distance from z_1 to z and further on, up to the formation of the meson wave function. Correspondingly, this term has the form,

$$F_2(b,z)=\frac{1}{2}\int_{-\infty}^{z}dz_1\rho_A(b,z_1)\int_0^1 d\alpha\int d^2r_1d^2r_2d^2r \times\Psi_V^*(\vec{r}_2,\alpha)G(z'\to\infty,\vec{r}_2;z,\vec{r})\sigma_{qq}^-(\vec{r},s) \times G(z,\vec{r};z_1,\vec{r}_1)\sigma_{qq}^-(\vec{r}_1,s)\Psi_{qq}^-(\vec{r}_1,\alpha). \quad (53)$$

Equation (52) correctly reproduces the limits (i)–(iii). At $l_c\to 0$ the second term $F_2(b,z)$ vanishes because of strong oscillations, and Eq. (52) reproduces the Glauber expression Eq. (3). At $l_c\gg R_A$ the phase shift in the Green functions can be neglected and they acquire the simple form $G(z_2,\vec{r}_2;z_1,\vec{r}_1)\to\delta(\vec{r}_2-\vec{r}_1)$. In this case the integration over longitudinal coordinates in Eqs. (50) and (53) can be performed explicitly and the asymptotic expression Eq. (51) is recovered as well.

B. Comparison with data for incoherent production of J/Ψ

Exclusive incoherent electroproduction of vector mesons off nuclei has been suggested in Ref. [37] to be very convenient for investigation of CT. Increasing the photon virtuality Q^2, one squeezes the produced $\bar{q}q$ wave packet. Such a small colorless system propagates through the nucleus with little attenuation, provided that the energy is sufficiently high ($l_f \gg R_A$) so the fluctuations of the $\bar{q}q$ separation are frozen during propagation. Consequently, a rise of nuclear transparency $\mathrm{Tr}_A^{inc}(Q^2)$ with Q^2 should give a signal for CT. Indeed, such a rise was observed in the E665 experiment [38] at Fermilab for exclusive production of ρ^0 mesons off nuclei, what has been claimed as a manifestation of CT.

However, the effect of coherence length [39,12] leads also to a rise of $\mathrm{Tr}_A^{inc}(Q^2)$ with Q^2 and so can imitate CT effects. This happens when the coherence length varies from long to short [see Eq. (2)] compared to the nuclear size, and the length of the path in nuclear matter becomes shorter. Consequently, the vector meson (or $\bar{q}q$) attenuates less in nuclear medium. This happens when Q^2 increases at fixed ν. Therefore one should carefully disentangle these two phenomena.

Unfortunately, the data on charmonium electroproduction off nuclei are very scanty so far. There are only data from the NMC experiment [40] concerning energy dependence of the ratio of nuclear transparencies Tr_{Sn}^{inc} and Tr_C^{inc} for incoherent production of J/Ψ at $Q^2=0$. The corresponding photon energy varies from 60 to 210 GeV. It allows to study the transition from medium long to long coherence length, which varies from 2.4 to 8.5 fm. For long $l_c \gtrsim 8.5$ fm the "frozen" approximation can be used with high accuracy. In this case, nuclear transparency Tr_A^{inc} of incoherent (quasielastic) J/Ψ production can be calculated using Eq. (52) and the simplified "frozen" approximation Eqs. (45), (51). For medium long coherence length one cannot use the "frozen" approximation and fluctuations of the size of the $\bar{q}q$ pair become important. Because of a strong inequality $l_c < l_f$ for charmonium production CT effects are expected to be dominant at small and moderate energies. Consequently, they should lead to a rise with energy of Tr_A^{inc}. Such a scenario is depicted in Fig. 3 by solid and dashed curves. Dashed curve show our results using the LC Green function approach in the limit of short coherence length $l_c \to 0$, Eq. (49). The solid curve includes in addition also CL effects. Thus, the effect of coherence length manifest itself as a separation between the solid and dashed curves. Energy rise of the ratio $\mathrm{Tr}_{Sn}^{inc}/\mathrm{Tr}_C^{inc}$ at small and medium energy is a net manifestation of CT. It follows from the rise of formation time, see Eq. (1). At larger energies when CL effects also become important the $\mathrm{Tr}_{Sn}^{inc}/\mathrm{Tr}_C^{inc}$ ratio starts to fall down gradually.[2] Unfortunately, the NMC data have quite large error bars and therefore give only an indication for such a behavior. More accurate data

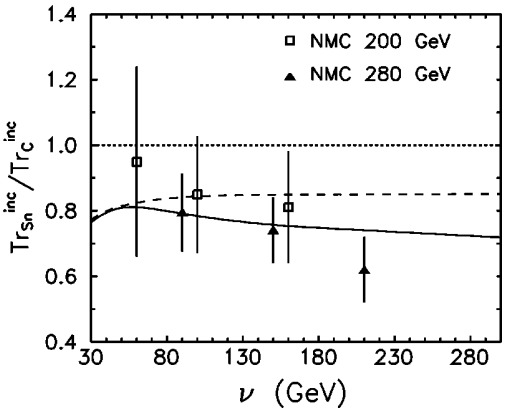

FIG. 3. Energy dependence of the ratio of nuclear transparencies Tr_{Sn} and Tr_C vs experimental points taken from the NMC experiment [40]. Solid and dashed curves show our results using the LC Green function approach in general case with no restriction for either l_c or l_f, Eq. (52), and in the limit of $l_c \to 0$, Eq. (49), respectively.

are needed for exploratory study of CT and CL effects. Charmonium real photoproduction off nuclei at small and large energies is very sensitive for investigation of CT and CL effect separately. However, it is not so for real photoproduction of light vector mesons when coherence and formation lengths are comparable and CT-CL mixing exists already at small energies.

Problem of separation of CT and CL effects was discussed in details in Ref. [10] with the main emphasis to light vector meson production where $l_c \gtrsim l_f$ at $Q^2 \lesssim 1-2$ GeV^2. In this paper we present the results for charmonium production, where a strong inequality $l_c < l_f$ in all discussed kinematic regions leads to a different scenario of CT-CL mixing compared to production of light vector mesons. Consequently, at fixed Q^2 and at small and medium energies the problem of CT-CL separation is not so acute. Besides, there is a prescription how to eliminate the effect of CL from the data on the Q^2 dependence of nuclear transparency [9]. One should simply bin the data in a way that keeps $l_c = \mathrm{const}$. It means that one should vary simultaneously ν and Q^2 maintaining the CL Eq. (2) constant,

$$\nu = \frac{1}{2} l_c (Q^2 + m_{J/\Psi}^2). \tag{54}$$

In this case the Glauber model predicts a Q^2 independent nuclear transparency, and any rise with Q^2 would signal CT [9].

The LC Green function technique incorporates both the effects of coherence and formation. We performed calculations of $\mathrm{Tr}_A^{inc}(Q^2)$ at fixed l_c starting from different minimal values of ν, which correspond to real photoproduction in Eq. (54),

$$\nu_{min} = \frac{1}{2} l_c m_{J/\Psi}^2 . \tag{55}$$

[2]In energy dependence of nuclear transparency at fixed Q^2, the effect of the coherence follows from variation of the coherence length from small to large values compared to the nuclear size, see Eq. (2).

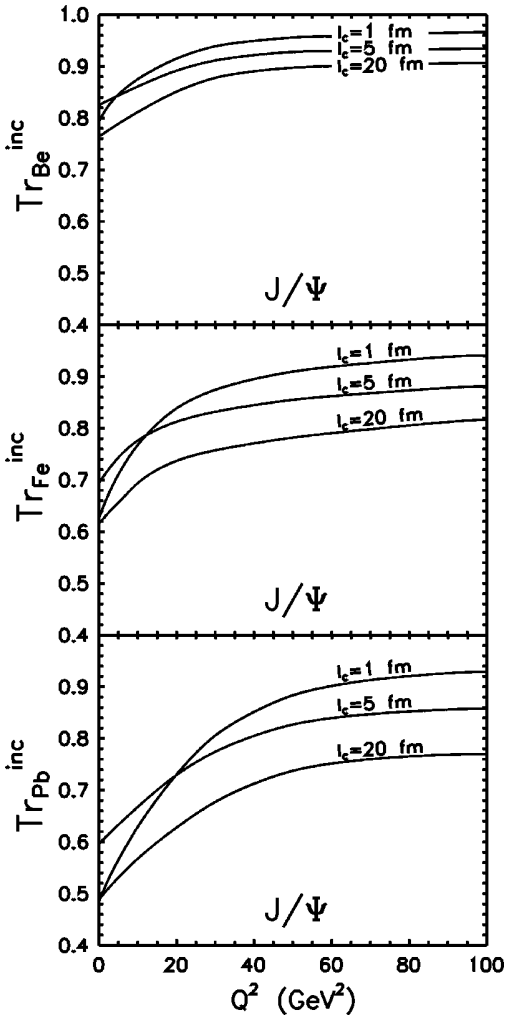

FIG. 4. Q^2 dependence of the nuclear transparency Tr_A^{inc} for exclusive electroproduction of J/Ψ on nuclear targets ^{9}Be, ^{56}Fe, and ^{207}Pb (from top to bottom). The CL is fixed at $l_c=1$, 5, and 20 fm.

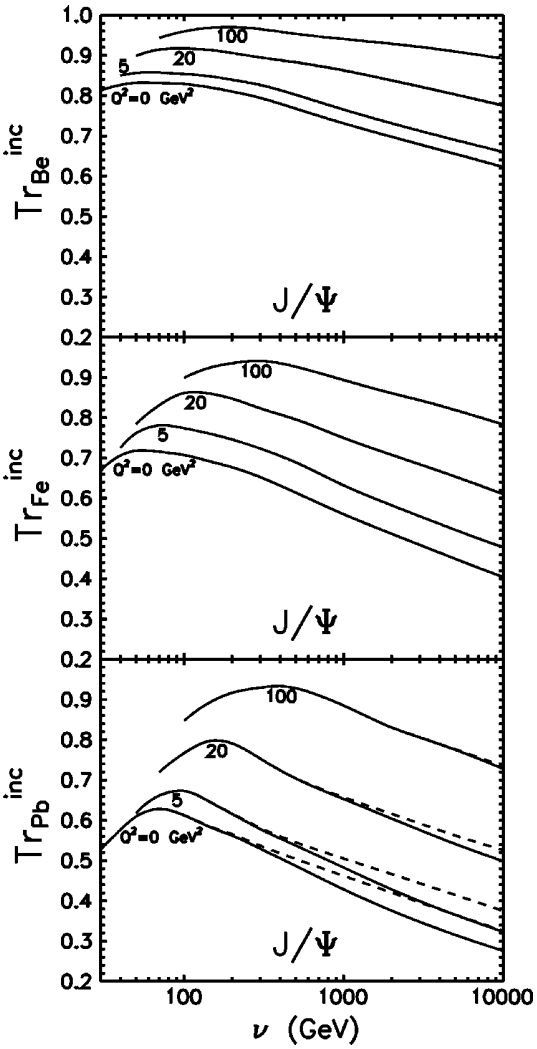

FIG. 5. Nuclear transparency for incoherent electroproduction $\gamma^* A \to J/\Psi\, X$ as a function of energy at $Q^2=0$, 5, 20, and 100 GeV^2 for beryllium, iron, and lead. The solid curves and dashed curves for lead correspond to calculations with and without gluon shadowing, respectively.

The results for incoherent production of J/Ψ at $\nu_{min}=24.3$, 121.7, and 487 GeV ($l_c=1$,5 and 20 fm) are presented in Fig. 4 for beryllium, iron, and lead. We use the nonperturbative LC wave function of the photon with the parameters of the LC potential $a_{0,1}$ fixed in accordance with Eq. (30) at $v=1/2$. We use quark mass $m_c=1.5$ GeV.

Although the predicted variation of nuclear transparency with Q^2 at fixed l_c is less than for light vector meson production [10], it is still sufficiently significant to be investigated experimentally even in the range of $Q^2 \lesssim 20$ GeV^2. CT effects (the rise with Q^2 of nuclear transparency) are more pronounced at low than at high energies and can be easily identified by the planned future experiments.

We also calculated the energy dependence of nuclear transparency at fixed Q^2. The results for beryllium, iron, and lead are shown in Fig. 5 for different values of Q^2. The interesting feature is the presence of a maximum of transparency at some energy, which is much more evident than in production of light vector mesons [10]. At small and moderate energies a strong rise of Tr_A^{inc} with energy, especially for the lead target, is a manifestation of net CT effects resulting from a strong inequality $l_c < l_f$. The existence of maxima of Tr_A^{inc} results from the interplay of coherence and formation effects. Indeed, the formation length rises with energy leading to an increasing nuclear transparency. At some energy, however, the effect of CL is switched on leading to a growth of the path length of the $\bar{q}q$ in the nucleus, i.e., to a suppression of nuclear transparency. This also explains the unusual ordering of curves at small and moderate Q^2 calculated for different values of l_c as is depicted in Fig. 4.

V. COHERENT PRODUCTION OF J/Ψ

First of all we present a short introduction to coherent production of vector mesons. One should replace $V \to J/\Psi$ and $\bar{q}q \to \bar{c}c$ when coherent production of charmonia is

treated. In general, in coherent (elastic) electroproduction of a vector meson the target nucleus remains intact, so all the vector mesons produced at different longitudinal coordinates and impact parameters add up coherently. This condition considerably simplifies the expressions for the production cross sections. The integrated cross section has the form

$$\sigma_A^{coh} \equiv \sigma^{coh}_{\gamma^* A\to VA} = \int d^2q \left| \int d^2b\, e^{i\vec{q}\cdot\vec{b}} \mathcal{M}^{coh}_{\gamma^* A\to VA}(b) \right|^2 = \int d^2b |\mathcal{M}^{coh}_{\gamma^* A\to VA}(b)|^2, \tag{56}$$

where

$$\mathcal{M}^{coh}_{\gamma^* A\to VA}(b) = \int_{-\infty}^{\infty} dz\, \rho_A(b,z) F_1(b,z), \tag{57}$$

with the function $F_1(b,z)$ defined in Eq. (50).

One should not use Eq. (42) for nuclear transparency anymore since the t-slopes of the differential cross sections for nucleon and nuclear targets are different and do not cancel in the ratio. Therefore, the nuclear transparency also includes the slope parameter B_V for the process $\gamma^* N\to VN$,

$$\mathrm{Tr}_A^{coh} = \frac{\sigma_A^{coh}}{A\sigma_N} = \frac{16\pi B_V \sigma_A^{coh}}{A|\mathcal{M}_{\gamma^* N\to VN}(s,Q^2)|^2}. \tag{58}$$

The energy dependent factor $C(s)$ in dipole cross section approximation Eq. (44) is adjusted in an analogical way as for incoherent charmonium production described in the preceding section. However, in contrast to Eq. (46) the factor $C(s)$ is fixed now by the following relation:

$$\frac{\int d^2b \left| \int d^2r \int d\alpha \Psi_V^{*T,L}(\vec{r},\alpha) \Psi_{q\bar{q}}^{T,L}(\vec{r},\alpha) \left\{ 1-\exp\left[-\frac{1}{2} C(s) r^2 T_A(b) \right] \right\} \right|^2}{\left| \int d^2r \int d\alpha \Psi_V^{*T,L}(\vec{r},\alpha) C(s) r^2 \Psi_{q\bar{q}}^{T,L}(\vec{r},\alpha) \right|^2} = \frac{\int d^2b \left| \int d^2r \int d\alpha \Psi_V^{*T,L}(\vec{r},\alpha) \Psi_{q\bar{q}}^{T,L}(\vec{r},\alpha) \left\{ 1-\exp\left[-\frac{1}{2} \sigma^-_{q\bar{q}}(r,s) T_A(b) \right] \right\} \right|^2}{\left| \int d^2r \int d\alpha \Psi_V^{*T,L}(\vec{r},\alpha) \sigma^-_{q\bar{q}}(r,s) \Psi_{q\bar{q}}^{T,L}(\vec{r},\alpha) \right|^2}. \tag{59}$$

A. Predictions for coherent production of J/Ψ

Unfortunately, there are no data yet on coherent electroproduction of charmonia. Therefore, we present only predictions that can be later verified and tested in the future planned experiments.

One can eliminate the effects of CL and single out the net CT effect in a way similar to what was suggested for incoherent reactions by selecting experimental events with l_c = const. We calculated nuclear transparency for the coherent reaction $\gamma^* A\to J/\Psi A$ at fixed values of l_c. The results for $l_c = 1$, 5, and 20 fm are depicted in Fig. 6 for several nuclei. We performed calculations of Tr_A^{coh} with the slope $B_V = B_{J/\Psi} = 4.7$ GeV^{-2}. The effect of a rise of Tr_A^{coh} is not sufficiently large to be observable in the range of $Q^2 \leqslant 20$ GeV^2. A wider range of $Q^2 \leqslant 100$ GeV^2 and heavy nuclei gives higher chances for experimental investigation of CT. However, it encounters the problem of low yields at high Q^2.

Note that in contrast to incoherent production where nuclear transparency is expected to saturate as $\mathrm{Tr}_A^{inc}(Q^2) \to 1$ at large Q^2, for the coherent process nuclear transparency reaches a higher limit, $\mathrm{Tr}_A^{coh}(Q^2) \to A^{1/3}$.

We also calculated nuclear transparency as function of energy at fixed Q^2. The results for J/Ψ produced coherently off beryllium, iron, and lead are depicted in Fig. 7 at $Q^2 = 0$, 5, 20, and 100 GeV^2. Tr_A^{coh} is very small at low energy, which of course does not mean that nuclear matter is not transparent, but the nuclear coherent cross section is suppressed by the nuclear form factor. Indeed, the longitudinal momentum transfer which is equal to the inverse CL, is large when the CL is short. However, at high energy $l_c \gg R_A$ and nuclear transparency nearly saturates (it decreases with ν only due to the rising dipole cross section). The saturation level is higher at larger Q^2, which is a manifestation of CT.

Note that in all calculations the effects of gluon shadowing are included in a way analogical to that described in the recent papers [10,11]. They are much smaller than in production of light vector mesons. For illustration, they are depicted in Figs. 5 and 7 for the lead target as a difference between solid and dashed lines at various values of Q^2. In the photoproduction limit $Q^2 = 0$ the onset of gluon shadowing becomes important at rather high photon energy $\nu > 1000$ GeV for incoherent and $\nu > 500$ GeV for coherent production. This corresponds to the claim made in Ref. [15] that the onset of gluon shadowing requires smaller x_{Bj} than the onset of quark shadowing. The reason is that the fluctuations containing gluons are, in general, heavier than the $\bar{q}q$ and have a shorter CL.

Although gluon shadowing is included in all calculations, it is small enough in the kinematic range important for in-

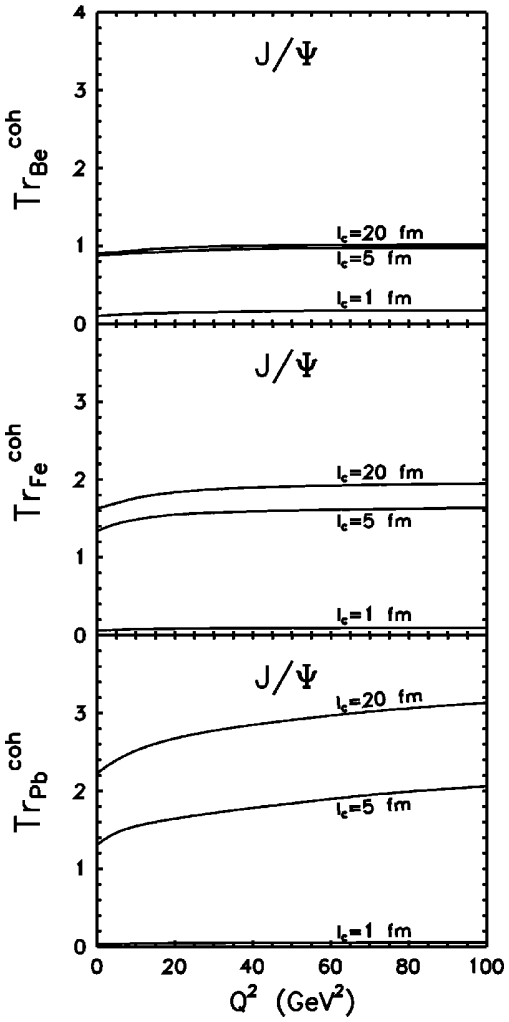

FIG. 6. The same as in Fig. 4, but for coherent production of J/Ψ, $\gamma^* A \to J/\Psi\, A$.

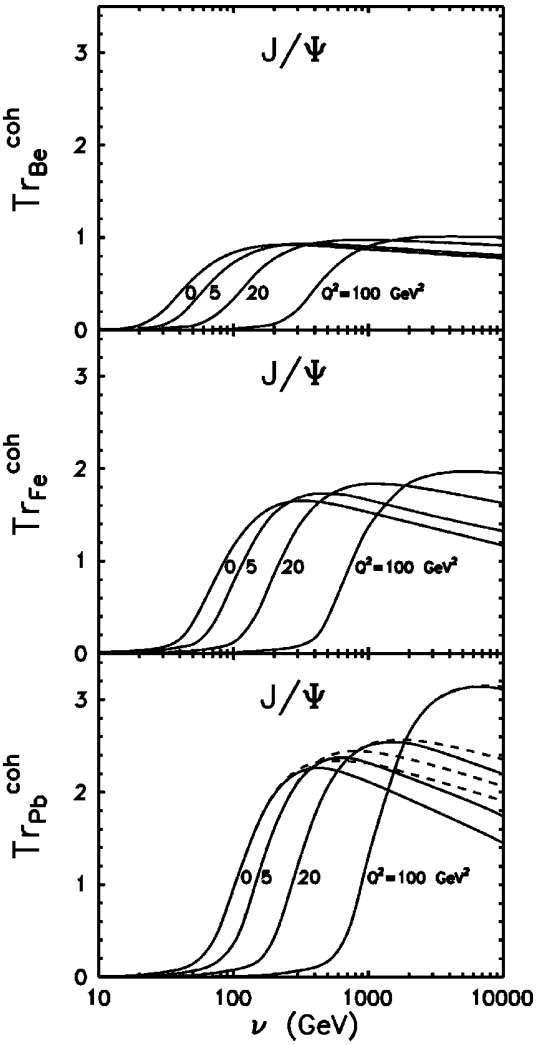

FIG. 7. Nuclear transparency for coherent electroproduction $\gamma^* A \to J/\Psi\, A$ as a function of energy at $Q^2 = 0$, 5, 20, and 100 GeV^2 for beryllium, iron, and lead. The solid curves and dashed curves for lead correspond to calculations with and without gluon shadowing, respectively.

vestigation of CT. Consequently, it does not affect the main achievements and conclusions important in the process of searching for CT effects in charmonium coherent and incoherent production off nuclei.

VI. SUMMARY AND CONCLUSIONS

In the present paper we focused the main emphasis on the production of charmonia due to advantages as compared with light vector meson production [10]. Electroproduction of charmonia off nuclei is a very convenient way to study the interplay between coherence (shadowing) and formation (color transparency) effects. A strong inequality $l_c < l_f$ in all kinematic region of ν and Q^2 leads to a different scenario of mixing of CT and CL effects as compared to light vector mesons where $l_c \gtrsim l_f$ at $Q^2 \lesssim 1-2$ GeV^2. Consequently, at small and moderate energies a problem of CT-CL separation is not so acute. Besides, due to quite a large mass of the c quark the relativistic corrections and nonperturbative effects are sufficiently small. They are negligible investigating the production of still heavier vector mesons (bottonium, toponium). However, one encounters the problem of very low yields as well as very small CT and CL effects (due to very large masses of $\overline{qq}$ fluctuactions and vector mesons) to be measured experimentally. Therefore production of charmonia represents some compromise, because the above mentioned theoretical uncertainties (typical for light vector mesons) and very small production rates (typical for still heavier vector mesons) are eliminated to a certain extent keeping sufficiently large CT and CL effects. This fact supports an enhanced interest to study electroproduction of charmonia off nuclei separately. We used from Ref. [10] a rigorous quantum-mechanical approach based on the light-cone QCD Green function formalism which naturally incorporates the interference effects of CT and CL. Our main results and observations are the following.

Within the suggested approach taken from Ref. [10], interpolating between the previously known low- and high-energy limits we studied for the first time CT effects in co-

herent and incoherent electroproduction of charmonia off nuclei.

As the first test we compare the model predictions with available data from the NMC experiment on energy dependence of the nuclear transparency ratio $\mathrm{Tr}_{Sn}^{inc}/\mathrm{Tr}_{C}^{inc}$ for incoherent production of J/Ψ at $Q^2=0$. We found a good agreement with the data, which confirms the dominance of CT effects at small and medium and CL effects at medium large and large energies.

The onset of coherence effects (shadowing) can mimic the expected signal of CT in incoherent electroproduction of charmonia at medium large and large energies. In order to single out the formation effect the data must be taken at such energy and Q^2 which keep $l_c=\mathrm{const}$. Then the observation of a rise with Q^2 of nuclear transparency for fixed l_c would give a signal of color transparency. Predictions of $\mathrm{Tr}_{A}^{inc}(Q^2)$ as a function of Q^2 at different fixed l_c show rather large CT effects in incoherent production of charmonia. Although the variation of nuclear transparency with Q^2 at fixed l_c is predicted to be less than for the production of light vector mesons [10], it is still sufficiently significant to be investigated experimentally even in the range of $Q^2 \lesssim 20$ GeV^2. CT effects (the rise with Q^2 of nuclear transparency) are more pronounced at low than at high energies and can be easily identified by the planned future experiments.

The effects of CT in coherent production of charmonia are found to be less pronounced, similarly as in production of light vector mesons [10]. A wider range $Q^2 \leqslant 100$ GeV^2 and heavy nuclei give higher chances for experimental investigation of CT. However, it faces the problem of low yields at high Q^2.

The effects of gluon shadowing were shown to be important only at much higher energies than in production of light vector mesons due to large mass of $\bar{c}c$ fluctuation. Nuclear suppression of gluons was calculated within the same LC approach and included in predictions. It was manifested that these corrections are quite small at medium energies which are dominant in the process of searching for CT effects.

Finally, one can compare the predictions for incoherent and coherent charmonium production off lead target (see Figs. 4, 5, 6, and 7) obtained within rigorous quantum-mechanical approach based on the light-cone QCD Green function formalism (incorporating naturally CT and CL effects) with the results of Ref. [11] evaluated in the approximation of long coherence length $l_c \gg R_A$ (without CT effects) allow to employ realistic light-cone wave functions of charmonia from Ref. [13] and to make corrections for finite values of l_c. We find a nice quantitative agreement at moderate and high energies and at low and medium values of Q^2. This fact confirms justification to use that high-energy approximation [11] for charmonium electroproduction off nuclei in the kinematic region where CL effects dominate. Besides, using advantages from both approaches, one can perform in the future fully realistic calculations using known LC dipole approach based on Green function formalism employing a realistic dipole cross section and using realistic LC wave functions of charmonia from [13].

In conclusion, the predicted rather large effects of CT in incoherent electroproduction of charmonia off nuclei open further possibilities to search for CT with medium energy electrons and can be tested in future experiments.

ACKNOWLEDGMENTS

This work was supported in part by the Slovak Funding Agency, Grant Nos. 2/1169 and 6114.

[1] T. Matsui and H. Satz, Phys. Lett. B **178**, 416 (1986).
[2] V.N. Gribov, Zh. Éksp. Teor. Fiz. **56**, 892 (1969) [Sov. Phys. JETP **29**, 483 (1969)].
[3] A.B. Zamolodchikov, B.Z. Kopeliovich, and L.I. Lapidus, Pis'ma Zh. Tekh. Fiz. **33**, 612 (1981) [JETP Lett. **33**, 595 (1981)].
[4] G. Bertsch, S.J. Brodsky, A.S. Goldhaber, and J.F. Gunion, Phys. Rev. Lett. **47**, 297 (1981).
[5] J.F. Gunion and D.E. Soper, Phys. Rev. D **15**, 2617 (1977).
[6] J. Hüfner and B. Povh, Phys. Rev. D **46**, 990 (1992).
[7] B. Povh, hep-ph/9806379.
[8] B.Z. Kopeliovich and B.G. Zakharov, Phys. Rev. D **44**, 3466 (1991).
[9] J. Hüfner and B.Z. Kopeliovich, Phys. Lett. B **403**, 128 (1997).
[10] B.Z. Kopeliovich, J. Nemchik, A. Schaefer, and A.V. Tarasov, Phys. Rev. C **65**, 035201 (2002).
[11] Yu.P. Ivanov, B.Z. Kopeliovich, A.V. Tarasov, and J. Huefner, Phys. Rev. C **66**, 024903 (2002).
[12] J. Hüfner, B.Z. Kopeliovich, and J. Nemchik, Phys. Lett. B **383**, 362 (1996).
[13] J. Huefner, Yu.P. Ivanov, B.Z. Kopeliovich, and A.V. Tarasov, Phys. Rev. D **62**, 094022 (2000).
[14] K. Golec-Biernat and M. Wüsthoff, Phys. Rev. D **59**, 014017 (1999); **60**, 114023 (1999).
[15] B.Z. Kopeliovich, A. Schäfer, and A.V. Tarasov, Phys. Rev. D **62**, 054022 (2000).
[16] A. Donnachie and P.V. Landshoff, Phys. Lett. B **478**, 146 (2000).
[17] Particle Data Group, D.E. Groom *et al.*, Eur. Phys. J. C **15**, 1 (2000).
[18] J.B. Bronzan, G.L. Kane, and U.P. Sukhatme, Phys. Lett. **49B**, 272 (1974).
[19] J.B. Kogut and D.E. Soper, Phys. Rev. D **1**, 2901 (1970).
[20] J.M. Bjorken, J.B. Kogut, and D.E. Soper, Phys. Rev. D **3**, 1382 (1971).
[21] N.N. Nikolaev and B.G. Zakharov, Z. Phys. C **49**, 607 (1991).
[22] R.P. Feynman and A.R. Gibbs, *Quantum Mechanics and Path Integrals* (McGraw-Hill, New York, 1965).
[23] H1 Collaboration, S. Aid *et al.*, Z. Phys. C **69**, 27 (1995).
[24] ZEUS Collaboration, M. Derrick *et al.*, Phys. Lett. B **293**, 465 (1992).
[25] M.V. Terent'ev, Yad. Fiz. **24**, 207 (1976) [Sov. J. Nucl. Phys. **24**, 106 (1976)].
[26] J. Nemchik, N.N. Nikolaev, E. Predazzi, and B.G. Zakharov, Z. Phys. C **75**, 71 (1997).

[27] I. Halperin and A. Zhitnitsky, Phys. Rev. D **56**, 184 (1997).
[28] H1 Collaboration, C. Adloff *et al.*, Phys. Lett. B **483**, 23 (2000).
[29] H1 Collaboration, C. Adloff *et al.*, Eur. Phys. J. C **10**, 373 (1999).
[30] ZEUS Collaboration, J. Breitweg *et al.*, Eur. Phys. J. C **6**, 603 (1999).
[31] E401 Collaboration, M. Binkley *et al.*, Phys. Rev. Lett. **48**, 73 (1982).
[32] E516 Collaboration, B.H. Denby *et al.*, Phys. Rev. Lett. **52**, 795 (1984).
[33] ZEUS Collaboration, J. Breitweg *et al.*, Z. Phys. C **75**, 215 (1997).
[34] B.Z. Kopeliovich, J. Raufeisen, and A.V. Tarasov, Phys. Lett. B **440**, 151 (1998).
[35] B.Z. Kopeliovich, J. Raufeisen, and A.V. Tarasov, Phys. Rev. C **62**, 035204 (2000).
[36] J. Hüfner, B.Z. Kopeliovich, and A. Zamolodchikov, Z. Phys. A **357**, 113 (1997).
[37] B.Z. Kopeliovich, J. Nemchik, N.N. Nikolaev, and B.G. Zakharov, Phys. Lett. B **324**, 469 (1994).
[38] E665 Collaboration, M.R. Adams *et al.*, Phys. Rev. Lett. **74**, 1525 (1995).
[39] B.Z. Kopeliovich and J. Nemchik, nucl-th/9511018.
[40] NMC Collaboration, M. Arneodo *et al.*, Phys. Lett. B **332**, 195 (1994).

PHYSICAL REVIEW C **76**, 025210 (2007)

Production of polarized vector mesons off nuclei

B. Z. Kopeliovich,[1,2] J. Nemchik,[3] and Ivan Schmidt[1]

[1]*Departamento de Física y Centro de Estudios Subatómicos, Universidad Técnica Federico Santa María, Valparaíso, Chile*

[2]*Joint Institute for Nuclear Research, Dubna, RU-141980 Moscow Region, Russia*

[3]*Institute of Experimental Physics SAS, Watsonova 47, SK-04001 Kosice, Slovakia*

(Received 13 March 2007; published 20 August 2007)

Using the light-cone QCD dipole formalism we investigate manifestations of color transparency (CT) and coherence length (CL) effects in electroproduction of longitudinally (L) and transversally (T) polarized vector mesons. Motivated by forthcoming data from the HERMES experiment we predict both the A and Q^2 dependence of the L/T ratios for ρ^0 mesons produced coherently and incoherently off nuclei. For an incoherent reaction the CT and CL effects add up and result in a monotonic A dependence of the L/T ratio at different values of Q^2. In contrast, for a coherent process the contraction of the CL with Q^2 causes an effect opposite to that of CT and we expect quite a nontrivial A dependence.

DOI: 10.1103/PhysRevC.76.025210 PACS number(s): 13.60.Le, 12.38.−t, 13.85.Lg, 24.85.+p

I. INTRODUCTION

Electroproduction of vector mesons has been intensively studied during the past three decades. Numerous fixed-target experiments have provided high-quality data: the OMEGA [1] and NMC [2] experiments at CERN, CHIO [3] and E665 experiments at Fermilab [4], etc. [5]. In particular, the E665 Collaboration [6] observed for the first time a manifestation of color transparency [7,8] in vector meson production on nuclear targets. The data confirmed the predictions for color transparency presented in Ref. [9].

Moreover, important dynamical information on vector meson electroproduction, in a wide range of Q^2 and energies and for different photon polarizations, transverse (T) and longitudinal (L), was provided by experiments performed by both the ZEUS [10] and H1 [11] Collaborations at HERA. In particular it was found that the longitudinal-to-transverse ratio, R_{LT}, for exclusive electroproduction of ρ^0 mesons, rises with Q^2, but has a weak energy dependence at fixed Q^2 [2,4,12–21]. Some correlation between the energy and Q^2 dependence was detected in the ZEUS experiment [12]. The energy dependence of the ratio R_{LT} is stronger at larger Q^2.

These observations can be understood within the dipole approach [22]. The shrinkage of the $\bar{q}q$ component of the photon with Q^2 and the small-size behavior of the dipole cross section [7], $\sigma_{\bar{q}q}(r) \sim r^2$,[1] lead to a *scanning effect* [9,22,23]. Namely, the vector meson production amplitude is dominated by the contribution of dipole sizes of the order of $r \sim r_S$, where

$$r_S \approx \frac{Y}{\sqrt{Q^2 + m_V^2}}, \tag{1}$$

and the product of the photon wave function and the dipole cross section forms a sharp peak. Varying Q^2 and the mass of vector meson m_V one can study the transition from the nonperturbative region of large r_S to the perturbative region of very small $r_S \ll R_V$, where R_V is the radius of the vector meson.

Factor Y in Eq. (1) was evaluated in [22] at $Y \approx 6$. However, this estimate made use of a nonrelativistic approximation, which is reasonable for charmonium and is rather accurate for bottonium production. Moreover, in the general case the parameter Y depends on polarization and increases slowly with Q^2. The Q^2 dependence of $Y_{T,L}$ is related to so-called aligned-jet configurations of the $\bar{q}q$ configurations when q or $\bar{q}$ carry almost the whole momentum of the photon. Since these end-point configurations in longitudinally polarized photons are suppressed, one should expect $Y_L < Y_T$. In another words, the production amplitude of longitudinal vector mesons scans their wave function at smaller transverse sizes. According to Eq. (1) higher Q^2 results in a smaller transverse size of the color $\bar{q}q$ dipole (i.e., in a smaller r_S). Stronger energy dependence of the dipole cross section $\sigma_{\bar{q}q}(r, s)$ at smaller dipole size causes a weak energy dependence of the ratio R_{LT} (see also Ref. [24]). However, large errors of available data do not allow this energy dependence to be seen clearly.

Equation (1) shows that one can reach small perturbative scanning radius only at very large scale ($Q^2 \gg m_V^2$).

There is much experimental and theoretical evidence [25,26] that a semihard scale of a nonperturbative origin exists in QCD [27]. Namely, the mean transverse distance of gluon propagation is small, of the order of $r_0 \sim 0.3$ fm. To rely on pQCD calculations one should make the scanning radius smaller than r_0, that is,

$$\left(Q^2 + m_V^2\right) \gtrsim Q^2_{\rm pQCD} = \frac{Y^2}{r_0^2}. \tag{2}$$

As was discussed in Refs. [28–30], nuclear targets represent unique analyzers of the dynamics of vector meson production. They allow us to study other phenomena such as color transparency (CT), coherence length (CL) effects, and gluon shadowing (GS). These effects were studied in Ref. [28] for coherent and incoherent electroproduction of vector mesons, and within a quantum-mechanical description of the $\bar{q}q$

[1] $\sigma_{\bar{q}q}(r)$ is the cross section for the interaction with a nucleon of the $\bar{q}q$ fluctuations of the photon having transverse separations $\vec{r}$.

evolution, based on the light-cone (LC) Green function technique [31]. The same LC Green function formalism has been applied also for Drell-Yan production in proton-nucleus and nucleus-nucleus interactions [32], and for nuclear shadowing in deep-inelastic scattering [33,34].

Data for vector meson production off nuclei are usually presented in the form of the so-called nuclear transparency, defined as a ratio

$$Tr_A = \frac{\sigma_{\gamma^* A\to VX}}{A\sigma_{\gamma^* N\to VX}} \tag{3}$$

for the diffractive incoherent (quasielasic) production of vector mesons, $\gamma^* A \to VX$, where one sums over all final states of the target nucleus except those that contain particle (pion) creation.

If electroproduction of a vector meson leaves the target intact, the process $\gamma^* A \to VA$ is usually called coherent or elastic. For this process one can formally define the nuclear transparency in the same way, Eq. (3); however, the coherent production cross section $\sigma^{\rm coh}_{\gamma^* A\to VA}$ has a form different from the incoherent cross section $\sigma^{\rm inc}_{\gamma^* A\to VX}$, as will be seen in Secs. IV and V [see Eqs. (65) and (73)].

There are two time scales that control the dynamics of vector meson production [28]. The first time scale, called formation time, is connected with the phenomenon called color transparency. This effect comes from QCD and has been studied intensively for almost two decades. The second time scale, known as the coherence time, is connected with quantum coherence effects. Both phenomena cause nuclear suppression.

The phenomenon of CT can be treated either in the hadronic or in the quark basis. The former approach leads to Gribov's inelastic corrections [35], whereas the latter manifests itself as a result of color screening [7,8]. Although these two approaches are complementary, the quark-gluon interpretation is more intuitive and straightforward, coming from the fact that colorless hadrons can interact only because color is distributed inside them. If the hadron transverse size r tends to zero then the interaction cross section $\sigma_{\bar qq}(r)$ vanishes as r^2 [7]. As a result, the nuclear medium is more transparent for smaller transverse size hadrons. Besides, this fact naturally explains the correlation between the cross sections of hadrons and their sizes [36–38].

Diffractive electroproduction of vector mesons off nuclei is one of the most effective processes for studying CT. According to Eq. (1), in this case a photon of high virtuality $Q^2 \gg m_V^2$ is expected to produce a pair with a small transverse separation $\sim 1/Q^2$.[2] Then CT manifests itself as a vanishing absorption of the small-size colorless $\bar qq$ wave packet during propagation through the nucleus. The dynamical evolution of this small-size $\bar qq$ pair into a normal-size vector meson is controlled by the time scale called formation time. Because of the uncertainty principle, one needs a time interval to resolve different levels V (the ground state) or V' (the next excited state) in the final state. In the rest frame of the nucleus this formation time is Lorentz dilated,

$$t_f = \frac{2\nu}{m_V'^2 - m_V^2}, \tag{4}$$

where ν is the photon energy. A rigorous quantum-mechanical description of the pair evolution was suggested in Ref. [31] and is based on the nonrelativistic light-cone Green function technique. A complementary description of the same process in the hadronic basis is presented in Ref. [39].

Another phenomenon known to cause nuclear suppression is quantum coherence, which results from the destructive interference of amplitudes for which the interaction takes place on different bound nucleons. It is controlled by the distance from the production to the absorption point when the pointlike photon becomes the hadronlike $\bar qq$ pair and may be also interpreted as the lifetime of $\bar qq$ fluctuation, thus providing the time scale that controls shadowing. Again, it can be estimated by relying on the uncertainty principle and Lorentz time dilation as

$$t_c = \frac{2\nu}{Q^2 + m_V^2}. \tag{5}$$

This is usually called coherence time, but we also will use the term coherence length, since light-cone kinematics is assumed, $l_c = t_c$ (similarly, for formation length $l_f = t_f$). The CL is related to the longitudinal momentum transfer in $\gamma^* N \to VN$ as $q_c = 1/l_c$, which controls the interference of the production amplitudes from different nucleons.

Since the exclusive production of vector mesons at high energies is controlled by small-x_{Bj} physics, gluon shadowing becomes an important issue [28]. In fact, GS suppresses electroproduction of vector mesons. Although it has been shown [40] that for electroproduction of charmonia off nuclei GS starts to be important at center-of-mass energies $\sqrt{(s)} \geqslant$ 30–60 GeV, the same does not happen for electroproduction of light vector mesons [28], where GS starts to be effective at smaller energy values $\sqrt{(s)} \geqslant$ 7–30 GeV. Nevertheless, GS in the HERMES kinematical range discussed in the present paper is negligible and does not need to be included in calculations.

In electroproduction of vector mesons off nuclei one needs to disentangle CT (absorption) and CL (shadowing) as the two sources of nuclear suppression. These effects can be associated with final- and initial-state interactions, respectively. A detailed analysis of the CT and CL effects in electroproduction of vector mesons off nuclei showed [28], for a vector dominance model (VDM) example, that one can easily identify the difference of the nuclear suppression corresponding to absorption and shadowing, in the two limiting cases:

(i) The limit of l_c shorter than the mean internucleon spacing ($\sim$2 fm). In this case only final-state absorption matters. The ratio of the quasielastic (or incoherent) $\gamma^* A \to VX$ and $\gamma^* N \to VX$ cross sections, usually called nuclear

[2] In fact, the situation is somewhat more complicated. For very asymmetric pairs, when the q or $\bar q$ carry almost the whole photon momentum, the pair can have a large separation; see Sec. II.

transparency, reads [31]

$$Tr_A^{\rm inc}\Big|_{l_c\ll R_A} \equiv \frac{\sigma_V^{\gamma^* A}}{A\sigma_V^{\gamma^* N}} = \frac{1}{A}\int d^2b \int_{-\infty}^{\infty} dz\, \rho_A(b,z) \times \exp\left[-\sigma_{\rm in}^{VN}\int_z^{\infty} dz'\, \rho_A(b,z')\right] = \frac{1}{A\sigma_{\rm in}^{VN}}\int d^2b\left\{1-\exp\left[-\sigma_{\rm in}^{VN}T_A(b)\right]\right\} = \frac{\sigma_{\rm in}^{VA}}{A\sigma_{\rm in}^{VN}}. \quad (6)$$

Here z is the longitudinal coordinate and $\vec{b}$ the impact parameter of the production point of vector meson. In Eq. (6) $\rho_A(b,z)$ is the nuclear density and $\sigma_{\rm in}^{VN}$ is the inelastic VN cross section.

(ii) The limit of long l_c, where the expression for the nuclear transparency takes a different form,

$$Tr_A^{\rm inc}\Big|_{l_c\gg R_A} = \int d^2b T_A(b)\exp\left[-\sigma_{\rm in}^{VN}T_A(b)\right], \quad (7)$$

and where we assume $\sigma_{el}^{VN} \ll \sigma_{\rm in}^{VN}$ for the sake of simplicity. Here $T_A(b)$ is the nuclear thickness function

$$T_A(b) = \int_{-\infty}^{\infty} dz\, \rho_A(b,z). \quad (8)$$

The exact expression that interpolates between the two regimes (6) and (7) can be found in Ref. [41].

The problem of CT-CL separation is different depending on the mass of the produced vector meson. In the production of light vector mesons (ρ^0, Φ^0) [28] the coherence length is larger or comparable with the formation length, $l_c \gtrsim l_f$, starting from the photoproduction limit up to $Q^2 \sim 1$–2 GeV^2. For charmonium production, however, there is a strong inequality $l_c < l_f$ independent of Q^2 and ν [29,30], which therefore leads to a different scenario of CT-CL mixing.

Recently, new HERMES data [42,43] for diffractive exclusive electroproduction of ρ^0 mesons on nitrogen target have gradually become available. At the beginning the data were presented as a dependence of nuclear transparencies (3) on coherence length (5). The data for incoherent ρ^0 production decrease with l_c, as expected from the effects of initial-state interactions. In contrast, the nuclear transparency for coherent ρ^0 production increases with coherence length, as expected from the effects of the nuclear form factor [28]. However, each l_c bin of the data contains different values of ν and Q^2 (i.e., there are different contributions from both effects, CT and CL). For this reason the l_c behavior of nuclear transparency does not allow us to study CT and CL effects separately. Therefore it was proposed in Refs. [28,39] that CT can be separately studied, eliminating the effect of CL from the data on the Q^2 dependence of nuclear transparency, in a way that keeps $l_c = $ const. According to this prescription, the HERMES data [43] were later presented as the Q^2 dependence of nuclear transparency, albeit at different fixed values of l_c. Then the rise of $Tr_A^{\rm inc}$ and $Tr_A^{\rm coh}$ with Q^2 represents a signature of CT. The HERMES data [43] are in a good agreement with the predictions from Ref. [28].

New HERMES data on neon and krypton targets should be presented soon and these will allow us to verify further the predictions for CT from Ref. [28]. In addition, gradually increasing the statistics of the HERMES data should allow us to also obtain results at different polarizations L and T, and this offers the interesting possibility of studying the polarization dependence of the CT and CL effects, in both coherent and incoherent production of vector mesons. The data are usually presented as the L/T ratio R_{LT}^A of the corresponding nuclear cross sections. Knowing the nucleon L/T ratio R_{LT} one can define the nuclear modification factor as

$$f(s,Q^2,A) = \frac{R_{LT}^A}{R_{LT}} \quad (9)$$

for both coherent and incoherent processes. The nuclear modification factor represents a modification of the nucleon L/T ratio, given by a nuclear environment. Its deviation from unity allows one to obtain information about a possible different onset of CT and CL effects in the production of L and T vector mesons. Therefore an exploratory study of the Q^2 and A dependence of the factors $f_{\rm inc}$ and $f_{\rm coh}$ gives an alternative way for investigating CT and CL effects in coherent and incoherent production of vector mesons, at different polarizations L and T. This is the main goal of the present paper.

The paper is organized as follows. In Sec. II we present the light-cone approach to diffractive electroproduction of vector mesons in the rest frame of the nucleon target. Here we also describe the individual ingredients contained in the production amplitude: (i) the dipole cross section, (ii) the LC wave function for a quark-antiquark fluctuation of the virtual photon, and (iii) the LC wave function of the vector meson.

In Sec. III we calculate the nucleon L/T ratio R_{LT} of the cross sections for exclusive electroproduction of L and T polarized ρ^0, Φ^0, and charmonia. The model calculations reproduce quite well the available data for the Q^2 dependence of R_{LT}. This is an important test of the model because R_{LT} is included in the calculations of the nuclear L/T ratio.

Section IV is devoted to the incoherent production of vector mesons off nuclei. First, in Sec. IV A we define the different transparency ratios, and in Sec. IV B, we briefly describe the formalism based on the LC Green function technique. In Sec. IV C we analyze different regimes of incoherent production of vector mesons, depending on the magnitude of the coherence length. Then in Sec. IV D we present a discussion on the A and Q^2 behavior of the nuclear L/T ratio in the limit of long coherence length $l_c \gg R_A$, because in this limit the corresponding formulas and theoretical treatment get simplified with respect to the general case $l_c \sim R_A$, where there is a strong CT-CL mixing. Here we also present the model predictions for the nuclear modification factor $f_{\rm inc}$ and nuclear L/T ratio. Finally, we study the general case when there is no restriction on the coherence length. The numerical calculations of Sec. IV E produce the prediction for the L/T ratio of nuclear cross sections, for production of L and T polarized vector mesons, as a function of the mass number A at different fixed values of $\langle Q^2\rangle$ corresponding to

the HERMES kinematics. We find a monotonic A dependence of this ratio. We discuss why this A behavior of $R_{LT}^A(\text{inc})$ only weakly changes with Q^2. Following the prescription of Refs. [28,39] we also investigate how a clear signal of CT effects manifests itself separately in the production of L and T polarized vector mesons. We present the model predictions for the Q^2 dependence of f_{inc} at different fixed values of the coherence length. Such a polarization dependence of CT effects can be analyzed by the HERMES Collaboration and in the experiments at JLab.

Coherent production of vector mesons off nuclei leaving the nucleus intact is studied in Sec. V. The formalism, with an emphasis on the nuclear L/T ratio, is described in Sec. V A. Then, just as for incoherent production, we analyze in Sec. V B the A and Q^2 behavior of the nuclear L/T ratio, in the limit of long coherence length. Here we also present the corresponding model predictions for the nuclear modification factor and the L/T ratio. The general case with no restriction on the coherence length is analyzed in Sec. V C. In contrast to incoherent vector meson production, here we find, at medium and large values of Q^2 (when $l_c \lesssim R_A$, where R_A is the nuclear radius), a nonmonotonic A dependence of the nuclear L/T ratio. This nontrivial and anomalous A dependence of $R_{LT}^A(\text{coh})$ is even more complicated at larger values of Q^2, as a result of a stronger interplay between CT and CL effects. We find also a different manifestation of the net CT effects in the production of L and T polarized vector mesons, by performing the predictions at fixed values of the coherence length.

Gluon shadowing starts to manifest itself at $\sqrt{s} \geqslant$ 7–30 GeV and is not significant in the HERMES energy range studied in the present paper. Therefore it is not included in the calculations.

The results of the paper are summarized and discussed in Sec. VI. The important conclusion of a nontrivial A dependence of the coherent nuclear L/T ratio for the expected new HERMES data and for the future planned experiments is stressed.

II. COLOR DIPOLE PHENOMENOLOGY FOR ELASTIC ELECTROPRODUCTION OF VECTOR MESONS $\gamma^* N \to V N$

The LC dipole approach for elastic electroproduction $\gamma^* N \to V N$ was already used in Ref. [44] to study the exclusive photo- and electroproduction of charmonia, and in Ref. [28] for elastic virtual photoproduction of the light vector mesons ρ^0 and Φ^0 (for a review see also Ref. [45]). Therefore, we present only a short review of this LC phenomenology, with the main emphasis on looking at the effects of the different polarizations L and T. In this approach a diffractive process is treated as elastic scattering of a $\bar{q}q$ fluctuation of the incident particle. The elastic amplitude is given by convolution of the universal flavor-independent dipole cross section for the $\bar{q}q$ interaction with a nucleon, $\sigma_{\bar{q}q}$ [7], and the initial and final wave functions. For the exclusive photo- or electroproduction of vector mesons $\gamma^* N \to V N$ the forward production amplitude is represented in the following form:

$$\begin{aligned}\mathcal{M}_{\gamma^* N \to V N}(s, Q^2) &= \langle V | \sigma_{\bar{q}q}(\vec{r}, s) | \gamma^* \rangle \\ &= \int_0^1 d\alpha \int d^2 r \Psi_V^*(\vec{r}, \alpha) \sigma_{\bar{q}q}(\vec{r}, s) \\ &\quad \times \Psi_{\gamma^*}(\vec{r}, \alpha, Q^2), \end{aligned} \tag{10}$$

with the normalization

$$\left.\frac{d\sigma(\gamma^* N \to V N)}{dt}\right|_{t=0} = \frac{|\mathcal{M}_{\gamma^* N \to V N}(s, Q^2)|^2}{16\pi}. \tag{11}$$

There are three ingredients contributing to the amplitude (10):

(i) the dipole cross section $\sigma_{\bar{q}q}(\vec{r}, s)$, which depends on the $\bar{q}q$ transverse separation $\vec{r}$ and the c.m. energy squared s,
(ii) the LC wave function of the photon $\Psi_{\gamma^*}(\vec{r}, \alpha, Q^2)$, which depends also on the photon virtuality Q^2 and the relative share α of the photon momentum carried by the quark, and
(iii) the LC wave function $\Psi_V(\vec{r}, \alpha)$ of the vector meson.

Notice that in the LC formalism the photon and meson wave functions also contain higher Fock states $|\bar{q}q\rangle$, $|\bar{q}qG\rangle$, $|\bar{q}q2G\rangle$, etc. The effects of higher Fock states are implicitly incorporated into the energy dependence of the dipole cross section $\sigma_{\bar{q}q}(\vec{r}, s)$, as is given in Eq. (10).

A. Dipole cross section

The dipole cross section $\sigma_{\bar{q}q}(\vec{r}, s)$ represents the interaction of a $\bar{q}q$ dipole of transverse separation $\vec{r}$ with a nucleon [7]. It is a flavor-independent universal function of $\vec{r}$ and energy, and allows us to describe in a uniform way various high-energy processes. It is known to vanish quadratically [$\sigma_{\bar{q}q}(r, s) \propto r^2$] as $r \to 0$, owing to color screening (CT property). The dipole cross section cannot be predicted reliably because of poorly known higher order pQCD corrections and nonperturbative effects. A detailed discussion of the dipole cross section in connection with production of vector mesons is presented in Ref. [28].

There are two popular parametrizations of $\sigma_{\bar{q}q}(\vec{r}, s)$. The first, suggested in Ref. [46], reflects the fact that at small separations the dipole cross section should be a function of r and $x_{Bj} \sim 1/(r^2 s)$, to reproduce Bjorken scaling. It describes well data for deep-inelastic scattering (DIS) at small x_{Bj} and medium and high Q^2. However, at small Q^2 it cannot be correct since it predicts energy-independent hadronic cross sections. Besides, x_{Bj} is no longer a proper variable at small Q^2 and should be replaced by energy. This defect is removed by the second parametrization proposed in Ref. [27], which is similar to the first one [46] but contains an explicit dependence on energy, and it is valid down to the limit of real photoproduction. Since we will consider HERMES data with a typical kinematical region of the photon energy, $5 < \nu < 24$ GeV, and virtuality, $0.8 < Q^2 < 5$ GeV^2, we choose the second parametrization, which has the following form:

$$\sigma_{\bar{q}q}(r, s) = \sigma_0(s)\left[1 - e^{-r^2/r_0^2(s)}\right], \tag{12}$$

where

$$\sigma_0(s) = \sigma_{\rm tot}^{\pi p}(s)\left[1 + \frac{3}{8}\frac{r_0^2(s)}{\langle r_{\rm ch}^2\rangle}\right] \text{ mb} \tag{13}$$

and

$$r_0(s) = 0.88\left(\frac{s}{s_0}\right)^{-0.14} \text{ fm}. \tag{14}$$

Here $\langle r_{\rm ch}^2\rangle = 0.44$ fm^2 is the mean pion charge radius squared, and $s_0 = 1000$ GeV^2. The cross section $\sigma_{\rm tot}^{\pi p}(s)$ was fitted to data in Ref. [47,48] and reads

$$\sigma_{\rm tot}^{\pi p}(s) = 23.6\left(\frac{s}{s_0}\right)^{0.079} + 1.425\left(\frac{s}{s_0}\right)^{-0.45} \text{ mb}. \tag{15}$$

This represents the Pomeron and Reggeon parts, corresponding to exchange of gluons and $\bar{q}q$, respectively. A detailed description of the incorporation of Reggeons into the LC dipole formalism can be found in Ref. [28].

The dipole cross section presented in Eqs. (12)–(15) provides the imaginary part of the elastic amplitude. It is known, however, that the energy dependence of the total cross section also generates a real part [49],

$$\sigma_{\bar{q}q}(r,s) \Rightarrow \left(1 - i\frac{\pi}{2}\frac{\partial}{\partial \ln(s)}\right)\sigma_{\bar{q}q}(r,s). \tag{16}$$

Therefore the energy dependence of the dipole cross section given by Eq. (12), which is rather steep at small r, leads to a large real part that should not be neglected.

B. The $\bar{q}q$ wave function of the photon

The perturbative distribution amplitude ("wave function") of the $\bar{q}q$ Fock component of the photon has the following form, for T and L polarized photons [50–52]:

$$\Psi_{\bar{q}q}^{T,L}(\vec{r},\alpha) = \frac{\sqrt{N_C\alpha_{\rm em}}}{2\pi} Z_q \bar{\chi}\hat{O}^{T,L}\chi K_0(\epsilon r), \tag{17}$$

where χ and $\bar{\chi}$ are the spinors of the quark and antiquark, respectively, Z_q is the quark charge, with $Z_q = 1/\sqrt{2}, 1/3\sqrt{2}, 1/3, 2/3$, and $1/3$ for $\rho^0, \omega^0, \Phi^0, J/\Psi$, and Υ production respectively, $N_C = 3$ is the number of colors. and $K_0(\epsilon r)$ is a modified Bessel function with

$$\epsilon^2 = \alpha(1-\alpha)Q^2 + m_q^2. \tag{18}$$

Here m_q is the quark mass, and α is the fraction of the LC momentum of the photon carried by the quark. The operators $\widehat{O}^{T,L}$ are given by

$$\widehat{O}^T = m_q\vec{\sigma}\cdot\vec{e} + i(1-2\alpha)(\vec{\sigma}\cdot\vec{n})(\vec{e}\cdot\vec{\nabla}_r) + (\vec{\sigma}\times\vec{e})\cdot\vec{\nabla}_r, \tag{19}$$

$$\widehat{O}^L = 2Q\alpha(1-\alpha)(\vec{\sigma}\cdot\vec{n}). \tag{20}$$

Here $\vec{\nabla}_r$ acts on the transverse coordinate $\vec{r}$, $\vec{e}$ is the polarization vector of the photon, $\vec{n}$ is a unit vector parallel to the photon momentum, and $\vec{\sigma}$ is the three-vector of the Pauli spin matrices.

The transverse separation of the $\bar{q}q$ pair contains an explicit α dependence and can be written uby sing the expression for the scanning radius, Eq. (1), as

$$r_{\bar{q}q} \sim \frac{1}{\epsilon} = \frac{1}{\sqrt{Q^2\alpha(1-\alpha)+m_q^2}} \sim \frac{r_S}{3} = \frac{\tilde{Y}}{\sqrt{Q^2+m_V^2}}, \tag{21}$$

where $\tilde{Y} = Y/3$. For very asymmetric $\bar{q}q$ pairs the LC variable α or $(1-\alpha) \lesssim m_q^2/Q^2$. Consequently, the transverse separation $r_{\bar{q}q} \sim \tilde{1}/m_q$ and the scanning radius r_S become large. However, this is not the case of charmonium and bottonium production because of the large quark masses $m_c = 1.5$ GeV and $m_b = 5.0$ GeV, respectively. Therefore in this latter case it is straightforward to include nonperturbative interaction effects between q and $\bar{q}$. In the production of light vector mesons there are two ways to fix the problem of a huge $\bar{q}q$ transverse separation. One can introduce an effective quark mass $m_q \approx \Lambda_{\rm QCD}$, which should represent the nonperturbative interaction effects between the q and $\bar{q}$, or one can introduce this interaction explicitly. We use the second possibility, with the corresponding phenomenology based on the LC Green function approach developed in Ref. [27].

The Green function $G_{\bar{q}q}(z_1,\vec{r}_1;z_2,\vec{r}_2)$ describes the propagation of an interacting $\bar{q}q$ pair between points with longitudinal coordinates z_1 and z_2, and with initial and final separations $\vec{r}_1$ and $\vec{r}_2$. This Green function satisfies the two-dimensional Schrödinger equation,

$$i\frac{d}{dz_2}G_{\bar{q}q}(z_1,\vec{r}_1;z_2,\vec{r}_2) = \left\{\frac{\epsilon^2-\Delta_{r_2}}{2\nu\alpha(1-\alpha)} + V_{\bar{q}q}(z_2,\vec{r}_2,\alpha)\right\}G_{\bar{q}q}(z_1,\vec{r}_1;z_2,\vec{r}_2). \tag{22}$$

Here ν is the photon energy, and the Laplacian Δ_r acts on the coordinate r.

The imaginary part of the LC potential $V_{\bar{q}q}(z_2,\vec{r}_2,\alpha)$ in Eq. (22) is responsible for the attenuation of the $\bar{q}q$ in the medium, whereas the real part represents the interaction between the q and $\bar{q}$. This potential is supposed to provide the correct LC wave functions of the vector mesons. For the sake of simplicity we use the oscillator form of the potential,

$$\mathrm{Re}V_{\bar{q}q}(z_2,\vec{r}_2,\alpha) = \frac{a^4(\alpha)\vec{r}_2^2}{2\nu\alpha(1-\alpha)}, \tag{23}$$

which leads to a Gaussian r dependence of the LC wave function of the meson ground state. The shape of the function $a(\alpha)$ will be discussed in the following.

In this case Eq. (22) has an analytical solution, leading to an explicit form of the harmonic oscillator Green function [53],

$$G_{\bar{q}q}(z_1,\vec{r}_1;z_2,\vec{r}_2) = \frac{a^2(\alpha)}{2\pi i\sin(\omega\Delta z)}\exp\left\{\frac{ia^2(\alpha)}{\sin(\omega\Delta z)}\left[\left(r_1^2+r_2^2\right)\cos(\omega\Delta z) - 2\vec{r}_1\cdot\vec{r}_2\right]\right\}\exp\left[-\frac{i\epsilon^2\Delta z}{2\nu\alpha(1-\alpha)}\right], \tag{24}$$

where $\Delta z = z_2 - z_1$ and

$$\omega = \frac{a^2(\alpha)}{\nu\alpha(1-\alpha)}. \tag{25}$$

The boundary condition is $G_{\bar{q}q}(z_1, \vec{r}_1; z_2, \vec{r}_2)|_{z_2=z_1} = \delta^2(\vec{r}_1 - \vec{r}_2)$.

The probability amplitude of finding the $\bar{q}q$ fluctuation of a photon at the point z_2 with separation $\vec{r}$ is given by an integral over the point z_1 where the $\bar{q}q$ is created by the photon with initial separation zero:

$$\Psi^{T,L}_{\bar{q}q}(\vec{r}, \alpha) = \frac{iZ_q\sqrt{\alpha_{\rm em}}}{4\pi\nu\alpha(1-\alpha)} \times \int_{-\infty}^{z_2} dz_1\, (\bar{\chi}\,\widehat{O}^{T,L}\chi) G_{\bar{q}q}(z_1, \vec{r}_1; z_2, \vec{r})\Big|_{r_1=0}. \tag{26}$$

The operators $\widehat{O}^{T,L}$ are defined by Eqs. (19) and (20). Here they act on the coordinate $\vec{r}_1$.

If we write the transverse part as

$$\bar{\chi}\,\widehat{O}^T\chi = \bar{\chi} m_q \vec{\sigma}\cdot\vec{e}\chi + \bar{\chi}[i(1-2\alpha)(\vec{\sigma}\cdot\vec{n})\vec{e} + (\vec{\sigma}\times\vec{e})]\chi\cdot\vec{\nabla}_r = E + \vec{F}\cdot\vec{\nabla}_r, \tag{27}$$

then the distribution functions read

$$\Psi^T_{\bar{q}q}(\vec{r}, \alpha) = Z_q\sqrt{\alpha_{\rm em}}[E\,\Phi_0(\epsilon, r, \lambda) + \vec{F}\cdot\vec{\Phi}_1(\epsilon, r, \lambda)], \tag{28}$$

$$\Psi^L_{\bar{q}q}(\vec{r}, \alpha) = 2Z_q\sqrt{\alpha_{\rm em}}Q\alpha(1-\alpha)\bar{\chi}\vec{\sigma}\cdot\vec{n}\chi\,\Phi_0(\epsilon, r, \lambda), \tag{29}$$

where

$$\lambda = \frac{2a^2(\alpha)}{\epsilon^2}. \tag{30}$$

The functions $\Phi_{0,1}$ in Eqs. (28) and (29) are defined as

$$\Phi_0(\epsilon, r, \lambda) = \frac{1}{4\pi}\int_0^\infty dt\,\frac{\lambda}{{\rm sh}(\lambda t)} \times \exp\left[-\frac{\lambda\epsilon^2 r^2}{4}\,{\rm cth}(\lambda t) - t\right], \tag{31}$$

$$\vec{\Phi}_1(\epsilon, r, \lambda) = \frac{\epsilon^2\vec{r}}{8\pi}\int_0^\infty dt\left[\frac{\lambda}{{\rm sh}(\lambda t)}\right]^2 \times \exp\left[-\frac{\lambda\epsilon^2 r^2}{4}{\rm cth}(\lambda t) - t\right], \tag{32}$$

where ${\rm sh}(x)$ and ${\rm cth}(x)$ are the hyperbolic sine and hyperbolic cotangent, respectively. Note that the $\bar{q}$-q interaction enters Eqs. (28) and (29) via the parameter λ defined in Eq. (30). In the limit of vanishing interaction ($\lambda \to 0$; i.e., $Q^2 \to \infty, \alpha$ fixed, $\alpha \neq 0$ or 1), Eqs. (28) and (29) produce the perturbative expressions of Eq. (17). As previously mentioned, for charmonium and bottonium production nonperturbative interaction effects are weak. Consequently, the parameter λ is then rather small owing to the large quark masses $m_c = 1.5$ GeV and $m_b = 5.0$ GeV, and it is given by

$$\lambda = \frac{8a^2(\alpha)}{Q^2 + 4m^2_{c,b}}. \tag{33}$$

With the choice $a^2(\alpha) \propto \alpha(1-\alpha)$ the end-point behavior of the mean-square interquark separation $\langle r^2\rangle \propto 1/\alpha(1-\alpha)$ contradicts the idea of confinement. Following Ref. [27] we fix this problem via a simple modification of the LC potential,

$$a^2(\alpha) = a_0^2 + 4a_1^2\alpha(1-\alpha). \tag{34}$$

The parameters a_0 and a_1 were adjusted in Ref. [27] to data on total photoabsorption cross section [54,55], diffractive photon dissociation, and shadowing in nuclear photoabsorption reactions. The results of our calculations vary within only 1% when a_0 and a_1 satisfy the relations

$$a_0^2 = v^{1.15}(0.112)^2\ {\rm GeV}^2, \qquad a_1^2 = (1-v)^{1.15}(0.165)^2\ {\rm GeV}^2, \tag{35}$$

where v takes any value in the range $0 < v < 1$. In view of this insensitivity of the observables we fix the parameters at $v = 1/2$. We checked that this choice does not affect our results beyond a few percent uncertainty.

C. Vector meson wave function

The last ingredient in the elastic production amplitude (10) is the vector meson wave function. We use the popular prescription of Ref. [56], obtained by applying a Lorentz boost to the rest-frame wave function, assumed to be Gaussian, which in turn leads to radial parts of transversely and longitudinally polarized mesons in the form (for an alternative description of the vector meson wave function see Refs. [57,58])

$$\Phi^{T,L}_V(\vec{r}, \alpha) = C^{T,L}\alpha(1-\alpha)f(\alpha)\exp\left[-\frac{\alpha(1-\alpha)\vec{r}^2}{2R^2}\right], \tag{36}$$

with the normalization defined in the following, and

$$f(\alpha) = \exp\left[-\frac{m_q^2R^2}{2\alpha(1-\alpha)}\right], \tag{37}$$

with the parameters, taken from Ref. [24], $R = 0.515$ fm, $m_q = 0.1$ GeV for ρ^0 production; $R = 0.415$ fm, $m_q = 0.3$ GeV for Φ^0 production; $R = 0.183$ fm, $m_q = 1.3$ GeV for charmonium production; and $R = 0.061$ fm, $m_q = 5.0$ GeV for bottonium production.

We assume that the distribution amplitude of the $\bar{q}q$ fluctuations for both the vector meson and the photon have a similar structure [24]. Then in analogy to Eqs. (28) and (29),

$$\Psi^T_V(\vec{r}, \alpha) = (E + \vec{F}\cdot\vec{\nabla}_r)\Phi^T_V(\vec{r}, \alpha), \tag{38}$$

$$\Psi^L_V(\vec{r}, \alpha) = 2m_V\alpha(1-\alpha)(\bar{\chi}\vec{\sigma}\cdot\vec{n}\chi)\Phi^L_V(\vec{r}, \alpha). \tag{39}$$

Correspondingly, the normalization conditions for the transverse and longitudinal vector meson wave functions read

$$N_C \int d^2r \int d\alpha \Big[m_q^2 \big|\Phi_V^T(\vec{r},\alpha)\big|^2 + [\alpha^2+(1-\alpha)^2]\big|\partial_r \Phi_V^T(\vec{r},\alpha)\big|^2\Big] = 1 \qquad (40)$$

and

$$4N_C \int d^2r \int d\alpha \alpha^2(1-\alpha)^2 m_V^2 \big|\Phi_V^L(\vec{r},\alpha)\big|^2 = 1. \qquad (41)$$

III. ELECTROPRODUCTION OF VECTOR MESONS ON A NUCLEON: COMPARISON WITH DATA

As the first test of the formalism, in this section we verify the LC approach by comparing its results with data for nucleon targets. Since the expected new HERMES data will be, at separate polarizations L and T, predominantly for electroproduction of ρ^0, we focus our attention on the production of light vector mesons. Using all the ingredients specified in the previous section [i.e., the nonperturbative photon equations (28) and (29) and vector meson wave function equations (38) and (39)], we can calculate the forward production amplitude $\gamma^* N \to VN$ for transverse and longitudinal photons and vector mesons. Under the assumption of s-channel helicity conservation (SCHC), the forward scattering amplitude reads

$$\mathcal{M}^T_{\gamma^* N\to VN}(s,Q^2)\big|_{t=0} = N_C Z_q \sqrt{2\alpha_{\rm em}} \int d^2r \sigma_{\bar{q}q}(\vec{r},s) \times \int_0^1 d\alpha \Big\{ m_q^2 \Phi_0(\epsilon,\vec{r},\lambda)\Phi_V^T(\vec{r},\alpha) - [\alpha^2+(1-\alpha)^2]\vec{\Phi}_1(\epsilon,\vec{r},\lambda) \times \vec{\nabla}_r \Phi_V^T(\vec{r},\alpha)\Big\}, \qquad (42)$$

$$\mathcal{M}^L_{\gamma^* N\to VN}(s,Q^2)\big|_{t=0} = 4N_C Z_q \sqrt{2\alpha_{\rm em}} m_V Q \int d^2r \sigma_{\bar{q}q}(\vec{r},s) \times \int_0^1 d\alpha \alpha^2(1-\alpha)^2 \times \Phi_0(\epsilon,\vec{r},\lambda)\Phi_V^L(\vec{r},\alpha). \qquad (43)$$

These amplitudes are normalized as $|\mathcal{M}^{T,L}|^2 = 16\pi d\sigma_N^{T,L}/dt|_{t=0}$, and their real parts are included according to the prescription described in Sec. II. The terms $\propto \Phi_0(\epsilon,\vec{r},\lambda)\Phi_V(\vec{r},\alpha)$ and $\propto \vec{\Phi}_1(\epsilon,\vec{r},\lambda)\cdot\vec{\nabla}_r\Phi_V(\vec{r},\alpha)$ in Eqs. (42) and (43) correspond to the helicity-conserving and helicity-flip transitions in the $\gamma^* \to \bar{q}q$, $V \to \bar{q}q$ vertices, respectively. The helicity-flip transitions represent the relativistic corrections. For heavy quarkonium these corrections become important only at large $Q^2 \gg m_V^2$. For production of light vector mesons, however, they are non-negligible even in the photoproduction limit, $Q^2 = 0$.

Usually the data are presented in the form of the production cross section $\sigma = \sigma^T + \epsilon'\sigma^L$, at fixed photon polarization ϵ'. Here the cross section integrated over t reads

$$\sigma^{T,L}(\gamma^* N \to VN) = \frac{|\mathcal{M}^{T,L}|^2}{16\pi B_{\gamma^* N}}, \qquad (44)$$

where $B_{\gamma^* N} \equiv B$ is the slope parameter in the reaction $\gamma^* p \to Vp$. The absolute value of the production cross section has already been checked by comparing with data for elastic ρ^0 and Φ^0 electroproduction in Ref. [28] and for charmonium exclusive electroproduction $\gamma^* p \to J/\Psi p$ in Refs. [29,30].

Motivated by the expected data from the HERMES Collaboration, we are going to make predictions for the production cross sections $\sigma^{L,T}(\gamma^* N \to VN)$ at separate polarizations L and T. However, the data are usually presented as the ratio $R_{LT} = \sigma_L(\gamma^* N \to VN)/\sigma_T(\gamma^* N \to VN)$ at different photon virtualities Q^2. Then a deviation of R_{LT} from unity indicates a difference in the production mechanisms of L and T polarized vector mesons. To calculate the ratio R_{LT}, using Eqs. (42) and (43) for forward production amplitudes at different polarizations L and T, one should know corresponding slope parameters $B_{\gamma_L^* N} \equiv B_L$ and $B_{\gamma_T^* N} \equiv B_T$:

$$R_{LT} = \frac{|\mathcal{M}^L|^2}{|\mathcal{M}^T|^2}\frac{B_T}{B_L} \approx \frac{|\mathcal{M}^L|^2}{|\mathcal{M}^T|^2}\left(1+\frac{\Delta B_{TL}}{B}\right), \qquad (45)$$

where $\Delta B_{TL} = B_T - B_L$.

The scanning phenomenon, Eq. (1), was already discussed in Refs. [22,24,59], and it can be understood qualitatively by analyzing the forward production amplitude (10). Here we assume for simplicity the perturbative distribution amplitudes of the $\bar{q}q$ Fock component of the photon containing the Bessel function $K_0(\epsilon r)$ [see Eq. (17)]. As was mentioned in the previous section, the most important property of the dipole cross section $\sigma_{\bar{q}q}(\vec{r},s)$ is the CT-driven dependence $\propto r^2$ at small r. Because of the smooth shape of the vector meson wave functions $\Phi_V^{L,T}(r,\alpha)$ [see Eq. (36)] and because of the behavior of the Bessel functions $K_{0,1}(x) \propto \exp(-x)$ at large values of x, the production amplitude is dominated by the contribution from $r_S \approx 3/\epsilon$. In the nonrelativistic approximation of $m_V \sim 2m_q$ and $\alpha \sim 0.5$, it leads to the scanning radius [Eq. (1)] and the estimate $Y \approx 6$ (see also Fig. 1). In general, to be more precise, the scanning property [see Eq. (1)] is quantified separately for L and T polarizations via the Q^2-dependent scale parameters Y_L and Y_T, as illustrated in Fig. 1. The dotted line represents the fact that for electroproduction of bottonia both scale parameters $Y_T \sim Y_L \sim 6$, and they practically do not depend on Q^2 as a consequence of the nonrelativistic approximation. Dashed lines describe the Q^2 dependence of Y_L and Y_T for charmonium electroproduction. One can see that both Y_L and Y_T smoothly rise with Q^2, do not differ much from each other, and are a little bit higher than the value 6 resulting from the nonrelativistic approximation. For this reason charmonium can be safely treated as a nonrelativistic object at small and medium values of Q^2 such that $r_S \gtrsim R_{J/\Psi}$.[3] At larger $Q^2 \gg m_{J/\Psi}^2$, the scale parameters $Y_{L,T}$ have a stronger Q^2 dependence, reaching $\sim$7.7 at $Q^2 = 100$ GeV^2, which differs from the nonrelativistic value $Y \sim 6$. This means that relativistic effects are no longer negligible and should be included in the calculations [59]. However, the situation is completely different for light vector meson production, as illustrated in Fig. 1 by the solid lines. In this case, the presence

[3] $R_{J/\Psi}$ is the radius of charmonium.

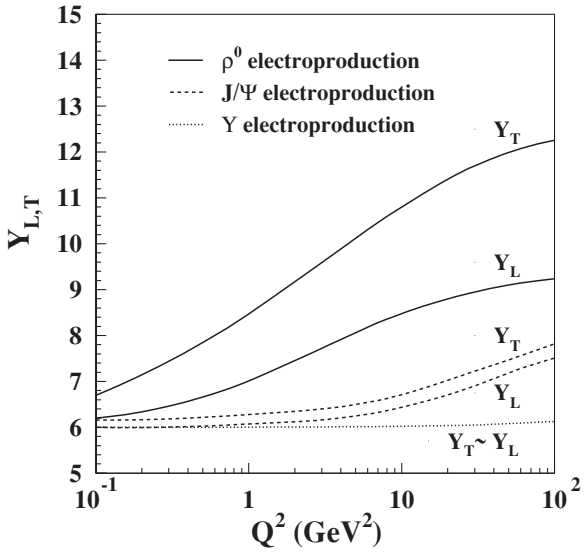

FIG. 1. Q^2 dependence of the scale parameters Y_L and Y_T, from the expression for the scanning radius [Eq. (1)], corresponding to the production of L and T polarized vector mesons. Solid, dashed, and dotted lines represent electroproduction of ρ^0, J/Ψ, and Υ, respectively.

of strong relativistic effects causes the scale parameters to rise with Q^2 much more rapidly than for the production of heavy vector mesons.

Compared to $\mathcal{M}_L$ [Eq. (42)] the transverse production amplitude $\mathcal{M}_T$ [Eq. (43)] receives larger contributions from large-size asymmetric end-point $\bar{q}q$ fluctuations with $\alpha(1-\alpha) \ll 1$. This is illustrated in Fig. 1, where $Y_T > Y_L$ in the whole Q^2 range, and the difference between Y_T and Y_L rises with Q^2. This fact is especially evident for the electroproduction of ρ^0 mesons, depicted by the solid lines. For electroproduction of charmonia the difference between Y_T and Y_L is small as a consequence of small relativistic effects, whereas for electroproduction of bottonia it was already indicated in Ref. [59] that $Y_T \sim Y_L \sim 6$ in a very broad Q^2 range, which supports the conclusion that the relativistic corrections are negligible.

At small $r_S \lesssim R_V$, the production amplitudes (42) and (43) can be evaluated as

$$\mathcal{M}_T \propto r_S^2 \sigma_{\bar{q}q}(r_S, s) \propto \frac{Y_T^4}{\left(Q^2 + m_V^2\right)^2}, \tag{46}$$

$$\mathcal{M}_L \propto \frac{\sqrt{Q^2}}{m_V} r_S^2 \sigma_{\bar{q}q}(r_S, s) \propto \frac{\sqrt{Q^2}}{m_V} \frac{Y_L^4}{\left(Q^2 + m_V^2\right)^2} \propto \frac{\sqrt{Q^2}}{m_V} \frac{Y_L^4}{Y_T^4} \mathcal{M}_T, \tag{47}$$

which means that the longitudinally polarized vector mesons dominate at $Q^2 \gg m_V^2$.

A detailed analysis of the diffraction cone [59,60] for exclusive vector meson electroproduction, within the color dipole generalized Balitskij-Fadin-Kuraev-Lipatov (BFKL) phenomenology, showed the presence of geometrical contributions from the target nucleon $\sim B_N$ and the beam dipole $\sim r^2$. At fixed energy and according to the scanning phenomenon [Eq. (1)], the diffraction slope is predicted to decrease with $(Q^2 + m_V^2)$ as

$$B(Q^2) \sim B_N + \tilde{C} r_S^2 \approx B_N + \text{const} \frac{Y^2}{Q^2 + m_V^2}. \tag{48}$$

One can see from Eq. (48) that different scanning properties for L and T polarized vector mesons ($Y_L < Y_T$; see Fig. 1 and subsequent discussion) lead also to an inequality $B_L < B_T$ of the slope parameters in the reactions $\gamma_L^* N \to V_L N$ and $\gamma_T^* N \to V_T N$. Consequently, the difference ΔB_{TL} in Eq. (45) is positive and can be estimated as

$$\Delta B_{TL} \propto \frac{\Delta Y_{TL}^2}{Q^2 + m_V^2}, \tag{49}$$

where

$$\Delta Y_{TL}^2 = Y_T^2 - Y_L^2. \tag{50}$$

For electroproduction of ρ^0 mesons at small $Q^2 \lesssim m_\rho^2$ the rise of ΔY_{TL}^2 with Q^2 can compensate or even overcompensate the decrease of ΔB_{TL} with $(Q^2 + m_\rho^2)$. Consequently, the difference ΔB_{TL} in Eq. (49) can weakly rise with Q^2. This does not happen at larger $Q^2 > m_\rho^2$, when ΔB_{TL} decreases slowly with Q^2. In the HERMES kinematical range $\Delta B_{TL} \sim 0.7\,\text{GeV}^{-2}$ at $Q^2 = 0.7\,\text{GeV}^2$, reaching a value of $\sim 0.4\,\text{GeV}^{-2}$ at $Q^2 = 5\ \text{GeV}^2$. Correspondingly, the factor $\Delta B_{TL}/B$ in Eq. (45), treated as a correction to unity in the brackets, is about 0.09 at $Q^2 = 0.7\ \text{GeV}^2$ and decreases very slowly with Q^2, reaching a value of ~ 0.07 at $Q^2 = 5\,\text{GeV}^2$. For this reason the factor $\Delta B_{TL}/B$ cannot be neglected in the calculations.

Using Eqs. (45) and (47) one can present the nucleon L/T ratio as

$$R_{LT} \propto \frac{Q^2}{m_V^2} \frac{Y_L^8}{Y_T^8} \frac{B_T}{B_L} \approx \frac{Q^2}{m_V^2} F_Y(Q^2) \left(1 + \frac{\Delta B_{TL}}{B}\right), \tag{51}$$

and thus R_{LT} is given mainly by three ingredients:

(i) The factor Q^2/m_V^2, which comes from σ_L [see Eq. (43)], represents a generic consequence of electromagnetic gauge invariance.

(ii) The Q^2-dependent factor $F_Y(Q^2) = Y_L^8/Y_T^8$, which comes from the scanning phenomenon [Eq. (1)], reflects the different relativistic corrections for the L and T production amplitudes. These corrections become important only at large $Q^2 \gg m_V^2$ (see Fig. 1). The factor F_Y leads to a substantial reduction of the rise of R_{LT} with Q^2, especially for the production of light vector mesons.

(iii) The factor B_T/B_L follows from the fact that the slope parameters B_L and B_T for the production of L and T polarized vector mesons are different. According to the scanning property ($B_L < B_T$), this factor decreases slightly with Q^2, tending to unity from above at large $Q^2 \gg m_V^2$ [59]. The ratio B_T/B_L leads to an additional but small reduction of the Q^2 rise of R_{LT}.

Our predictions are plotted in Figs. 2 and 3, together with the data on the Q^2 dependence of the ratio R_{LT} for the production of ρ^0 and Φ^0 mesons, taken from Ref. [21]. We added also the

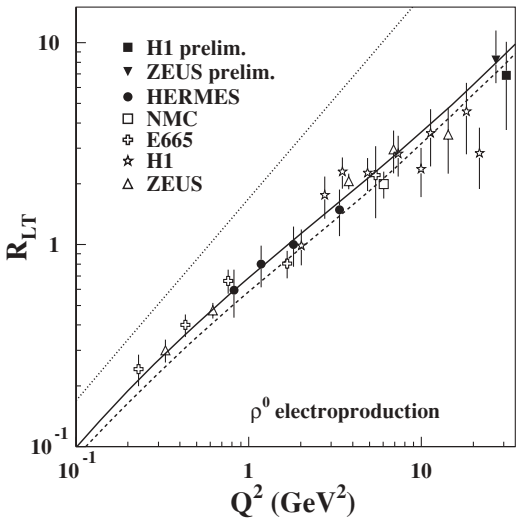

FIG. 2. Q^2 dependence of the ratio R_{LT} of the integrated cross sections for the reactions $\gamma_L^* p \to \rho_L^0 p$ and $\gamma_T^* p \to \rho_T^0 p$. The solid and dashed lines represent model calculations at $W = 15$ and 90 GeV, respectively. The data are taken from Ref. [21]. The preliminary H1 and ZEUS data can be found in Refs. [18] and [14], respectively. The dotted curve represents the Q^2/m_V^2 rise of R_{LT}.

last published data from H1 [16] and preliminary data from the H1 [18] and ZEUS [14,15] Collaborations. The analogous Q^2 dependence of R_{LT} for electroproduction of charmonia is plotted in Fig. 4 together with results from the H1 [61] and ZEUS [62] Collaborations.

One can see from Eq. (51) that the Q^2 rise of the nucleon ratio R_{LT} gets diminished by the factor F_Y, coming from the different scanning properties of the L and T production amplitudes, and by the ratio of the slope parameters B_T

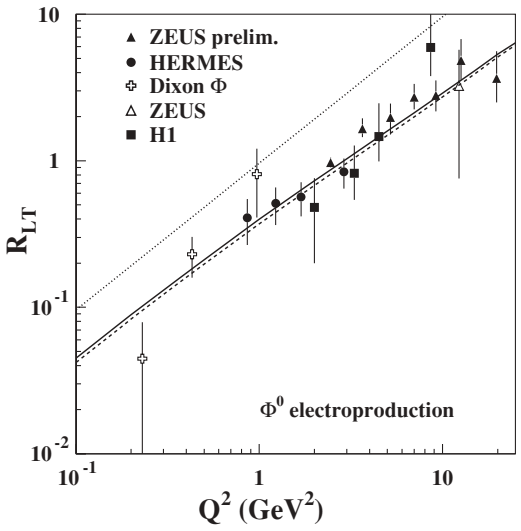

FIG. 3. Q^2 dependence of the ratio R_{LT} of the integrated cross sections for the reactions $\gamma_L^* p \to \Phi_L^0 p$ and $\gamma_T^* p \to \Phi_T^0 p$. The solid and dashed lines represent model calculations at $W = 15$ and 90 GeV, respectively. The data are taken from Ref. [21] and H1 data are from Ref. [16]. The preliminary ZEUS data can be found in Ref. [15]. The dotted curve represents the Q^2/m_V^2 rise of R_{LT}.

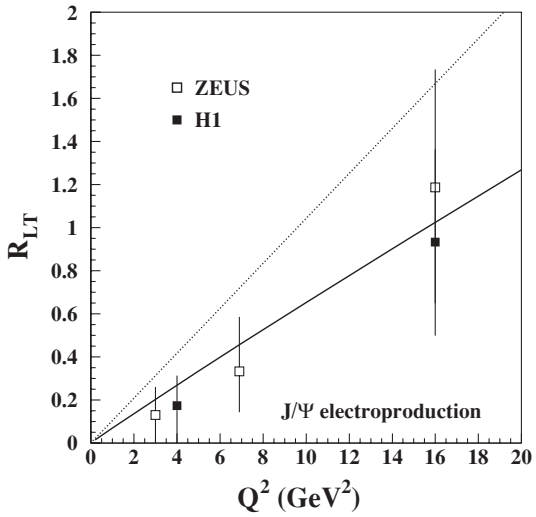

FIG. 4. Q^2 dependence of the ratio R_{LT} of the integrated cross sections for the reactions $\gamma_L^* p \to (J/\Psi)_L p$ and $\gamma_T^* p \to (J/\Psi)_T p$. The model calculations are performed at $W = 90$ GeV. The H1 and ZEUS data are taken from Refs. [61] and [62], respectively. The dotted curve represents the Q^2/m_V^2 rise of R_{LT}.

and B_L. In the nonrelativistic approximation, represented by the electroproduction of bottonia, the factor $F_Y \sim 1$ [see Eq. (51) and Fig. 1] and $B_T \sim B_L$. Consequently, the ratio R_{LT} rises with Q^2 as $\sim Q^2/m_V^2$ [59]. However, electroproduction of light vector mesons has large relativistic effects and the different scanning properties for the L and T production amplitudes ($Y_L < Y_T$) lead to a large decrease of the dominance of the longitudinal cross section $\propto |\mathcal{M}_L|^2$. Thus the ratio R_{LT} rises with Q^2 much less rapidly than Q^2/m_V^2. This is illustrated in Figs. 2 and 3 as a difference between the solid (dashed) and dotted lines. For charmonium production the decrease of the rise of the ratio R_{LT} with $Q^2/m_{J/\Psi}^2$ is much less effective because of smaller relativistic effects, as one can see in Fig. 4 as a difference between the solid and dotted lines. Notice that in all calculations we assumed SCHC as the consequence of the spin independence of the dipole cross section $\sigma_{\bar{q}q}(r, s)$ in the forward production amplitude [Eq. (10)]. This assumption is supported by the low-energy data, indicating that the amplitude for the photon-vector meson transition is predominantly s-channel conserving (i.e., the helicity of the vector meson is equal to that of the photon when the spin-quantization axis is chosen along the direction of the meson momentum in the $\gamma^* p$ center-of-mass system). In general, however, small helicity-single-flip and helicity-double-flip contributions to the production amplitude have been reported in $\pi^+\pi^-$ photoproduction in the ρ^0 mass region, at $W \lesssim 4$ GeV [63]. Helicity-single-flip amplitudes have also been observed in ρ^0 electroproduction for $1.3 < W < 2.8$ GeV and $0.3 < Q^2 < 1.4$ GeV^2 [64]. A helicity-single-flip contribution of $(14 \pm 8)\%$ was measured in ρ^0 muo production at $W = 17$ GeV [3].

At high energy the breaking of SCHC has been measured by the ZEUS [65] and H1 [17] Collaborations at HERA. The size of the SCHC-breaking effects was quantified by evaluating the ratios of the helicity-single-flip and helicity-double-flip

amplitudes to the helicity-conserving amplitudes. The ratio of T_{01} (for production of L polarized ρ^0 mesons from T photons) to the helicity-conserving amplitudes,

$$\tau_{01} = \frac{|T_{01}|}{\sqrt{|T_{00}|^2 + |T_{11}|^2}}, \tag{52}$$

gives the values $\tau_{01} = (6.9 \pm 2.7)\%$ for $0.25 < Q^2 < 0.85$ GeV^2 and $\tau_{01} = (7.9 \pm 2.6)\%$ for $3 < Q^2 < 30$ GeV^2, determined by the ZEUS Collaboration [65]. The H1 result for this quantity is $(8 \pm 3)\%$ [17]. The ratio of helicity-double-flip amplitudes to the helicity-conserving amplitudes τ_{1-1}, defined analogously as τ_{01} in Eq. (52), gives the values $\tau_{1-1} = (4.8 \pm 2.8)\%$ for $0.25 < Q^2 < 0.85$ GeV^2 and $\tau_{1-1} = (1.4 \pm 6.5)\%$ for $3 < Q^2 < 30$ GeV^2 [65]. In addition, the ZEUS Collaboration [65] also determined the nucleon L/T ratio for ρ^0 electroproduction, without assuming SCHC. Those results differ from those derived from the SCHC hypothesis by less than 3%. Similarly, the last data from the HERMES Collaboration [21] on electroproduction of ρ^0 and Φ^0 mesons at $4 < W < 6$ GeV and $0.7 < Q^2 < 5$ GeV^2 confirm the breaking of SCHC and are consistent with the H1 [17] and ZEUS [65] results. The observed deviation from SCHC changes the ratio R_{LT} by only a few percent. Because in the present paper we will focus predominantly on theoretical predictions for the ratio of the L and T production cross sections on nucleon and nuclear targets we can safely assume SCHC.

The second test of our approach is the description of the energy dependence of the production amplitudes [Eqs. (42) and (43)], which is given by the energy-dependent dipole cross section. As we mentioned in the previous section $\sigma_{\bar{q}q}(r, s)$ has a stronger energy dependence at smaller dipole sizes. According to the scanning phenomenon, the dipole cross section is scanned at smaller transverse size in the L than in the T production amplitude. Consequently, the L production amplitude has a stronger energy dependence and so we expect a weak energy dependence of the ratio R_{LT}. Model predictions at $W = 15$ and 90 GeV are depicted in Figs. 2 and 3 by the dashed and solid lines. One can see that the data error bars are too large to see such a weak energy dependence.

IV. INCOHERENT PRODUCTION OF VECTOR MESONS OFF NUCLEI

A. Introduction

In diffractive incoherent (quasielastic) production of vector mesons off nuclei, $\gamma^* A \to VX$, one sums over all final states of the target nucleus, except those that contain particle (pion) creation. The observable that is usually studied experimentally is the nuclear transparency, defined as

$$Tr_A^{\rm inc} = \frac{\sigma^{\rm inc}_{\gamma^* A \to VX}}{A\sigma_{\gamma^* N \to VN}}. \tag{53}$$

The t slope of the differential quasielastic cross section is the same as on a nucleon target. Therefore, instead of integrated cross sections one can also use the forward differential cross sections given in Eq. (11) to write

$$Tr_A^{\rm inc} = \frac{1}{A}\left|\frac{\mathcal{M}_{\gamma^* A \to VX}(s, Q^2)}{\mathcal{M}_{\gamma^* N \to VN}(s, Q^2)}\right|^2. \tag{54}$$

We consider also the production of either longitudinal or transverse polarized vector mesons on nucleon and nuclear targets, and then one can define nuclear transparency separately for incoherent production of L and T vector mesons as

$$Tr_A^{\rm inc}(L) = \frac{1}{A}\left|\frac{\mathcal{M}_{\gamma_L^* A \to V_L X}(s, Q^2)}{\mathcal{M}_{\gamma_L^* N \to V_L N}(s, Q^2)}\right|^2 \tag{55}$$

and

$$Tr_A^{\rm inc}(T) = \frac{1}{A}\left|\frac{\mathcal{M}_{\gamma_T^* A \to V_T X}(s, Q^2)}{\mathcal{M}_{\gamma_T^* N \to V_T N}(s, Q^2)}\right|^2. \tag{56}$$

However, to study the ratio of L and T polarized vector meson production on nuclear targets using forward differential cross sections we should also include the difference between the L and T slope parameters, as was done in the previous section [see Eq. (45)]:

$$\begin{aligned} R_{LT}^A({\rm inc}) &= \frac{\sigma^{\rm inc}_{\gamma_L^* A \to V_L X}}{\sigma^{\rm inc}_{\gamma_T^* A \to V_T X}} = \left|\frac{\mathcal{M}_{\gamma_L^* A \to V_L X}(s, Q^2)}{\mathcal{M}_{\gamma_T^* A \to V_T X}(s, Q^2)}\right|^2 \frac{B_T}{B_L} \\ &= R_{LT}\frac{Tr_A^{\rm inc}(L)}{Tr_A^{\rm inc}(T)} = R_{LT} f_{\rm inc}(s, Q^2, A), \end{aligned} \tag{57}$$

where the nuclear transparencies $Tr_A^{\rm inc}(L)$ and $Tr_A^{\rm inc}(T)$ for L and T polarized vector mesons are given by Eqs. (55) and (56), respectively. The variable $f_{\rm inc}$ in Eq. (57) represents the nuclear modification factor already introduced by Eq. (9).

B. The LC Green function formalism

The nuclear forward production amplitude $\mathcal{M}_{\gamma^* A \to VX}(s, Q^2)$ was calculated by using the LC Green function approach in Ref. [28]. In this approach the physical photon $|\gamma^*\rangle$ is decomposed into different Fock states, namely, the bare photon $|\gamma^*\rangle_0$ plus $|\bar{q}q\rangle$, $|\bar{q}qG\rangle$, etc. As we mentioned earlier the higher Fock states containing gluons describe the energy dependence of the photoproduction reaction on a nucleon. In addition, these Fock components also lead to gluon shadowing as far as nuclear effects are concerned. However, these fluctuations are heavier and have a shorter coherence time (lifetime) than the lowest $|\bar{q}q\rangle$ state, and therefore at medium energies only the $|\bar{q}q\rangle$ fluctuations of the photon matter. Consequently, gluon shadowing, related to the higher Fock states, will dominate at high energies. A detailed description and calculation of gluon shadowing for the case of vector meson production off nuclei is presented in Refs. [28,40]. In the HERMES kinematical range studied in the present paper gluon shadowing is negligible and therefore is not included in the calculations.

The propagation of an interacting $\bar{q}q$ pair in a nuclear medium is described by the Green function satisfying the evolution equation (22). However, the potential in this case acquires an imaginary part, which represents absorption in the

medium [see Eq. (6) for notation],

$$\mathrm{Im}V_{\bar{q}q}(z_2,\vec{r},\alpha) = -\frac{\sigma_{\bar{q}q}(\vec{r},s)}{2}\rho_A(b,z_2). \quad (58)$$

The evolution equation (22), with the potential $V_{\bar{q}q}(z_2,\vec{r}_2,\alpha)$ containing this imaginary part, was used in Refs. [33,34]. In particular, nuclear shadowing in deep-inelastic scattering was calculated, in good agreement with data.

Analytical solutions of Eq. (22) are only known for the harmonic oscillator potential $V(r) \propto r^2$. Furthermore, to keep the calculations reasonably simple we use the dipole approximation

$$\sigma_{\bar{q}q}(r,s) = C(s)r^2, \quad (59)$$

which allows us to obtain the Green function in an analytical form [see Eq. (24)].

The energy-dependent factor $C(s)$ was adjusted by demanding that the calculations employing the approximation of Eq. (59) reproduce correctly the results based on the realistic cross section [Eq. (12)], in the limit $l_c \gg R_A$ (the so-called frozen approximation), when the Green function takes the simple form

$$G_{\bar{q}q}(z_1,\vec{r}_1;z_2,\vec{r}_2) \Rightarrow \delta(\vec{r}_1-\vec{r}_2)\exp\left[-\frac{1}{2}\sigma_{\bar{q}q}(r_1)\int_{z_1}^{z_2} dz\,\rho_A(b,z)\right], \quad (60)$$

where the dependence of the Green function on impact parameter has been dropped. A detailed description of the determination of the factors $C(s)$, separately for coherent and incoherent vector meson production, is presented in Ref. [28].

With the potential given by Eqs. (58) and (59), the solution of Eq. (22) has the same form as Eq. (24), except that one should replace ω with Ω, where

$$\Omega = \frac{\sqrt{a^4(\alpha) - i\rho_A(b,z)\nu\alpha(1-\alpha)C(s)}}{\nu\alpha(1-\alpha)}. \quad (61)$$

The evolution equation (22), with the potential $V_{\bar{q}q}(z_2, \vec{r}_2,\alpha)$ containing the imaginary part [Eq. (58)], and with the realistic dipole cross section [Eq. (12)], was recently solved numerically for the first time in Ref. [66]. There it was shown that the nuclear shadowing in deep-inelastic scattering depends on the form of the dipole cross section $\sigma_{\bar{q}q}$. However, the approximation (59) gives a nuclear shadowing that is very close to realistic numerical calculations using the parametrization of Eq. (12), in the HERMES kinematical range under consideration in the present paper. For this reason we can safely use the dipole approximation (59) for the calculation of vector meson production.

C. Different regimes for incoherent production of vector mesons

As we discussed in Ref. [28], the value of l_c can distinguish different regimes of vector meson production.

(i) When the CL is much shorter than the mean nucleon spacing in a nucleus ($l_c \to 0$), $G(z_2,\vec{r}_2;z_1,\vec{r}_1) \to \delta(z_2-z_1)$. Correspondingly, the formation time of the meson wave function is very short, and it is given by Eq. (4). For light vector mesons $l_f \sim l_c$, and since the formation and coherence lengths are proportional to the photon energy, both must be short. Consequently, nuclear transparency is given by the simple formula [Eq. (6)] corresponding to the Glauber approximation.

(ii) In the production of charmonia and other heavy flavors, the intermediate case $l_c \to 0$, but $l_f \sim R_A$, can be realized. Then the formation of the meson wave function is described by the Green function, and the numerator of the nuclear transparency ratio, Eq. (54), has the form [31]

$$|\mathcal{M}_{\gamma^*A\to VX}(s,Q^2)|^2_{l_c\to 0;l_f\sim R_A} = \int d^2b\int_{-\infty}^{\infty} dz\,\rho_A(b,z)|F_1(b,z)|^2, \quad (62)$$

where

$$F_1(b,z) = \int_0^1 d\alpha\int d^2r_1 d^2r_2\Psi_V^*(\vec{r}_2,\alpha) \times G(z',\vec{r}_2;z,\vec{r}_1)\sigma_{\bar{q}q}(r_1,s)\Psi_{\gamma^*}(\vec{r}_1,\alpha)|_{z'\to\infty}. \quad (63)$$

(iii) In the high-energy limit ($l_c \gg R_A$; in fact, it is more correct to compare with the mean free path of the $\bar{q}q$ in a nuclear medium if the latter is shorter than the nuclear radius), $G(z_2,\vec{r}_2;z_1,\vec{r}_1) \to \delta(\vec{r}_2-\vec{r}_1)$ (i.e., all fluctuations of the transverse $\bar{q}q$ separation are "frozen" by Lorentz time dilation). Then, the numerator on the right-hand side (r.h.s.) of Eq. (54) takes the form [31]

$$|\mathcal{M}_{\gamma^*A\to VX}(s,Q^2)|^2_{l_c\gg R_A} = \int d^2bT_A(b) \times \left|\int d^2r\int_0^1 d\alpha\Psi_V^*(\vec{r},\alpha)\sigma_{\bar{q}q}(r,s) \times \exp\left[-\frac{1}{2}\sigma_{\bar{q}q}(r,s)T_A(b)\right]\Psi_{\gamma^*}(\vec{r},\alpha,Q^2)\right|^2. \quad (64)$$

In this case the $\bar{q}q$ pair attenuates with a constant absorption cross section, as in the Glauber model, except that the whole exponential is averaged rather than just the cross section in the exponent. The difference between the results of the two prescriptions are the well-known inelastic corrections of Gribov [7].

(iv) In the general case when there are no restrictions for either l_c or l_f, the corresponding theoretical tool has been developed for the first time only recently in Ref. [28] and has been applied to electroproduction of light vector mesons at medium and high energies. The same approach was used later for the study of virtual photoproduction of heavy vector mesons [29,30]. Even within the VDM the Glauber model expression interpolating between the limiting cases of low [(i) and (ii)] and high [(iii)] energies has also been derived only recently [41]. In this general case the incoherent nuclear production amplitude squared is represented as a sum of two terms [67],

$$|\mathcal{M}_{\gamma^*A\to VX}(s,Q^2)|^2 = \int d^2b\int_{-\infty}^{\infty} dz\,\rho_A(b,z) \times |F_1(b,z)-F_2(b,z)|^2. \quad (65)$$

The first term, $F_1(b,z)$, introduced in Eq. (63), corresponds to the short l_c limit (ii). The second term, $F_2(b,z)$, in Eq. (65) corresponds to the situation when the incident photon produces

a $\bar{q}q$ pair diffractively and coherently at the point z_1, prior to incoherent quasielastic scattering at point z. The LC Green functions describe the evolution of the $\bar{q}q$ over the distance from z_1 to z and further on, up to the formation of the meson wave function. Correspondingly, this term has the form

$$F_2(b,z) = \frac{1}{2}\int_{-\infty}^{z} dz_1\, \rho_A(b,z_1)\int_0^1 d\alpha \int d^2r_1 d^2r_2 d^2r \times \Psi_V^*(\vec{r}_2,\alpha)G(z'\to\infty,\vec{r}_2;z,\vec{r})\sigma_{\bar{q}q}(\vec{r},s) \times G(z,\vec{r};z_1,\vec{r}_1)\sigma_{\bar{q}q}(\vec{r}_1,s)\Psi_{\gamma^*}(\vec{r}_1,\alpha). \quad (66)$$

Equation (65) correctly reproduces the limits (i)–(iii). At $l_c \to 0$ the second term, $F_2(b,z)$, vanishes because of strong oscillations, and Eq. (65) reproduces the Glauber expression [Eq. (6)]. At $l_c \gg R_A$ the phase shift in the Green functions can be neglected and they acquire the simple form $G(z_2,\vec{r}_2;z_1,\vec{r}_1)\to\delta(\vec{r}_2-\vec{r}_1)$. In this case the integration over longitudinal coordinates in Eqs. (63) and (66) can be performed explicitly, and the asymptotic expression [Eq. (64)] is recovered as well.

D. The nuclear ratio R_{LT}^A(inc) in the limit of long coherence length ($l_c \gg R_A$)

One can see from Eqs. (9) and (57) that the nuclear ratio R_{LT}^A(inc) differs from the nucleon ratio R_{LT} by the nuclear modification factor for the incoherent process $f_{\rm inc}(s,Q^2,A)$, given also as the ratio $Tr_A^{\rm inc}(L)/Tr_A^{\rm inc}(T)$ of nuclear transparencies for the corresponding polarizations L and T. To understand more intuitively and simply the Q^2 and A dependence of the nuclear ratio R_{LT}^A(inc), it is convenient to present the nuclear transparency in the high-energy limit [$l_c \gg R_A$; see Eq. (64)]:

$$Tr_A^{\rm inc}\big|_{l_c\gg R_A} = \frac{\int d^2b T_A(b)\left|\int d^2r\int_0^1 d\alpha\Psi_V^*(\vec{r},\alpha)\sigma_{\bar{q}q}(r,s)\exp\left[-\frac{1}{2}\sigma_{\bar{q}q}(r,s)T_A(b)\right]\Psi_{\gamma^*}(\vec{r},\alpha,Q^2)\right|^2}{A\left|\int d^2r\int_0^1 d\alpha\Psi_V^*(\vec{r},\alpha)\sigma_{\bar{q}q}(r,s)\Psi_{\gamma^*}(\vec{r},\alpha,Q^2)\right|^2} = 1-\Sigma\frac{1}{A}\int d^2bT_A(b)^2+\cdots, \quad (67)$$

where the CT observable [9]

$$\Sigma = \frac{\int d^2r\int_0^1 d\alpha\Psi_V^*(\vec{r},\alpha)\sigma_{\bar{q}q}^2(r,s)\Psi_{\gamma^*}(\vec{r},\alpha,Q^2)}{\int d^2r\int_0^1 d\alpha\Psi_V^*(\vec{r},\alpha)\sigma_{\bar{q}q}(r,s)\Psi_{\gamma^*}(\vec{r},\alpha,Q^2)} \quad (68)$$

measures the strength of the intranuclear final-state interaction (FSI).

For the sake of clarity in the subsequent discussion we have explicitly shown in Eq. (67) only the leading term of the FSI. Evaluation of the strength of the FSI can be done by using the scanning phenomenon [Eq. (1); see also Eq. (21) and Fig. 1]. Since the integrand of the matrix element in the numerator of Eq. (68) is peaked at $r\sim r_{\rm FSI}=5/3r_S$,[4] the FSI is dominated by the contribution from $\bar{q}q$ pairs of transverse size $r\sim r_{\rm FSI}$. At large $Q^2\gg m_V^2$ and/or for production of heavy vector mesons, when $r_{\rm FSI}\ll R_V$, the observable $\Sigma\approx\sigma_{\bar{q}q}(r_{\rm FSI},s)$ and the nuclear transparency tend to unity from below:

$$1-Tr_A^{\rm inc}\propto\langle T_A\rangle\frac{Y^2}{Q^2+m_V^2}, \quad (69)$$

where $\langle T_A\rangle$ is the mean nuclear thickness given by

$$\langle T_A\rangle = \frac{\int d^2bT_A(b)^2}{A}. \quad (70)$$

The proportionality in Eq. (69) holds for $1-Tr_A^{\rm inc}\ll 1$.

The nuclear modification factor $f_{\rm inc}(s,Q^2,A)$ in Eq. (57) measures the nuclear modification of the nucleon L/T ratio. Using Eq. (69) and different scanning properties for the production of L and T polarized vector mesons, one can write the following expression:

$$f_{\rm inc}(Q^2,A)-1\propto\langle T_A\rangle\frac{\Delta Y_{TL}^2}{Q^2+m_V^2}, \quad (71)$$

where ΔY_{TL}^2 is given by Eq. (50). Thus at large $Q^2\gg m_V^2$ the factor $f_{\rm inc}$ tends to unity from above. On the r.h.s. of Eq. (71) the mean nuclear thickness causes a rise of $f_{\rm inc}$ with A, whereas the fraction is responsible for the Q^2 dependence.

As was already mentioned in Sec. II, different scale parameters Y_L and Y_T lead to different scanning properties for the production of L and T polarized vector mesons. In fact, the L production amplitude is controlled by a smaller dipole size than the T amplitude ($Y_L<Y_T$). Therefore, the following can be concluded:

(i) For bottonium production $Y_T\doteq Y_L\sim 6$, the variable $\Delta Y_{TL}^2\to 0$, and the nuclear modification factor $f_{\rm inc}\sim 1$, for any fixed mass number A of the nuclear target. Consequently, the Q^2 dependence of the nuclear L/T ratio is almost exactly given by the analogous ratio R_{LT} for the process on a nucleon target.

(ii) For charmonium production both parameters Y_L and Y_T slightly depend on Q^2 and do not differ much from each other. Consequently, the factor $f_{\rm inc}>1$ does not differ much from unity, and it gradually decreases with Q^2, tending to unity at large $Q^2\gg m_V^2$. According to Eq. (71), this deviation of $f_{\rm inc}$ from unity rises weakly with A.

(iii) The most interesting situation is in the production of light vector mesons, where one should expect a much stronger

[4]Extension to the higher order rescattering is straightforward.

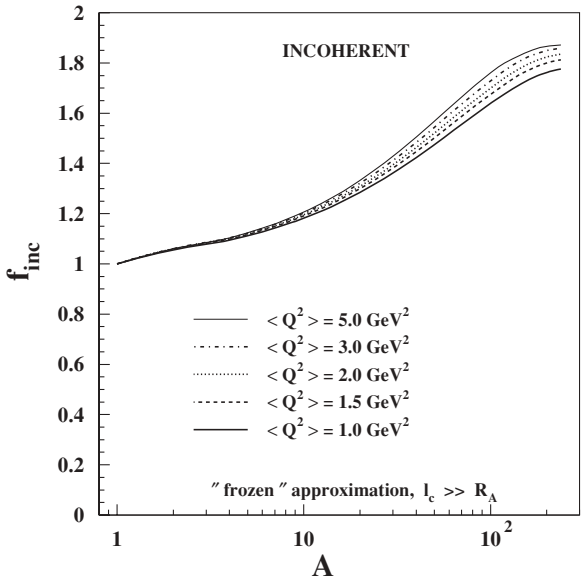

FIG. 5. A dependence of the nuclear modification factor $f_{\rm inc} = Tr_A^{\rm inc}(L)/Tr_A^{\rm inc}(T)$ as the ratio of nuclear transparencies for incoherent production of L and T polarized ρ^0 mesons, at different fixed values of $\langle Q^2\rangle$. Calculations are performed in the limit of long coherence length, $l_c \gg R_A$.

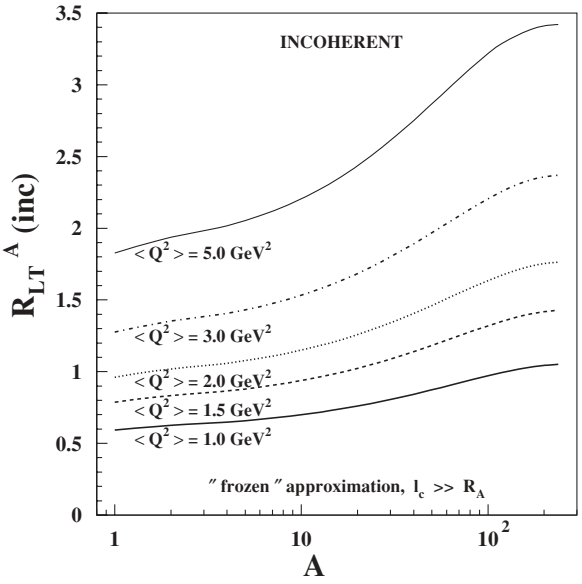

FIG. 6. A dependence of the nuclear ratio R_{LT}^A(inc) [Eq. (57)] of the cross sections [Eq. (64)], for incoherent production of L and T polarized ρ^0 mesons off nuclei, and at different fixed values of $\langle Q^2\rangle$. Calculations are performed in the limit of long coherence length, $l_c \gg R_A$.

nuclear modification of the nucleon ratio R_{LT} than for heavy mesons. At small and medium values of Q^2, such as $r_S \gtrsim R_V$, there is a strong Q^2 dependence of both scale parameters Y_L and Y_T. Moreover, the difference between Y_T and Y_L rises very rapidly with Q^2 (see Fig. 1), resulting in a strong Q^2 behavior of ΔY_{TL}^2. The rise with Q^2 of ΔY_{TL}^2 in the numerator of the r.h.s. of Eq. (71) can fully compensate or even overcompensate a decrease of the r.h.s. of Eq. (71), with $(Q^2 + m_V^2)$. This fact causes a weak Q^2 rise of the nuclear modification factor. Such expectation is confirmed by Fig. 5, where we present the A dependence of $f_{\rm inc}$ for incoherent production of ρ^0 mesons, at several values of $\langle Q^2\rangle$ and at $\nu = 15$ GeV, corresponding to HERMES kinematics.

According to Eq. (71), at fixed value of $\langle Q^2\rangle$ one should expect a monotonic A rise of $f_{\rm inc}$, caused by the mean nuclear thickness $\langle T_A\rangle$. This is in accordance with the predictions presented in Fig. 5, where one can see quite a strong nuclear modification of the nucleon L/T ratio for heavy nuclei.

Using our results for the nucleon L/T ratio (see Fig. 2) and for the nuclear modification factor $f_{\rm inc}$ (see Fig. 5), we calculated the nuclear L/T ratio. The results are depicted in Fig. 6. One can see again a monotonic A dependence of R_{LT}^A(inc), coming from the A behavior of $f_{\rm inc}$.

Finally, we emphasize that the discussion presented here concerns the high-energy limit $l_c \gg R_A$, when the $\bar{q}q$ fluctuations can be treated as frozen during the propagation through the nuclear target. This simplification was used for a better and more intuitive qualitative understanding of the Q^2 and A behavior of the nuclear ratio R_{LT}^A(inc). In this frozen approximation any rise of nuclear transparency with Q^2 represents a net manifestation of CT [28–30], because CL effects are negligible. Generally, at smaller $l_c \lesssim R_A$, when fluctuations of the size of the $\bar{q}q$ pair become important, one should include in addition CL effects, and therefore go beyond the simplified frozen approximation. Thus in this kinematical region one should solve the problem of CT-CL mixing. Both CT and CL effects are naturally incorporated in the LC Green function formalism, and the corresponding formulas become much more complicated, as one can see here. As was analyzed in detail in Ref. [28], the effects of CL can mock the signal of CT if the coherence length varies from long to short compared to the nuclear size. In this case the nuclear transparency rises with Q^2 because the length of the path in nuclear matter becomes shorter, and the vector meson (or $\bar{q}q$) attenuates less. Consequently, the effects of CL lead to a stronger Q^2 dependence of $Tr_A^{\rm inc}$ than in the frozen approximation, because both effects work in the same direction. This leads to the following expectations:

(i) According to the scanning phenomenon [Eq. (1)] and Eq. (71) one should expect a little bit stronger Q^2 dependence of $f_{\rm inc}$. However, in the HERMES kinematical range the formation length $l_f \gtrsim l_c$ and the CL $l_c \sim R_A$ and varies with Q^2 approximately from 4 to 1 fm. Then a different interplay of coherence and formation effects at different values of Q^2 and A can modify or even change the expected monotonic Q^2 dependence of $f_{\rm inc}$ (see Sec. IV E).

(ii) The monotonic A dependence of $f_{\rm inc}$ and/or R_{LT}^A(inc) should remain. The CT-CL mixing can only modify the rate of the A rise of the nuclear modification factor $f_{\rm inc}$ and/or R_{LT}^A(inc).

In conclusion, we expect that the realistic calculations performed within the LC Green function approach do not affect

significantly the expectations and conclusions concerning the Q^2 and A dependence of the nuclear ratio $R^A_{LT}(\text{inc})$ as presented here in the frozen approximation.

E. Realistic predictions for the nuclear ratio $R^A_{LT}(\text{inc})$

Exclusive incoherent electroproduction of vector mesons off nuclei has been suggested in Ref. [9,28] to be a very convenient process for the investigation of CT. By increasing the photon virtuality Q^2 one squeezes the produced $\bar{q}q$ wave packet, and such a small colorless system propagates through the nucleus with little attenuation, provided that the energy is sufficiently high ($l_f \gg R_A$), so the fluctuations of the $\bar{q}q$ separation become frozen during propagation. Consequently, a rise of nuclear transparency $Tr^{\text{inc}}_A(Q^2)$ with Q^2 should give a signal for CT. Indeed, such a rise was observed in the E665 experiment [6] at Fermilab for exclusive production of ρ^0 mesons off nuclei, and this has been claimed as a manifestation of CT. However, the effect of coherence length [41,68] leads also to a rise of $Tr^{\text{inc}}_A(Q^2)$ with Q^2, therefore imitating the CT effects. Both effects work in the same direction and so from this the problem of CT-CL separation arises, although this has been already solved in Refs. [28,39], where a simple prescription for the elimination of CL effects from the data on the Q^2 dependence of nuclear transparency was presented. One should bin the data in a way that keeps $l_c = \text{const}$. This means that one should vary simultaneously ν and Q^2, maintaining the CL Eq. (5) constant,

$$\nu = \tfrac{1}{2} l_c \left(Q^2 + m_V^2\right). \tag{72}$$

In this case any rise with Q^2 of nuclear transparency signals CT [28,39].

In the present paper we investigate differences and peculiarities in the production of vector mesons at different polarizations. The data are usually presented as the ratio of the nuclear cross sections for production of L and T polarized vector mesons. Dependence of this ratio on various variables demonstrates different properties and phenomena in the production of vector mesons, at separated polarizations. Therefore it is interesting to study the Q^2 and A behavior of the nuclear ratio $R^A_{LT}(\text{inc}) = \sigma^{\text{inc}}_A(L)/\sigma^{\text{inc}}_A(T)$ as a manifestation of the polarization dependence of the CT and CL effects. Because new data from the HERMES Collaboration will appear soon we provide predictions for the nuclear ratio $R^A_{LT}(\text{inc})$ in the HERMES kinematical range and analyze the corresponding phenomena.

Motivated by the expected new data from the HERMES Collaboration we concentrate in the present paper on the production of light vector mesons (ρ^0 and Φ^0). Because the results of the calculation for the production of ρ^0 and Φ^0 are quite similar we present predictions only for ρ^0 mesons. However, as was discussed in Refs. [28–30], the coherence and formation effects in electroproduction of vector mesons off nuclei are much more visible for light than for heavy vector mesons, as is the case for differences in electroproduction of L and T polarized vector mesons. The LC Green function technique is a very effective tool for such studies because both CT and CL effects are naturally incorporated.

According to Eqs. (9) and (57) the nuclear modification factor f_{inc} [or ratio $Tr^{\text{inc}}_A(L)/Tr^{\text{inc}}_A(T)$ of nuclear transparencies] for incoherent production of L and T polarized vector mesons represents the strength of the nuclear modification of the nucleon ratio R_{LT}. Therefore besides the nuclear ratio $R^A_{LT}(\text{inc})$ the ratio f_{inc} is also a very effective variable for the study of differences in the production of L and T polarized vector mesons off nuclei.

First we investigate different manifestations of net CT effects in incoherent electroproduction of L and T polarized ρ^0 mesons, using the Eq. (72) prescription, which states that one should study the Q^2 dependence of the factor f_{inc} at fixed values of the CL Eq. (5). According to the scanning phenomenon [see Eq. (1) and Fig. 1], for incoherent electroproduction of L polarized vector mesons one expects a stronger CT effect than for T polarized vector mesons. Consequently, at arbitrary Q^2 the nuclear transparency $Tr^{\text{inc}}_A(L) > Tr^{\text{inc}}_A(T)$ and the nuclear modification factor $f_{\text{inc}} > 1$. The results of f_{inc} for incoherent production of ρ^0 at values of $l_c =$ 0.6, 1.0, 2.0, 3.0, 5.0, and 7 fm are presented in Fig. 7 for nitrogen, krypton, and lead. One can see the following:

(i) The nuclear modification factor decreases slightly with Q^2, and at fixed l_c the photon energy rises with Q^2.

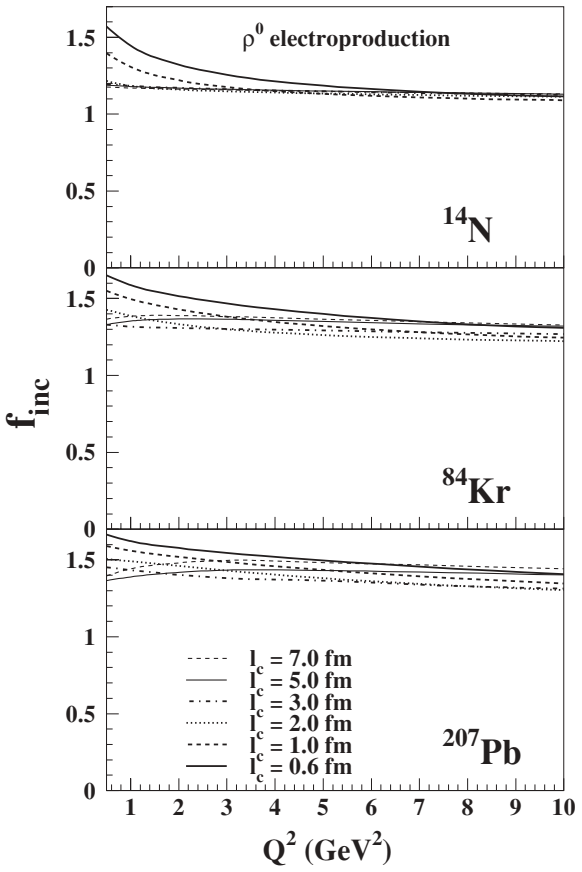

FIG. 7. Q^2 dependence of the ratio $f_{\text{inc}} = Tr^{\text{inc}}_A(L)/Tr^{\text{inc}}_A(T)$ of nuclear transparencies for incoherent production of L and T polarized ρ^0 mesons on nuclear targets ^{14}N, ^{84}Kr, and ^{207}Pb (from top to bottom). The CL Eq. (5) is fixed at $l_c = 0.6$, 1.0, 2.0, 3.0, 5.0, and 7.0 fm.

Because of a weaker Q^2 dependence of the nuclear transparency at larger photon energy, there is also a smaller difference between $Tr_A^{\rm inc}(L)$ and $Tr_A^{\rm inc}(T)$ (i.e., a smaller value of $f_{\rm inc}$).

(ii) The Q^2 dependence of $f_{\rm inc}$ is stronger at smaller l_c. In fact, if the coherence length is long then the formation length is also long, $l_f \gtrsim l_c \gg R_A$, and nuclear transparency rises with Q^2 only because the mean transverse separation of the $\bar{q}q$ fluctuation decreases. Because the production of L polarized vector mesons is scanned at smaller $\bar{q}q$ transverse separations, the nuclear transparency $Tr_A^{\rm inc}(L) > Tr_A^{\rm inc}(T)$ and $f_{\rm inc} > 1$. If, however, $l_c \lesssim R_A$ and is fixed, the photon energy rises with Q^2 and the formation length [Eq. (4)] rises as well. Thus, these two effects, the Q^2 dependence of l_f and the $\bar{q}q$ transverse size, add up and lead to a steeper growth of $Tr_A^{\rm inc}(Q^2)$ for short l_c. Consequently, this stronger Q^2 dependence leads to a larger difference between $Tr_A^{\rm inc}(L)$ and $Tr_A^{\rm inc}(T)$ (i.e., to a larger value of $f_{\rm inc}$).

(iii) The weak Q^2 rise of $f_{\rm inc}$ at large $l_c \gtrsim 5$ fm is given by the Reggeon part contribution to the dipole cross section, Eq. (15).

In Fig. 8 we present the A dependence of the ratio $f_{\rm inc}$ at $\nu = 15$ GeV and at several fixed values of Q^2, corresponding to the HERMES kinematical range. One can see that $f_{\rm inc} > 1$ as a consequence of the different scanning properties of $Tr_A^{\rm inc}(L)$ and $Tr_A^{\rm inc}(T)$ [see Eq. (71) and subsequent discussion]. Notice the weak Q^2 dependence of $f_{\rm inc}$, coming from the factor $\Delta Y_{TL}^2/(Q^2 + m_V^2)$ on the r.h.s. of Eq. (71). However, in contrast to the results from the frozen approximation (see Fig. 5) the nuclear modification factor $f_{\rm inc}$ decreases now slightly with Q^2 as a consequence of a strong CT-CL mixing. Moreover, at larger values of $A \gtrsim 84$ there is a change in the order of the curves calculated for different values of Q^2. This change is a manifestation of a different interplay of coherence and formation effects as a function of Q^2 and A. At larger Q^2 the effects of CL become more important also for lighter nuclei, when the condition $l_c \lesssim R_A$ starts to be effective.

As we already discussed in Sec. IV D, the A dependence of the nuclear factor $f_{\rm inc}$ comes, in the high-energy limit, from the A-dependent mean nuclear thickness [see Eqs. (69) and (70)]. Figure 8 shows that by performing realistic calculations (without restrictions on the coherence length) we also predict a monotonic A rise of $f_{\rm inc}$, similar to that obtained in the frozen approximation (see Fig. 5), because both CT and CL effects work in the same direction. However, in comparison with the frozen approximation, the A dependence of the CL-CT mixing causes a decrease of the A growth of $f_{\rm inc}$.

According to Eq. (57), using known values for the nuclear modification factor $f_{\rm inc}$ (see Fig. 8) and the nucleon L/T ratio (see Fig. 2), we present in Fig. 9 the A dependence of the nuclear ratio R_{LT}^A(inc). The predictions are shown at several values of $\langle Q^2 \rangle$ and at $\nu = 15$ GeV, corresponding to the HERMES kinematical range. The Q^2 dependence of R_{LT}^A(inc) is given by the convolution of the Q^2 behavior of the nucleon ratio R_{LT} (see Fig. 2) with nuclear factor $f_{\rm inc}$ (see Fig. 8). One can see a monotonic increase of the A dependence of R_{LT}^A(inc) as a consequence of the monotonic increase with A behavior of $f_{\rm inc}$.

V. COHERENT PRODUCTION OF VECTOR MESONS

A. The LC Green function formalism

If electroproduction of a vector meson leaves the target intact, the process is usually called coherent or elastic, and the mesons produced at different longitudinal coordinates and impact parameters add up coherently. This fact considerably

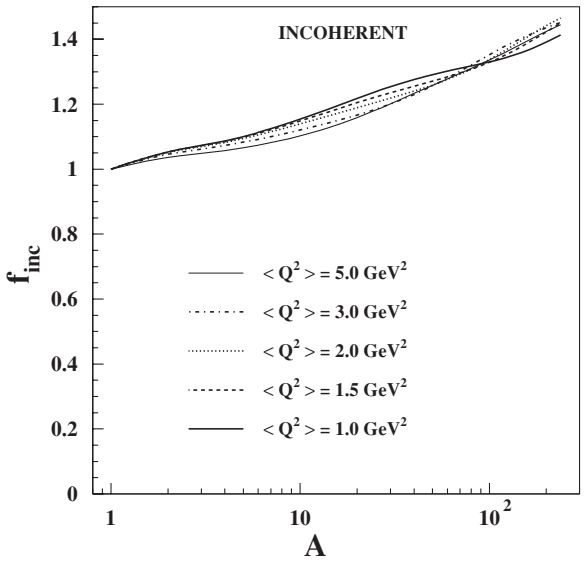

FIG. 8. A dependence of the ratio $f_{\rm inc} = Tr_A^{\rm inc}(L)/Tr_A^{\rm inc}(T)$ of nuclear transparencies for incoherent production of L and T polarized ρ^0 mesons at different fixed values of $\langle Q^2 \rangle$. Calculations are performed at the photon energy $\nu = 15$ GeV.

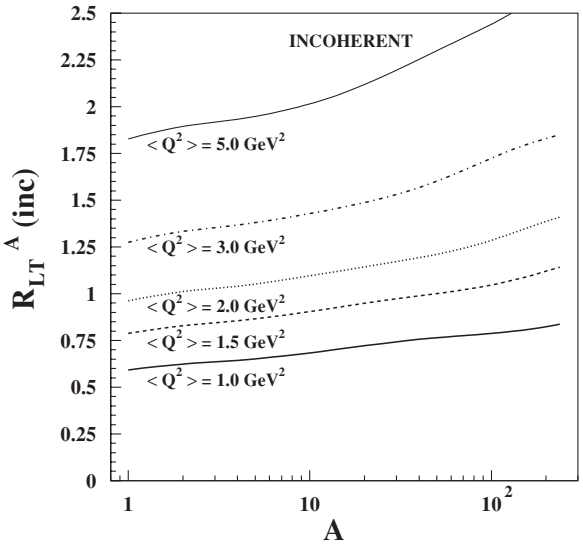

FIG. 9. A dependence of the nuclear ratio R_{LT}^A(inc) [Eq. (57)] of the cross sections for incoherent production of L and T polarized ρ^0 mesons off nuclei, at different fixed values of $\langle Q^2 \rangle$. Calculations are performed at the photon energy $\nu = 15$ GeV.

simplifies the expressions for the cross sections, compared to the case of incoherent production. The integrated cross section has the form

$$\sigma_A^{\rm coh} \equiv \sigma_{\gamma^* A\to VA}^{\rm coh} = \int d^2q \left| \int d^2b e^{i\vec{q}\cdot\vec{b}} \mathcal{M}_{\gamma^* A\to VA}^{\rm coh}(b) \right|^2 = \int d^2b |\mathcal{M}_{\gamma^* A\to VA}^{\rm coh}(b)|^2, \quad (73)$$

where the coherent nuclear production amplitude is expressed as

$$\mathcal{M}_{\gamma^* A\to VA}^{\rm coh}(b) = \int_{-\infty}^{\infty} dz\, \rho_A(b,z) F_1(b,z) \quad (74)$$

and the function $F_1(b,z)$ is defined by Eq. (63).

In contrast to incoherent vector meson production, the t slopes of the differential cross sections for nucleon and nuclear targets are different and do not cancel in the ratio. Therefore, the coherent nuclear transparency also includes the slope parameter $B_{\gamma^* N}$ for the process $\gamma^* N \to VN$,[5]

$$Tr_A^{\rm coh} = \frac{\sigma_A^{\rm coh}}{A\sigma_N} = \frac{16\pi B_{\gamma^* N}\sigma_A^{\rm coh}}{A|\mathcal{M}_{\gamma^* N\to VN}(s,Q^2)|^2}. \quad (75)$$

Because we study the L/T ratio of nuclear cross sections, just as for incoherent vector meson production [see Eq. (57)] one can define the coherent nuclear ratio $R_{LT}^A({\rm coh})$ as

$$R_{LT}^A({\rm coh}) = \frac{\sigma_{\gamma_L^* A\to V_L A}^{\rm coh}}{\sigma_{\gamma_T^* A\to V_T A}^{\rm coh}} = R_{LT}\frac{Tr_A^{\rm coh}(L)}{Tr_A^{\rm coh}(T)} = R_{LT} f_{\rm coh}(s,Q^2,A), \quad (76)$$

where $Tr_A^{\rm coh}(L)$ and $Tr_A^{\rm coh}(T)$ are defined by Eq. (75) and represent the nuclear transparencies for coherent production of L and T polarized vector mesons, respectively. The nucleon L/T ratio R_{LT} in Eq. (76) is defined by Eq. (45).

B. The nuclear ratio R_{LT}^A(coh) in the limit of long coherence length ($l_c \gg R_A$)

Expression (73) is simplified in the limit of long coherence time ($l_c \gg R_A$) as

$$\sigma_A^{\rm coh}\big|_{l_c\gg R_A} = 4\int d^2b \left| \int d^2r \left\{ 1 - \exp\left[-\frac{1}{2}\sigma_{\bar{q}q}(\vec{r},s) T_A(b) \right] \right\} \times \int_0^1 d\alpha \Psi_V^*(\vec{r},\alpha)\Psi_{\gamma^*}(\vec{r},\alpha) \right|^2. \quad (77)$$

Here, again, for the sake of clarity in the subsequent discussion we assume the frozen approximation ($l_c \gg R_A$), which simplifies the expressions for the cross sections and allows us to understand on a qualitative level the differences between coherent production of L and T polarized vector mesons. The generalization of this long-l_c limit to a more complicated realistic case using the LC Green function approach will be discussed in Sec. V C.

In the limit $l_c \gg R_A$ the total integrated cross section for coherent vector meson production is given by Eq. (77), and consequently the nuclear ratio $R_{LT}^A({\rm coh})$ can be written as

$$R_{LT}^A({\rm coh}) = R_{LT}\frac{B_L}{B_T}\cdot\frac{\int d^2b T_A^2(b)\left[1-\frac{1}{2}\Sigma_L T_A(b)+\cdots\right]}{\int d^2b T_A^2(b)\left[1-\frac{1}{2}\Sigma_T T_A(b)+\cdots\right]} = R_{LT}\frac{B_L}{B_T}\cdot\frac{\langle T_A\rangle - \frac{1}{2}\Sigma_L\langle T_A^2\rangle + \cdots}{\langle T_A\rangle - \frac{1}{2}\Sigma_T\langle T_A^2\rangle + \cdots}, \quad (78)$$

where the mean nuclear thickness $\langle T_A\rangle$ is defined by Eq. (70), and the mean nuclear thickness squared $\langle T_A^2\rangle$ is given by

$$\langle T_A^2\rangle = \frac{\int d^2b T_A(b)^3}{A}. \quad (79)$$

In Eq. (78) the variable Σ is defined by Eq. (68) and for simplicity we have explicitly shown only the leading term of the FSI.

As we discussed in Sec. IV, the FSI is dominated by the contribution from $\bar{q}q$ pairs of transverse size $r \sim r_{\rm FSI} = 5/3r_S$. At large $Q^2 \gg m_V^2$ and/or for production of heavy vector mesons, when $r_{\rm FSI} \ll R_V$ the observable $\Sigma \approx \sigma_{\bar{q}q}(r_{\rm FSI}, s)$, and according to the scanning phenomenon [Eq. (1)] the function $1 - g(Q^2)Tr_A^{\rm coh}$ scales with $(Q^2 + m_V^2)$ [compare with Eq. (69)],

$$1 - g(Q^2)Tr_A^{\rm coh} \propto \langle T_A\rangle \frac{Y^2}{Q^2+m_V^2}, \quad (80)$$

where the Q^2-dependent function $g(Q^2)$ reads

$$g(Q^2) = \frac{1}{\langle T_A\rangle}\frac{1}{16\pi B(Q^2)}. \quad (81)$$

The relation (80) holds for $1 - g(Q^2)Tr_A^{\rm coh} \ll 1$.

It can be seen from Eq. (76) that, in analogy with $f_{\rm inc}$, one can define the coherent nuclear modification factor $f_{\rm coh}$ as the ratio of the coherent nuclear and nucleon L/T ratio. A deviation of $f_{\rm coh}$ from unity as a function of Q^2 and A provides information about how the coherence and formation effects manifest themselves in coherent electroproduction of vector mesons at different polarizations L and T. Therefore now we discuss the Q^2 and A dependence of $f_{\rm coh}$. For this purpose it is convenient to write the following expression, using Eqs. (78), (80), and (81):

$$\frac{B_T}{B_L} f_{\rm coh} - 1 \propto \frac{\Delta Y_{TL}^2}{Q^2+m_V^2}\frac{\langle T_A^2\rangle}{\langle T_A\rangle} \approx \langle T_A\rangle \frac{\Delta Y_{TL}^2}{Q^2+m_V^2}, \quad (82)$$

where $\langle T_A^2\rangle$ is defined by Eq. (79). Within the discussed frozen approximation we include for simplicity in Eq. (82) only the leading term of the FSI, when $Q^2 \gg m_V^2$.

By assuming the equality $B_L = B_T$, Eq. (82) leads to an analogous Q^2 and A behavior of $f_{\rm coh}$, as the one in Eq. (71) for the incoherent nuclear modification factor $f_{\rm inc}$. This is fulfilled at large $Q^2 \gg m_V^2$ and/or for the production of heavy vector mesons, when the relativistic effects are small enough to apply safely the nonrelativistic approximation. At small and medium Q^2, however, $B_L < B_T$ [59] and the B_T/B_L ratio

[5]Note that, in contrast to incoherent production, where nuclear transparency is expected to saturate as $Tr_A^{\rm inc}(Q^2) \to 1$ at large Q^2, for the coherent process nuclear transparency reaches a higher limit, $Tr_A^{\rm coh}(Q^2) \to A^{1/3}$.

on the left-hand side (l.h.s.) of Eq. (82) reduces the coherent nuclear factor $f_{\rm coh}$. Consequently, for light nuclear targets $A \lesssim 10$ the factor $f_{\rm coh}$ can be less than unity.

As was discussed in detail in Sec. IV D, for bottonium production $Y_T \doteq Y_L \sim 6$, and the slope parameters $B_L \approx B_T$. Consequently, $f_{\rm coh} \sim 1$ and the Q^2 dependence of the nuclear L/T ratio for coherent reactions is almost exactly given by the analogous ratio R_{LT} for the process on a nucleon. This conclusion is essentially the same as the one expected for incoherent production of bottonia.

For charmonium production both Y_L and Y_T depend slightly on Q^2 and do not differ much from each other. Consequently, the difference ΔY^2_{TL} acquires a small value and rises very weakly with Q^2. Because $B_T/B_L \approx 1.03$ in the photoproduction limit, the nuclear factor $f_{\rm coh}$ can go below unity at small values of Q^2 and A. As Q^2 increases the ratio B_T/B_L tends to unity from above and $f_{\rm coh}$ gradually comes to unity from below at small A or from above at medium and large A.

In contrast to the production of heavy vector mesons, for the production of light vector mesons we expect much larger nuclear modifications of the nucleon ratio R_{LT}, just as for the incoherent processes discussed in Sec. IV. At small and medium Q^2 such as $r_S \gtrsim R_V$, there is a strong Q^2 dependence of ΔY^2_{TL}, which can even overcompensate the rise of $(Q^2 + m_V^2)$ in the denominator of Eq. (82). This fact can lead to a weak rise with Q^2 of the coherent nuclear factor $f_{\rm coh}$, which is further enhanced by the decrease of the B_T/B_L ratio on the l.h.s. of Eq. (82). As a result, we expect a stronger Q^2 dependence of $f_{\rm coh}$ than of $f_{\rm inc}$. Such an expectation is supported by calculations performed in the limit of long coherence length and is shown in Fig. 10 (compare with Fig. 5).

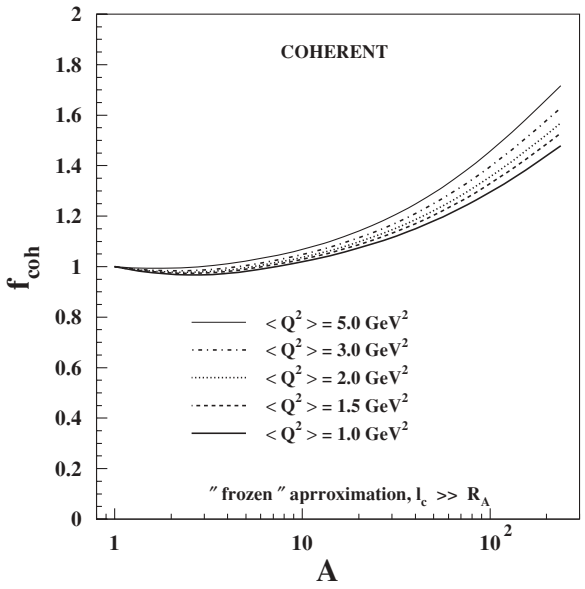

FIG. 10. A dependence of the nuclear modification factor $f_{\rm coh} = Tr_A^{\rm coh}(L)/Tr_A^{\rm coh}(T)$ as the ratio of nuclear transparencies for coherent production of L and T polarized ρ^0 mesons, at different fixed values of $\langle Q^2 \rangle$. Calculations are performed in the limit of long coherence length, $l_c \gg R_A$.

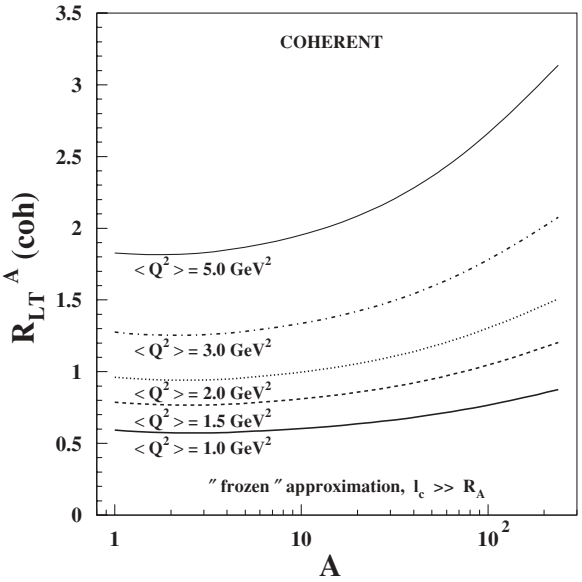

FIG. 11. A dependence of the nuclear ratio R^A_{LT}(coh) [Eq. (76)] of the cross sections [Eq. (77)] for coherent production of L and T polarized ρ^0 mesons off nuclei, at different fixed values of $\langle Q^2 \rangle$. Calculations are performed in the limit of long coherence length, $l_c \gg R_A$.

Concluding, in the HERMES kinematical range, $\sim 1 < Q^2 < 5$ GeV^2, studied in the present paper, we expect a rise with Q^2 of the nuclear modification factor $f_{\rm coh}$. The rate of this rise is then given by the mean nuclear thickness, as follows from Eq. (82). Consequently, we expect a monotonic rise of $f_{\rm coh}$ with A, just as for the incoherent nuclear modification factor $f_{\rm inc}$ (see also Fig. 5). Monotonic A-increase behavior of $f_{\rm coh}$ is confirmed also by the predictions depicted in Fig. 10 at several values of $\langle Q^2 \rangle$, corresponding to the HERMES kinematical range.

For completeness we also calculated the nuclear L/T ratio using the known nuclear modification factor $f_{\rm coh}$ and the nucleon L/T ratio. The results are presented in Fig. 11. One can see a monotonic A dependence of R^A_{LT}(coh) as a consequence of a corresponding monotonic A-increase behavior of $f_{\rm coh}$.

In the following section we demonstrate, however, that in contrast to incoherent vector meson production such a picture of Q^2 and A behavior for $f_{\rm coh}$ and/or R^A_{LT}(coh) drastically changes going beyond this frozen approximation. This is the crucial point that leads to interesting physics in the investigation of light vector mesons produced coherently off nuclei.

C. Realistic predictions for the nuclear ratio R^A_{LT}(coh)

Analogously as was done for incoherent production of vector mesons, here we study the differences in coherent electroproduction of L and T polarized vector mesons off nuclei, performing a realistic calculation without restrictions on the CL. We focus on the production of ρ^0 mesons, where CT and CL effects are the most visible. This is also

supported by our expectations about the new data from the HERMES Collaboration, and therefore our calculations cover the corresponding kinematical range. We use the LC Green function formalism, which naturally incorporates both CT and CL effects.

First, we study the net CT effect in L and T polarizations, by eliminating the effects of CL in a way similar to what was suggested for incoherent reactions, which involves selecting experimental data with $l_c = \text{const}$. We calculated the nuclear modification factor $f_{\rm coh}$ for the coherent reaction $\gamma^* A \to \rho^0 A$ as a function of Q^2, at different fixed values of l_c. The results for $l_c = 0.6, 1.0, 2.0, 3.0, 5.0,$ and 7.0 fm are depicted in Fig. 12. In contrast to the incoherent processes one can observe a much more complicated Q^2 behavior, which is the result of an interplay between CT and CL effects when a contraction of the CL causes an effect opposite to that of CT. This CL-CT mixing as a function of Q^2 changes the order of curves calculated at different values of l_c.

Following Eq. (76) we give the coherent nuclear factor $f_{\rm coh}$ as the ratio $Tr_A^{\rm coh}(L)/Tr_A^{\rm coh}(T)$ of nuclear transparencies for coherent production of L and T polarized vector mesons. It represents the strength of the nuclear modification of the nucleon ratio R_{LT}. In Fig. 13 we present the A dependence of $f_{\rm coh}$ for ρ^0 production, at photon energy $\nu = 15$ GeV

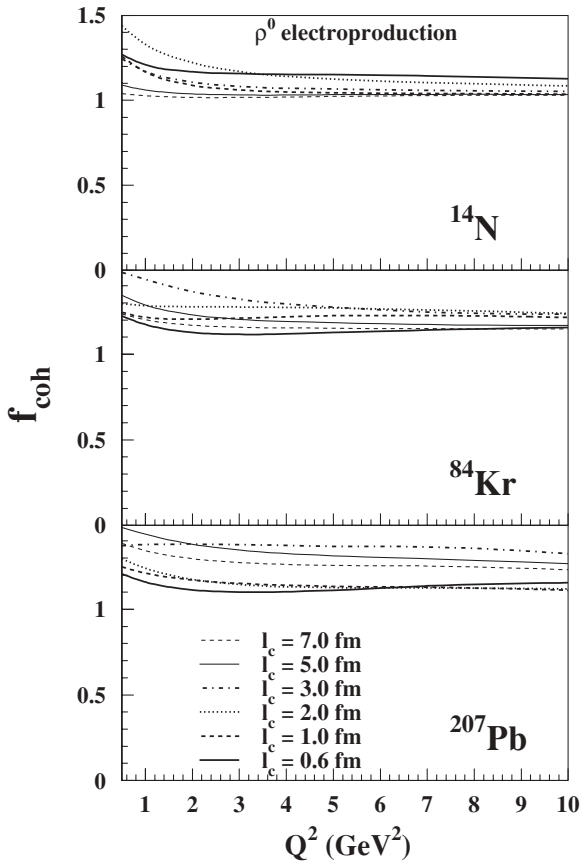

FIG. 12. Q^2 dependence of the ratio $f_{\rm coh} = Tr_A^{\rm coh}(L)/Tr_A^{\rm coh}(T)$ of nuclear transparencies for coherent production of L and T polarized ρ^0 mesons on nuclear targets ^{14}N, ^{84}Kr, and ^{207}Pb (from top to bottom). The CL Eq. (5) is fixed at $l_c = 0.6, 1.0, 2.0, 3.0, 5.0,$ and 7.0 fm.

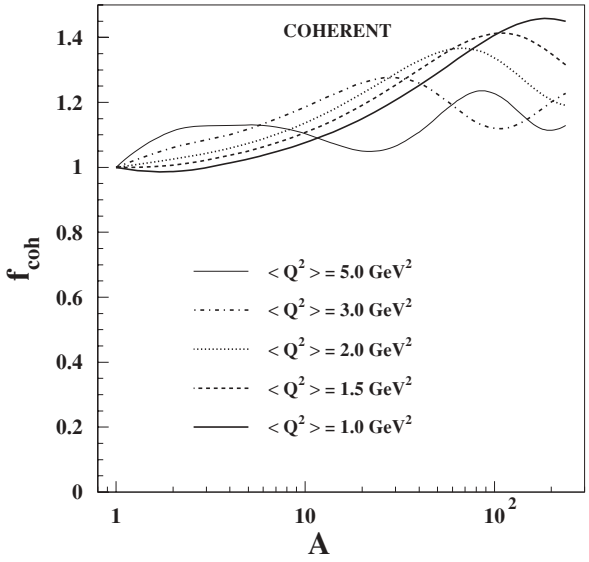

FIG. 13. A dependence of the ratio $f_{\rm coh} = Tr_A^{\rm coh}(L)/Tr_A^{\rm coh}(T)$ of nuclear transparencies for coherent production of L and T polarized ρ^0 mesons at different fixed values of $\langle Q^2 \rangle$. Calculations are performed at the photon energy $\nu = 15$ GeV.

and several fixed values of $\langle Q^2 \rangle$, corresponding to the HERMES kinematical range. One can see that the predictions dramatically changed from those that we found for the limit of long CL, $l_c \gg R_A$, in Sec. V B. This is because the HERMES kinematics does not allow us to neglect the effects of CL. Only at very small $A \lesssim 4$ and at $Q^2 \lesssim 3$ GeV^2 can one assume small CL effects, because $l_c > R_A$. Then the A and Q^2 behavior of $f_{\rm coh}$ follows the scenario described within the frozen approximation (see Sec. V B), which means that $f_{\rm coh}$ rises with Q^2 and has a monotonic A dependence.

In Ref. [28] it was demonstrated that for coherent production of vector mesons the contraction of the CL with Q^2 causes an effect opposite to that of CT. Nuclear transparency is suppressed rather than enhanced. At large Q^2, when $l_c \lesssim R_A$, and at medium energies, corresponding to the HERMES kinematics, the suppression of nuclear transparency can be so strong that it fully compensates or even overcompensates the rise of nuclear transparency with Q^2 given by CT. Because $Tr_A^{\rm coh}(L)$ is scanned at smaller dipole sizes than $Tr_A^{\rm coh}(T)$, one can expect that at fixed Q^2 the former nuclear transparency has stronger CL effects than the latter one. This different manifestation of CL effects for L and T polarizations depends also on A. Consequently, one may expect a nontrivial and nonmonotonic A and Q^2 dependence of the nuclear modification factor $f_{\rm coh}$.

Mainly because of the effects of CL, there is an unusual order of curves at different values of $\langle Q^2 \rangle$, as is shown in Fig. 13. Moreover, the order of curves is changed at various values of A, as a consequence of the fact that the condition $l_c \gg R_A$ is broken in a different degree for different nuclear targets. At $\langle Q^2 \rangle = 1$ GeV^2 the effects of CL start to be important at $A \gtrsim 100$ and lead to a diminishing of the A rise of the nuclear factor $f_{\rm coh}$. One can see by the thick solid line in Fig. 13 that there is even a maximum of $f_{\rm coh}$ at $A \sim 200$,

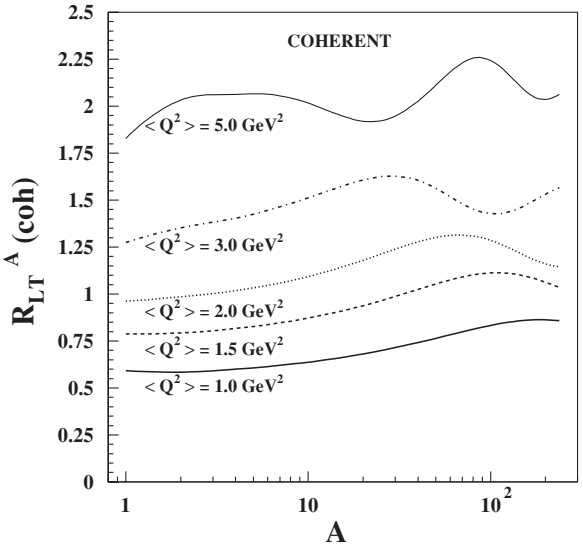

FIG. 14. A dependence of the nuclear ratio $R_{LT}^A(\text{coh})$ (76) of the cross sections for coherent production of L and T polarized ρ^0 mesons off nuclei at different fixed values of $\langle Q^2 \rangle$. Calculations are performed at the photon energy $\nu = 15$ GeV.

as a natural demonstration of the effectiveness of CL effects. Larger $\langle Q^2 \rangle$ leads to a contraction of the CL. Consequently, the effect of CL-contraction becomes also important for lighter nuclear targets, which means that the maximum is shifted to smaller values of A. The combination of the A rise of f_{coh} through the nuclear profile function [Eq. (8)], together with the different manifestation of CL effects as a function of Q^2 and A, lead to a nontrivial and nonmonotonic A dependence of f_{coh}, as is shown in Fig. 13. This A dependence is even more complicated at larger values of $\langle Q^2 \rangle$, when the CL effects are effective at a different level, for a broader range of nuclear targets.

In Fig. 14 we present the A dependence of the nuclear ratio $R_{LT}^A(\text{coh})$, obtained from the nuclear modification factor f_{coh} and the nucleon L/T ratio [see Eq. (76)]. The predictions are shown at several values of $\langle Q^2 \rangle$, and at $\nu = 15$ GeV, corresponding to the HERMES kinematical range. One can see that a nonmonotonic A dependence of f_{coh} is projected into a nonmonotonic A dependence of $R_{LT}^A(\text{coh})$. The Q^2 dependence of $R_{LT}^A(\text{coh})$ is given by the convolution of the Q^2 behavior of the nucleon ratio R_{LT} (see Fig. 2) with the nuclear factor f_{coh} (see Fig. 13). The predicted anomalous A behavior of the coherent nuclear ratio $R_{LT}^A(\text{coh})$ at different values of $\langle Q^2 \rangle$ is a undeniable and irrefutable manifestation of strong CL effects and can be tested by the HERMES Collaboration or at JLab.

VI. SUMMARY AND CONCLUSIONS

Electroproduction of vector mesons off nuclei is a very effective tool for the study of the interplay between coherence (shadowing) and formation (color transparency) effects. In the present paper we investigated how these effects manifest themselves differently in the production of L and T polarized vector mesons off nuclei. The data are usually presented as the L/T ratio of the nuclear production cross sections. Then an investigation of the behavior of this ratio as a function of various variables (Q^2, A, etc.), and a deviation of this ratio from unity, allows the study of different properties and manifestations of corresponding phenomena in the production of vector mesons, at separated polarizations. We used, from Ref. [28], a rigorous quantum-mechanical approach based on the light-cone QCD Green function formalism, which naturally incorporates these interference effects. We focused on the production of light vector mesons, because here the polarization dependence of CT and CL effects is much more visible than in the production of heavy vector mesons. Because new data from the HERMES Collaboration are expected to appear soon, we presented predictions for the nuclear L/T ratios [see Eqs. (57) and (76)] within the corresponding kinematical range. These predictions are made for ρ^0 mesons produced both coherently and incoherently off nuclei.

The strength of the nuclear modification of the nucleon L/T ratio [Eq. (45)] is given by the nuclear modification factors f_{inc} and f_{coh}, which are defined as the ratio of nuclear transparencies for electroproduction of L and T polarized vector mesons [see Eqs. (57) and (76)]. If these factors are equal to unity there are no nuclear effects. Therefore in addition tp the nuclear L/T ratios, the nuclear modification factors are also very effective variables for the study of differences in the production of L and T polarized vector mesons off nuclei. The nuclear L/T ratio is then given as the product of the nucleon L/T ratio and the nuclear modification factor.

As the first step we compare the nucleon L/T ratio as a function of Q^2 with available data on electroproduction of ρ^0 and Φ^0 mesons and charmonia and find a nice agreement (see Figs. 2, 3, and 4). This is a very important achievement because the nucleon L/T ratio represents a basis for the correct determination of the nuclear L/T ratio via the nuclear modification factor.

To obtain more intuitive information about the A and Q^2 behavior of the nuclear L/T ratio and/or nuclear modification factor we presented on the qualitative level, using the scanning phenomenon [Eq. (1)], the corresponding predictions in the high-energy limit ($l_c \gg R_A$). Here the expressions for nuclear production cross sections are sufficiently simplified. This so-called frozen approximation includes only CT because there are no fluctuations of the transverse size of the $\bar{q}q$ pair. For incoherent electroproduction of ρ^0 mesons we predict a very weak Q^2 growth of f_{inc} in the HERMES kinematical range (see Fig. 5) owing to a strong Q^2 rise of a difference between the scanning radii corresponding to T and L polarizations [see Fig. 1 and Eq. (1)]. In contrast to incoherent processes, for ρ^0 mesons produced coherently off nuclei one should include in f_{coh} also the slope parameters B_L and B_T for different polarizations L and T [see Eq. (82)]. Consequently, we expect a stronger Q^2 dependence of f_{coh} (see Fig. 10) owing to different Q^2 dependences of the corresponding slope parameters. We predict a monotonic rise with A of both nuclear factors f_{inc} and f_{coh}, which comes from the A-dependent mean nuclear thickness.

The "frozen" approximation cannot be applied for the study of differences in electroproduction of vector mesons off nuclei at different polarizations, in the HERMES kinematical range. Therefore we use the approach of Ref. [28], which interpolates between the previously known low- and high-energy limits for incoherent production [see Eq. (65)]. Equation (74) does the same for coherent production.

In the incoherent electroproduction of vector mesons at low and medium energies, the onset of coherence effects (shadowing) can mimic the expected signal of CT. Both effects, CT and CL, work in the same direction. In comparison with the high-energy limit, the onset of CL has little effect on the A and Q^2 behavior of $f_{\rm inc}$. Consequently, we predict again a weak Q^2 dependence of $f_{\rm inc}$ (see Fig. 8). An investigation of the A dependence of $f_{\rm inc}$ reveals that the interplay between CT and CL effects changes the order of curves calculated at different values of Q^2. The CL-CT mixing also modifies the rate of the A rise of $f_{\rm inc}$, but it conserves the monotonic A dependence typical for the frozen approximation (see Fig. 8). Therefore we predict a monotonic A increase behavior of the nuclear L/T ratio as well at different values of Q^2 (see Fig. 9).

In coherent production of vector mesons the natural incorporation of the CL effects in the Green function formalism changes drastically the A and Q^2 behavior of $f_{\rm coh}$ predicted for the high-energy limit. The contraction of the CL with Q^2 causes an effect opposite to that of CT. There is a different manifestation of CL effects at various values of Q^2 and A, which together with CT effects leads to a nontrivial and anomalous A and Q^2 dependence of the nuclear modification factor. The nonmonotonic A dependence is even more complicated at larger values of Q^2 as a result of stronger CL effects for a broader range of nuclear targets (see Fig. 8). Consequently, we predict also a nonmonotonic and anomalous A dependence of the nuclear L/T ratio at different values of Q^2 (see Fig. 14), which gives a motivation to detect such anomalous manifestations of strong CL effects in experiments with the HERMES spectrometer and especially at JLab.

We also investigated different manifestations of net CT effects at different polarizations L and T, using a prescription from Refs. [28,39], calculating the nuclear modification factor as a function of Q^2 at various fixed values of the coherence length.

(i) In incoherent production of ρ^0 mesons, we found a stronger CT effects for L than for T polarization (i.e., $f_{\rm inc} > 1$). Moreover, $f_{\rm inc}$ rises toward small values of Q^2 at short $l_c \lesssim R_A$ (see Fig. 7). The two effects, that is, the Q^2 dependence of l_f and the $\bar{q}q$ transverse size, add up and lead to a steeper Q^2 growth of nuclear transparency, and consequently to larger values of $f_{\rm inc}$.

(ii) In coherent production of ρ^0 mesons we predicted also $f_{\rm coh} > 1$ (see Fig. 12). However, the Q^2 behavior of $f_{\rm coh}$ is more complicated in comparison with the incoherent reaction, which follows from the fact that a contraction of the CL with Q^2 causes an effect opposite to that of CT. Then the CT-CL mixing as a function of Q^2 changes the order of curves calculated at different values of l_c.

In conclusion, the exploratory study of the A dependence of the nuclear L/T ratio, especially in coherent electroproduction of light vector mesons off nuclei, opens new possibilities for the search for the CL effects and their different manifestations at different polarizations with medium-energy electrons.

ACKNOWLEDGMENTS

This work was supported in part by Fondecyt (Chile) Grant No. 1050519, by DFG (Germany) Grant No. PI182/3-1, and by the Slovak Funding Agency, Grant No. 2/7058/27.

[1] OMEGA Collaboration, D. Aston *et al.*, Nucl. Phys. **B172**, 1 (1980); **B209**, 56 (1982).
[2] NMC Collaboration, M. Arneodo *et al.*, Nucl. Phys. **B429**, 503 (1994).
[3] CHIO Collaboration, W. D. Shambroom *et al.*, Phys. Rev. D **26**, 1 (1982).
[4] E665 Collaboration, M. R. Adams *et al.*, Z. Phys. C **74**, 237 (1997).
[5] R. Erbe *et al.*, Phys. Rev. **175**, 1669 (1968); W. G. Jones *et al.*, Phys. Rev. Lett. **21**, 586 (1968); C. Berger *et al.*, Phys. Lett. **B39**, 659 (1972); J. Park *et al.*, Nucl. Phys. **B36**, 404 (1972); SBT Collaboration, J. Ballam *et al.*, Phys. Rev. D **5**, 545 (1972); G. E. Gladding *et al.*, *ibid.* **8**, 3721 (1973); H. J. Bersh *et al.*, Nucl. Phys. **B70**, 257 (1974); H. J. Behrend *et al.*, Phys. Lett. **B56**, 408 (1975); D. P. Barber *et al.*, *ibid.* **B79**, 150 (1978); R. M. Egloff *et al.*, Phys. Rev. Lett. **43**, 657 (1979); M. Atkinson *et al.*, Z. Phys. C **27**, 233 (1985); J. Busenitz *et al.*, Phys. Rev. D **40**, 1 (1989), and references therein.
[6] E665 Collaboration, M. R. Adams *et al.*, Phys. Rev. Lett. **74**, 1525 (1995).
[7] A. B. Zamolodchikov, B. Z. Kopeliovich, and L. I. Lapidus, Pis'ma Zh. Eksp. Teor. Fiz. **33**, 612 (1981); Sov. Phys. JETP Lett. **33**, 595 (1981).
[8] G. Bertsch, S. J. Brodsky, A. S. Goldhaber, and J. G. Gunion, Phys. Rev. Lett. **47**, 297 (1981).
[9] B. Z. Kopeliovich, J. Nemchik, N. N. Nikolaev, and B. G. Zakharov, Phys. Lett. **B324**, 469 (1994).
[10] ZEUS Collaboration, M. Derrick *et al.*, Z. Phys. C **63**, 391 (1994); Phys. Lett. **B356**, 601 (1995); Z. Phys. C **69**, 39 (1995); Phys. Lett. **B377**, 259 (1996); **B380**, 220 (1996); paper pa02-050, submitted to the XXVIII International Conference on HEP, 25–31 July, 1996, Warsaw, Poland; ZEUS Collaboration, J. Breitweg *et al.*, Z. Phys. C **73**, 253 (1997); Eur. Phys. J. C **2**, 247 (1998); abstract 793, submitted to the XXIX International Conference on HEP, 23–29 July, 1998, Vancouver, Canada.
[11] H1 Collaboration, S. Aid *et al.*, Nucl. Phys. **B463**, 3 (1996); **B468**, 3 (1996); H1 Collaboration, C. Adloff *et al.*, Z. Phys. C **75**, 607 (1997).
[12] ZEUS Collaboration, J. Breitweg *et al.*, Eur. Phys. J. C **6**, 603 (1999).
[13] ZEUS Collaboration, J. Breitweg *et al.*, abstract 880, submitted to the XXX International Conference on HEP, 27 July–2 August, 2000, Osaka, Japan.

[14] ZEUS Collaboration, J. Breitweg *et al*., abstract 594, submitted to the International Europhysics Conference on HEP, 12–18 July, 2001, Budapest, Hungary.
[15] ZEUS Collaboration, J. Breitweg *et al*., paper ZEUS-prel-04-11, abstract 6-0248, submitted to the International Conference on HEP, 16–22 August, 2004, Beijing, China.
[16] H1 Collaboration, C. Adloff *et al*., Phys. Lett. **B483**, 360 (2000).
[17] H1 Collaboration, C. Adloff *et al*., Eur. Phys. J. C **13**, 371 (2000).
[18] H1 Collaboration, C. Adloff *et al*., abstract 989, submitted to the International Conference on HEP, 24–31 July, 2002, Amsterdam, Netherlands.
[19] H1 Collaboration, A. Aktas *et al*., abstract 092, submitted to the International Europhysics Conference on HEP, 17–23 July, 2003, Aachen, Germany.
[20] HERMES Collaboration, A. Airapetyan *et al*., Eur. Phys. J. C **17**, 389 (2000); HERMES Collaboration, M. Hartig *et al*., *Diffractive Vector Meson Production at HERMES*, paper DESY-HERMES-01-18, prepared for the International Conference on Quark Nuclear Physics (QNP2000), 21–25 February, 2000, Adelaide, Australia, Nucl. Phys. **A680**, 264 (2000); HERMES Collaboration, M. Tytgat *et al*., *Diffractive Vector Meson Production at Intermediate Energies*, paper DESY-HERMES-01-15, prepared for the IX Blois Workshop on Elastic and Diffractive Scattering, 9–15 June, 2001, Pruhonice, Czech Republic, published in *Pruhonice 2001, Elastic and diffractive scattering*, 77.
[21] HERMES Collaboration, A. B. Borissov *et al*., *Spin Physics of Vector Meson Production at Intermediate W and* Q^2, paper DESY-HERMES-01-60, prepared for the IX Workshop on High Energy Spin Physics, 2–7 August, 2001, Dubna, Russia, and references therein; A. B. Borissov *et al*., *Spin Physics of Vector Meson Production at HERMES*, paper DESY-HERMES-02-63, prepared for the X NATO Advanced Spin Physics Workshop, 30 June–3 July, 2002, Nor Amberd Conference Center, Armenia, and references therein, published in *Nor-Ambered 2002, Spin structure of the nucleon*, 201.
[22] J. Nemchik, N. N. Nikolaev, and B. G. Zakharov, Phys. Lett. **B341**, 228 (1994).
[23] B. Z. Kopeliovich, J. Nemchik, N. N. Nikolaev, and B. G. Zakharov, Phys. Lett. **B309**, 179 (1993).
[24] J. Nemchik, N. N. Nikolaev, E. Predazzi, and B. G. Zakharov, Z. Phys. C **75**, 71 (1997).
[25] B. Z. Kopeliovich and B. Povh, J. Phys. G **30**, S999 (2004).
[26] Z. Kopeliovich, B. Povh, and I. Schmidt, Nucl. Phys. **A782**, 24 (2007).
[27] B. Z. Kopeliovich, A. Schäfer, and A. V. Tarasov, Phys. Rev. D **62**, 054022 (2000).
[28] B. Z. Kopeliovich, J. Nemchik, A. Schaefer, and A. V. Tarasov, Phys. Rev. C **65**, 035201 (2002).
[29] J. Nemchik, Phys. Rev. C **66**, 045204 (2002).
[30] J. Nemchik, Czech. J. Phys. **53**, 301 (2003).
[31] B. Z. Kopeliovich and B. G. Zakharov, Phys. Rev. D **44**, 3466 (1991).
[32] B. Z. Kopeliovich, J. Raufeisen, and A. V. Tarasov, Phys. Lett. **B503**, 91 (2001); B. Z. Kopeliovich, J. Raufeisen, A. V. Tarasov, and M. B. Johnson, Phys. Rev. C **67**, 014903 (2003).
[33] B. Z. Kopeliovich, J. Raufeisen, and A. V. Tarasov, Phys. Lett. **B440**, 151 (1998).
[34] B. Z. Kopeliovich, J. Raufeisen, and A. V. Tarasov, Phys. Rev. C **62**, 035204 (2000).
[35] V. N. Gribov, Zh. Eksp. Teor. Fiz. **56**, 892 (1969); Sov. Phys. JETP **29**, 483 (1969).
[36] J. F. Gunion and D. E. Soper, Phys. Rev. D **15**, 2617 (1977).
[37] J. Hüfner and B. Povh, Phys. Rev. D **46**, 990 (1992).
[38] B. Povh, invited talk at the 14th International Workshop on Nuclear Dynamics, January 31–February 7, 1998, Snowbird, USA, hep-ph/9806379; preprint MPIH-V21-1998.
[39] J. Hüfner and B. Z. Kopeliovich, Phys. Lett. **B403**, 128 (1997).
[40] Yu. P. Ivanov, B. Z. Kopeliovich, A. V. Tarasov, and J. Hüfner, Phys. Rev. C **66**, 024903 (2002).
[41] J. Hüfner, B. Z. Kopeliovich, and J. Nemchik, Phys. Lett. **B383**, 362 (1996).
[42] HERMES Collaboration, K. Ackerstaff *et al*., Phys. Rev. Lett. **82**, 3025 (1999).
[43] HERMES Collaboration, A. Airapetian *et al*., Acta Phys. Pol. B **33**, 3639 (2002); Nucl. Phys. Proc. Suppl. **126**, 232 (2004); Phys. Rev. Lett. **90**, 052501 (2003).
[44] J. Hüfner, Yu. P. Ivanov, B. Z. Kopeliovich, and A. V. Tarasov, Phys. Rev. D **62**, 094022 (2000).
[45] I. P. Ivanov, N. N. Nikolaev, and A. A. Savin, Phys. Part. Nuclei **37**, 1 (2006).
[46] K. Golec-Biernat and M. Wüsthoff, Phys. Rev. D **59**, 014017 (1999); **60**, 114023 (1999).
[47] A. Donnachie and P. V. Landshoff, Phys. Lett. **B478**, 146 (2000).
[48] Particle Data Group, Eur. Phys. J. C **15**, 1 (2000).
[49] J. B. Bronzan, G. L. Kane, and U. P. Sukhatme, Phys. Lett. **B49**, 272 (1974).
[50] J. B. Kogut and D. E. Soper, Phys. Rev. D **1**, 2901 (1970).
[51] J. M. Bjorken, J. B. Kogut, and D. E. Soper, Phys. Rev. D **3**, 1382 (1971).
[52] N. N. Nikolaev and B. G. Zakharov, Z. Phys. C **49**, 607 (1991).
[53] R. P. Feynman and A. R. Gibbs, *Quantum Mechanics and Path Integrals* (McGraw-Hill, New York, 1965).
[54] H1 Collaboration, S. Aid *et al*., Z. Phys. C **69**, 27 (1995).
[55] ZEUS Collaboration, M. Derrick *et al*., Phys. Lett. **B293**, 465 (1992).
[56] M. V. Terent'ev, Yad. Fiz. **24**, 207 (1976); Sov. J. Nucl. Phys. **24**, 106 (1976).
[57] H. G. Dosch, T. Gousset, G. Kulzinger, and H. J. Pirner, Phys. Rev. D **55**, 2602 (1997).
[58] G. Kulzinger, H. G. Dosch, and H. J. Pirner, Eur. Phys. J. C **7**, 73 (1999).
[59] J. Nemchik, N. N. Nikolaev, E. Predazzi, B. G. Zakharov, and V. R. Zoller, J. Exp. Theor. Phys. **86**, 1054 (1998).
[60] J. Nemchik, Czech. J. Phys. **51**, 531 (2001).
[61] H1 Collaboration, C. Adloff *et al*., Eur. Phys. J. C **10**, 373 (1999).
[62] ZEUS Collaboration, S. Chekanov *et al*., Nucl. Phys. **B695**, 3 (2004).
[63] SBT Collaboration, J. Ballam *et al*., Phys. Rev. D **7**, 3150 (1973).
[64] P. Joos *et al*., Nucl. Phys. **B113**, 53 (1976).
[65] ZEUS Collaboration, J. Breitweg *et al*., Eur. Phys. J. C **12**, 393 (2000).
[66] J. Nemchik, Phys. Rev. C **68**, 035206 (2003).
[67] J. Hüfner, B. Z. Kopeliovich, and A. Zamolodchikov, Z. Phys. A **357**, 113 (1997).
[68] B. Z. Kopeliovich and J. Nemchik, preprint MPIH-V41-1995, nucl-th/9511018.

Gluon shadowing in DIS off nuclei

To cite this article: B Z Kopeliovich *et al* 2008 *J. Phys. G: Nucl. Part. Phys.* **35** 115010

J. Phys. G: Nucl. Part. Phys. **35** (2008) 115010 (25pp) doi:10.1088/0954-3899/35/11/115010

Gluon shadowing in DIS off nuclei

B Z Kopeliovich[1,2], J Nemchik[3,4], I K Potashnikova[1,2] and Ivan Schmidt[1]

[1] Departamento de Física y Centro de Estudios Subatómicos, Universidad Técnica Federico Santa María, Valparaíso, Chile
[2] Joint Intitute for Nuclear Research, Dubna, Russia
[3] Institute of Experimental Physics SAS, Watsonova 47, 04001 Kosice, Slovakia
[4] Czech Technical University, FNSPE, Brehova 7, 11519 Praque, Czech Republic

Received 30 May 2008
Published 26 September 2008
Online at stacks.iop.org/JPhysG/35/115010

Abstract

Within a light-cone quantum-chromodynamics dipole formalism based on the Green function technique, we study nuclear shadowing in deep-inelastic scattering at small Bjorken $x_{\rm Bj} \lesssim 0.01$. Such a formalism incorporates naturally color transparency and coherence length effects. Calculations of the nuclear shadowing for the $\bar{q}q$ Fock component of the photon are based on an exact numerical solution of the evolution equation for the Green function, using a realistic form of the dipole cross section and nuclear density function. Such an exact numerical solution is unavoidable for $x_{\rm Bj} \gtrsim 10^{-4}$, when a variation of the transverse size of the $\bar{q}q$ Fock component must be taken into account. The eikonal approximation, used so far in most other models, can be applied only at high energies, when $x_{\rm Bj} \lesssim 10^{-4}$ and the transverse size of the $\bar{q}q$ Fock component is 'frozen' during propagation through the nuclear matter. At $x_{\rm Bj} \leqslant 0.01$, we find quite a large contribution of gluon suppression to nuclear shadowing, as a shadowing correction for the higher Fock states containing gluons. Numerical results for nuclear shadowing are compared with the available data from the E665 and NMC collaborations. Nuclear shadowing is also predicted at very small $x_{\rm Bj}$ corresponding to LHC kinematical range. Finally, the model predictions are compared and discussed with the results obtained from other models.

1. Introduction

Nuclear shadowing in deep-inelastic scattering (DIS) off nuclei is usually studied via nuclear structure functions. In the shadowing region of small Bjorken, $x_{\rm Bj} \lesssim 0.01$, the structure function F_2 per nucleon turns out to be smaller in nuclei than in a free nucleon (see the review [1], for example). This affects then the corresponding study of nuclear effects, mainly in connection with the interpretation of the results coming from hadron–nucleus and heavy-ion experiments.

0954-3899/08/115010+25$30.00

Nuclear shadowing, intensively investigated during the last two decades, can be treated differently depending on the reference frame. In the infinite momentum frame of the nucleus, it can be interpreted as a result of parton fusion [2–5], leading to a reduction of the parton density at low Bjorken, $x_{\rm Bj}$. In the rest frame of the nucleus, however, this phenomenon looks like nuclear shadowing of the hadronic fluctuations of the virtual photon, and occurs due to their multiple scattering inside the target [6–18]. Although these two physical interpretations are complementary, the one based on the rest frame of the nucleus is more intuitive and straightforward.

The dynamics of nuclear shadowing in DIS is controlled by the effect of quantum coherence, which results from the destructive interference of amplitudes for which the interaction takes place on different bound nucleons. Taking into account the $|\bar{q}q\rangle$ Fock component of the photon, quantum coherence can be characterized by the lifetime of the $\bar{q}q$ fluctuation, which, in turn, can be estimated by relying on the uncertainty principle and Lorentz time dilation as

$$t_c = \frac{2\nu}{Q^2 + M^2_{\bar{q}q}}, \tag{1}$$

where ν is the photon energy, Q^2 is photon virtuality, and $M_{\bar{q}q}$ is the effective mass of the $\bar{q}q$ pair. This is usually called coherence time, but we will also use the term coherence length (CL), since light-cone kinematics is assumed, $l_c = t_c$. The CL is related to the longitudinal momentum transfer by $q_c = 1/l_c$. Note that for higher Fock states containing gluons $|\bar{q}qG\rangle, |\bar{q}q2G\rangle, \ldots$, the corresponding effective masses are larger than $M_{\bar{q}q}$. Consequently, these fluctuations have a shorter coherence time than the lowest $|\bar{q}q\rangle$ state. The effect of CL is naturally incorporated in the Green function formalism, which has already been applied to DIS, Drell–Yan pair production [17–19], and vector meson production [20, 21] (see also the following section).

In the present paper, nuclear shadowing in DIS will be treated using again the Green function approach. Such a quantum mechanical treatment requires us to solve the evolution equation for the Green function. Usually, for simplicity this equation is set up in a such way as to obtain the Green function in an analytical form (see [17, 19], for example), which requires, however, to implement several approximations into a rigorous quantum-mechanical approach, such as a constant nuclear density function (36) and a specific quadratic form (35) of the dipole cross section. The solution obtained in a such way is the harmonic oscillator Green function [22] (see also equation (16)), usually used for the calculation of nuclear shadowing [17, 19, 23]. Then, the question about the accuracy of the predictions for nuclear shadowing using such approximations naturally arises.

In the process of searching for the corresponding answer, in 2003 the evolution equation for the Green function was solved numerically for the first time in [18]. This allowed us to exclude any additional assumptions and avoid supplementary approximations, which caused theoretical uncertainties. The corresponding predictions for nuclear shadowing in DIS at small $x_{\rm Bj}$, based on the exact numerical solution of the evolution equation for the Green function [17, 18], showed quite a large difference in comparison with approximate calculations [19] obtained within the harmonic oscillator Green function approach, in the kinematic region, when $l_c \lesssim R_A$ (R_A is the nuclear radius). However, no comparison with data was performed using this path integral technique based on an exact numerical solution of the two-dimensional Schrödinger equation for the Green function. This is one of the main goals of the present paper. Such a comparison with data provides a better baseline for future studies of the QCD dynamics, not only in DIS off nuclei but

also in further processes occurring in lepton (proton)–nucleus interactions and in heavy-ion collisions.

The calculations of nuclear shadowing in DIS off nuclei presented so far within the light-cone (LC) Green function approach [17–19] were performed assuming only $\bar{q}q$ fluctuations of the photon, and neglecting higher Fock components containing gluons and sea quarks. The effects of higher Fock states are included in the energy dependence of the dipole cross section, $\sigma_{\bar{q}q}(\vec{r}, s)$[5]. However, as soon as nuclear effects are considered, these Fock states $|\bar{q}qG\rangle, |\bar{q}q2G\rangle, \ldots$, lead to gluon shadowing (GS), which, for simplicity, has been neglected so far when the model predictions were compared with experimental data. The contribution of the gluon suppression to nuclear shadowing represents a shadowing correction for the multigluon higher Fock states. It was shown in [24] that GS becomes effective at small $x_{\rm Bj} \lesssim 0.01$. The present available experimental data cover the shadowing region $\sim 0.0001 \lesssim x_{\rm Bj} \lesssim 0.01$, and therefore, the contribution of GS to the overall nuclear shadowing should be included. This is a further goal of the present paper.

Different (but equivalent) descriptions of GS are known, depending on the reference frame. In the infinite momentum frame of the nucleus it looks like fusion of gluons, which overlap in the longitudinal direction at small $x_{\rm Bj}$, leading to a reduction of the gluon density. In the rest frame of the nucleus the same phenomenon looks as a specific part of Gribov's inelastic corrections [25]. The lowest order inelastic correction related to diffractive dissociation $\gamma^* N \to XN$ [26] contains PPR and PPP contributions (in terms of the triple-Regge phenomenology, see [27]). The former is related to quark shadowing, while the latter, the triple-Pomeron term, corresponds to gluon shadowing. Indeed, only diffractive gluon radiation can provide the M_X dependence $\mathrm{d}\sigma_{\rm dd}/\mathrm{d}M_X^2 \propto 1/M_X^2$ of the diffractive dissociation cross section. In terms of the light-cone QCD approach the same process is related to the inclusion of higher Fock components, $|\bar{q}qnG\rangle$, containing gluons [28]. Such fluctuations might be quite heavy compared to the simplest $|\bar{q}q\rangle$ fluctuation, and therefore have a shorter lifetime (see equation (1)), and need higher energies to be relevant.

Calculations of the GS contribution to nuclear suppression have been already performed within the light-cone QCD approach, for both coherent and incoherent productions of vector mesons [20, 21], and also for production of Drell–Yan pairs [17]. They showed (except for the specific case of incoherent production of vector mesons) that GS is a non-negligible effect, especially for heavy nuclear targets at small and medium values of photon virtualities $Q^2 \lesssim$ a few GeV^2 and at large photon energies ν. This is another reason to include the effect of GS for the calculation of nuclear shadowing, especially for making more realistic comparison of the predictions with experimental data.

Note also that by investigating shadowing in the region of small $x_{\rm Bj} \lesssim 0.01$ we can safely omit the nuclear antishadowing effect that assumed to be beyond the shadowing dynamics [8, 9].

The paper is organized as follows. In section 2, we present a short description of the light-cone dipole phenomenology for nuclear shadowing in DIS, together with the Green function formalism. In section 3, we discuss how gluon shadowing modifies the total photoabsorption cross section on a nucleus. In section 4, numerical results are presented and compared with experimental data, and also with the results from other models, in a broad range of $x_{\rm Bj}$. Finally, in section 5, we summarize our main results and discuss the possibility of future experimental evidence of the GS contribution to the overall nuclear shadowing in DIS at small values of $x_{\rm Bj}$.

[5] Here $\vec{r}$ represents the transverse separation of the $\bar{q}q$ photon fluctuation, and s is the center-of-mass energy squared.

2. Light-cone dipole approach to nuclear shadowing

In the rest frame of the nucleus the nuclear shadowing in the total virtual photoabsorption cross section $\sigma_{\rm tot}^{\gamma^* A}(x_{\rm Bj}, Q^2)$ (or in the structure function $F_2^A(x_{\rm Bj}, Q^2)$) can be decomposed over different Fock components of the virtual photon. Then the total photoabsorption cross section on a nucleus can be formally represented in the form

$$\sigma_{\rm tot}^{\gamma^* A}(x_{\rm Bj}, Q^2) = A\sigma_{\rm tot}^{\gamma^* N}(x_{\rm Bj}, Q^2) - \Delta\sigma_{\rm tot}(x_{\rm Bj}, Q^2), \tag{2}$$

where

$$\Delta\sigma_{\rm tot}(x_{\rm Bj}, Q^2) = \Delta\sigma_{\rm tot}(\bar{q}q) + \Delta\sigma_{\rm tot}(\bar{q}qG) + \Delta\sigma_{\rm tot}(\bar{q}q2G) + \cdots. \tag{3}$$

Here the Bjorken variable $x_{\rm Bj}$ is given by

$$x_{\rm Bj} = \frac{Q^2}{2m_N\nu} \approx \frac{Q^2}{Q^2 + s}, \tag{4}$$

where s is the γ^*-nucleon center-of-mass (cm) energy squared, m_N is the mass of the nucleon, and $\sigma_{\rm tot}^{\gamma^* N}(x_{\rm Bj}, Q^2)$ in (2) is the total photoabsorption cross section on a nucleon:

$$\sigma_{\rm tot}^{\gamma^* N}(x_{\rm Bj}, Q^2) = \int {\rm d}^2 r \int_0^1 {\rm d}\alpha |\Psi_{\bar{q}q}(\vec{r}, \alpha, Q^2)|^2 \sigma_{\bar{q}q}(\vec{r}, s). \tag{5}$$

In this last expression, $\sigma_{\bar{q}q}(\vec{r}, s)$ is the dipole cross section, which depends on the $\bar{q}q$ transverse separation $\vec{r}$ and the cm energy squared s, and $\Psi_{\bar{q}q}(\vec{r}, \alpha, Q^2)$ is the LC wavefunction of the $\bar{q}q$ Fock component of the photon, which depends also on the photon virtuality Q^2 and the relative share α of the photon momentum carried by the quark. Note that $x_{\rm Bj}$ is related to the cm energy squared s via equation (4). Consequently, hereafter we will write the energy dependence of variables in subsequent formulae also via an $x_{\rm Bj}$-dependence, whenever convenient.

The total photoabsorption cross section on a nucleon target (5) contains two ingredients. The first ingredient is given by the dipole cross section $\sigma_{\bar{q}q}(\vec{r}, s)$, representing the interaction of a $\bar{q}q$ dipole of transverse separation $\vec{r}$ with a nucleon [29]. It is a flavor-independent universal function of $\vec{r}$ and energy, and allows us to describe various high-energy processes in an uniform way. It is also known to vanish quadratically, $\sigma_{\bar{q}q}(r, s) \propto r^2$ as $r \to 0$, due to color screening (property of color transparency [29–31]), and cannot be predicted reliably because of poorly known higher order perturbative QCD (pQCD) corrections and nonperturbative effects. However, it can be extracted from experimental data on DIS and structure functions using reasonable parametrizations, and in this case pQCD corrections and nonperturbative effects are naturally included in $\sigma_{\bar{q}q}(r, s)$.

There are two popular parameterizations of $\sigma_{\bar{q}q}(\vec{r}, s)$: GBW presented in [32], and KST proposed in [24]. Detailed discussions and comparison of these two parametrizations can be found in [18, 20, 23]. Whereas the GBW parametrization cannot be applied in the nonperturbative region of Q^2, the KST parametrization gives a good description of the transition down to the limit of real photoproduction, $Q^2 = 0$. Because we will study the shadowing region of small $x_{\rm Bj} \lesssim 0.01$, where available experimental data from the E665 and NMC collaborations cover small and moderate values of $Q^2 \lesssim 2 \div 3$ GeV^2, we will prefer the latter parametrization.

The KST parametrization [24] has the following form, which contains an explicit dependence on energy:

$$\sigma_{\bar{q}q}(r, s) = \sigma_0(s)\left[1 - \exp\left(-\frac{r^2}{R_0^2(s)}\right)\right]. \tag{6}$$

The explicit energy dependence in the parameter $\sigma_0(s)$ is introduced in a such way that it guarantees that the correct hadronic cross sections is reproduced:

$$\sigma_0(s) = \sigma_{\rm tot}^{\pi p}(s)\left(1 + \frac{3R_0^2(s)}{8\langle r_{\rm ch}^2\rangle_\pi}\right), \tag{7}$$

where $\sigma_{\rm tot}^{\pi p}(s) = 23.6(s/s_0)^{0.079} + 1.432(s/s_0)^{-0.45}$ mb, which contains the Pomeron and Reggeon parts of the πp total cross section [33], and $R_0(s) = 0.88(s/s_0)^{-\lambda/2}$ fm, with $\lambda = 0.28$, and where $s_0 = 1000$ GeV^2 is the energy-dependent radius. In equation (7), $\langle r_{\rm ch}^2\rangle_\pi = 0.44$ fm^2 is the mean pion charge radius squared. The form of equation (6) successfully describes the data for DIS at small $x_{\rm Bj}$ only up to $Q^2 \approx 10$ GeV^2. Nevertheless, this interval of Q^2 is sufficient for the purpose of the present paper, which is focused on the study of nuclear shadowing at small $x_{\rm Bj} \lesssim 0.01$ in the kinematic range, $Q^2 \lesssim 4$ GeV^2, covered by the available E665 and NMC data.

However, as we will present the predictions for nuclear shadowing at very small $x_{\rm Bj}$ down to 10^{-7} accesible by the prepared experiments at LHC and at larger values of $Q^2 \gtrsim 10$ GeV^2, we will also use the second GBW parametrization [32] of the dipole cross section.

The second ingredient of $\sigma_{\rm tot}^{\gamma^* N}(x_{\rm Bj}, Q^2)$ in (5) is the perturbative distribution amplitude ('wavefunction') of the $\bar{q}q$ Fock component of the photon. For transversely (T) and longitudinally (L) polarized photons it has the form [34, 35, 10]

$$\Psi_{\bar{q}q}^{T,L}(\vec{r}, \alpha, Q^2) = \frac{\sqrt{N_C\alpha_{\rm em}}}{2\pi} Z_q \bar{\chi}\hat{O}^{T,L}\chi K_0(\epsilon r), \tag{8}$$

where χ and $\bar{\chi}$ are the spinors of the quark and antiquark respectively, Z_q is the quark charge, $N_C = 3$ is the number of colors, and $K_0(\epsilon r)$ is a modified Bessel function with

$$\epsilon^2 = \alpha(1-\alpha)Q^2 + m_q^2, \tag{9}$$

where m_q is the quark mass. The operators $\widehat{O}^{T,L}$ read

$$\widehat{O}^T = m_q\vec{\sigma}\cdot\vec{e} + {\rm i}(1-2\alpha)(\vec{\sigma}\cdot\vec{n})(\vec{e}\cdot\vec{\nabla}_r) + (\vec{\sigma}\times\vec{e})\cdot\vec{\nabla}_r, \tag{10}$$

$$\widehat{O}^L = 2Q\alpha(1-\alpha)(\vec{\sigma}\cdot\vec{n}). \tag{11}$$

Here $\vec{\nabla}_r$ acts on the transverse coordinate $\vec{r}$, $\vec{e}$ is the polarization vector of the photon, $\vec{n}$ is a unit vector parallel to the photon momentum, and $\vec{\sigma}$ is the 3-vector of the Pauli spin-matrices.

The distribution amplitude equation (8) controls the transverse $\bar{q}q$ separation with the mean value

$$\langle r\rangle \sim \frac{1}{\epsilon} = \frac{1}{\sqrt{Q^2\alpha(1-\alpha)+m_q^2}}. \tag{12}$$

For very asymmetric $\bar{q}q$ pairs with α or $(1-\alpha) \lesssim m_q^2/Q^2$ the mean transverse separation $\langle r\rangle \sim 1/m_q$ becomes huge, since one must use current quark masses within pQCD. A popular recipe to fix this problem is to introduce an effective quark mass, $m_{\rm eff} \sim \Lambda_{\rm QCD}$, which represents the nonperturbative interaction effects between q and $\bar{q}$. It is more consistent and straightforward, however, to introduce this interaction explicitly through a phenomenology based on the light-cone Green function approach, and which has been developed in [24].

The Green function $G_{\bar{q}q}(\vec{r}_2, z_2; \vec{r}_1, z_1)$ describes the propagation of an interacting $\bar{q}q$ pair between points with longitudinal coordinates z_1 and z_2 and with initial and final separations $\vec{r}_1$ and $\vec{r}_2$. This Green function satisfies the two-dimensional Schrödinger equation:

$${\rm i}\frac{\rm d}{{\rm d}z_2}G_{\bar{q}q}(\vec{r}_2, z_2; \vec{r}_1, z_1) = \left[\frac{\epsilon^2 - \Delta_{r_2}}{2\nu\alpha(1-\alpha)} + V_{\bar{q}q}(z_2, \vec{r}_2, \alpha)\right] G_{\bar{q}q}(\vec{r}_2, z_2; \vec{r}_1, z_1), \tag{13}$$

with the boundary condition

$$G_{\bar{q}q}(\vec{r}_2, z_2; \vec{r}_1, z_1)|_{z_2=z_1} = \delta^2(\vec{r}_1 - \vec{r}_2). \tag{14}$$

In equation (13) ν is the photon energy, and the Laplacian Δ_r acts on the coordinate r.

We start with the propagation of a $\bar{q}q$ pair in vacuum. The LC potential $V_{\bar{q}q}(z_2, \vec{r}_2, \alpha)$ in (13) contains only the real part, which is responsible for the interaction between q and $\bar{q}$. For the sake of simplicity we use an oscillator form of this potential. Although more realistic models for the real part of the potential are available [36, 37], however, the solution of the corresponding Schrödinger equation for the light-cone Green function is a challenge. The analytic solution has been known so far only for the oscillator potential. Otherwise one has to solve the Schrödinger equation numerically, which needs a dedicated study.

On the other hand, the mean $\bar{q}q$ transverse separation which is fitted to diffraction data is important. Any form of the potential must comply with this condition. The same restriction is imposed on the quark–gluon Fock states. The mean quark–gluon separation, which matters for shadowing, is fixed by high-mass diffraction data and should not be much affected by the choice of a model for the potential:

$$\mathrm{Re}\, V_{\bar{q}q}(z_2, \vec{r}_2, \alpha) = \frac{a^4(\alpha)\vec{r}_2^{\,2}}{2\nu\alpha(1-\alpha)}. \tag{15}$$

Then, one can solve the two-dimensional Schrödinger equation (13) analytically, and the solution is given by the harmonic oscillator Green function [38]:

$$G_{\bar{q}q}(\vec{r}_2, z_2; \vec{r}_1, z_1) = \frac{a^2(\alpha)}{2\pi \mathrm{i}\sin(\omega\Delta z)} \exp\left\{\frac{\mathrm{i}a^2(\alpha)}{\sin(\omega\Delta z)}\left[\left(r_1^2 + r_2^2\right)\cos(\omega\Delta z) - 2\vec{r}_1\cdot\vec{r}_2\right]\right\}$$
$$\times \exp\left[-\frac{\mathrm{i}\epsilon^2\Delta z}{2\nu\alpha(1-\alpha)}\right], \tag{16}$$

where $\Delta z = z_2 - z_1$, and

$$\omega = \frac{a^2(\alpha)}{\nu\alpha(1-\alpha)}. \tag{17}$$

The shape of the function $a(\alpha)$ in equation (15) will be discussed below.

The probability amplitude to find the $\bar{q}q$ fluctuation of a photon at the point z_2, with separation $\vec{r}$, is given by an integral over the point z_1, where the $\bar{q}q$ is created by the photon with initial separation zero:

$$\Psi^{T,L}_{\bar{q}q}(\vec{r}, \alpha) = \frac{\mathrm{i}Z_q\sqrt{\alpha_{\mathrm{em}}}}{4\pi E\alpha(1-\alpha)} \int_{-\infty}^{z_2} \mathrm{d}z_1 (\bar{\chi}\widehat{O}^{T,L}\chi) G_{\bar{q}q}(\vec{r}, z_2; \vec{r}_1, z_1)|_{r_1=0}. \tag{18}$$

The operators $\widehat{O}^{T,L}$ are defined by equations (10) and (11), and here they act on the coordinate $\vec{r}_1$.

If we write the transverse part as

$$\bar{\chi}\widehat{O}^T\chi = \bar{\chi}m_c\vec{\sigma}\cdot\vec{e}\chi + \bar{\chi}[\mathrm{i}(1-2\alpha)(\vec{\sigma}\cdot\vec{n})\vec{e} + (\vec{\sigma}\times\vec{e})]\chi\cdot\vec{\nabla}_r = E + \vec{F}\cdot\vec{\nabla}_r, \tag{19}$$

then the distribution functions read

$$\Psi^T_{\bar{q}q}(\vec{r}, \alpha) = Z_q\sqrt{\alpha_{\mathrm{em}}}[E\Phi_0(\epsilon, r, \lambda) + \vec{F}\vec{\Phi}_1(\epsilon, r, \lambda)], \tag{20}$$

$$\Psi^L_{\bar{q}q}(\vec{r}, \alpha) = 2Z_q\sqrt{\alpha_{\mathrm{em}}}Q\alpha(1-\alpha)\bar{\chi}\vec{\sigma}\cdot\vec{n}\chi\Phi_0(\epsilon, r, \lambda), \tag{21}$$

where

$$\lambda = \frac{2a^2(\alpha)}{\epsilon^2}. \tag{22}$$

The functions $\Phi_{0,1}$ in equations (20) and (21) are defined as

$$\Phi_0(\epsilon, r, \lambda) = \frac{1}{4\pi}\int_0^\infty \mathrm{d}t\,\frac{\lambda}{\mathrm{sh}(\lambda t)}\exp\left[-\frac{\lambda\epsilon^2 r^2}{4}\,\mathrm{cth}(\lambda t) - t\right], \tag{23}$$

$$\vec{\Phi}_1(\epsilon, r, \lambda) = \frac{\epsilon^2\vec{r}}{8\pi}\int_0^\infty \mathrm{d}t\left[\frac{\lambda}{\mathrm{sh}(\lambda t)}\right]^2\exp\left[-\frac{\lambda\epsilon^2 r^2}{4}\,\mathrm{cth}(\lambda t) - t\right], \tag{24}$$

where $\mathrm{sh}(x)$ and $\mathrm{cth}(x)$ are the hyperbolic sine and hyperbolic cotangent, respectively.

Note that the $\bar{q}$–q interaction enters in equations (20) and (21) via the parameter λ defined in equation (22). In the limit of vanishing interaction $\lambda \to 0$ (i.e. $Q^2 \to \infty$, α is fixed, $\alpha \neq 0$ or 1) equations (20) and (21) produce the perturbative expressions of equation (8).

With the choice of $a^2(\alpha) \propto \alpha(1-\alpha)$, the end-point behavior of the mean-square interquark separation is $\langle r^2\rangle \propto 1/\alpha(1-\alpha)$, which contradicts the idea of confinement. Following [24], we fix this problem via a simple modification of the LC potential:

$$a^2(\alpha) = a_0^2 + 4a_1^2\alpha(1-\alpha). \tag{25}$$

The parameters a_0 and a_1 were adjusted in [24] to the data on total photoabsorption cross section [39, 40], diffractive photon dissociation and shadowing in nuclear photoabsorption reaction. The results of our calculations vary within only 1% when a_0 and a_1 satisfy the relation

$$\begin{aligned} a_0^2 &= v^{1.15}(0.112)^2\ \mathrm{GeV}^2, \\ a_1^2 &= (1-v)^{1.15}(0.165)^2\ \mathrm{GeV}^2, \end{aligned} \tag{26}$$

where v takes any value, $0 < v < 1$. In view of this insensitivity of the observables we fix the parameters at $v = 1/2$. We checked that this choice does not affect our results beyond a few percent uncertainty.

The matrix element (5) contains the LC wavefunction squared, which has the following form for T and L polarizations, in the limit of vanishing interaction between $\bar{q}$ and q:

$$\left|\Psi^T_{\bar{q}q}(\vec{r}, \alpha, Q^2)\right|^2 = \frac{2N_C\alpha_{\mathrm{em}}}{(2\pi)^2}\sum_{f=1}^{N_f} Z_f^2\left[m_f^2 K_0(\epsilon, r)^2 + [\alpha^2 + (1-\alpha)^2]\epsilon^2 K_1(\epsilon r)^2\right] \tag{27}$$

and

$$\left|\Psi^L_{\bar{q}q}(\vec{r}, \alpha, Q^2)\right|^2 = \frac{8N_C\alpha_{\mathrm{em}}}{(2\pi)^2}\sum_{f=1}^{N_f} Z_f^2 Q^2\alpha^2(1-\alpha)^2 K_0(\epsilon r)^2, \tag{28}$$

where K_1 is the modified Bessel function,

$$K_1(z) = -\frac{\mathrm{d}}{\mathrm{d}z}K_0(z). \tag{29}$$

If one includes the nonperturbative $\bar{q}$–q interaction, the perturbative expressions (27) and (28) should be replaced by

$$\left|\Psi^T_{\mathrm{npt}}(\vec{r}, \alpha, Q^2)\right|^2 = 2N_C\alpha_{\mathrm{em}}\sum_{f=1}^{N_f} Z_f^2\left[m_f^2\Phi_0^2(\epsilon, r, \lambda) + [\alpha^2 + (1-\alpha)^2]|\vec{\Phi}_1(\epsilon, r, \lambda)|^2\right] \tag{30}$$

and

$$\left|\Psi^L_{\mathrm{npt}}(\vec{r}, \alpha, Q^2)\right|^2 = 8N_C\alpha_{\mathrm{em}}\sum_{f=1}^{N_f} Z_f^2 Q^2\alpha^2(1-\alpha)^2\Phi_0^2(\epsilon, r, \lambda). \tag{31}$$

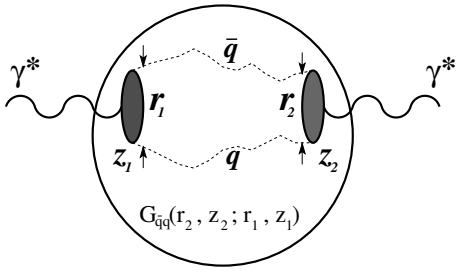

Figure 1. A cartoon for the shadowing term $\Delta\sigma_{\rm tot}(x_{\rm Bj}, Q^2) = \Delta\sigma_{\rm tot}(\bar{q}q)$ in (2). Propagation of the $\bar{q}q$ pair through the nucleus is described by the Green function $G_{\bar{q}q}(\vec{r}_2, z_2; \vec{r}_1, z_1)$, which results from the summation over different paths of the $\bar{q}q$ pair.

Note that in the LC formalism the photon wavefunction contains also higher Fock states $|\bar{q}q\rangle$, $|\bar{q}qG\rangle$, $|\bar{q}q2G\rangle$, etc, but its effect can be implicitly incorporated into the energy dependence of the dipole cross section $\sigma_{\bar{q}q}(\vec{r}, s)$, as is given in equation (5). The energy dependence of the dipole cross section is naturally included in the realistic KST parametrization of equation (6).

Now we will continue with our discussion of DIS on nuclear targets, and will study the propagation of a $\bar{q}q$ pair in nuclear matter. Some work has already been done in this direction. In fact, the derivation of the formula for nuclear shadowing, keeping only the first shadowing term in equation (2), $\Delta\sigma_{\rm tot}(x_{\rm Bj}, Q^2) = \Delta\sigma_{\rm tot}(\bar{q}q)$, can be found in [41]. This term represents the shadowing correction for the lowest $\bar{q}q$ Fock state, and has the following form:

$$\Delta\sigma_{\rm tot}(x_{\rm Bj}, Q^2) = \frac{1}{2}\,{\rm Re}\int {\rm d}^2b \int_{-\infty}^{\infty} {\rm d}z_1\, \rho_A(b, z_1) \int_{z_1}^{\infty} {\rm d}z_2\, \rho_A(b, z_2) \int_0^1 {\rm d}\alpha\, A(z_1, z_2, \alpha), \qquad (32)$$

with

$$A(z_1, z_2, \alpha) = \int {\rm d}^2r_2\, \Psi^*_{\bar{q}q}(\vec{r}_2, \alpha, Q^2)\sigma_{\bar{q}q}(r_2, s) \times \int {\rm d}^2r_1\, G_{\bar{q}q}(\vec{r}_2, z_2; \vec{r}_1, z_1)\sigma_{\bar{q}q}(r_1, s)\Psi_{\bar{q}q}(\vec{r}_1, \alpha, Q^2). \qquad (33)$$

When nonpertubative interaction effects between $\bar{q}$ and q are explicitly included, one should replace in equation (33) $\Psi_{\bar{q}q}(\vec{r}, \alpha, Q^2) \Longrightarrow \Psi_{\rm npt}(\vec{r}, \alpha, Q^2)$ and $\Psi^*_{\bar{q}q}(\vec{r}, \alpha, Q^2) \Longrightarrow \Psi^*_{\rm npt}(\vec{r}, \alpha, Q^2)$.

In equation (32), $\rho_A(b, z)$ represents the nuclear density function defined at the point with longitudinal coordinate z and impact parameter $\vec{b}$.

The shadowing term $\Delta\sigma_{\rm tot}(x_{\rm Bj}, Q^2) = \Delta\sigma_{\rm tot}(\bar{q}q)$ in (2) is illustrated in figure 1. At the point z_1, the initial photon diffractively produces the $\bar{q}q$ pair ($\gamma^*N \to \bar{q}qN$) with transverse separation $\vec{r}_1$. The $\bar{q}q$ pair then propagates through the nucleus along arbitrary curved trajectories, which are summed over, and arrives at the point z_2 with transverse separation $\vec{r}_2$. The initial and final separations are controlled by the LC wavefunction of the $\bar{q}q$ Fock component of the photon $\Psi_{\bar{q}q}(\vec{r}, \alpha, Q^2)$. During propagation through the nucleus the $\bar{q}q$ pair interacts with bound nucleons via the dipole cross section $\sigma_{\bar{q}q}(r, s)$, which depends on the local transverse separation $\vec{r}$. The Green function $G_{\bar{q}q}(\vec{r}_2, z_2; \vec{r}_1, z_1)$ describes the propagation of the $\bar{q}q$ pair from z_1 to z_2.

Describing the propagation of the $\bar{q}q$ pair in a nuclear medium, the Green function $G_{\bar{q}q}(\vec{r}_2, z_2; \vec{r}_1, z_1)$ satisfies again the time-dependent two-dimensional Schrödinger

equation (13). However, the potential in this case acquires in addition an imaginary part. This imaginary part of the LC potential $V_{\bar{q}q}(z_2, \vec{r}_2, \alpha)$ in equation (13) is responsible for the attenuation of the $\bar{q}q$ photon fluctuation in the medium, and has the following form:

$$\mathrm{Im}V_{\bar{q}q}(z_2, \vec{r}, \alpha) = -\frac{\sigma_{\bar{q}q}(\vec{r}, s)}{2}\rho_A(b, z_2). \tag{34}$$

As was already mentioned above, the analytical solution of equation (13) is known only for the harmonic oscillator potential $V_{\bar{q}q}(r) \propto r^2$. Consequently, in order to keep such an analytical solution one should also use a quadratic approximation for the imaginary part of $V_{\bar{q}q}(z_2, \vec{r}_2, \alpha)$, i.e.,

$$\sigma_{\bar{q}q}(r, s) = C(s)r^2 \tag{35}$$

and uniform nuclear density

$$\rho_A(b, z) = \rho_0\Theta\big(R_A^2 - b^2 - z^2\big). \tag{36}$$

In this case, the solution of equation (13) has the same form as equation (16), except that one should replace $\omega \Longrightarrow \Omega$ and $a^2(\alpha) \Longrightarrow b(\alpha)$, where

$$\Omega = \frac{b(\alpha)}{\nu\alpha(1-\alpha)} = \frac{\sqrt{a^4(\alpha) - \mathrm{i}\rho_A(b, z)\nu\alpha(1-\alpha)C(s)}}{\nu\alpha(1-\alpha)}. \tag{37}$$

The determination of the energy-dependent factor $C(s)$ in equation (35) and the mean nuclear density ρ_0 in equation (36) can be realized by the procedure described in [17, 18, 23], and will be discussed below.

Investigating nuclear shadowing in DIS one can distinguish between two regimes, depending on the value of the coherence length:

(i) We start with the general case when there are no restrictions for l_c. If $l_c \sim R_A$ one has to take into account the variation of the transverse size r during propagation of the $\bar{q}q$ pair through the nucleus, which is naturally included using a correct quantum-mechanical treatment based on the Green function formalism presented above. The overall total photoabsorption cross section on a nucleus is given as a sum over T and L polarizations, $\sigma^{\gamma^* A} = \sigma_T^{\gamma^* A} + \epsilon'\sigma_L^{\gamma^* A}$, assuming that the photon polarization $\epsilon' = 1$. If one takes into account only the $\bar{q}q$ Fock component of the photon, the full expression after summation over all flavors, colors, helicities and spin states becomes [42]

$$\begin{aligned}
\sigma^{\gamma^* A}(x_{\mathrm{Bj}}, Q^2) &= A\sigma^{\gamma^* N}(x_{\mathrm{Bj}}, Q^2) - \Delta\sigma(x_{\mathrm{Bj}}, Q^2) \\
&= A\int \mathrm{d}^2 r \int_0^1 \mathrm{d}\alpha\, \sigma_{\bar{q}q}(r, s)\Big(\big|\Psi_{\bar{q}q}^T(\vec{r}, \alpha, Q^2)\big|^2 + \big|\Psi_{\bar{q}q}^L(\vec{r}, \alpha, Q^2)\big|^2\Big) \\
&\quad - \frac{N_C\alpha_{\mathrm{em}}}{(2\pi)^2}\sum_{f=1}^{N_f} Z_f^2\,\mathrm{Re}\int \mathrm{d}^2 b \int_{-\infty}^{\infty}\mathrm{d}z_1 \int_{z_1}^{\infty}\mathrm{d}z_2 \int_0^1 \mathrm{d}\alpha \int \mathrm{d}^2 r_1 \int \mathrm{d}^2 r_2 \\
&\quad \times \rho_A(b, z_1)\rho_A(b, z_2)\sigma_{\bar{q}q}(r_2, s)\sigma_{\bar{q}q}(r_1, s) \\
&\quad \times \Big\{[\alpha^2 + (1-\alpha)^2]\epsilon^2\frac{\vec{r}_1\cdot\vec{r}_2}{r_1 r_2}K_1(\epsilon r_1)K_1(\epsilon r_2) \\
&\quad + \big[m_f^2 + 4Q^2\alpha^2(1-\alpha)^2\big]K_0(\epsilon r_1)K_0(\epsilon r_2)\Big\}G_{\bar{q}q}(\vec{r}_2, z_2; \vec{r}_1, z_1)
\end{aligned} \tag{38}$$

Here, $\big|\Psi_{\bar{q}q}^{T,L}(\vec{r}, \alpha, Q^2)\big|^2$ are the absolute squares of the LC wavefunctions for the $\bar{q}q$ fluctuation of T and L polarized photons, summed over all flavors, and with the form given by equations (27) and (28), respectively.

If one takes into account the nonperturbative interaction effects between $\bar{q}$ and q of the virtual photon the expression for $\sigma^{\gamma^* A}(x_{\rm Bj}, Q^2)$ equation (38) takes the following form:

$$\begin{aligned}\sigma_{\rm npt}^{\gamma^* A}(x_{\rm Bj}, Q^2) &= A\sigma_{\rm npt}^{\gamma^* N}(x_{\rm Bj}, Q^2) - \Delta\sigma_{\rm npt}(x_{\rm Bj}, Q^2)\\ &= A\int {\rm d}^2 r \int_0^1 {\rm d}\alpha\, \sigma_{\bar{q}q}(r,s)\left(\left|\Psi_{\rm npt}^T(\vec{r},\alpha,Q^2)\right|^2 + \left|\Psi_{\rm npt}^L(\vec{r},\alpha,Q^2)\right|^2\right)\\ &\quad - N_C\alpha_{\rm em}\sum_{f=1}^{N_f} Z_f^2\,{\rm Re}\int {\rm d}^2 b\int_{-\infty}^{\infty}{\rm d}z_1\int_{z_1}^{\infty}{\rm d}z_2\int_0^1{\rm d}\alpha\int {\rm d}^2 r_1\int {\rm d}^2 r_2\\ &\quad \times \rho_A(b,z_1)\rho_A(b,z_2)\sigma_{\bar{q}q}(r_2,s)\sigma_{\bar{q}q}(r_1,s)\\ &\quad \times\left\{[\alpha^2+(1-\alpha)^2]\vec{\Phi}_1(\epsilon,r_1,\lambda)\cdot\vec{\Phi}_1(\epsilon,r_2,\lambda)\right.\\ &\quad \left.+\left[m_f^2+4Q^2\alpha^2(1-\alpha)^2\right]\Phi_0(\epsilon,r_1,\lambda)\Phi_0(\epsilon,r_2,\lambda)\right\}G_{\bar{q}q}(\vec{r}_2,z_2;\vec{r}_1,z_1)\end{aligned} \tag{39}$$

where $\left|\Psi_{\rm npt}^{T,L}(\vec{r},\alpha,Q^2)\right|^2$ is now given by equations (30) and (31), respectively.

(ii) The CL is much larger than the mean nucleon spacing in a nucleus ($l_c \gg R_A$), which is the high-energy limit. Correspondingly, the transverse separation r between $\bar{q}$ and q does not vary during propagation through the nucleus (Lorentz time dilation). In this case, the eikonal formula for the total photoabsorption cross section on a nucleus can be obtained as a limiting case of the Green function formalism. Indeed, in the high-energy limit $\nu\to\infty$, the kinetic term in equation (13) can be neglected, and the Green function reads

$$G_{\bar{q}q}(b;\vec{r}_2,z_2;\vec{r}_1,z_1)|_{\nu\to\infty} = \delta(\vec{r}_2-\vec{r}_1)\exp\left[-\frac{1}{2}\sigma_{\bar{q}q}(r_2,s)\int_{z_1}^{z_2}{\rm d}z\rho_A(b,z)\right] \tag{40}$$

Including nonperturbative interaction effects between $\bar{q}$ and q, after substitution of expression (40) into equation (39), one arrives at the following results:

$$\begin{aligned}\sigma_{\rm npt}^{\gamma^* A}(x_{\rm Bj}, Q^2) &= 2\int {\rm d}^2 b\int {\rm d}^2 r\int_0^1 {\rm d}\alpha\left\{1-\exp\left[-\frac{1}{2}\sigma_{\bar{q}q}(r,s)T_A(b)\right]\right\}\\ &\quad \times 2N_C\alpha_{\rm em}\sum_{f=1}^{N_f} Z_f^2\left\{[\alpha^2+(1-\alpha)^2]|\vec{\Phi}_1(\epsilon,r,\lambda)|^2\right.\\ &\quad \left.+\left[m_f^2+4Q^2\alpha^2(1-\alpha)^2\right]\Phi_0^2(\epsilon,r,\lambda)\right\},\end{aligned}$$

where

$$T_A(b) = \int_{-\infty}^{\infty}{\rm d}z\rho_A(b,z) \tag{42}$$

is the nuclear thickness calculated with the realistic Wood–Saxon form of the nuclear density, with parameters taken from [43].

At the photon polarization parameter $\epsilon' = 1$ the structure function ratio F_2^A/F_2^N is related to nuclear shadowing $R(A/N$, and can be expressed via a ratio of the total photoabsorption cross sections,

$$\frac{F_2^A(x_{\rm Bj},Q^2)}{F_2^N(x_{\rm Bj},Q^2)} = AR(A/N) = \frac{\sigma_T^{\gamma^* A}(x_{\rm Bj},Q^2)+\sigma_L^{\gamma^* A}(x_{\rm Bj},Q^2)}{\sigma_T^{\gamma^* N}(x_{\rm Bj},Q^2)+\sigma_L^{\gamma^* N}(x_{\rm Bj},Q^2)}, \tag{43}$$

where the numerator on the right-hand side (rhs) is given by equation (39), whereas the denominator can be expressed as the first term of equation (39) divided by the mass number A.

As already mentioned above, an explicit analytical expression for the Green function $G_{\bar{q}q}(\vec{r}_2, z_2; \vec{r}_1, z_1)$ (16) can be found only for the quadratic form of the dipole cross section (35), and for uniform nuclear density function (36). It was shown in [17–19, 23] that such an approximation gives results of reasonable accuracy, especially at small $x_{\rm Bj} \lesssim 10^{-4}$ and for heavy nuclei. Nevertheless, it can be even more precise if one considers the fact that expression (41) in the high-energy limit can be easily calculated using realistic parametrizations of the dipole cross section (see equation (6) for the KST parametrization and [32] for the GBW parametrization) and a realistic nuclear density function $\rho_A(b, z)$ [43]. Consequently, one needs to know the full Green function only in the transition region from non-shadowing ($x_{\rm Bj} \sim 0.1$) to a fully developed shadowing given when coherence length $l_c \gg R_A$, which corresponds to $x_{\rm Bj} \lesssim 10^{-4}$ depending on the value of Q^2. Therefore, the value of the energy-dependent factor, $C(s)$, in equation (35) can be determined by the procedure described in [17, 23, 20]. According to this procedure, the factor $C(s)$ is adjusted by demanding that calculations employing the approximation (35) reproduce correctly the results for nuclear shadowing in DIS based on the realistic parametrizations of the dipole cross section equation (6) in the limit $l_c \gg R_A$, when the Green function takes the simple form (40). Consequently, the factor $C(s)$ is fixed by the relation

$$\frac{\int \mathrm{d}^2b \int \mathrm{d}^2r |\Psi_{\bar{q}q}(\vec{r}, \alpha, Q^2)|^2 \left\{1 - \exp\left[-\frac{1}{2}C(s)r^2 T_A(b)\right]\right\}}{\int \mathrm{d}^2r |\Psi_{\bar{q}q}(\vec{r}, \alpha, Q^2)|^2 C(s) r^2} = \frac{\int \mathrm{d}^2b \int \mathrm{d}^2r |\Psi_{\bar{q}q}(\vec{r}, \alpha, Q^2)|^2 \left\{1 - \exp\left[-\frac{1}{2}\sigma_{\bar{q}q}(r, s)T_A(b)\right]\right\}}{\int \mathrm{d}^2r |\Psi_{\bar{q}q}(\vec{r}, \alpha, Q^2)|^2 \sigma_{\bar{q}q}(r, s)}. \tag{44}$$

Correspondingly, the value ρ_0 of the uniform nuclear density (36) is fixed in an analogous way using the following relation:

$$\int \mathrm{d}^2b \left[1 - \exp\left(-\sigma_0 \rho_0 \sqrt{R_A^2 - b^2}\right)\right] = \int \mathrm{d}^2b \left[1 - \exp\left(-\frac{1}{2}\sigma_0 T_A(b)\right)\right], \tag{45}$$

where the value of ρ_0 was found to be practically independent of the cross section σ_0, when this changed from 1 to 50 mb [17, 23]. Such a procedure for the determination of the factors $C(s)$ and ρ_0 was applied also in [20, 21], in the case of incoherent and coherent production of vector mesons off nuclei.

In order to remove the above-mentioned uncertainties, the evolution equation for the Green function was solved numerically for the first time in [18]. Such an exact solution can be performed for arbitrary parametrization of the dipole cross section and for realistic nuclear density functions, although a nice analytical form for the Green function is lost in this case.

In the process of numerical solution of the Schrödinger equation (13) for the Green function $G_{\bar{q}q}(\vec{r}_2, z_2; \vec{r}_1, z_1)$ with the initial condition (14), it is much more convenient to use the following substitutions [18]:

$$g_0(\vec{r}_2, z_2; z_1, \lambda) = \int \mathrm{d}^2r_1 \, \Phi_0(\epsilon, r_1, \lambda) \sigma_{\bar{q}q}(r_1, s) G_{\bar{q}q}(\vec{r}_2, z_2; \vec{r}_1, z_1), \tag{46}$$

and

$$\frac{\vec{r}_2}{r_2} g_1(\vec{r}_2, z_2; z_1, \lambda) = \int \mathrm{d}^2r_1 \, \vec{\Phi}_1(\epsilon, r_1, \lambda) \sigma_{\bar{q}q}(r_1, s) G_{\bar{q}q}(\vec{r}_2, z_2; \vec{r}_1, z_1). \tag{47}$$

After some algebra with equation (13) these new functions $g_0(\vec{r}_2, z_2; z_1, \lambda)$ and $g_1(\vec{r}_2, z_2; z_1, \lambda)$ can be shown to satisfy the following evolution equations:

$$\mathrm{i}\frac{\mathrm{d}}{\mathrm{d}z_2} g_0(\vec{r}_2, z_2; z_1, \lambda) = \left\{\frac{1}{2\mu_{\bar{q}q}}\left[\epsilon^2 - \frac{\partial^2}{\partial r_2^2} - \frac{1}{r_2}\frac{\partial}{\partial r_2}\right] + V_{\bar{q}q}(z_2, \vec{r}_2, \alpha)\right\} g_0(\vec{r}_2, z_2; z_1, \lambda) \tag{48}$$

and

$$\mathrm{i}\frac{\mathrm{d}}{\mathrm{d}z_2}g_1(\vec{r}_2, z_2; z_1, \lambda) = \left\{\frac{1}{2\mu_{\bar{q}q}}\left[\epsilon^2 - \frac{\partial^2}{\partial r_2^2} - \frac{1}{r_2}\frac{\partial}{\partial r_2} + \frac{1}{r_2^2}\right] + V_{\bar{q}q}(z_2, \vec{r}_2, \alpha)\right\} g_1(\vec{r}_2, z_2; z_1, \lambda), \tag{49}$$

with the boundary conditions

$$g_0(\vec{r}_2, z_2; z_1, \lambda)|_{z_2=z_1} = \Phi_0(\epsilon, r_2, \lambda)\sigma_{\bar{q}q}(r_2, s) \tag{50}$$

and

$$g_1(\vec{r}_2, z_2; z_1, \lambda)|_{z_2=z_1} = \tilde{\Phi}_1(\epsilon, r_2, \lambda)\sigma_{\bar{q}q}(r_2, s), \tag{51}$$

where $\tilde{\Phi}_1(\epsilon, r, \lambda)$ is connected with $\vec{\Phi}_1(\epsilon, r, \lambda)$ by the following relation:

$$\vec{\Phi}_1(\epsilon, r, \lambda) = \frac{\vec{r}}{r}\tilde{\Phi}_1(\epsilon, r, \lambda). \tag{52}$$

In equations (48) and (49), the quantity,

$$\mu_{\bar{q}q} = \nu\alpha(1-\alpha), \tag{53}$$

plays the role of the reduced mass of the $\bar{q}q$ pair.

Now expression (39) for total photoabsorption cross section on a nucleus reads

$$\begin{aligned}\sigma_{\mathrm{npt}}^{\gamma^* A}(x_{\mathrm{Bj}}, Q^2) &= A\sigma_{\mathrm{npt}}^{\gamma^* N}(x_{\mathrm{Bj}}, Q^2) - \Delta\sigma(x_{\mathrm{Bj}}, Q^2)\\ &= A\int \mathrm{d}^2 r \int_0^1 \mathrm{d}\alpha\, \sigma_{\bar{q}q}(r, s)\left(\left|\Psi_{\mathrm{npt}}^T(\vec{r}, \alpha, Q^2)\right|^2 + \left|\Psi_{\mathrm{npt}}^L(\vec{r}, \alpha, Q^2)\right|^2\right)\\ &\quad - 3\alpha_{\mathrm{em}}\sum_{f=1}^{N_f} Z_f^2\,\mathrm{Re}\int \mathrm{d}^2 b \int_{-\infty}^{\infty}\mathrm{d}z_1\int_{z_1}^{\infty}\mathrm{d}z_2\int_0^1\mathrm{d}\alpha\int \mathrm{d}^2 r_2\\ &\quad \times \rho_A(b, z_1)\rho_A(b, z_2)\sigma_{\bar{q}q}(r_2, s)\\ &\quad \times \left\{[\alpha^2 + (1-\alpha)^2]\tilde{\Phi}_1(\epsilon, r_2, \lambda)g_1(\vec{r}_2, z_2; z_1, \lambda)\right.\\ &\quad \left. + \left[m_f^2 + 4Q^2\alpha^2(1-\alpha)^2\right]\Phi_0(\epsilon, r_2, \lambda)g_0(\vec{r}_2, z_2; z_1, \lambda)\right\}\end{aligned} \tag{54}$$

Note that this equation explicitly includes nonperturbative interaction effects between $\bar{q}$ and q. Details of the algorithm for the numerical solution of equations (48) and (49) can be found in [18].

Finally, we would like to emphasize that the $\bar{q}q$ Fock component of the photon represents the highest twist shadowing correction [17], and vanishes at large quark masses as $1/m_f^2$. This does not happen for higher Fock states containing gluons, which lead to GS. Therefore GS represents the leading twist shadowing correction [24, 44]. Moreover, a steep energy dependence of the dipole cross section $\sigma_{\bar{q}q}(r, s)$ (see equation (6)) especially at smaller dipole sizes r causes a steep energy rise in both corrections.

3. Gluon shadowing

In the LC Green function approach [17–21], the physical photon $|\gamma^*\rangle$ is decomposed into different Fock states, namely, the bare photon $|\gamma^*\rangle_0$, plus $|\bar{q}q\rangle$, $|\bar{q}qG\rangle$, etc. As mentioned above, the higher Fock states containing gluons describe the energy dependence of the photoabsorption cross section on a nucleon, and also lead to GS in the nuclear case. However, these fluctuations are heavier and have a shorter coherence time (lifetime) than the lowest $|\bar{q}q\rangle$ state, and therefore at small and medium energies only the $|\bar{q}q\rangle$ fluctuations of the photon

matter. Consequently, GS, which is related to the higher Fock states, will dominate at higher energies, i.e. at small values of $x_{\rm Bj} \lesssim 0.01$. Since we will study the shadowing region of $x_{\rm Bj} \lesssim 0.01$ and the available experimental data reach values of $x_{\rm Bj}$ down to $\sim 10^{-4}$, we will include GS in our calculations and show that it is not a negligible effect. Besides, no data for gluon shadowing are available, and one has to rely on calculations.

In the previous section, we discussed the nuclear shadowing for the $|\bar{q}q\rangle$ Fock component of the photon. It is dominated by the transverse photon polarizations, because the corresponding photoabsorption cross section is scanned at larger dipole sizes than for the longitudinal photon polarization. The transverse $\bar{q}q$ separation is controlled by the distribution amplitude equation (8), with the mean value given by equation (12). Contributions of large size dipoles come from the asymmetric $\bar{q}q$ fluctuations of the virtual photon, when the quark and antiquark in the photon carry a very large ($\alpha \to 1$) and a very small fraction ($\alpha \to 0$) of the photon momentum, and vice versa. The LC wavefunction for longitudinal photons (28) contains a term $\alpha^2(1-\alpha)^2$, which makes considerably smaller the contribution from asymmetric $\bar{q}q$ configurations than for transversal photons (see equation (27)). Consequently, in contrast to transverse photons, all $\bar{q}q$ dipoles from longitudinal photons have a size squared $\propto 1/Q^2$ and the double-scattering term vanishes as $\propto 1/Q^4$. The leading-twist contribution for the shadowing of longitudinal photons arises from the $|\bar{q}qG\rangle$ Fock component of the photon because the gluon can propagate relatively far from the $\bar{q}q$ pair, although the $\bar{q}$–q separation is of the order $1/Q^2$. After radiation of the gluon the pair is in an octet state, and consequently the $|\bar{q}qG\rangle$ state represents a GG dipole. Then, the corresponding correction to the longitudinal cross section is just gluon shadowing.

The phenomenon of GS, as for the case of nuclear shadowing discussed in the introduction, can be treated differently depending on the reference frame. In the infinite momentum frame this phenomenon looks similar to gluon–gluon fusion, corresponding to a nonlinear term in the evolution equation [45]. This effect should lead to a suppression of the small $x_{\rm Bj}$ gluons also in a nucleon, and to a precocious onset of the saturation effects for heavy nuclei. Within a parton model interpretation, in the infinite momentum frame of the nucleus the gluon clouds of nucleons which have the same impact parameter overlap at small $x_{\rm Bj}$ in the longitudinal direction. This allows gluons originated from different nucleons to fuse, leading to a gluon density which is not proportional to the density of nucleons any more. This is gluon shadowing.

The same phenomenon looks quite different in the rest frame of the nucleus. It corresponds to the process of gluon radiation and shadowing corrections, related to multiple interactions of the radiated gluons in the nuclear medium [28]. This is a coherence phenomenon known as the Landau–Pomeranchuk effect, namely the suppression of bremsstrahlung by interference of radiation from different scattering centers, demanding a sufficiently long coherence time of radiation, a condition equivalent to a small Bjorken $x_{\rm Bj}$ in the parton model.

Although these two different interpretations are not Lorentz invariant, they represent the same phenomenon, related to the Lorentz invariant Reggeon graphs. It was already discussed in detail in [20, 46] that the double-scattering correction to the cross section of gluon radiation can be expressed in Regge theory via the triple-Pomeron diagram. It is interpreted as a fusion of two Pomerons originated from different nucleons, $2\mathbb{P} \to \mathbb{P}$, which leads to a reduction of the nuclear gluon density G_A.

Note that in the hadronic representation such a suppression of the parton density corresponds to Gribov's inelastic shadowing [25], which is related to the single diffraction cross section. In particular, GS corresponds to the triple-Pomeron term in the diffractive dissociation cross section, which enters the calculations of inelastic corrections.

There are still very few numerical evaluations of gluon shadowing in the literature, all of them done in the rest frame of the nucleus, using the idea from [28]. As was discussed

above, gluon shadowing can be identified as the shadowing correction to the longitudinal cross section coming from the GG dipole representing the $|\bar{q}qG\rangle$ Fock component of the photon. An important point for the evaluation of GS is to know about the transverse size of this GG dipole. This size has been extracted in [24] from data for diffractive excitation of the incident hadrons to the states of large mass, the so-called triple-Pomeron region. The corresponding diffraction cross section ($\propto r^4$) is a more sensitive probe of the mean transverse separation than the total cross section ($\propto r^2$). Consequently, it was found in [24] that the mean dipole size of the GG system (radius of propagation of the LC gluons) is rather small, $r_0 \approx 0.3$ fm [47]. Such a small quark–gluon fluctuation represents the only known way how to resolve the long-standing problem of the small size of the triple-Pomeron coupling.

In order to incorporate the smallness of the size of quark–gluon fluctuations into the LC dipole approach, a nonperturbative LC potential describing the quark–gluon interaction was introduced into the Schrödinger equation for the LC Green function describing the propagation of a quark–gluon system. The strength of the potential was fixed by data on high mass $\left(M_X^2\right)$ diffraction $pp \to pX$ [24]. This approach allows us to extend the methods of pQCD to the region of small Q^2. Since a new semihard scale $1/r_0 \sim 0.65$ GeV is introduced, one should not expect a substantial variation of gluon shadowing at $Q^2 \lesssim 4/r_0^2$. Indeed, the calculations performed in [24] for $Q^2 = 0$ and 4 GeV^2, using different techniques, led to about the same gluon shadowing. At higher Q^2 shadowing slowly (logarithmically) decreases, in accordance with the expectations based on the evolution equation [4], which clearly demonstrates that GS is a leading-twist effect.

In this paper, we repeated the calculations [24] of the ratio of the gluon densities in nuclei and nucleon:

$$R_G(x_{\rm Bj}, Q^2) = \frac{G_A(x_{\rm Bj}, Q^2)}{AG_N(x_{\rm Bj}, Q^2)} \approx 1 - \frac{\Delta\sigma_{\rm tot}(\bar{q}qG)}{\sigma_{\rm tot}^{\gamma^* A}}, \tag{55}$$

where $\Delta\sigma_{\rm tot}(\bar{q}qG)$ is the inelastic correction to the total cross section $\sigma_{\rm tot}^{\gamma^* A}$, related to the creation of a $|\bar{q}qG\rangle$ intermediate Fock state,

$$\begin{aligned}\Delta\sigma_{\rm tot}(\bar{q}qG) = {\rm Re}\int_{-\infty}^{\infty} {\rm d}z_2 \int_{-\infty}^{z_2} {\rm d}z_1\, \rho_A(b, z_1)\rho_A(b, z_2) \int {\rm d}^2x_2\, {\rm d}^2y_2\, {\rm d}^2x_1\, {\rm d}^2y_1 \int {\rm d}\alpha_q \frac{{\rm d}\alpha_G}{\alpha_G} \\ \times F^{\dagger}_{\gamma^*\to\bar{q}qG}(\vec{x}_2, \vec{y}_2, \alpha_q, \alpha_G) G_{\bar{q}qG}(\vec{x}_2, \vec{y}_2, z_2; \vec{x}_1, \vec{y}_1, z_1) \\ \times F_{\gamma^*\to\bar{q}qG}(\vec{x}_1, \vec{y}_1, \alpha_q, \alpha_G).\end{aligned} \tag{56}$$

Here, $\vec{x}$ and $\vec{y}$ are the transverse distances from the gluon to the quark and antiquark, respectively, α_q is the fraction of the LC momentum of the $\bar{q}q$ carried by the quark, and α_G is the fraction of the photon momentum carried by the gluon. $F_{\gamma^*\to\bar{q}qG}$ is the amplitude of diffractive $\bar{q}qG$ production in a $\gamma^* N$ interaction [24], and it is given by

$$\begin{aligned}F_{\gamma^*\to\bar{q}qG}(\vec{x}, \vec{y}, \alpha_q, \alpha_G) = \frac{9}{8}\Psi_{\bar{q}q}(\alpha_q, \vec{x} - \vec{y})\left[\Psi_{qG}\left(\frac{\alpha_G}{\alpha_q}, \vec{x}\right) - \Psi_{\bar{q}G}\left(\frac{\alpha_G}{1-\alpha_q}, \vec{y}\right)\right] \\ \times [\sigma_{\bar{q}q}(x) + \sigma_{\bar{q}q}(y) - \sigma_{\bar{q}q}(\vec{x} - \vec{y})],\end{aligned} \tag{57}$$

where $\Psi_{\bar{q}q}$ and $\Psi_{\bar{q}G}$ are the LC distribution functions of the $\bar{q}q$ fluctuations of a photon and qG fluctuations of a quark, respectively.

In the above equation $G_{\bar{q}qG}(\vec{x}_2, \vec{y}_2, z_2; \vec{x}_1, \vec{y}_1, z_1)$ is the LC Green function which describes the propagation of the $\bar{q}qG$ system from the initial state with longitudinal and transverse coordinates z_1 and $\vec{x}_1, \vec{y}_1$, respectively, to the final coordinates $(z_2, \vec{x}_2, \vec{y}_2)$. For the calculation of gluon shadowing one should suppress the intrinsic $\bar{q}q$ separation, i.e. assume $\vec{x} = \vec{y}$. In this case, the Green function simplifies, and effectively describes the propagation of a gluon–gluon dipole through a medium.

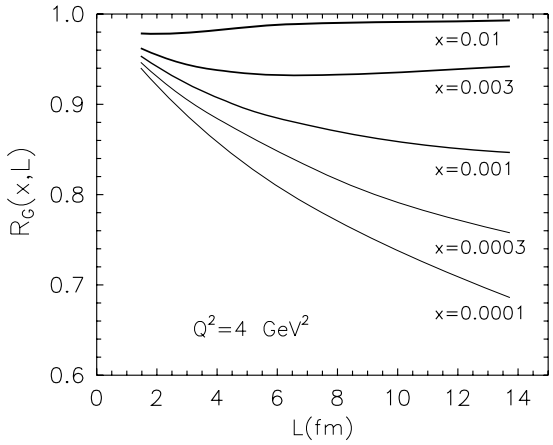

Figure 2. The ratio of the nucleus-to-nucleon gluon densities as a function of the thickness of the nucleus, $L = T(b)/\rho_0$, at $Q^2 = 4$ GeV^2 and different fixed values of $x_{\rm Bj}$. Figure is taken from [20].

An important finding of [24] is the presence of a strong nonperturbative interaction which squeezes the gluon–gluon wavepacket and substantially diminishes gluon shadowing. The smallness of the gluon–gluon transverse separation is not a model assumption, but is dictated by data for hadronic diffraction into large masses (triple-Pomeron regime), which is controlled by diffractive gluon radiation.

Further calculational details can be found in [24]. In our case we calculated the gluon shadowing only for the lowest Fock component containing just one LC gluon. In terms of the parton model it reproduces the effects of fusion of many gluons to one gluon (in terms of Regge approach it corresponds to the $n\mathbb{P} \to \mathbb{P}$ vertex). Inclusion of higher multigluon Fock components is still a challenge. However, their effect can be essentially taken into account by the eikonalization of the calculated $R_G(x_{\rm Bj}, Q^2)$, as argued in [48]. In other words, the dipole cross section, which is proportional to the gluon density at small separations, should be renormalized everywhere, in the form

$$\sigma_{\bar{q}q} \Rightarrow R_G \sigma_{\bar{q}q}. \tag{58}$$

Such a procedure makes the nuclear medium more transparent. This could be expected since Gribov's inelastic shadowing is known to suppress the total hadron–nucleus cross sections, i.e., to make nuclei more transparent [29, 49].

As an illustration of not very strong onset of GS, here we present $R_G(x_{\rm Bj}, Q^2)$, equation (55), for different nuclear thicknesses $T_A(b)$. Using an approximation of constant nuclear density (see equation (36)), $T_A(b) = \rho_0 L$, where $L = 2\sqrt{R_A^2 - b^2}$, the ratio $R_G(x_{\rm Bj}, Q^2)$ is also implicitly a function of L. An example for the calculated L-dependence of $R_G(x_{\rm Bj}, Q^2)$ at $Q^2 = 4$ GeV^2 is depicted in figure 2 for different values of $x_{\rm Bj}$.

One can expect intuitively from equation (58) that GS should always diminish the nuclear cross sections of various processes in nuclear targets, and that the onset of GS is stronger for heavier nuclei. However, this is not so for incoherent electroproduction of vector mesons, analyzed in [20]. The specific structure of the expression for the nuclear production cross section causes that the cross section of incoherent electroproduction of vector mesons is rather

insensitive to GS. Furthermore, the effect of GS is stronger for light than for heavy nuclear targets, in contradiction with the standard intuition. Moreover, for heavy nuclei the effect GS can lead even to a counterintuitive enhancement (antishadowing), as was analyzed in [20]. For the case of coherent vector meson production $\gamma^* A \to V A$ [20], GS was shown to be a much stronger effect in comparison with incoherent production, which confirms the expected reduction of the nuclear production cross section.

Similarly, it was analyzed in [46] that multiple scattering of higher Fock states containing gluons leads to an additional suppression of the Drell–Yan cross section. In the present paper, we will demonstrate that gluon shadowing also suppresses the total photoabsorption cross section on a nucleus $\sigma_{\rm tot}^{\gamma^* A}(x_{\rm Bj}, Q^2)$. Here we expect quite a strong effect of GS on the shadowing region of small $x_{\rm Bj} \lesssim (0.01 \div 0.001)$, in the kinematic range of available data corresponding to small and medium values of $Q^2 \sim$ a few GeV^2.

4. Numerical results

As mentioned above, the main goal of this paper is to compare for the first time available experimental data with realistic predictions for nuclear shadowing in DIS, based on exact numerical solutions of the evolution equation for the Green function. Such a comparison is performed for the shadowing region of small $x_{\rm Bj} \lesssim 0.01$. As was discussed in the previous section one should take into account also a contribution of gluon shadowing, which increases the overall nuclear suppression. The effect of GS was already calculated in [50], but only for the F_2^C/F_2^D ratio of structure functions. Although the quark shadowing was compute approximately via a longitudinal form factor of the nucleus and assuming only the leading shadowing term, it was shown that GS is a rather large effect at $x_{\rm Bj} \sim 10^{-4}$. In the present paper, we will also show that GS is not a negligible effect, and can, in principle, be detected by the data on the total photoabsorption nuclear cross section in future experiments.

The predictions for nuclear shadowing based on an exact numerical solution of the evolution equation was compared in [18] with approximate results obtained by using the harmonic oscillatory form of the Green function (16). Quite a large discrepancy was found in the range of $x_{\rm Bj} \gtrsim 0.001$, where the variation of the transverse size of the $\bar{q}q$ pair during propagation through the nucleus becomes important. Such a variation is naturally included in the Green function formalism and consequently the exact shape of the Green function is extremely important.

We use an algorithm for the numerical solution of the Schrödinger equation for the Green function, as developed and described in [18]. This gives the possibility of calculating nuclear shadowing for arbitrary LC potentials $V_{\bar{q}q}(z, \vec{r}, \alpha)$ and nuclear density functions. Because the available data from the E665 [51, 52] and NMC [53, 54] collaborations cover the region of small and medium values of $Q^2 \lesssim 4$ GeV^2, we prefer the KST parametrization of the dipole cross section (6), which is valid down to the limit of real photoproduction. In contrast, the second GBW parametrization [32] of the dipole cross section cannot be applied in the nonperturbative region and therefore we do not use it in our calculations.

In the process of exact numerical solutions of the evolution equation for the Green function, the imaginary part of the LC potential (34) contains the corresponding KST dipole cross section as well. The nuclear density function $\rho_A(b, z)$ was taken in the realistic Wood–Saxon form, with parameters taken from [43]. The nonperturbative interaction effects between $\bar{q}$ and q are included explicitly via the real part of the LC potential of the form (15), which is supported also by the fact that the data from E665 and NMC collaborations correspond to very small values of $Q^2 \lesssim 1$ GeV^2 in the region of small $x_{\rm Bj} \lesssim 0.004$.

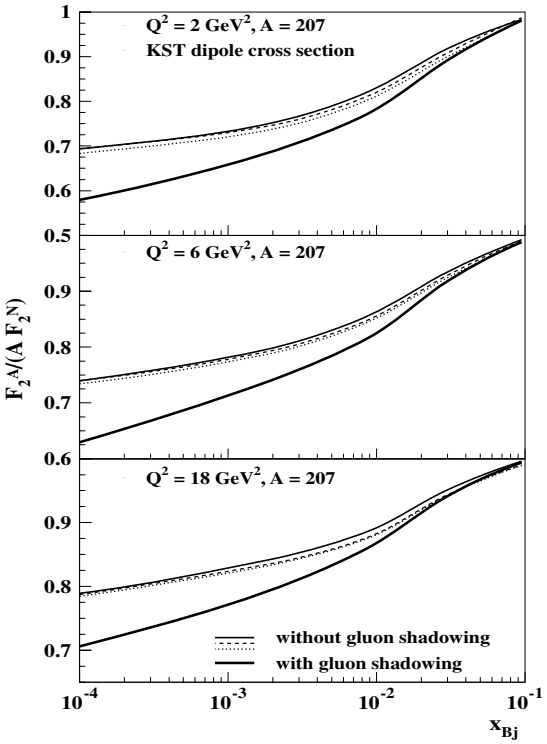

Figure 3. Nuclear shadowing for lead. Calculations correspond to exact numerical solution of the evolution equation for the Green function using the KST [24] parametrization of the dipole cross section and a realistic nuclear density function of the Woods–Saxon form [43]. The thick and thin solid curves represent the predictions calculated with and without contribution of gluon shadowing, respectively. The dotted lines are calculated using a constant nuclear density function (36) and the quadratic form of the dipole cross section, $\sigma(r, s) = C(s)r^2$, where the energy-dependent factor $C(s)$ is determined by equation (44). The dashed curves are calculated for the same quadratic form of the dipole cross section, but for the realistic nuclear density function ([43]).

We included also the effects of gluon shadowing for the lowest Fock component containing just one LC gluon. Although the inclusion of higher Fock components with more gluons is complicated, their effect was essentially taken into account by eikonalization of the calculated $R_G(x_{\rm Bj}, Q^2)$ [48], i.e., using the renormalization (58).

Nuclear shadowing effects were studied via the $x_{\rm Bj}$-behavior of the ratio of proton structure functions (43) divided by the mass number A. First we present nuclear shadowing for a lead target in figure 3 at different fixed values of Q^2. The thick and thin solid curves represent the predictions obtained with and without the contribution of gluon shadowing, respectively.

One can see that the onset of GS happens at smaller $x_{\rm Bj}$ than the quark shadowing, which is supported by the fact that higher Fock fluctuations containing gluons are in general heavier than $\bar{q}q$, and have a shorter coherence length. Figure 3 demonstrates quite a strong effect of GS on the range of $x_{\rm Bj} \in (0.01, 0.0001)$, where most of the available data exist. This is a result of the suppression of the dipole cross section by the renormalization (58), which can result only in a reduction of the total photoabsorption cross section on a nuclear target. Besides, the

effect of GS is stronger at smaller Q^2 because corresponding Fock fluctuations of the photon have a larger transverse size.

In figure 3 we also present, for comparison and by the dotted lines, the approximate predictions for nuclear shadowing in DIS using constant nuclear density (36) and the quadratic form of the dipole cross section, $\sigma(r, s) = C(s)r^2$. The energy-dependent factor $C(s)$ is determined by equation (44), and the uniform nuclear density is fixed by the condition (45). One can see that these approximate predictions overestimate the values of nuclear shadowing obtained by means of an exact numerical solution of the evolution equation for the Green function. The difference from the exact calculation (thin solid lines) is not large and rises toward small values of Q^2. The reason is that the quadratic approximation of the dipole cross section cannot be applied exactly at large dipole sizes. Since the available data from the E665 [51, 52] and NMC [53, 54] collaborations at smallest values of $x_{\rm Bj}$ correspond also to small $Q^2 \ll 1$ GeV^2, one can expect a larger difference between the exact and approximate results in comparison with what is shown in figure 3 at $Q^2 = 2$ GeV^2. Keeping the quadratic form of the dipole cross section, but using the realistic nuclear density [43], one can obtain the results depicted in figure 3 by the dashed lines. It brings a better agreement with the exact calculations.

At low $x_{\rm Bj} \lesssim 10^{-4}$ one should expect a saturation of nuclear shadowing at the level given by equation (41). This is realized only for the dipole cross section, without energy dependence, i.e., for example, for parametrization (35) of the dipole cross section with constant factor $C(s) \approx 3$ [19]. However, this is not so for the realistic KST parametrization equation (6), where the saturation level is not fixed exactly due to energy (Bjorken $x_{\rm Bj}$-)dependence of the dipole cross section $\sigma_{\bar{q}q}(r, s)$.

In figure 4, we present a comparison of the model predictions with experimental data at small $x_{\rm Bj}$, from the E665 [51, 52] and NMC [53, 54] collaborations. One can see a quite reasonable agreement with experimental data, in spite of the absence of any free parameters in the model. Several comments are in order: first, if GS is not taken into account, for the C/D and Ca/D ratios the nuclear shadowing looks overestimated in comparison with the E665 data for $x_{\rm Bj} \sim 0.01$, while it looks in a good agreement for C/D, and a little bit underestimated for Ca/D in comparison with the NMC data. This is affected by the known incompatibility of the results from both experiments for the ratios over D. Second, as was discussed in the previous section, the effect of GS produces an additional nuclear shadowing which rises with mass number A. Consequently, it leads to a small overestimation of the nuclear shadowing for the C/D and Ca/D ratios in comparison with the E665 data, but it seems to be in good agreement with the NMC data.

For heavy nuclear targets there is only E665 data for the ratios Xe/D and Pb/D. Figure 4 shows a reasonable good description of these data, even if the effect of GS is taken into account. The difference between the solid and dashed lines in figure 4 represents quite a large effect of GS, which was neglected up to the present time in calculations of nuclear shadowing in DIS [17, 19, 23] assuming that it would be a very small effect in the kinematic range covered by the available experimental data. In contrast, looking at figure 4 one can see that the effect of GS as an additional nuclear shadowing cannot be neglected and should be included in calculations already in the region of $x_{\rm Bj} \lesssim 0.01 \div 0.001$. Very large error bars especially at small $x_{\rm Bj} \sim 10^{-4}$ do not allow us to investigate separately the effect of GS, and therefore more exact new data on nuclear shadowing in DIS at small $x_{\rm Bj}$ are very important for further exploratory studies on the nuclear modification of structure functions and also for gluon shadowing.

For completeness we present also in figures 5 and 6 predictions for nuclear shadowing down to very small $x_{\rm Bj} = 10^{-7}$ accessible by experiments at LHC using two different realistic

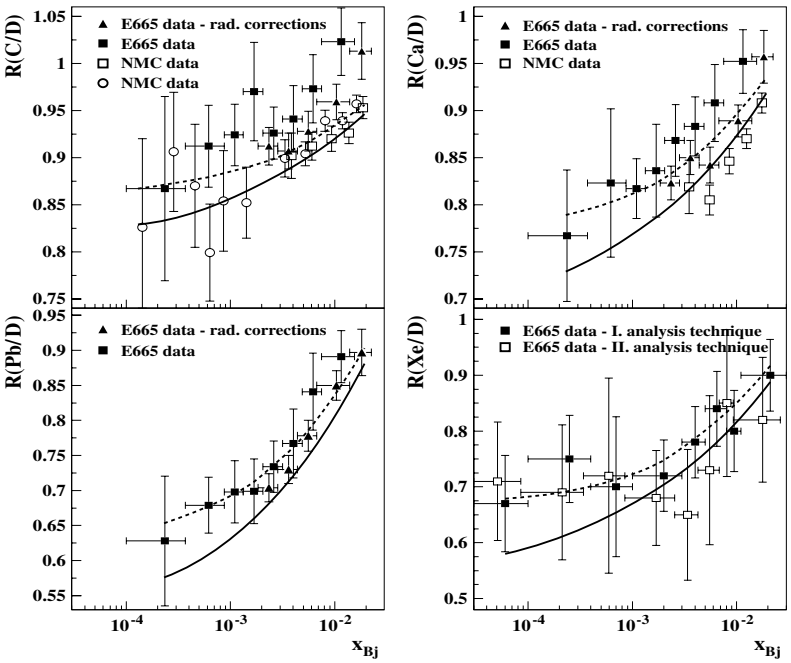

Figure 4. Comparison of the model with experimental data from the E665 [51, 52] and NMC [53, 54] collaborations. Calculations correspond to the exact numerical solution of the evolution equation for the Green function using KST [24] parametrization of the dipole cross section and a realistic nuclear density function of the Woods–Saxon form [43]. The solid and dashed curves are calculated with and without the contribution of gluon shadowing, respectively.

parametrizations of the dipole cross section, KST [24] and GBW [32]. Again, one can see quite large effect of GS as a difference between the solid and dashed lines.

Here, we would like to emphasize that at $x_{\rm Bj} \lesssim 10^{-4}$ transverse size separations of the photon fluctuations are 'frozen' during propagation through nuclear medium and one can use the simplified expressions, equations (40) and (41) for calculation of nuclear shadowing.

Finally, we present, in figure 7, a comparison of the nuclear shadowing calculated using our model with the results of other models, for $Q^2 = 3$ GeV^2 (except the results of [55], which are at $Q^2 = 4$ GeV^2). Note that the difference between models rises toward small values of $x_{\rm Bj}$, as a result of the different treatment of various nuclear effects, and absence of relevant experimental information at such small $x_{\rm Bj}$. At $x_{\rm Bj} = 10^{-5}$ we predict quite a large effect of GS (compare upper and lower thick solid lines).

In [56], nuclear structure functions were studied using the relation with diffraction on nucleons known as Gribov inelastic corrections. The results of these calculations are depicted in figure 7 by dotted curves.

The model presented in [55] employs again a parametrization of hard diffraction at the scale Q_0^2, which gives nuclear shadowing in terms of Gribov's corrections similar to [56]. Then the nuclear suppression calculated at Q_0^2 is used as an initial condition for Dokshitzer–Gribov–Lipatov–Altareli–Parisi (DGLAP) [57] evolution. This results are presented in figure 7 by dashed curves.

The model based on a numerical solution of the nonlinear equation for small-$x_{\rm Bj}$ evolution in nuclei was employed in [58]. The result is shown in figure 7 by thin solid curve.

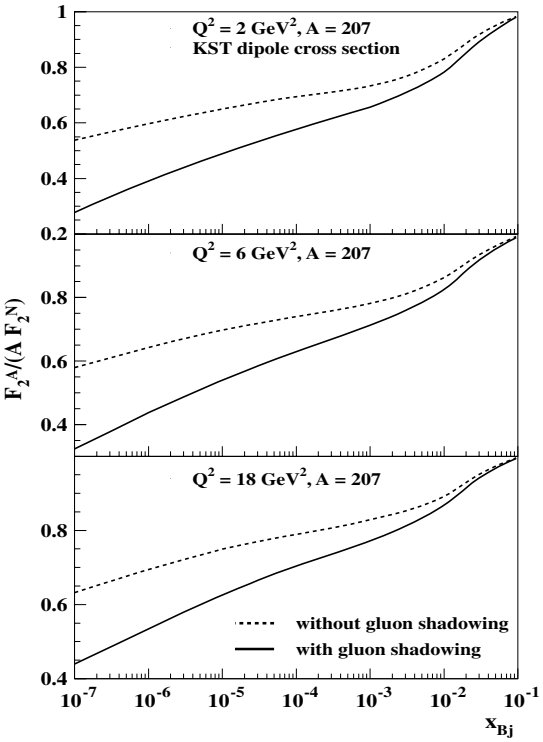

Figure 5. Model predictions for nuclear shadowing for a broad $x_{\rm Bj}$-region down to 10^{-7} corresponding to LHC kinematical range at three different values of $Q^2 = 2, 6$ and 18 GeV^2. Calculations of the nuclear shadowing for the $\bar{q}q$ Fock component of the photon correspond to the exact numerical solution of the evolution equation for the Green function using KST [24] parametrization of the dipole cross section and a realistic nuclear density function of the Woods–Saxon form [43]. The solid and dashed curves are calculated with and without the contribution of gluon shadowing, respectively.

At very small $x_{\rm Bj}$ our model predictions, including the effect of GS, roughly agrees with those of [56], but lie below the results of other models. If the effect of GS is not taken into account the situation is substantially different and the corresponding curve (see the upper thick solid line) lies in between the results from other models.

Most models presented above are based on eikonal formulae, which should be used only in the high-energy limit, when the coherence length $l_c \gg R_A$, i.e. at $x_{\rm Bj} \lesssim 10^{-4}$. However, they were applied also in the region when $l_c \lesssim R_A$. In this transition shadowing region, $x_{\rm Bj} \in (0.0001, 0.01)$, such approximations lead in general to a larger nuclear shadowing than a realistic situation, when more exact expressions should be more appropriate (compare equations (39) and (41)). For this reason, theoretical predictions of most models overestimate nuclear shadowing in the range of $x_{\rm Bj}$ where available experimental data exist.

So far, the main source of experimental information on gluon shadowing was DIS on nuclei. Although it probes only quark distributions, the Q^2-dependence of nuclear effects is related via the evolution equations to the gluon distribution. For the smallest value of $x_{\rm Bj} = 0.01$ reached in the NMC experiment the gluon suppression factor $R_G(Sn)/R_G(C) = 0.87 \pm 0.05$ was obtained in [59] within the leading-log (LL) approximation. This result

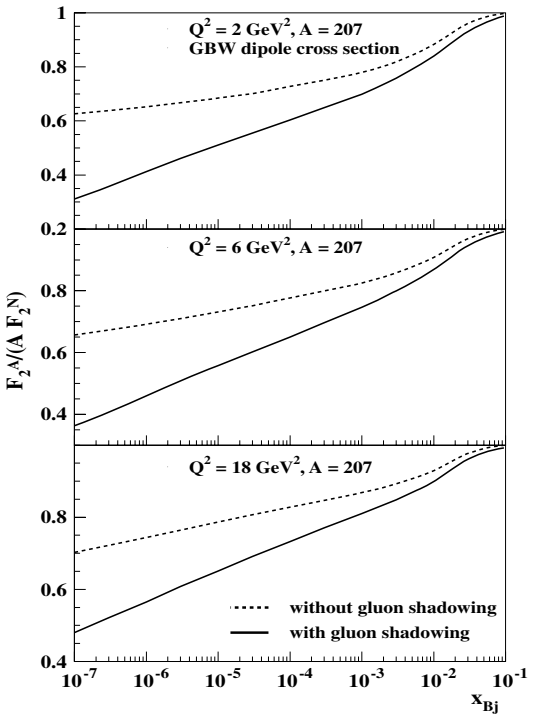

Figure 6. The same as figure 5, but with GBW [32] parametrization of the dipole cross section.

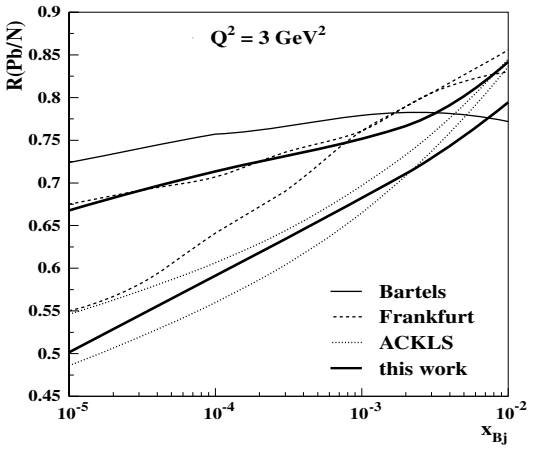

Figure 7. Comparison of the model results for the ratio Pb/nucleon obtained without (upper thick solid line) and with (lower thick solid line) gluon shadowing, with other models, versus $x_{\rm Bj}$, at fixed $Q^2 = 3$ GeV^2. Bartels are the results from [58], Frankfurt from [55] ($Q^2 = 4$ GeV^2), and ACKLS from [56].

is somewhat lower that our expectation $R_G \sim 0.98$ which can be read out from figure 2. However, according to [59] the next-to-LL corrections at $x_{\rm Bj} = 0.01$ are about 10–20%,

which apparently eliminates the disagreement with our calculations. Furthermore, the full leading-order (LO) DGLAP analysis of the NMC data [53, 54] in [60], which should not be less accurate than LL calculations, led to a conclusion that the NMC data are not sensitive to gluon shadowing. Moreover, the recent next-to-LO (NLO) analysis by de Florian and Sassot [61] was claimed to be sensitive to gluons. This analysis found almost no GS at $x_{\rm Bj} = 0.01$ in good agreement with our calculations.

Other possible sources of information about gluon shadowing were considered in [62–64]. It was proposed in [62] to probe gluons in nuclei by direct photons produced in p–A collisions in the proton fragmentation region where one can access smallest values of the light-front momentum fraction variable x_2 in nuclei. This, however, should not work, since at large value of the light-front momentum fraction variable x_1 in the proton (i.e., at large Feynman x_F) one faces the energy sharing problem [65]: it is more difficult to give the whole energy to one particle in p–A, than in p–p collision. This effect leads to a breakdown of QCD factorization and to nuclear suppression observed at forward rapidities [65–68] in any reaction measured so far, even at low energies, where no shadowing is possible.

An attempt to impose a restriction on GS analyzing the nuclear effects in J/Ψ production observed in p–A collisions by the E866 experiment [69], was made in [63]. The mechanisms of J/Ψ production and nuclear effects are so complicated that it would be risky to rely on oversimplified models. Indeed, the analysis performed in this paper completely misses the color transparency effects, which are rather strong [70] and vary throughout the interval of x_F studied in this paper. For this reason the results of the analysis are not trustable.

The new analysis of nuclear parton distribution functions performed in [64] included the BRAHMS data for high-p_T pion production at forward rapidities [71]. As mentioned above, hadron production in this kinematic region of large x_1 (x_F) is suppressed by multiple parton interactions [65], rather than by shadowing. Consequently, the results of this analysis are not trustable either. Moreover, it seems to provide another confirmation for an alternative dynamics for the suppression observed in the data [71]. Indeed, it was concluded in [64] that gluons in lead target are completely terminated at $x_{\rm Bj} = 10^{-4}$ where $R_G < 0.05$ is predicted. This cannot be true because in the limit of strong shadowing the gluon ratio has a simple form $R_G = \pi R_A^2/(A\sigma_{\rm eff})$, where $\sigma_{\rm eff}$ is the effective cross section responsible for shadowing. The strong effect predicted in [64] needs $\sigma_{\rm eff} > 150$ mb.

5. Summary and conclusions

We presented a rigorous quantum-mechanical approach based on the light-cone QCD Green function formalism which naturally incorporates the interference effects of CT and CL. Within this approach [17–19, 41] we studied nuclear shadowing in deep-inelastic scattering at small Bjorken $x_{\rm Bj}$.

Calculations of nuclear shadowing corresponding to the $\bar{q}q$ component of the virtual photon performed so far were based only on efforts to solve the evolution equation for the Green function analytically, and unfortunately an analytical harmonic oscillatory form of the Green function (16) could be obtained only by using additional approximations, like a constant nuclear density function (36) and the dipole cross section of the quadratic form (35). This brings additional theoretical uncertainties in the predictions for nuclear shadowing. In order to remove these uncertainties we solve the evolution equation for the Green function numerically, which does not require additional approximations.

In [18], it was found for the first time the exact numerical solution of the evolution equation for the Green function, using two realistic parametrizations of the dipole cross section (GBW [32] and KST [24]), and a realistic nuclear density function of the Woods–Saxon form [43].

It was demonstrated that the corresponding nuclear shadowing shows quite large differences from approximate results [17, 19]. On the other hand, we showed that approximate calculations corresponding to uniform nuclear density (48) and quadratic dipole cross section (47), but with the energy-dependent factor $C(s)$ determined by equation (44), bring a better agreement with exact realistic calculations (see figure 3). However, the difference from the exact calculations rises toward small values of Q^2, where available data exist at smallest values of $x_{\rm Bj} \sim 10^{-4}$. This confirms the claim that the quadratic approximation of the dipole cross section cannot be applied at large dipole sizes.

Since the available data from the shadowing region of $x_{\rm Bj} \lesssim 0.01$ comes mostly from the E665 and NMC collaborations, and cover only small and medium values of $Q^2 \lesssim 4$ GeV^2, we used only the KST realistic parametrization [24] of the dipole cross section, which is more suitable for this kinematic region, and the corresponding expressions can be applied down to the limit of real photoproduction. On the other hand, the data obtained at the lower part of the $x_{\rm Bj}$-kinematic interval correspond to very low values of $Q^2 < 1$ GeV^2 (nonperturbative region). For this reason we include explicitly the nonperturbative interaction effects between $\bar{q}$ and q, taking into account the real part of the LC potential $V_{\bar{q}q}$ (15) in the time-dependent two-dimensional Schrödinger equation (13).

In order to compare the realistic calculations with data on nuclear shadowing, the effects of GS are taken into account. The same path integral technique [24] can be applied in this case, and GS was calculated only for the lowest Fock component containing just one LC gluon. Although the inclusion of higher Fock components containing more gluons is still a challenge, their effect was essentially taken into account by eikonalization of the calculated $R_G(x_{\rm Bj}, Q^2)$,using the renormalization (58). We found quite a large effect of GS, which starts to be important already at $x_{\rm Bj} \sim 0.01$. The effect of GS rises toward small $x_{\rm Bj}$ because higher Fock components with more gluons having shorter coherence time will contribute to overall nuclear shadowing. Such a situation is illustrated in figure 3.

Performing numerical calculations, we find that our model is in reasonable agreement with existing experimental data (see figure 4). Large error bars and incompatibility of the experimental results from the E665 and NMC collaborations do not allow us to study separately the effect of GS, and therefore more accurate new data on nuclear shadowing in DIS off nuclei at still smaller $x_{\rm Bj} \lesssim 10^{-5}$ are very important for further exploratory studies of GS effects.

Comparison among various models shows large differences for the Pb/nucleon ratio of structure functions at $x_{\rm Bj} = 10^{-5}$ and $Q^2 = 3$ GeV^2 (see figure 7), which has a large impact on the calculation of high-p_T particles in nuclear collisions at RHIC and LHC. Such large differences at small $x_{\rm Bj}$ among different models should be testable by the new more precise data on nuclear structure functions, which can be obtained in lepton–ion collider planned at BNL [72].

In most models presented above, the final formulae for nuclear shadowing are based on the eikonal approximation, which can be used exactly only in the high-energy limit, $l_c \gg R_A$. Consequently, such an approach cannot be really applied in the transition shadowing region, $l_c \approx R_A$, where $x_{\rm Bj} \in (0.0001, 0.01)$, because it produces a larger nuclear shadowing than in a realistic case when more appropriate expressions should be taken into account (compare equations (39) and (41)).

Concluding, a combination of the exact numerical solution of the evolution equation for the Green function with the universality of the LC dipole approach based on the Green function formalism provides us with a very powerful tool for realistic calculations of many processes. It allows us to minimize theoretical uncertainties in the predictions of nuclear shadowing in DIS off nuclei, which gives the possibility of obtaining reliable information about nuclear modification of the structure functions at low $x_{\rm Bj}$, with an important impact on

the physics performed in heavy-ion collisions at RHIC and in lepton–ion interactions planned at BNL.

Acknowledgments

This work was supported in part by Fondecyt (Chile) grants 1050589 and 1050519, by DFG (Germany) grant PI182/3-1, by the Slovak Funding Agency, grant no 2/7058/27 and the grant VZ MSM 6840770039 and LC 07048 (Czech Republic).

References

[1] Arneodo M 1994 *Phys. Rep.* **240** 301
[2] Kancheli O V 1973 *Sov. Phys. JETP Lett.* **18** 274
[3] Gribov V N, Levin E M and Ryskin M G 1983 *Phys. Rep.* **100** 1
[4] Mueller A H and Qiu J 1986 *Nucl. Phys.* B **268** 427
[5] Qiu J 1987 *Nucl. Phys.* B **291** 746
[6] Bauer T H, Spital R D, Yennie D R and Pipkin F M 1978 *Rev. Mod. Phys.* **50** 261
[7] Frankfurt L L and Strikman M I 1988 *Phys. Rep.* **160** 235
[8] Brodsky S J and Lu H J 1990 *Phys. Rev. Lett.* **64** 1342
[9] Brodsky S J, Schmidt I and Yang J-J 2004 *Phys. Rev.* D **70** 116003
[10] Nikolaev N N and Zakharov B G 1991 *Z. Phys.* C **49** 607
[11] Melnitchouk W and Thomas A W 1993 *Phys. Lett.* B **317** 437
[12] Nikolaev N N, Piller G and Zakharov B G 1995 *JETP* **81** 851
[13] Piller G, Ratzka W and Weise W 1995 *Z. Phys.* A **352** 427
[14] Kopeliovich B Z and Povh B 1996 *Phys. Lett.* B **367** 329
[15] Kopeliovich B Z and Povh B 1997 *Z. Phys.* A **356** 467
[16] Piller G and Weise W 2000 *Phys. Rep.* **330** 1
[17] Kopeliovich B Z, Raufeisen J and Tarasov A V 2000 *Phys. Rev.* C **62** 035204
[18] Nemchik J 2003 *Phys. Rev.* C **68** 035206
[19] Kopeliovich B Z, Raufeisen J and Tarasov A V 1998 *Phys. Lett.* B **440** 151
[20] Kopeliovich B Z, Nemchik J, Schaefer A and Tarasov A V 2002 *Phys. Rev.* C **65** 035201
[21] Nemchik J 2002 *Phys. Rev.* C **66** 045204
[22] Kopeliovich B Z and Zakharov B G 1991 *Phys. Rev.* D **44** 3466
[23] Raufeisen J 2000 *PhD Thesis* Heidelberg (arXiv:hep-ph/0009358)
[24] Kopeliovich B Z, Schäfer A and Tarasov A V 2000 *Phys. Rev.* D **62** 054022
[25] Gribov V N 1969 *Sov. Phys.—JETP* **29** 483
[26] Karmanov V and Kondratyuk L A 1973 *Sov. Phys. JETP Lett.* **18** 266
[27] Kazarinov Yu M, Kopeliovich B Z, Lapidus L I and Potashnikova I K 1976 *JETP* **70** 1152
[28] Mueller A H 1990 *Nucl. Phys.* B **335** 115
[29] Zamolodchikov A B, Kopeliovich B Z and Lapidus L I 1981 *Sov. Phys. JETP Lett.* **33** 595
[30] Bertsch G, Brodsky S J, Goldhaber A S and Gunion J F 1981 *Phys. Rev. Lett.* **47** 297
[31] Brodsky S J and Mueller A 1988 *Phys. Lett.* B **206** 685
[32] Golec-Biernat K and Wüsthoff M 1999 *Phys. Rev.* D **59** 014017
Golec-Biernat K and Wüsthoff M 1999 *Phys. Rev.* D **60** 114023
[33] Barnett R M *et al* 1996 *Phys. Rev.* D **54** 191 (Review of Particle Physics)
[34] Kogut J B and Soper D E 1970 *Phys. Rev.* D **1** 2901
[35] Bjorken J M, Kogut J B and Soper D E 1971 *Phys. Rev.* D **3** 1382
[36] Pirner H J and Nurpeissov N 2004 *Phys. Lett.* B **595** 379
[37] Pirner H J, Galow B and Schlaudt O 2008 Light-cone constituent quark model *Preprint* arXiv:0804.3490
[38] Feynman R P and Gibbs A R 1965 *Quantum Mechanics and Path Integrals* (New York: McGraw-Hill)
[39] Aid S *et al* (H1 Collaboration) 1995 *Z. Phys.* C **69** 27
[40] Derrick M *et al* (ZEUS Collaboration) 1992 *Phys. Lett.* B **293** 465
[41] Raufeisen J, Tarasov A V and Voskresenskaya O O 1999 *Eur. Phys. J.* A **5** 173
[42] Zakharov B G 1998 *Phys. Atom. Nucl.* **61** 838
[43] De Vries H, De Jager C W and De Vries C 1987 *Atomic Data Nucl. Data Tables* **36** 469
[44] Kopeliovich B Z and Tarasov A V 2002 *Nucl. Phys.* A **710** 180

[45] Gribov L V, Levin E M and Ryskin M G 1981 *Nucl. Phys.* B **188** 555
[46] Kopeliovich B Z, Raufeisen J, Tarasov A V and Jonson M B 2003 *Phys. Rev.* C **67** 014903
[47] Kopeliovich B Z, Potashnikova I K, Povh B and Predazzi E 2000 *Phys. Rev. Lett.* **85** 507
[48] Kopeliovich B Z, Tarasov A V and Hüfner J 2001 *Nucl. Phys.* A **696** 669
[49] Kopeliovich B Z and Nemchik J 1996 *Phys. Lett.* B **368** 187
[50] Johnson M B *et al* 2002 *Phys. Rev.* C **65** 025203
[51] Adams M R *et al* (E665 Collaboration) 1995 *Z. Phys.* C **67** 403
[52] Adams M R *et al* (E665 Collaboration) 1992 *Phys. Rev. Lett.* **68** 3266
[53] Amaudruz P *et al* (NMC Collaboration) 1995 *Nucl. Phys.* B **441** 3
[54] Arneodo M *et al* (NMC Collaboration) 1995 *Nucl. Phys.* B **441** 12
[55] Frankfurt L, Guzey V, McDermott M and Strikman M 2002 *J. High Energy Phys.* JHEP02(2002)027
Frankfurt L, Guzey V and Strikman M 2005 *Phys. Rev.* D **71** 054001
[56] Armesto N, Capella A, Kaidalov A B, López-Albacete J and Salgado C A 2003 *Eur. Phys. J.* C **29** 531
[57] Dokshitzer Yu L 1977 *Sov. Phys.—JETP* **46** 641
Dokshitzer Yu L 1977 *Zh. Eksp. Teor. Fiz.* **73** 1216
Gribov V N and Lipatov L N 1972 *Yad. Fiz.* **15** 781
Gribov V N and Lipatov L N 1972 *Sov. J. Nucl. Phys.* **15** 438
Altareli G and Parisi G 1977 *Nucl. Phys.* B **126** 298
[58] Bartels J, Gotsman E, Levin E M, Lublinsky M and Maor U 2003 *Phys. Rev.* D **68** 054008
[59] Gousset T and Pirner H J 1996 *Phys. Lett.* B **375** 349
[60] Eskola K J, Kolhinen V J and Ruuskanen P V 1998 *Nucl. Phys.* B **535** 351
Eskola K J, Kolhinen V J and Salgado C A 1999 *Eur. Phys. J.* C **9** 61
[61] de Florian D and Sassot R 2004 *Phys. Rev.* D **69** 074208
[62] Arleo F and Gousset T 2008 Probing gluon shadowing with forward photons at RHIC arXiv:0806.0769
[63] Arleo F 2008 Constraints on nuclear gluon densities from J/Ψ data arXiv:0804.2802
[64] Eskola K J, Paukkunen H and Salgado C A 2008 An improved global analysis of nuclear parton distribution functions including RHIC data arXiv:0802.0139
[65] Kopeliovich B Z, Nemchik J, Potashnikova I K, Schmidt I and Johnson M B 2005 *Phys. Rev.* C **72** 054606
[66] Kopeliovich B Z, Nemchik J, Potashnikova I K, Schmidt I and Johnson M B 2005 *Nucl. Phys.* B **146** 171
[67] Nemchik J, Petracek V, Potashnikova I K and Sumbera M 2008 Study of nuclear suppression at large forward rapidities in d–Au collisions at RHIC arXiv:0805.4267
[68] Nemchik J and Potashnikova I K 2008 Forward physics in proton–nucleus and nucleus–nucleus collisions arXiv:0807.1605
[69] Leitch M J *et al* (E866 Collaboration) 2000 *Phys. Rev. Lett.* **84** 3256
[70] He Y B, Huefner J and Kopeliovich B Z 2000 *Phys. Lett.* B **477** 93
[71] Arsene I *et al* (BRAHMS Collaboration) 2004 *Phys. Rev. Lett.* **93** 242303
Yang Hongyan *et al* 2007 *J. Phys. G: Nucl. Part. Phys.* **34** S619
[72] Milner R G 2004 *Proc. 12th Int. Workshop on DIS ée Pleso, Slovakia, 14–18 April)* pp 173–82

Bibliography

[1] J. Adam *et al.* [ALICE Collaboration] Phys. Lett. B**751**, 358 (2015).

[2] J. Adam *et al.* [ALICE Collaboration] JHEP **09**, 095 (2015).

[3] T. Matsui and H. Satz, Phys. Lett. B**178**, 416 (1986).

[4] V.N. Gribov, Sov. Phys. JETP **29**, 483 (1969); [Zh. Eksp. Teor. Fiz. **56**, 892 (1969)].

[5] A.B. Zamolodchikov, B.Z. Kopeliovich and L.I. Lapidus, Pis'ma Zh. Eksp. Teor. Fiz. **33**, 612 (1981); Sov. Phys. JETP Lett. **33**, 595 (1981).

[6] G. Bertsch, S.J. Brodsky, A.S. Goldhaber and J.F. Gunion, Phys. Rev. Lett. **47**, 297 (1981).

[7] P. Jain, B. Pire and J.P. Ralston, Phys. Rept. **271**, 67 (1996).

[8] J.F. Gunion and D.E. Soper, Phys. Rev. D**15**, 2617 (1977).

[9] J. Hüfner and B. Povh, Phys. Rev. D**46**, 990 (1992).

[10] B. Povh, *Hadron Interactions - Hadron Sizes*, **hep-ph/9806379**.

[11] B.Z. Kopeliovich and B.G. Zakharov, Phys. Rev. D**44**, 3466 (1991).

[12] J. Hüfner and B.Z. Kopeliovich, Phys. Lett. B**403**, 128 (1997).

[13] B.Z. Kopeliovich, J. Nemchik, A. Schäfer and A.V. Tarasov, Phys. Rev. C**65**, 035201 (2002).

[14] T.H. Bauer et al., Rev. Mod. Phys. **50**, 261 (1978).

[15] M. Arneodo *et al.* [NMC Collaboration], Nucl. Phys. **441**, 12 (1995); Nucl. Phys. **481**, 3 (1996).

[16] M.R. Adams *et al.* [E665 Collaboration], Z. Phys. C**67**, 403 (1995).

[17] B.Z. Kopeliovich, Phys. Lett. B**227**, 461 (1989).

[18] D.M. Alde *et al.* [E772 Collaboration], Phys. Rev. Lett. **64**, 2470 (1990).

[19] M. Vasiliev *et al.* [E866 Collaboration], Phys. Rev. Lett. **83**, 2304 (1999).

[20] J. Hüfner, B.Z. Kopeliovich and J. Nemchik, Phys. Lett. B**383**, 362 (1996).

[21] J. Nemchik, Phys. Rev. C**66**, 045204 (2002).

[22] A.H. Mueller, Nucl. Phys. B**335**, 115 (1990).

[23] B.Z. Kopeliovich, J. Raufeisen and A.V. Tarasov, Phys. Rev. C**62**, 035204 (2000).

[24] Yu.P. Ivanov, B.Z. Kopeliovich, A.V. Tarasov and J. Hufner, Phys. Rev. C**66**, 024903 (2002).

[25] K. Golec-Biernat and M. Wüsthoff, Phys. Rev. D**59**, 014017 (1999); Phys. Rev. D**60**, 114023 (1999).

[26] H. Kowalski, L. Motyka and G. Watt, Phys. Rev. D**74**, 074016 (2016).

[27] J. Bartels, Golec-Biernat, J. Krzysztof and H. Kowalski, Phys. Rev. D**66**, 014001 (2002).

[28] J.L. Albacete, N. Armesto, J.G. Milhano and C.A. Salgado, Phys. Rev. D**80**, 034031 (2009).

[29] A.H. Rezaeian, M. Siddikov, M. Van de Klundert and R. Venugopalan, Phys. Rev. D**87**, 034002 (2013).

[30] B.Z. Kopeliovich, A. Schäfer and A.V. Tarasov, Phys. Rev. D**62**, 054022 (2000).

[31] A. Donnachie and P.V. Landshoff, Phys. Lett. B**478**, 146 (2000).

[32] Review of Particle Physics, Particle Data Group, Eur. Phys. J. C**15**, 1 (2000).

[33] J.B. Bronzan, G.L. Kane and U.P. Sukhatme, Phys. Lett. B**49**, 272 (1974).

[34] J.B. Kogut and D.E. Soper, Phys. Rev. D**1**, 2901 (1970).

[35] J.M. Bjorken, J.B. Kogut and D.E. Soper, Phys. Rev. D**3**, 1382 (1971).

[36] N.N. Nikolaev and B.G. Zakharov, Z. Phys. C**49**, 607 (1991).

[37] R.P. Feynman and A.R. Gibbs, *Quantum Mechanics and Path Integrals*, McGraw-Hill Book Company, NY 1965.

[38] S. Aid *et al.* [H1 Collaboration], Z. Phys. C**69**, 27 (1995).

[39] M. Derrick *et al.* [ZEUS Collaboration], Phys. Lett. B**293**, 465 (1992).

[40] M.V. Terent'ev, Sov. J. Nucl. Phys. **24**, 106 (1976).

[41] I. Halperin and A. Zhitnitsky, Phys. Rev. D**56**, 184 (1997).

[42] J. Nemchik, N.N. Nikolaev, E. Predazzi and B.G. Zakharov, Z. Phys. C**75**, 71 (1997).

[43] M. Arneodo *et al.* [NMC Collaboration], Nucl. Phys. B**429**, 503 (1994).

[44] C. Adloff *et al.* [H1 Collaboration], Eur. Phys. J. C**13**, 371 (2000).

[45] J. Breitweg *et al.* [ZEUS Collaboration], Eur. Phys. J. C**6**, 603 (1999).

[46] C. Adloff *et al.* [H1 Collaboration], Z. Phys. C**75**, 607 (1997);
C. Adloff *et al.* [H1 Collaboration], Phys. Lett. B**483**, 360 (2000);
M. Derrick *et al.* [ZEUS Collaboration], Phys. Lett. B**380**, 220 (1996);
J. Breitweg *et al.* [ZEUS Collaboration], "Exclusive Electroproduction of Φ Mesons at HERA", presented at the XXIX International Conference on HEP, Vancouver, 1998, paper-**793**.

[47] J. Nemchik, N.N. Nikolaev, E. Predazzi, B.G. Zakharov and V.R. Zoller, J. Exp. Theor. Phys. **86**, 1054 (1998).

[48] W.D. Shambroom *et al.* [CHIO Collaboration], Phys. Rev. D**26**, 1 (1982);
M.R. Adams *et al.* [E665 Collaboration], Z. Phys. C**74**, 237 (1997).

[49] S. Aid *et al.* [H1 Collaboration], Nucl. Phys. B**463**, 3 (1996).

[50] S. Aid *et al.* [H1 Collaboration], Nucl. Phys. B**468**, 3 (1996).

[51] M. Derrick *et al.* [ZEUS Collaboration], Z. Phys. C**69**, 39 (1995).

[52] J. Breitweg *et al.* [ZEUS Collaboration], Z. Phys. C**73**, 253 (1997);
J. Breitweg *et al.* [ZEUS Collaboration], Eur. Phys. J. C**2**, 247 (1998).

[53] M. Derrick *et al.* [ZEUS Collaboration], Phys. Lett. B**356**, 601 (1995).

[54] J. Busenitz *et al.*, Phys. Rev. D**40**, 1 (1989), and references therein;
R. Erbe *et al.*, Phys. Rev. **175**, 1669 (1968);
J. Ballam *et al.*, Phys. Rev. D**7**, 3150 (1973);
H.J. Bersh *et al.*, Nucl. Phys. B**70**, 257 (1974);
H.J. Behrend *et al.*, Phys. Lett. B**56**, 408 (1975);
D.P. Barber *et al.*, ibid. B**79**, 150 (1978);
D. Aston *et al.*, Nucl. Phys. B**172**, 1 (1980);
M. Atkinson *et al.*, Z. Phys. C**27**, 233 (1985).

[55] M. Derrick *et al.* [ZEUS Collaboration], Phys. Lett. B**377**, 259 (1996).

[56] D. Aston *et al.* [OMEGA Collaboration], Nucl. Phys. B**209**, 56 (1982).

[57] J. Park *et al.*, Nucl. Phys. B**36**, 404 (1972);
R.M. Egloff *et al.*, Phys. Rev. Lett. **43**, 657 (1979).

[58] M. Derrick *et al.* [ZEUS Collaboration], Z. Phys. C**63**, 391 (1994);
M. Derrick *et al.*, paper **pa02-050**, submitted to the 28th International Conference on HEP, 25-31 July, 1996, Warsaw, Poland.

[59] W.G. Jones *et al.*, Phys. Rev. Lett. **21**, 586 (1968);
C. Berger *et al.*, Phys. Lett. B**39**, 659 (1972);
J. Ballam *et al.* [SBT Collaboration], Phys. Rev. D**5**, 545 (1972);
G.E. Gladding *et al.*, ibid. **8**, 3721 (1973).

[60] J. Nemchik, N.N. Nikolaev and B.G. Zakharov, Phys. Lett. B**341**, 228 (1994).

[61] J. Nemchik, N.N. Nikolaev, E. Predazzi and B.G. Zakharov, Phys. Lett. B**374**, 199 (1996).

[62] J. Nemchik, Eur. Phys. J. C**18**, 711 (2001).

[63] B.Z. Kopeliovich, J. Raufeisen and A.V. Tarasov, Phys. Lett. B**440**, 151 (1998).

[64] J. Hüfner, B.Z. Kopeliovich and A. Zamolodchikov, Z. Phys. A**357**, 113 (1997).

[65] B.Z. Kopeliovich, J. Nemchik, N.N. Nikolaev and B.G. Zakharov, Phys. Lett. B**324**, 469 (1994).

[66] M.R. Adams *et al.* [E665 Collaboration], Phys. Rev. Lett. **74**, 1525 (1995).

[67] B.Z. Kopeliovich and J. Nemchik, *Where is the Baseline for Color Transparency Studies with Moderate Energy Electron Beams ?*, preprint **MPIH-V41-1995**; **nucl-th/9511018**.

[68] B.Z. Kopeliovich, A.V. Tarasov and O.O. Voskresenskaya, Eur. Phys. J. A**11**, 345 (2001).

[69] B.Z. Kopeliovich, J. Nemchik, N.N. Nikolaev and B.G. Zakharov, Phys. Lett. B**309**, 179 (1993).

[70] J. Nemchik, N.N. Nikolaev and B.G. Zakharov, Phys. Lett. B**339**, 194 (1994).

[71] B.Z. Kopeliovich, J. Nemchik and I, Schmidt, Phys. Rev. C**76**, 025210 (2007).

[72] B.Z. Kopeliovich, J. Nemchik and I, Schmidt, Phys. Rev. C**76**, 015205 (2007).

[73] J. Nemchik, Phys. Rev. C**68**, 035206 (2003).

[74] B.Z. Kopeliovich, J. Nemchik, I.K. Potashnikova and I, Schmidt, J. Phys. G**35**, 115010 (2008).

[75] L.V. Gribov, E.M. Levin and M.G. Ryskin, Nucl. Phys. B**188**, 555 (1981).

[76] B.Z. Kopeliovich, J. Raufeisen, A.V. Tarasov and M.B. Jonson, Phys. Rev. C**67**, 014903 (2003).

[77] B.Z. Kopeliovich, I.K. Potashnikova, B. Povh and E. Predazzi, Phys. Rev. Lett. **85**, 507 (2000).

[78] B.Z. Kopeliovich, A.V. Tarasov and J. Hüfner, Nucl. Phys. A**696**, 669 (2001).

[79] B.Z. Kopeliovich and J. Nemchik, Phys. Lett. B**368**, 187 (1996).

[80] A.H. Mueller and J. Qiu, Nucl. Phys. B**268**, 427 (1986).

[81] E. Basso, V.P. Goncalves, M. Krelina, J. Nemcik and R. Pasechnik, Phys. Rev. D**93**, 094027 (2016).

[82] V.P. Goncalves, M. Krelina, J. Nemcik and R. Pasechnik, Phys. Rev. D**94**, 114009 (2016).

[83] K. Ackerstaff *et al.* [HERMES Collaboration], Phys. Rev. Lett. **82**, 3025 (1999).